UNIVERSITY OF OKLAHOMA

GRADUATE COLLEGE

HIGH RESOLUTION SEQUENCE STRATIGRAPHY OF THE LEONARDIAN BONE SPRING FORMATION OUTCROP OF BONE CANYON, GUADALUPE MOUNTAINS, WEST TEXAS AND ITS CORRELATION TO THE SUBSURFACE

A THESIS

SUBMITTED TO THE GRADUATE FACULTY

in partial fulfillment of the requirements for the

Degree of

MASTER OF SCIENCE

By

ANDREW BROWN
Norman, Oklahoma
2020

HIGH RESOLUTION SEQUENCE STRATIGRAPHY OF THE LEONARDIAN BONE SPRING FORMATION OUTCROP OF BONE CANYON, GUADALUPE MOUNTAINS, WEST TEXAS AND ITS CORRELATION TO THE SUBSURFACE

A THESIS APPROVED FOR THE
SCHOOL OF GEOSCIENCES

BY THE COMMITTEE CONSISTING OF:

Dr. John D. Pigott, Chair

Dr. R. Douglas Elmore

Dr. Kulwadee Pigott

This thesis is dedicated In Loving Memory of,

my life-long best friend, Patrick Ryan Carver. Pat showed me what true friendship is and means. With his charismatic, bold, and unique personality, Pat encouraged me to believe in myself and to accomplish my dreams.

I'd also like to dedicate this In Loving Memory of

my uncles, Tom Kemp and Kelly Rogers, my grandmother, Sue Brown, my grandfather, Thomas - Elwood Kemp, and my step-grandfather, Paul Rogers.

As I have grown older, I have gained a better understanding of the impact each of them has had, and continues to have, on my life. They all have set extraordinary examples of how to love and how to live life to its fullest. Their love and support will continue to guide me through life and eternity.

Acknowledgements

When I was young, I dreamed of winning awards for making imaginary scientific breakthroughs that saved the world and brought all of humanity to a greater love and understanding of themselves, their families, others, and the Earth. As I grew older, I began to dream of having a career in science and especially in the study of the Earth, where I could someday possibly play a part in some great scientific breakthrough for the common good. These early dreams set me on the path to study science and geology.

Has this path been easy? Definitely not! Nevertheless, life's struggles have played a positive role in my development and in my understanding of my inner self. My parents and family deserve much credit in guiding me through my life. They helped form my life's framework, instilling values - love, hope, empathy, compassion, courage, persistence, spirituality, hard work and a strong belief in the importance of education, and especially in science. Most importantly, their unconditional love has taught me to love and trust myself.

I think of the framework I received from my family of origin as a "low order" sequence. Yes, it fluctuates just like the lowest order sea level fluctuations- fluctuating, but not controlled by, the "higher order" fluctuations in my life (i.e. friends, girlfriends, careers, death of loved ones, etc.). I want to emphasize and acknowledge the importance of my family here, since the "low order" sequence has provided me with a solid base for my own path during the "higher order" sequences of life.

Through my studies, I now have the tools to start my career in geology and work toward my childhood dreams of having a challenging and interesting career in science and making a difference in the world. For this, I acknowledge God, my father, Ron, mother, Liz, brother Matt (sister in-law, Ryanne, nephews, Michael and Daniel), sister Lauren (brother in-law Eric), my

extended family (that I could argue is closer than many immediate families), all of my friends, and all of creation: the Universe, the Galaxies, and the Earth. My friends and family have played a huge role in making me, me and I have great gratitude for, and appreciation of, them. I would be remiss if I did not also acknowledge my dog, Auri (Aurora Borealis Brown), who has been a constant companion to me while I have been working on this thesis.

I would especially like to acknowledge my faculty advisor, Dr. John D. Pigott, who has helped me immensely in my master's journey. We spent a lot of time together in the Guadalupe Mountains National Park studying the geology of the Permian Basin and collecting data for this thesis. I appreciate all his advice and assistance in my geology coursework and my research, as well as in my life. His views on science and spirituality and his extensive knowledge of the geology of the Earth have been, and will continue to be, inspiring. I am forever grateful for my time in the School of Geosciences studying under Dr. P.

I would also like to acknowledge my advisory committee; Dr. Kulwadee Pigott and Dr. R. Doug Elmore. Their knowledge in geochemistry, sedimentology, and diagenesis is unrivaled. I sincerely thank Dr. K. Pigott for helping me to understand geochemistry and for helping me along my journey. Our discussions about science, meditation, and our life's path(s) have inspired and motivated me to dig deep to find a better understanding of geology, my true self, and my place within the world.

Dr. Elmore played a very important role, especially, in the development of my love for geology. My early interest in geology is in large part attributed to what I learned in Dr. Elmore's geology classes where he passed on his knowledge and passion for geology to me. The class field trips took with Dr. Elmore across the United States and Italy, including the Dolomite Mountains, were truly life changing. I am so thankful for the education I received through my

work with my faculty advisor, advisory committee, and the entire geoscience department at OU. With their guidance through school and their knowledge of geology, my time at The University of Oklahoma Mewbourne College of Earth and Energy has galvanized my continued pursuit and interest in geology.

Table of Contents

List of Tables

List of Figures

Abstract

The purpose of this Thesis is to analyze the Upper Leonardian Bone Spring Formation, Cutoff Formation, and Early Guadalupian Brushy Canyon Formation in the outcrop of Bone Canyon located along the Western Escarpment of the Guadalupe Mountains in West Texas. The stratigraphy in Bone Canyon reveals numerous sea-level fluctuations that influenced the depositional processes and paleo-environments. By analyzing the outcrop, new data was obtained of lateral variations in the strata through in-depth field and laboratory analysis, including XRF and petrographic analysis. This data provides insight into the lithology and diagenetic processes impacting reservoir characterization that could only be obtained through outcrop analysis. Lateral studies provide a detailed look into various depositional processes that occurred within the same sea level sequence and show the importance of understanding lateral (dis)continuity, erosion, and deposition that transcend both chrono- and stratigraphic boundaries previously defined in the stratigraphy.

The high-resolution study shows similar elemental concentrations in the strata despite variations in sea level between strata. The study seems to indicate that chert formation and dolomite concentrations were sometimes affected by depositional processes independently of sea level fluctuations. TSTs-HSTs reveal alternating beds of carbonate and post-diagenetic chert, RSTs-LSTs reveal nodular-mottled chert formation along with mass transport deposits, which are also seen during TSTs. These mass transport deposits provided the rapid burial and compaction processes necessary for dolomitization to occur during lowstands in sea level.

According to this analysis, evidence illustrates that the Avalon deposit, which has been recognized to be comprised of the Bone Spring and Cutoff Formation, is much thicker near the slope-basin transition zone at this location than it is on the shelf and in the basin as many

subsurface studies have suggested. Outcrop analysis allows a more detailed look into the Avalon sequences than can be seen in the subsurface. The Avalon Shale is shown to cross chronostratigraphic boundaries, which originates from the L5 HFS of the Bone Spring Formation and ends at the G1 HFS of the Cutoff Formation. The alternation between high terrigeneous and carbonate concentrations in these Avalon deposits is interpreted as the result of the effects of lowstands and highstands in sea levels, which turned out providing finer-scale observations into the depositional environments and processes. The elemental and XRF analyses of this study are used as paleoenvironment proxies that aid in revealing the ideal source and reservoir rocks potential in these deposits during the fluctuations in sea level. Furthermore, results also suggested that during transgressive system tracts, pervasive permeable gravity debris flows could deposit in a more anoxic environment that resulted in a higher potential for hydrocarbon generation.

Chapter 1: Introduction

The Permian Basin, which includes the Midland and Delaware Basins, is a very prolific oil and gas province. From its record over close to a century, the Permian Basin has produced more than 33.4 billion barrels of oil and around 118 trillion cubic feet of natural gas (EIA, 2018). In 2014, the basin produced 5.6 percent of the total oil production of the world and in 2017, it was recorded to have produced 20 percent of the total crude oil production of the U.S. and 9% of total natural gas production (EIA, 2018). The Permian Basin is recognized as one of the largest hydrocarbon-producing basins in the world with proven reserves exceeding 5 billion barrels of oil and 19.1 cubic feet of natural gas (EIA, 2018). Research studies show that the Permian Basin has the greatest potential for additional oil production in the U.S. with recent advancements in technology and geological knowledge of the area. The oil and gas produced for industry has increased enormously due to additional horizontal oil and gas production which is presently seen throughout the large Permian of both Midland and Delaware basins.

The Midland and Delaware Basins were both formed during the Permian and are considered as a part of the greater prolific Permian Basin. Although the Delaware Basin is one of the two basins holding the most prolific hydrocarbon generation for the Permian Basin, nevertheless its petroleum is still mysterious due to the complication of regional tectonic development, including deformation and subsidence, degrees of sedimentary fill, thermal maturities, and remaining exploration and production potential (Lew et al., 2013). The main purpose of this research is to provide a further detailed study of the Delaware Basin in terms of higher-order stratigraphic sequences (> 3rd) by investigating its depositional formation and processes, and to increase the knowledge and appreciation of its extensive economic potential.

Advancements in technology and the continued success rate of the Delaware Basin have created further interest in the area and a greater understanding of how the basin has become so prolific. The Bone Spring formation is one of the top three oil producers of the Delaware Basin in Texas and New Mexico, and is recognized as one of the most active formations in the United States and even the world. Production from these top three formations increased from 140,000 BBl/d in 2007 to around 600,000 BBl/d in 2013, an increase from 16 to 44 percent (Figure-EIA, 2014). In 2017, the Bone Spring and two other formations accounted for 36 percent of U.S. tight oil production and the production is expected to increase to 43 percent through 2050. Tight oil production accounted for over half (54%) of the total U.S oil production in 2017(EIA, 2018)

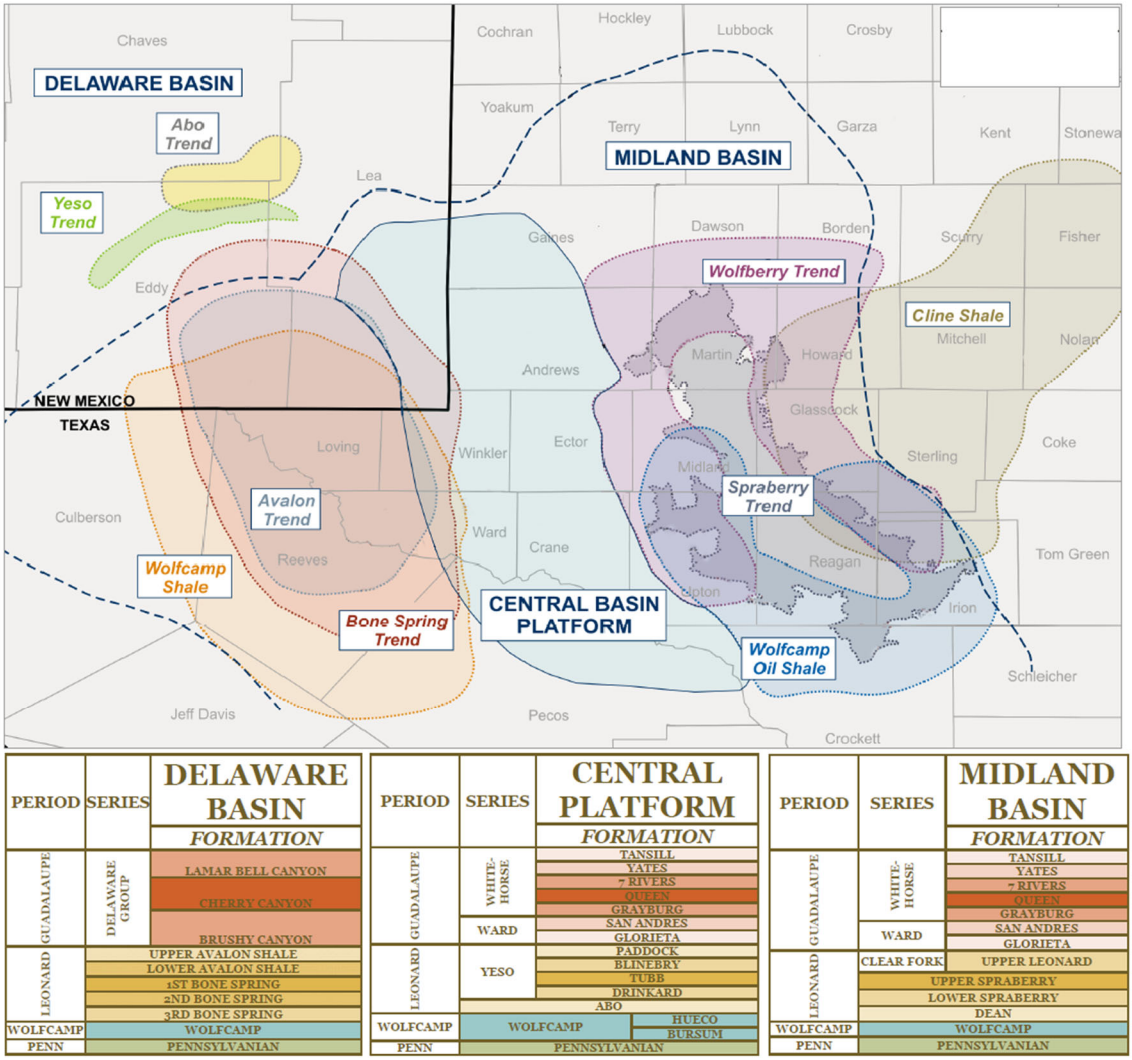

PERIOD	SERIES	DELAWARE BASIN FORMATION
GUADALAUPE	DELAWARE GROUP	LAMAR BELL CANYON
		CHERRY CANYON
		BRUSHY CANYON
LEONARD		UPPER AVALON SHALE
		LOWER AVALON SHALE
		1ST BONE SPRING
		2ND BONE SPRING
		3RD BONE SPRING
WOLFCAMP		WOLFCAMP
PENN		PENNSYLVANIAN

PERIOD	SERIES	CENTRAL PLATFORM FORMATION
GUADALAUPE	WHITE-HORSE	TANSILL
		YATES
		7 RIVERS
		QUEEN
		GRAYBURG
	WARD	SAN ANDRES
		GLORIETA
LEONARD	YESO	PADDOCK
		BLINEBRY
		TUBB
		DRINKARD
		ABO
WOLFCAMP	WOLFCAMP	HUECO
		BURSUM
PENN	PENNSYLVANIAN	

PERIOD	SERIES	MIDLAND BASIN FORMATION
GUADALAUPE	WHITE-HORSE	TANSILL
		YATES
		7 RIVERS
		QUEEN
		GRAYBURG
	WARD	SAN ANDRES
		GLORIETA
LEONARD	CLEAR FORK	UPPER LEONARD
		UPPER SPRABERRY
		LOWER SPRABERRY
		DEAN
WOLFCAMP		WOLFCAMP
PENN		PENNSYLVANIAN

Figure 1: Showing the (extent of) major plays within the Permian Basin. Taken from ShaleExperts.com (2019).

The Bone Spring Formation is subdivided into carbonate and clastic beds deposited as a result of reciprocal sedimentation on a slope to basin environment. Hydrocarbon production is from both carbonate and clastic intervals but especially from shelf and slope margin carbonates that were deposited into the basin by gravity deposits (i.e. debris flow, slumps). Most porosity found within the carbonates was suggested to be secondary by Hart (1997). The carbonate members were interpreted to be deposited during highstands, or transgressions, while the clastic-

siliciclastic members were deposited during lowstands sea levels. These siliciclastic members are hypothesized as turbidites deposits and as some sediments settling from aeolian transport (Hart, 1997).

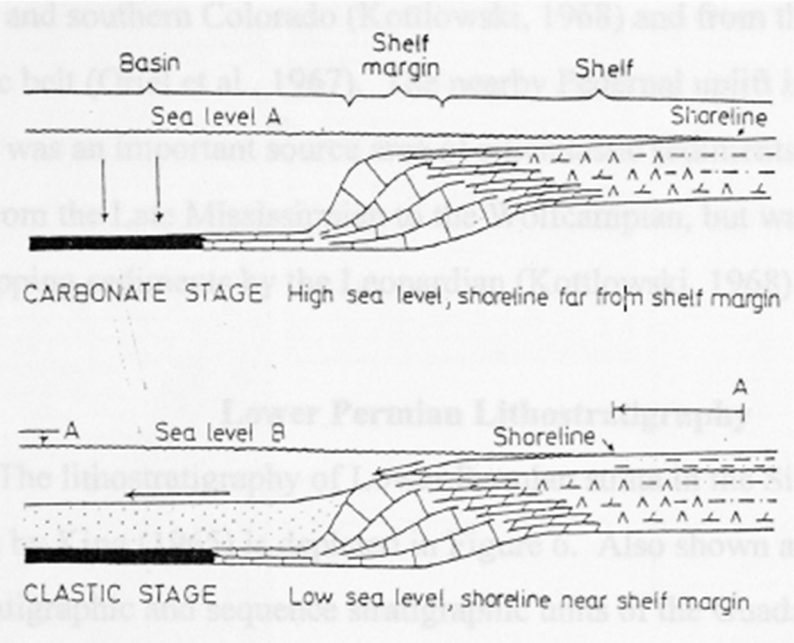

Figure 2: Figure showing Reciprocal Sedimentation. Highstands are defined by a high sea level, a shoreline far from the shelf margin, and carbonate deposition. Lowstands are defined by a low sea level, a shoreline near the shelf margin, and clastic deposition. Taken from Fitchen (1997).

Historically, the Bone Spring was thought of as a secondary target. As technology and production increased, so did the means to drill, and the focus locations shifted from slope production, to basinal sands, and now include basinal carbonates. Presently, more studies have emphasized on basinal deposits in order to increase and improve production, for the local and industrial national economy. The additional geological background and increased knowledge of the area will provide detailed information on how this Bone Spring Formation became so prolific. Even through the continued success of the Bone Spring, it is still far less studied than

the other top plays in the area including the Eagle Ford, Woodford, and Barnett Shales. Increasing knowledge of sources, reservoirs, and seals in the Bone Spring will allow for more efficient recovery and more production potential. Hart (1998) discussed and suggested that the best ways to study and optimize exploration activities in the Bone Spring is through well log analysis and chemostratigraphy; these suggestions were subsequently implemented by the study of Crosby (2015). In this research, detailed study is following Crosby's but by an outcrop investigation instead of from subsurface cores, and is based upon chemostratigraphy, geochemistry (XRF and pseudo-gamma ray), and thin-section analysis on the Late Permian formations, the Bone Spring and Cutoff Formations, especially in regard to 3^{rd}-4^{th} order stratigraphic sequences. Bone Canyon is one location which consists of out crops that can provides a unique understanding of the lithology, stratigraphy, depositional history, and paleoenvironment of the Bone Spring and Cutoff Formations where the well-known Avalon Shale Play also exists. The study of the Avalon Shale is crucial when trying to understand the source rocks, reservoirs, seals, and migration pathways in these two formations. The instant project aims to assist the on-going success of oil and gas production of the present Delaware Basin and the successful exploration and production of similar basins around the world.

Study Location

Figure 3 is an image of the West Texas and Southeast New Mexico Permian Basin and within it, the Delaware Basin. The stratigraphy investigated is confined to the outcrops present in Bone Canyon, located in Culbersum County in the Northwestern part of the Delaware Basin along the Western Escarpment of the Guadalupe Mountains (**Figure 4**). The area was subjected to sediment inputs, primarily sediment gravity flows, from the Diablo Platform,

Northwestern Shelf, and Central Basin Platform. Owing to its position in the Delaware Basin, Bone Cayon provides a good look into the basinal carbonates and basinal clastics, which are the major hydrocarbon producing units, that were transported from the surrounding shelves and slopes. Bone Canyon, and the formations within, are for the study of paleoenvironments and depositional processes through high-resolution, high-order sequence stratigraphic investigations owing to the amount of detail that can be observed, visually as well as the amount of data that can be collected in outcrops.

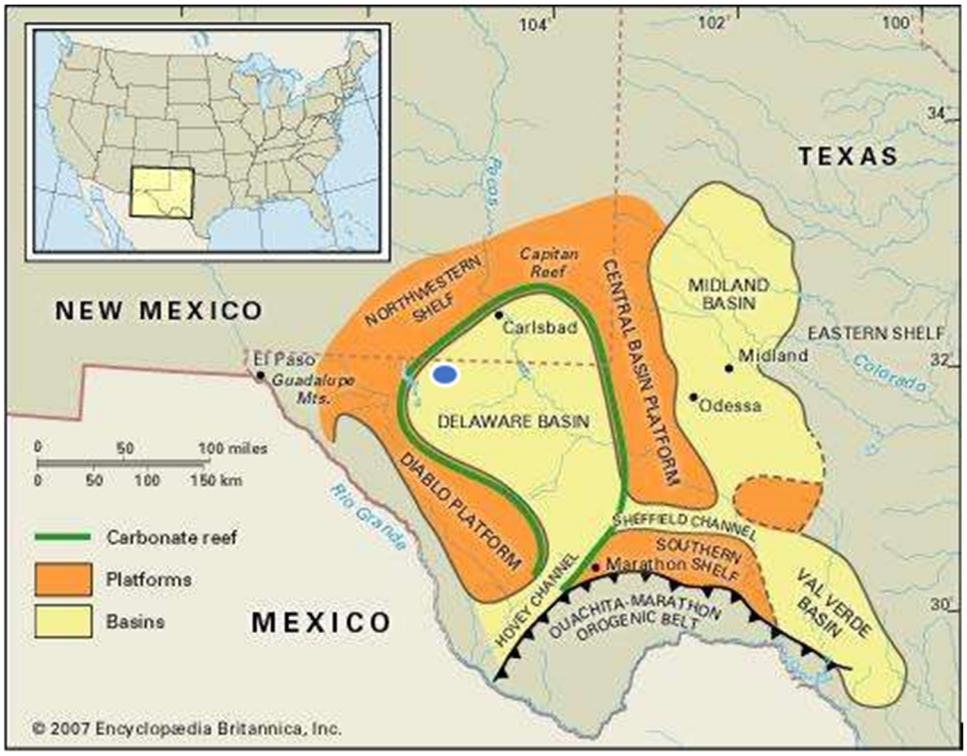

Figure 3: Simplified Map of the Permian Basin and the Geologic Provinces within. Bone Canyon is represented by the blue oval. Modified from (Tang, 2007).

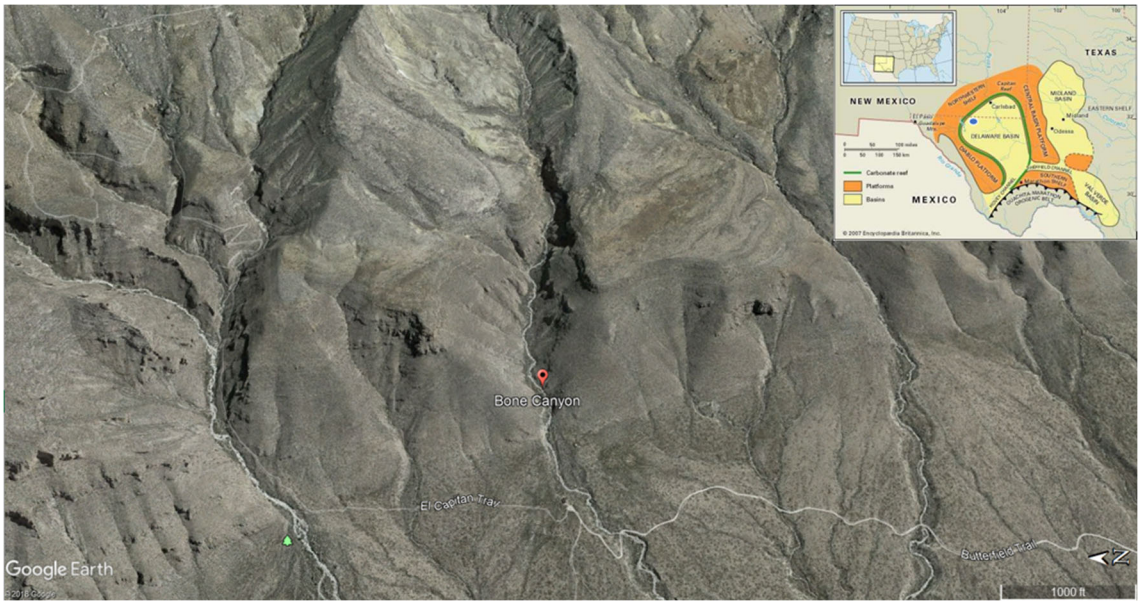

Figure 4: Location of Bone Canyon taken from Google Earth. Basin map included for reference that was modified from Tang (2007).

Previous Work

This study relies heavily upon numerous previous detailed works regarding the tectonics, stratigraphy, geochemistry, geophysics, and oil and gas history of the Permian Basin and, more specifically, the Delaware Basin. Many studies were reviewed as background research into the Basin. However, the studies listed below are directly related to the Bone Spring formation inside the Permian Basin.

Geological research began in the Delaware Basin around 160 years ago in order to find the best path for the future railroad going from the Mississippi River to the west coast. The leader of the research team was G.G. Shumard, the man who originally named the Bone Spring "black basal limestone" (King, 1948; Crosby, 2015). The name was changed to the Bone Spring Limestone in a bulletin from Texas University in 1916 by J.A. Udden et. Al (King, 1948; Crosby, 2015).

Bone Canyon, the area of this investigation, is also the original geographic location where the Bone Spring was first discovered. Bone Canyon and Shumard Canyon to the North-Northwest both have great outcrops of the Bone Spring. P.B. King is known as the father of the Delaware Basin because of his original work regarding its geology. (Hill, 1996). King provides a detailed analysis of the Permian strata where they crop out in the southern Guadalupe Mountains, including exposures of the Bone Spring, the Cutoff, and the Victoria Peak Limestone (King, 1948). Ever since King's classic study, the Delaware Basin has been subject to extensive research regarding the tectonic history, stratigraphy, and lithology of the basin (Adams, 1939; Galley, 1958; Adams, 1965; Silver and Todd 1969; Keller et al., 1980; Hills 1984; Ross and Ross, 1994; Crosby, 2015). In order to focus the study on one specific formation, the Bone Spring, it is crucial to understand the history of the basin as a whole. Numerous studies have also been done in the Delaware Basin regarding oil and gas exploration and production. Oxygen isotopes from fluid inclusions found within the Bone Spring provided a geothermal gradient of 2.2 degrees F/100ft in the Delaware Basin (Barker and Halley, 1986; Crosby, 2015). Wiggins and Harris (1985) conducted a diagenetic and geochemical study within the Bone Spring and found that the carbonate debris flows had been dolomitized syn-depositionally and the formation of the dolomite can be correlated to the high presence of organic matter. The geochemical findings show that the Bone Spring exhibits type II and III kerogen total organic carbon (TOC) is greater than 2%, and that the Formation has been in the oil generation window since 200 ma. (Wiggins and Harris, 1985; Crosby, 2015). Although this study focuses more on the 1st Bone Spring Carbonate, Wiggins and Harris suggest a max porosity of 10.4% and a max permeability of 12 millidarcies (mD), which they found from core measurements of the 2nd Bone Spring Carbonate (Wiggins and Harris, 1985).

Before Saller et al. (1989) studied the Mescalero Escarpe Field, the carbonate debris flows found within the Bone Spring were thought to have possibly been subjected to subaerial exposure. Their study changed this assumption and stated that the debris flows were being eroded by subaqueous biodegradation or bioerosion from organisms. This discovery further supported the deposition of debris flows during highstands of sea level (Saller et al., 1989; Crosby, 2015).

An overall geological analysis of the Delaware Basin was conducted by Hill in 1996. Her work focuses on the stratigraphic sequences that make up the basin and explains how the various tectonic events helped to shape the stratigraphic record that is currently seen.

In 1998, Hart and Montgomery both provided background studies on the Bone Spring. Hart (1998) analyzed the stratigraphic sequences and how they relate to tectonics, concluding the paleobathymetric lows in the basin act as gravity lows where submarine turbidites form (Hart, 1998). Similarly, but not as in depth, Montgomery's (1998) study discussed tectonics and the stratigraphy during Bone Spring deposition. However, his work focused more on a full production history of the Bone Spring. The facies established by Montgomery provided an important guide for this study.

The New Mexico Bureau of Geology and Mineral Resources also recently conducted a geochemical study that complements that of Wiggins and Harris (1985). By using the rock evaluation process that factors in TOC, Tmax, hydrogen index, oxygen index, S1, S2, and S3 peaks, as well as vitrinite reflectance. The study showed once again Type II and Type III kerogen, good to excellent TOC, and the source rock to be in the generation and expulsion phases of hydrocarbon production (NM Bureau; Crosby, 2015).

In 2008, Bassett published a thesis focusing on chemostratigraphic packages and how they can be used in correlating wells. Using well cuttings, Bassett (2008) was able to distinguish certain geochemical packages found within the 1st shale interval of the Bone Spring. The importance of this study is owing to the use of certain major, trace, and rare-earth elements as proxies for paleoenvironmental reconstruction (Bassett, 2008).

Since around 2013, numerous studies have focused on the shale-rich or mudstone-rich facies within the Bone Spring. Nance and Rowe (2013) used x-ray diffraction (XRD), x-ray fluorescence (XRF), and total organic carbon (TOC) methods to correlate facies with changes in organic and inorganic constituents throughout the history of deposition. Their studies continued and included a discussion regarding the silica and carbonate depositional cycles found within the mudstone packages (Nance and Rowe, 2014).

Crosby (2015) provided a very detailed thesis regarding the depositional history and sequence stratigraphy of the Bone Spring Formation. Using 451 well logs, subsurface mapping, and five cores from the slope to basin transect, Crosby (2015) found eight sequences within the Bone Spring primarily controlled by global and relative sea level fluctuations, basin physiography, and subaqueous erosion (Crosby, 2015). These sequences correspond to 3rd order parasequence sets that overlie the Wolfcampian Unconformity and are bounded at the top by the Leonardian Unconformity. The unconformities are 2nd order sequence boundaries that reflect tectonic, subsidence, sediment supply, and eustatic influences (Crosby, 2015). Using spectral gamma ray (SGR) and x-ray fluorescence (XRF) techniques, Crosby (2015) was able to show just how complex this siliciclastic and carbonate petroleum system really is. The proxies in his work related siliciclastic terrigenous, detrital concentrations to lowstands and carbonate-rich concentrations to highstands (Crosby, 2015). Perhaps the most important part of the study, as it

pertains to this investigation, is the use of elemental concentrations to investigate paleoenvironmental conditions and controls. Crosby's (2014) proxies showed sporadic intervals of anoxia with increasing anoxia from the slope to basin. By compounding paleoenvironmental proxies with compositional proxies, Crosby (2015) found internal heterogeneities within individual members of the Bone Spring that represent good source rocks, reservoir rocks, and even self-sourced reservoirs (Crosby, 2015).

The exposure in Bone Canyon is almost entirely comprised of the 1st Bone Spring Carbonate Member. Within this package is a subdivision known as the Avalon Shale. Stoltz (2014) conducted a thesis study regarding the Avalon Shale, the carbonate-rich sediment gravity flows (SGF) that are found within it, the depositional controls, and its reservoir potential. The Avalon is made up of dark, organic-rich siliciclastic mudstones interbedded with deposits of carbonate-rich sediment gravity flows, indicating source areas in every cardinal direction of the basin (Stoltz, 2014). Owing to changes in source direction and sediment dispersal through time, depositional trends consistently change throughout the Avalon deposition (Stolz et. al., 2015). SGFs allow shelf and slope carbonates to be deposited lower on the slope and deeper into the basin. Aprons, sheets, fans, and linear geobodies are all found within the Avalon. Stoltz found two phases of carbonate fan development, those that formed during regressions and and those during lowstands, and are separated by a phase of apron development deposited during transgression and highstand. Furthermore, the mudstone facies indicated high-quality unconventional reservoir with higher porosity, permeability, and TOC than the carbonate facies (Stoltz, 2014). As the thickest mudstone facies are found on the fan lobe margins owing to their reservoir quality, these are the best places to drill.

Problem Definition and Objectives

The deposition of the Bone Spring and Cutoff Formations is complex, a product of cyclic siliciclastic and carbonate composition, (Leonardian-Guadalupian) sea level fluctuations, effects of regional tectonic phases, and local paleoenvironmental conditions during deposition. The focus of this study is to provide a better understanding of those processes on the Bone Spring and Cutoff Formation(s) from the outcrops in Bone Canyon, through an investigation employing high resolution sequence stratigraphy.

Once the sequence stratigraphy is completed on the outcrop, it can then be correlated to the subsurface in order to better confine this petroleum system within the Delaware Basin. The chemostratigraphic information will be used in high-order sequence stratigraphic analyses to build a high-resolution framework for the Bone Spring and Cutoff formations for the first time. The combination of using chemostratigraphic proxies and pseudo-gamma ray data from the XRF, along with thin-section analysis and well logs from previous studies, will provide a detailed outcrop analysis with the ability to correlate these units in the subsurface, resulting in a more detailed and higher resolution sequence stratigraphic framework of the Bone Spring and Cutoff Formations which can aid in future oil and gas exploration and production in the Delaware Basin.

Chapter 2: Geologic Background

A generalized stratigraphic column for the Delaware Basin and, specifically, the Bone Spring Formation is shown in **Figure 5**. It is important to remember that although this column provides a good visual representation of the Bone Spring Formation, the composition of the strata that make up this formation is relative to the location within the Delaware Basin and, unfortunately, the naming of the strata is relative to the company or researcher. The problematic nature of naming the strata will become more apparent later on when discussing the Avalon Shale Play and correlating outcrops to the subsurface.

The tectonic history of any province is crucial when trying to understand its complete and complex geology. Once the tectonic history is better understood, the information can be combined with the depositional and stratigraphic histories of the province, providing such an understanding of the basin that the potential causes for its evolution into such a prolific oil and gas province can be inferred. This deep understanding of the basin as a whole will then provide insight into the environmental forces that impacted and helped to shape the stratigraphy during the time of deposition, in this instance, the Permian.

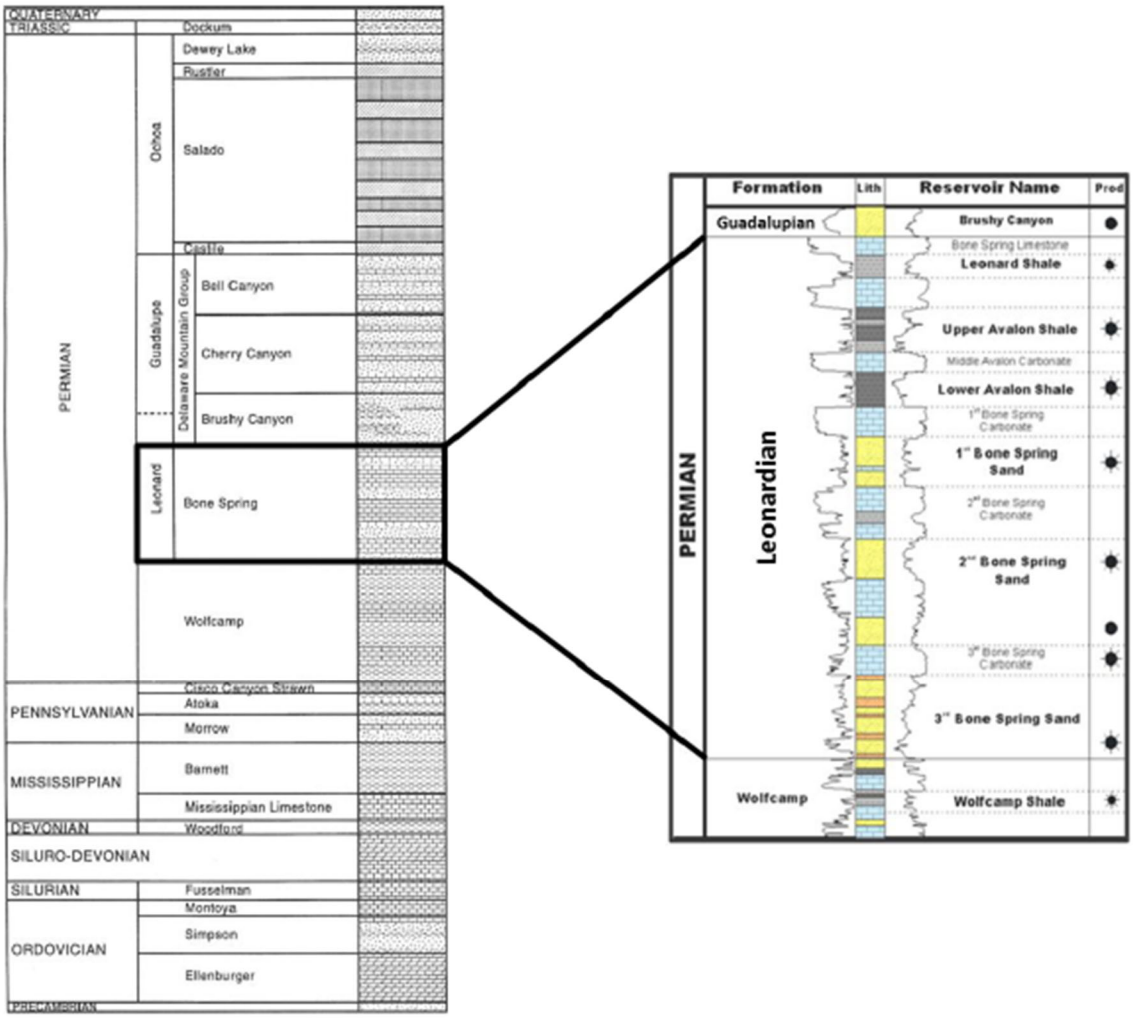

Figure 5: Generalized stratigraphic column for the Delaware Basin. The focus is on the Leonardian Bone Spring Formation (enlarged to the right). The Bone Spring is comprised of alternating carbonate and clastic units. HC production zones to the far right. Taken from Crosby (2014) that was modified from Hardage et al. (1998) and Concho Resources from Core Laboratories (2014).

2.1: Tectonic History

The Delaware Basin occupies a negative structural depression located in western Texas and southeastern New Mexico that reaches 200 miles long and 100 miles wide, covering around 86,000 square miles comprised of 52 counties in Texas and New Mexico (Adams, 1965; ShaleExperts, 2019). The basin is bounded by the Northwestern Shelf to the North, the Central

Basin Platform to the East, the Marathon-Ouachita Belt to the South, and the Diablo Platform to the West. The San Simon Channel to the northeast, the Hovey Channel to the southwest, and the Sheffield Channel to the southeast, played important roles connecting the Delaware Basin, Midland Basin, and Panthalassic Ocean together during the Permian (Crosby, 2015). Tectonism is a major control on stratigraphic sequences and thus tectonism has implications on hydrocarbon development, migration, accumulation, and preservation- Crosby. Knowing the structural development and the subsidence history of a basin provides a better understanding of the stratigraphic variability within it (Yang and Dorobek, 1995).

Through time the formation, and eventually the separation, of Rodinia and Pangea likely created the structural features found within the Delaware Basin and were inherited or modified during the Permian. This structural inheritance is likely owing to the fact that the Proterozoic zones of weakness follow trends brought on by the Grenville orogeny and the rifting of Rodinia (Shumaker, 2002; Crosby, 2015). The Variscan orogeny later reactivated these lines of weakness as Pangea formed and further influenced the structural development. The Laramide Orogeny during the Cretaceous-Cenozoic eventually created the structural features that are seen today in the Guadalupe Mountains. Organizing, or dividing, these major processes by geological ages provides an easy and clear understanding of the tectonic and depositional phases that occurred throughout time.

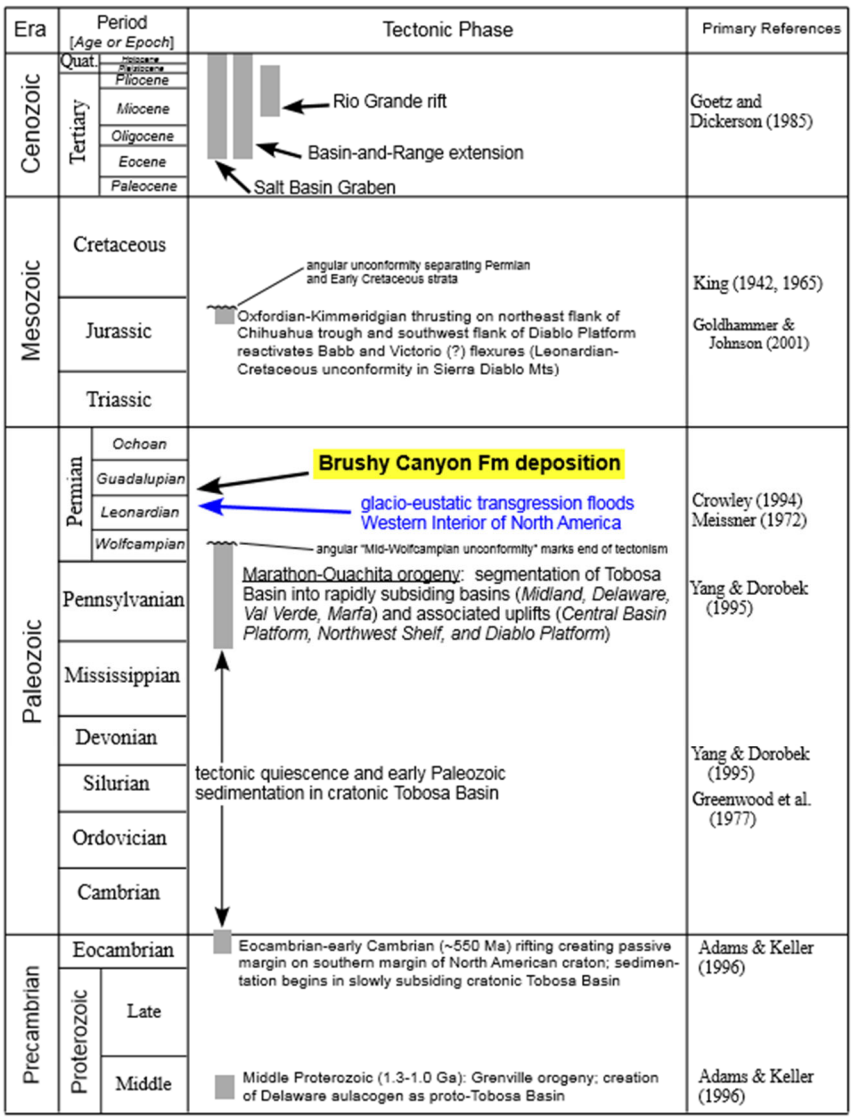

Figure 6: Tectonic Events in the Permian Basin and the Delaware Basin within. Taken from Romans (2000).

2.1.1: Precambrian-Cambrian

During the end of the Precambrian and into the Early Cambrian, a peninsular spur (protrusion) off the Transcontinental Arch was the original structure in which the Delaware Basin evolved (Adams, 1965). Likely caused by shrinking and cooling of the underlying crust and mantle, the crest of this peninsular ridge subsided into a negative depression and developed

into the axis of the, future, Permian Basin. Rather than becoming a structural basin after this early subsidence, the peninsular arch turned into a flat and shallow coastal plain where the Early Ordovician ocean transgressed (Adams, 1965). At the end of the Precambrian the entire region was welded to the southwestern edge of the craton and began to gradually subside, forming the Tobosa Basin. Soon after, the tectonic activity along the Proterozoic lines of weakness ended and the Tobosa Basin was well established (Hills, 1984).

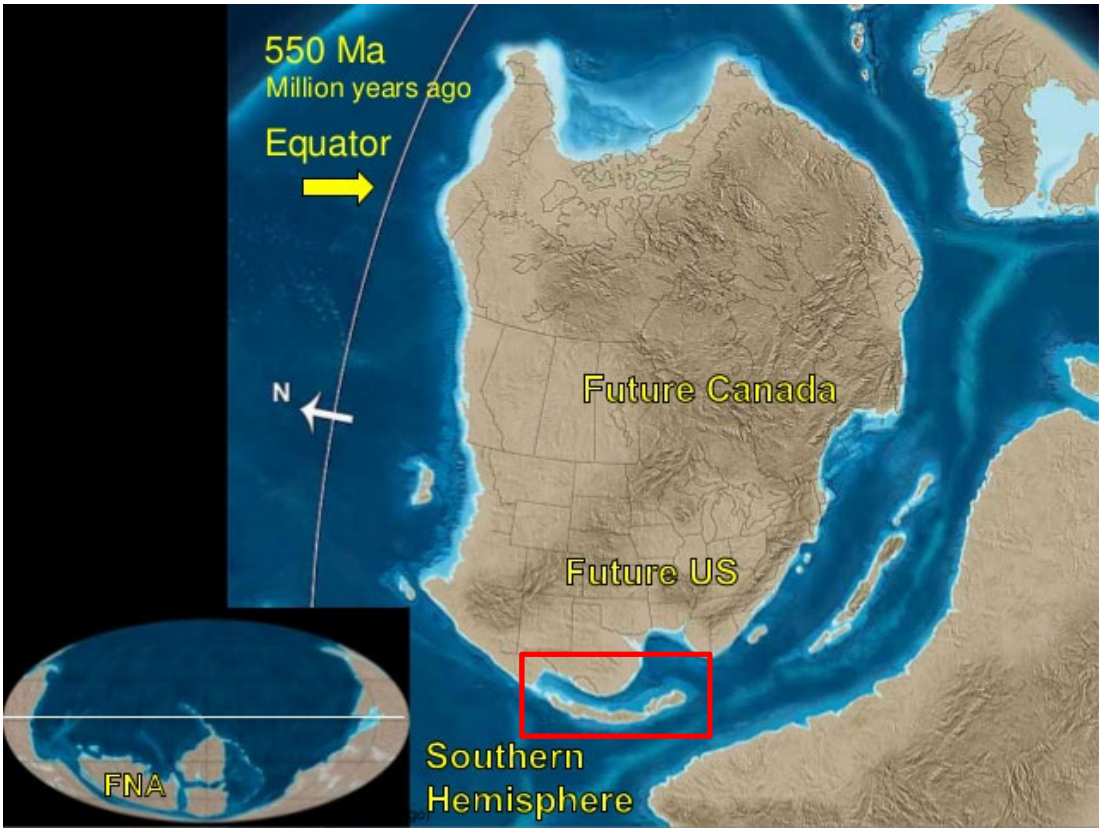

Figure 7: Paleogeographic image of North America during the Late Precambrian. The red rectangle shows the peninsular arch welded onto the southwestern edge of the craton that later evolved into the Permian Basin. Modified from Blakely (2014).

2.1.2: Mid-Ordovician

In the Middle Ordovician, between the Texas Arch to the east and the Diablo Arch to the west, sagging of the continental crust at the negative depression, mentioned earlier, created the Tobosa Basin, the precursor basin to the Permian and, more specifically, the Delaware Basin (**Figure 8**). The southern Tobosa Basin merged with the Marathon embayment permitting ocean water circulation (Adams, 1965).

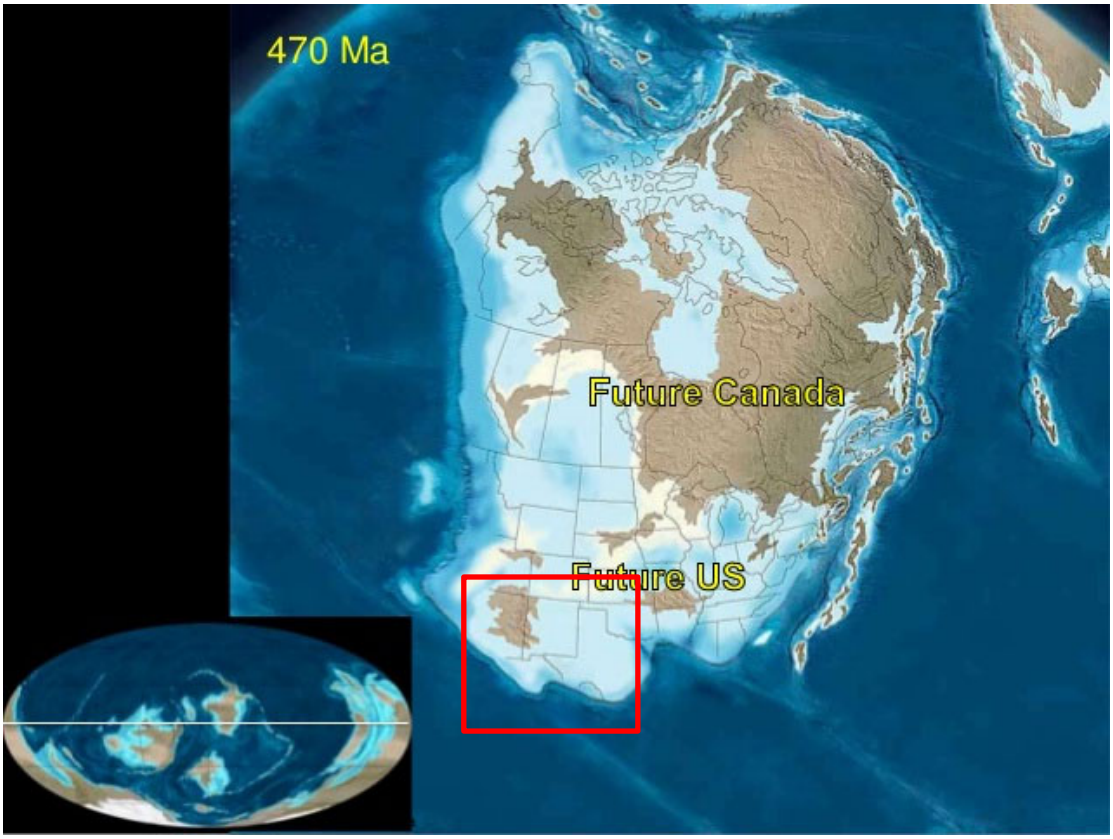

Figure 8: Paleogeographic image of North America during the Middle Ordovician. The red square shows the merging of the Tobosa Basin with the Marathon embayment which was time equivalent to the subsidence of the Michigan basin (red square). Modified from Blakely (2014).

2.1.3: Late-Ordovician – Silurian – Devonian

From the Ordovician-Silurian, the center, axial part of the Tobosa Basin contained relatively deep water. Owing to deep waters, possibly acidic, limestone deposition was limited. Subsidence rates were greater than those of sedimentation, consequently many areas were sediment starved during this time and eventually the disconformity expanded shoreward. During the Devonian structural stability was temporarily re-established (Adams, 1965).

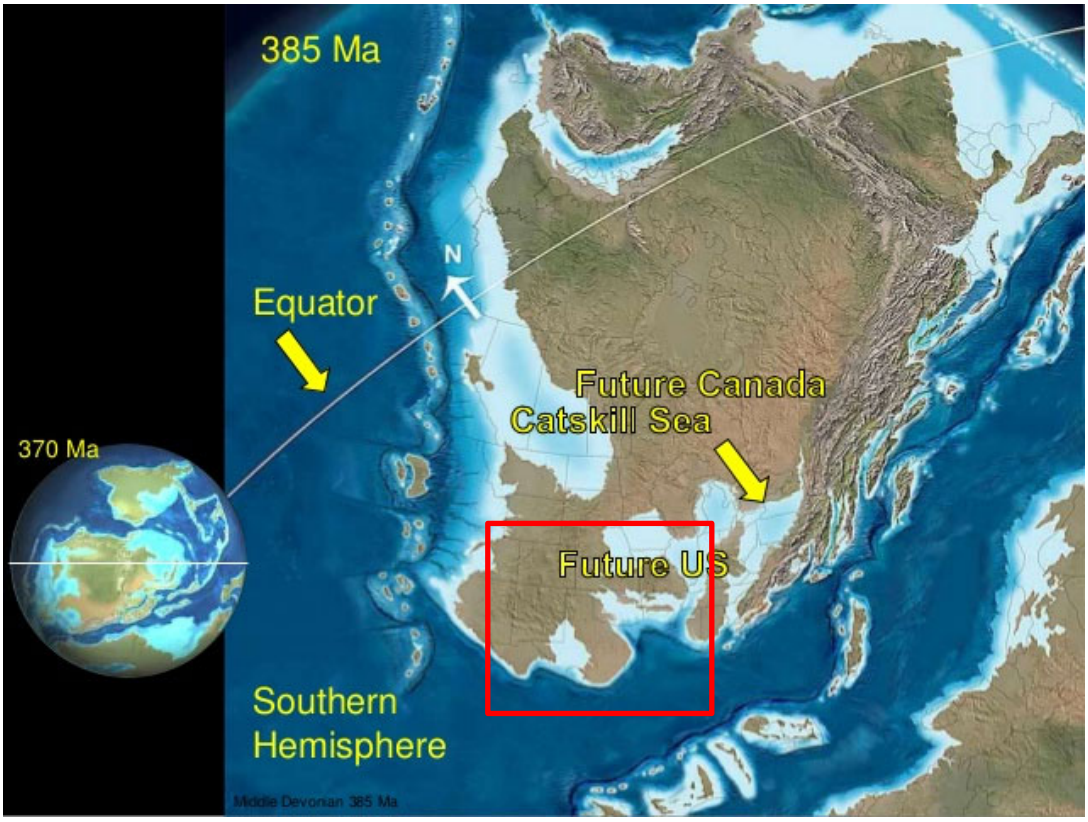

Figure 9: Paleogeographic image of North America during the Late Devonian. The red square shows the structure of the Permian Basin. Modified from Blakely (2014).

2.1.4: Mississippian

During the Early-Middle Mississippian the formation of Pangea began to cause tectonic pulses that resulted in slight uplift and reactivation of zones of weakness along the semi-vertical Proterozoic fault planes located on the axis (median ridge) of the Tobosa Basin (Crosby, 2015). Compressional forces associated with the Variscan Orogeny resulted in extensive vertical movement along these Proterozoic zones of weakness in the Tobosa Basin. The movement along this ridge, later known as the Central Basin Platform, caused the separation of the Tobosa (Permian) Basin into the Delaware and Midland Basins (Hills], 1984).

Around 7000 ft of sediments filled the axial portions of the Tobosa sag by late Mississippian. The extensive and long lived autogeosynclinal sagging of the Tobosa Basin, in which these sediments filled, is not fully understood, after all sedimentation was still less than subsidence (Adams, 1965). Later compression of sediments cannot explain subsidence of a 350-mile-wide, and flat, basin as Adams (1965) believes that densification along with compaction of the underlying crust or mantle layers better explains the continued subsidence of the Tobosa Basin.

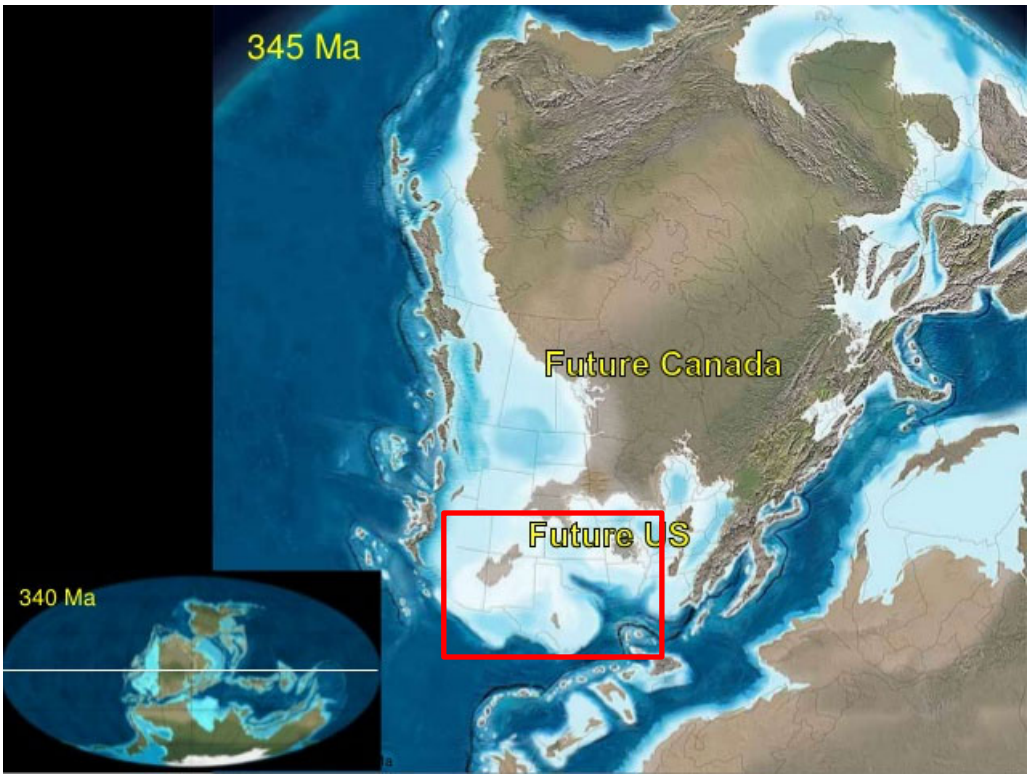

Figure 10: Paleogeographic image of North America during the Early Mississippian. Red box outlines the separation of basins. Modified from Blakely (2014).

2.1.5: Central Basin Platform

The Permian is comprised of various uplifts and sub-basins, specifically, the Central Basin Platform (CBP), Delaware Basin, and Midland Basin respectfully. **Figure 11** shows the structural features that bound the uplift and basins. To the East, the Delaware Basin is bounded by the CBP which separates it from the Midland Basin and is composed of fault-bounded, left-stepping, en echelon structural domains (Yang & Dorobek, 1995). Faults and boundary fault zones separate these structural domains from each other and adjacent basinal areas. To the east, the Midland Basin is bounded by the Fort Chadbourne Fault Zone, to the south, by the Ozona Arch, which is an eastern extension of the Central Basin Platform that separates the Midland from the Val Verde Basins. Although the Ozona Arch is considered an extension of the Central

Basin Platform differ in structural styles and therefore suggest different tectonic mechanisms associated with their formation (Yang & Dorobek, 1995). The Puckett-Grey Ranch Fault (Fig. 11) is a steeply dipping fault that runs south from the western boundary fault zone of the Central Basin Platform and separates the Delaware Basin from the Val Verde Basin.

Yang and Dorobeck (1995) proposed the compressional forces from the Variscan Orogeny created the CBP, thus separating the Delaware and Midland Basins. The CBP is composed of numerous (around six) crustal blocks, or sub provinces, that have different structural styles from adjacent blocks or areas. Yang and Dorobek (1995) have divided the Central Basin Platform into two dominant structural blocks, known as the Andector and Fort Stockton Blocks (**Figure 11**), because these block boundaries include the multiple domains, with similar vergence, relief, and structural orientations, that were found in other studies. The Fort Stockton Block corresponds with the southern portion, while the Andector Block corresponds with the northern portion of the CBP. The SW and NE corners of the Fort Stockton Block are characterized by steep reverse faults that dip inward of the block and display the greatest amounts of vertical displacement along the CBP's boundaries. On the western side of the block, displacement decreases from South to North while on the eastern side of the block displacement decreases from North to South (Yang & Dorobek, 1995). Similar to the FSB, the SW and NE corners of the Andector Block are also characterized by steep reverse faults that dip inward of the block. The SW corner of the Andector Block displays the greatest amount of vertical displacement and, on the western side, displacement decreases from south to north while on the eastern side displacement decreases from north to south. The fault zone on the northern boundary of the Andector Block shows steep reverse faults that dip southward (Yang & Dorobek, 1995).

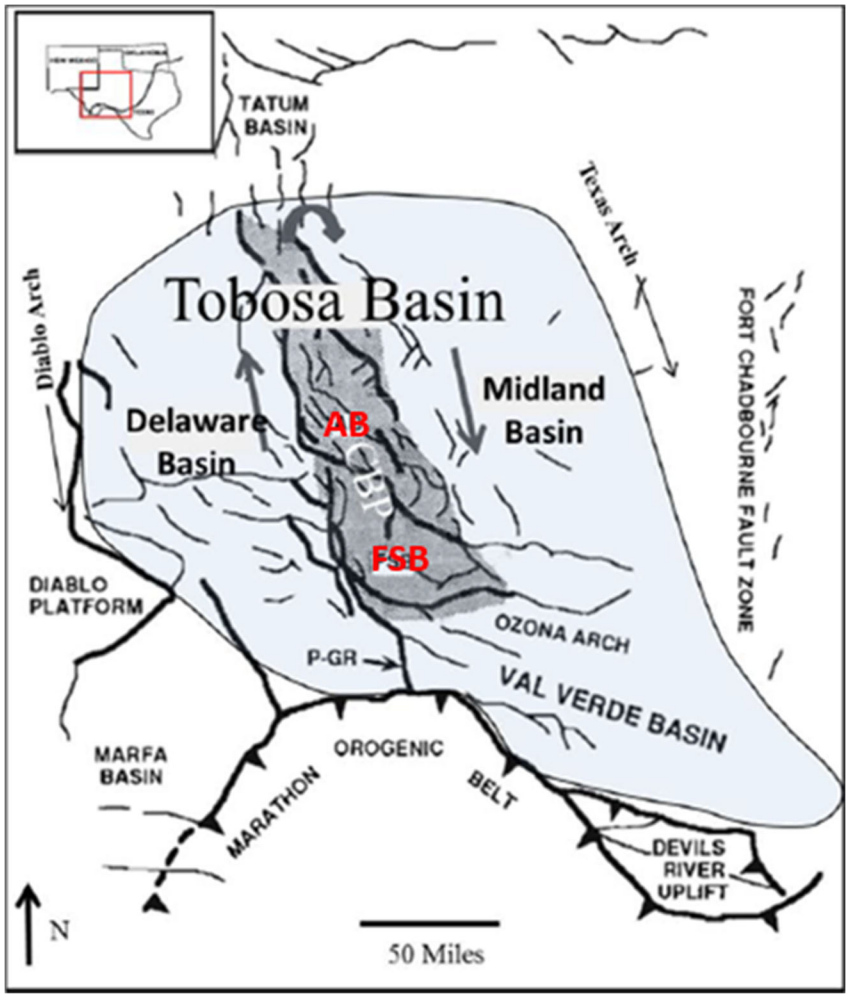

Figure 11: Generalized structural features of the Tobosa Basin showing fault zones and the direction of movement. The light blue shaded area outlines the Taboso Basin, while the dark grey shaded area outlines the Central Basin Platform (CBP). The two main fault blocks, the Andector Block (AB) and the Fort Stockton Block (FSB) are seen within the CBP. PsGR indicates the Puckett-Grey Ranch Fault. Image taken from Yang and Dorobek, 1995.

2.1.6: Pennsylvanian

The Pennsylvanian was a time of high tectonism and rapid subsidence as evidence by several structural activities in the area. The left stepping, en echelon pattern of the two blocks, the thrust and reverse faults found at the SW and NE corner of the blocks and normal faults

found at the NW corner of the FSB, the greatest displacement found at the boundary fault zones on the SW and NE block corners, and decreasing displacement, or basement shortening, from South to North on the western side and from North to South on the eastern side of the two blocks can be explained as a result of the clockwise rotation of the FSB and AB (Yang & Dorobek, 1995). This is more evidence that the compressional forces were derived from the Marathon-Ouachita thrust belt in the south and caused the CBP uplift (Crosby, 2015). Tectonic activity and compression associated with the CBP uplift continued into the Pennsylvanian followed by rapid subsidence. The primary factor causing the extensive subsidence during this time was the flexural loading of the CBP onto the Delaware Basin and, later, sediment loading during the Permian (Crosby, 2015, Yang and Dorobek, 1995).

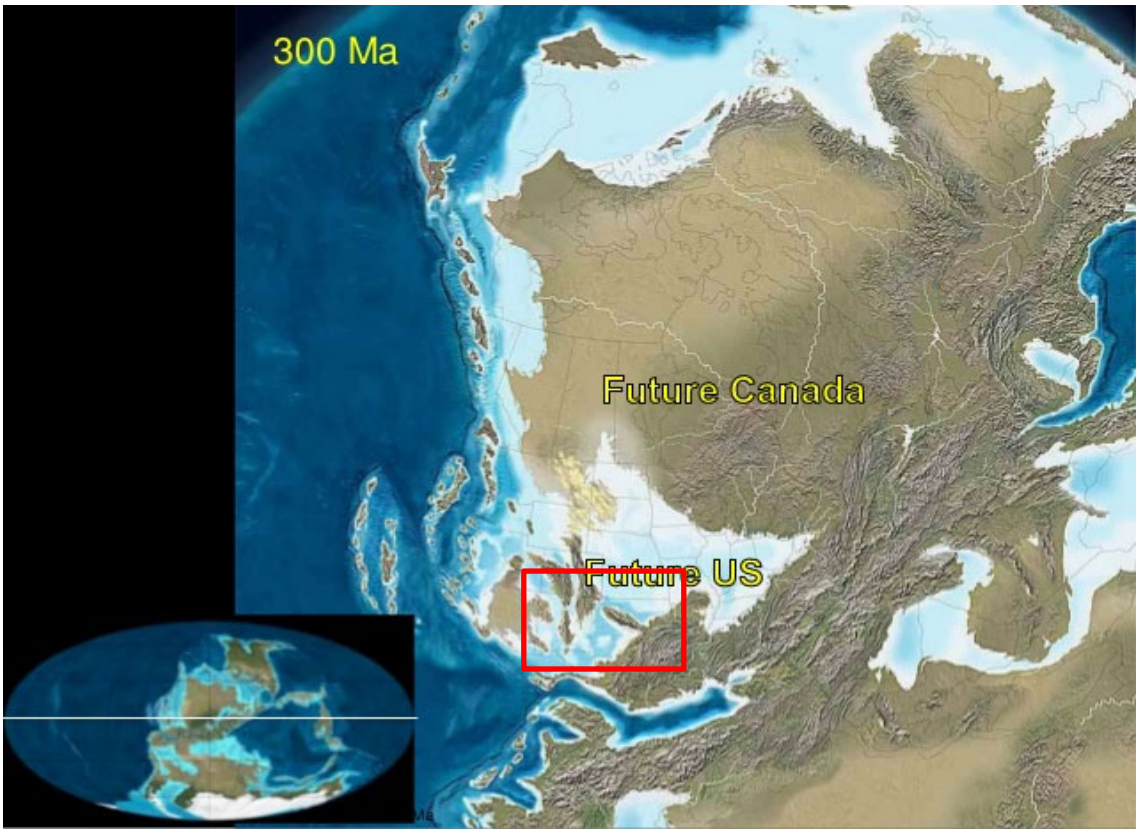

Figure 12: Paleogeographic image of North America during the Late Pennsylvanian. Red square showing location of Permian Basin. Modified from Blakely (2014).

2.1.7: Permian

Tectonism during the Permian period accompanied waning events associated with the Variscan Orogeny that caused short periods of tectonic pulses and vigorous sedimentation as a result of the accommodation created during the subsiding, sediment starved Pennsylvanian (Crosby, 2015). The Permian Basin can be separated into 4 depositional stages, from oldest to youngest, including the Wolfcampian, Leonardian, Guadalupian, and Ochoan, respectively. In the Early-Permian (Wolfcampian) the Delaware Basin foundered. Rapid basin subsidence allowed thousands of feet of sediment to accumulate, causing compressional stress to the underlying crust and permitting several thousands of additional feet of uplift of the CBP as well

as the formation of ridges around the Delaware Basin (Adams, 1965). The variation in relief, subsidence, and sedimentation between the Delaware and Midland Basins during this time gives credence as to why there is stratigraphic differentiation between the two basins during this time (Crosby, 2015). Throughout the Early Permian, compaction and movement along old, weak zones on the eastern margin of the DB caused continued subsidence and thus significant relief (>1,000 feet) between the shelf and central basin floor (Hills, 1984). As carbonate shelves continued to develop in the Middle Permian, Leonardian to Early Guadalupian, the basinal circulation became more constricted, however, owing to the shelf channels, the Hovey Channel and Val Verde basin surface water was able to circulate and continue to be organically productive (Hills, 1984). By the time of the Late Permian, tectonism and subsidence slowed and eastward tilting and deepening of the Delaware Basin eventually became the only tectonic effect (Crosby, 2015).

During the Late Guadalupian and Ochoan, rapid subsidence continued while global sea level dropped and the continuing restriction of water circulation from the Panthalassic Ocean caused the deposition of evaporites that ceased the vertical migration of fluids and caused the fluids to migrate laterally into traps on carbonate platforms (Hills, 1984; Blakely, 2013). The general lack of tectonic deformation during this time means that no structural traps formed within the basin and hydrocarbons were forced to migrate to the surrounding shelves. The evaporites prolonged petroleum generation and caused less gas generation in Late Permian beds owing to heat conduction. By Ochoan the basin had become tectonically stable and was no longer a subsiding geological province (Crosby, 2015). Stability of the basin continued until the Late Cretaceous to Cenozoic when the Laramide Orogeny and Basin and Range took place. The tectonic activity associated with these events in the Late Paleozoic created the structural features

including the Guadalupe Mountains, Delaware Mountains, Sierra Diablos, and the Salt Basin that are seen today (Yang and Dorobek, 2995; Crosby, 2015).

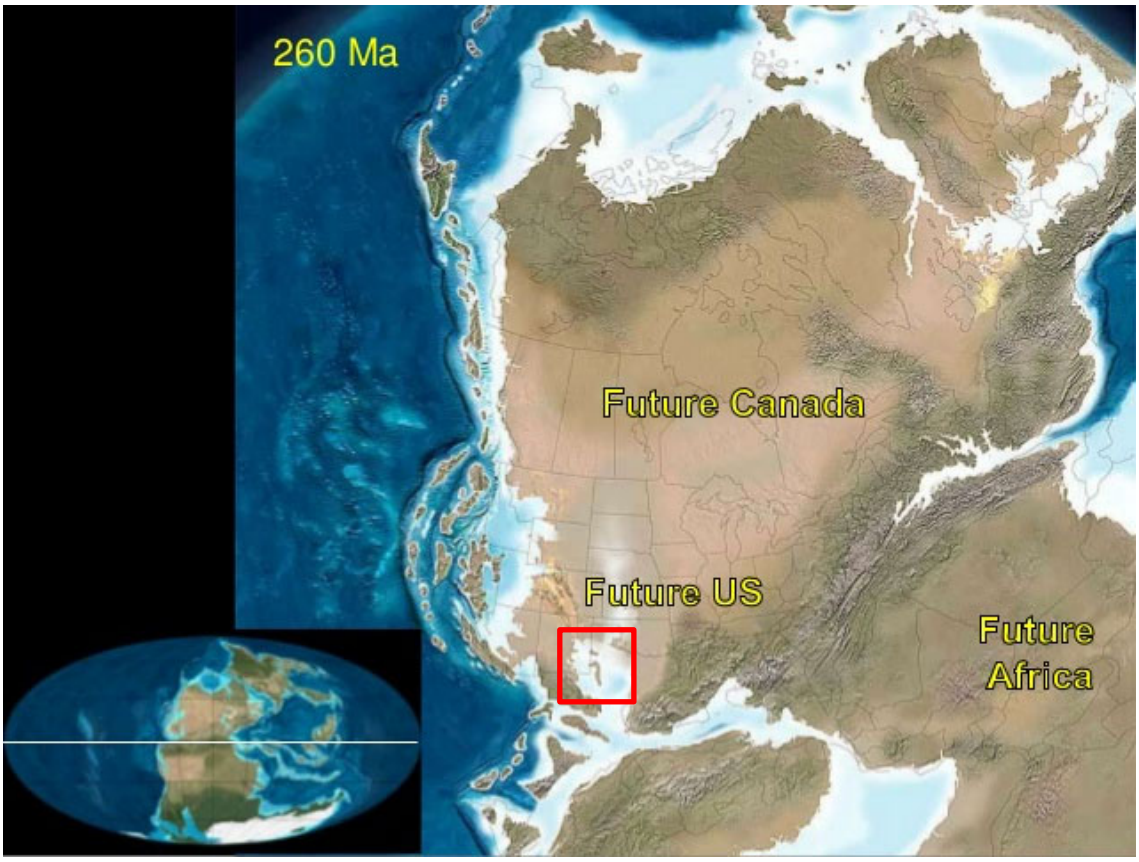

Figure 13: Paleogeographic image of North America during the Late Permian. At this time the DB, CBP, and MB which are within the red rectangle are well established. Modified from Blakely (2014).

2.2 Deposition

By the end of the Permian, the sub-basins were filled with sediments. The two main sub-basins, the Delaware Basing and Midland Basin, were filled with similar aged lithologies. However, as the sub-basins subsided and the platform remained uplifted, the different depths and development of the sub-basins caused varying water depths and, therefore, different depositional

environments (Sutton, 2014). **Figure 14** below shows the varying degrees of structural relief/subsidence between the sub-basins and platform(s).

.

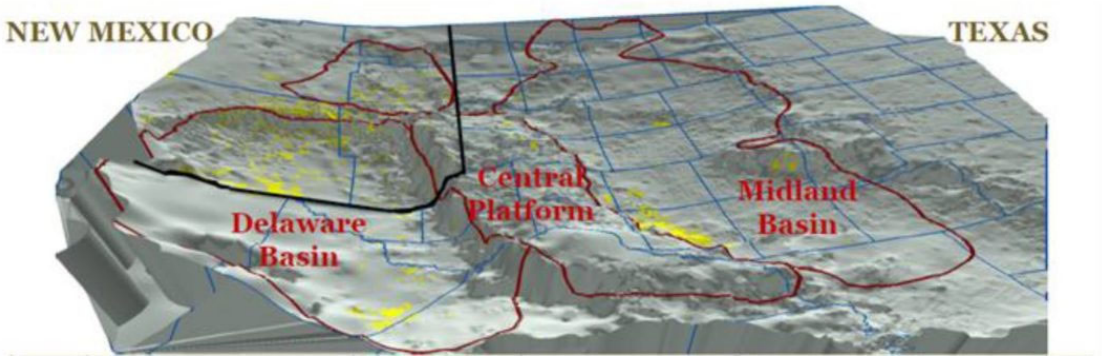

Figure 14: Structural variation between the Delaware and Midland Basins and Central Basin Platform. Taken from Sutton (2014) from Kelly et al. (2014).

During the Pennsylvanian (323-299 ma), large accumulations of clastic sediments sourced from the Ouachita orogenic belt filled the eastern Midland Basin quickly filled the eastern portions of the sub-basin as deltaics and spread westward to the Central Basin Platform. By the Middle Permian, this deltaic system was covered with floodplains and the Midland Basin was almost entirely filled (Sutton, 2014). The Delaware Basin, on the other hand, had a different evolution.

This western, topographically, and structurally low sub-basin became an inlet for the sea water during the Permian. Unlike the Midland Basin, the Delaware Basin had low accumulations of clastic sediments sourced from the surrounding low coastal plains and the eastern Ouachita source. With a semi-continuous connection to the ocean through the Hovey Channel and a low rate of clastic sedimentation, the basin's environment was perfect for reef builders (sponges, algae, and microbial organisms) to flourish. Through the Permian, these conditions allowed

carbonate buildups that then separated the shallow shelf from deep-water deposits (Sutton, 2014).

The Delaware Basin was close to 2,000 ft. deeper relative to the Midland Basin (Sutton, 2014). The differences in depths of the sub-basins and platform(s) (**Figure 15**), compounded with their varied overburden pressures from the filled sediments, leads to the major stratigraphic variations found within these sub-basins. Both basins were filled with terrigenous clastic sediments in the deep-water environments while the shallow reef environments along the platform accumulated coarser grains and carbonates.

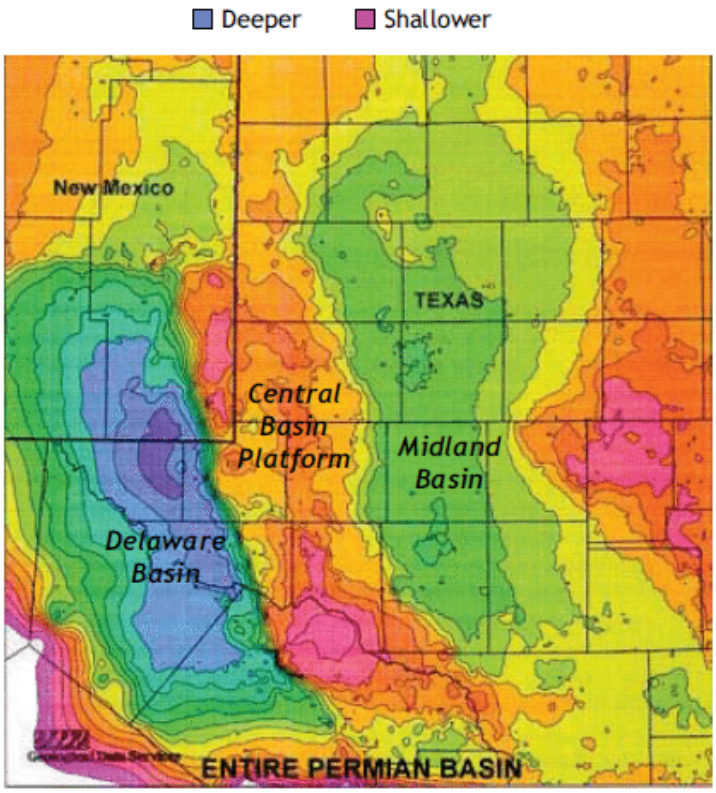

Figure 15: Permian Basin depth variation. Darker colors represent deep areas and lighter colors represent shallow areas. Image taken from Sutton (2014) from searchanddiscovery.com.

One of the most important aspects defining the Delaware Basin is the accumulation of Phanerozoic, organic-rich sediments in the deep, poorly circulated basin and the conversion of these sediments into kerogen (Hills, 1984). Although some hydrocarbons became trapped in the basin, without significant tectonics to create structural traps, large amounts of hydrocarbons migrated into the shallower lateral carbonate reservoirs. During the end of the Permian, thick evaporite beds were deposited that created seals to the traps and allowed the preservation of the migrated conventional hydrocarbons (Hills, 1984).

For reference when discussing the deposition, **Figure 16** provides the relative timing of tectonic events that were major factors controlling deposition. Bone Canyon outcrops represent numerous phases of deposition and erosion, which correlate to the Bone Spring, Cutoff, and Brushy Canyon Formations. Organizing, or dividing, deposition phases into pre-, syn-, and post-Bone Canyon, or Middle Permian, deposition provides an easy and clear understanding of the major depositional phases that occurred in the Delaware Basin through geologic time.

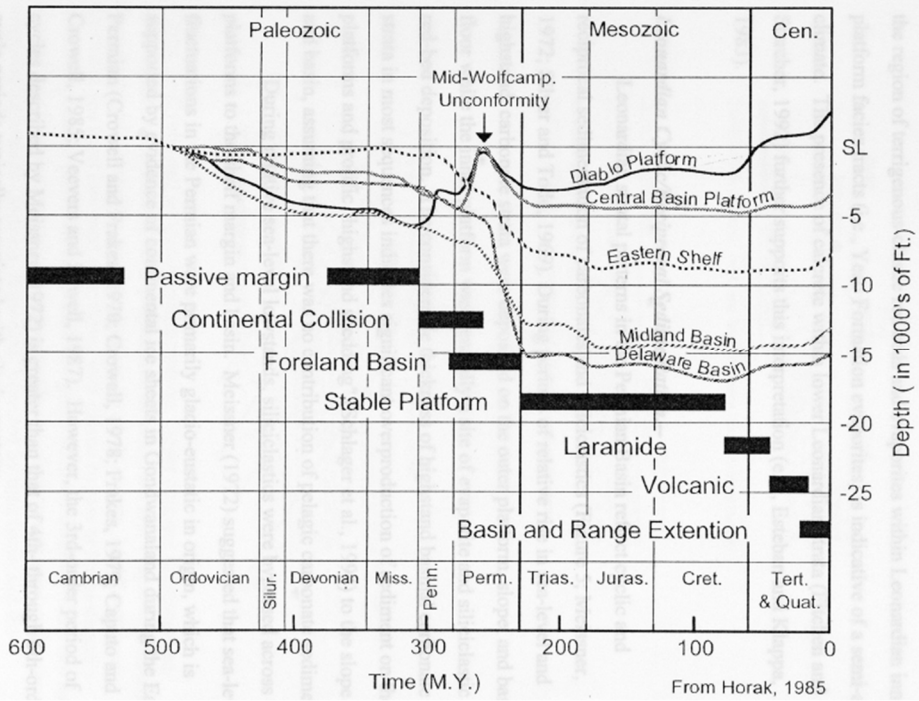

Figure 16: Subsidence Evolution showing the timing of formation of the major structural provinces of the Permian Basin. Taken from Fitchen (1997), modified from Horak (1985).

2.2.1 Pre-Middle Permian Deposition

In the Late Proterozoic, the Central Basin Platform was likely part of a continental wedge of sediments bounded by faults, a spreading oceanic ridge to the south, and was covered by a shallow sea that progressively deepened into an oceanic basin to the south (Hills, 1984). The rifting that caused the formation of the basin is hypothesized to have occurred in the Late Proterozoic because of the fact that the Phanerozoic is associated with moderate, episodic subsidence and mild tectonic activity, possibly a result of a thick granitic crust in the center of the basin (Hills, 1984).

Late Cambrian sediments in the region include the deposition of the Dagger Flat Sandstone, which was a result of the sea advancing over intensely weathered, mature granitic rocks followed by the widespread deposition of the Ellenburger carbonates deposited on broad

shelves covered by a shallow sea until the Early Ordovician. Owing to a slow transgressing sea, the oldest Ellenburger strata are found in the south and progressively get younger to the northwest (Adams, 1995). During the Middle Ordovician the Simpson Formation, composed equally of shales and limestones, was deposited over the southern portion of the present day North American craton (Hills, 1984). The majority of the clastics were derived from the North and the northwest highlands and grade to the South into limestone (Adams, 1995). The Tobosa Basin continued to extend and deepen.

From Late Ordovician to Devonian the axial areas of the Tobosa Basin contained relatively deep-water inhibiting limestone deposition and clastic sedimentation was to slow to keep up with subsidence resulting in numerous areas to be sediment starved during this time (Adams, 1995). Platform and shelf carbonates were deposited and, especially in the Devonian, contained siliceous input. During times of rapid subsidence, the starved basinal areas expanded shoreward and during times of stability carbonate shelves would start to fore step (Adams, 1995). Dolomite and white chert are typical of shelf carbonates and dense limestone and dark chert are typical of starved depressions (Adams, 1995). The rate of subsidence, at this time, controlled variations in limestone, dolomite, chert, and shale (Adams, 1995).

In the Late Devonian and, in many areas, through the Early Mississippian, the Woodford Shale was deposited in the Delaware Basin. Much of the region was covered by restricted shallow seas and sediment starved. These characteristics allowed the deposition of organic rich, black shales (Hills, 1984). The Woodford Shale extends through the majority of the Permian Basin and extends eastward beyond Oklahoma, providing an idea of how much area this sea covered. The Woodford Shale is the major source rock for oil in the Mississippian rocks in this region (Adams, 1995). Deposition began to change and by the Middle Mississippian, carbonates

were primarily deposited. The Late Mississippian is dominated by thick, organic rich black shales. During this time, the Central Basin Platform began to be uplifted causing fine clastic sediments to be deposited off the platform and into the basin (Hills, 1984).

As the Delaware Basin continued to grow through the Early Pennsylvanian it was filled with deltaic sediments from the northwestern uplift. Broad carbonate shelves and banks began to grow on perimeters through the Middle and Late Pennsylvanian (Hills, 1984). The carbonate banks trapped clastic sediments coming in from the northeast and thus starved the basin to the south (Hills, 1984). The sediments within the basin began to compact and the poorly circulated bottom waters allowed the preservation of organisms coming in from the platforms and shelves ("photic zone and shelf margins").

During the Early Permian, the Marathon orogeny caused further thrusting northward and mud and fine sediments flooded into the southern and central Delaware Basin. Intervals of dormancy allowed deposition of thin limestones and, by the Late Wolfcampian, clastic sediment deposition decreased permitting thick carbonate beds (several thousands of feet) to replace the thin limestones (Hills, 1984). Although marginal shelves and platforms were developing, they were not sufficient enough to restrict circulation within the basin and "normal marine salinity prevailed". Compaction and uplift on the eastern margin of the basin resulted in the basin being at least 1,000 ft. deeper than the shelves allowing organic carbon rich sediments to accumulate (Hills, 1984). As the carbonate shelves continued to develop, circulation of the bottom waters in the basin was progressively constricting. Water circulation through channels in the shelf, Hovey channel and Val Verde Basin, however, allowed the surface water to aerate and remain organically productive (Hills, 1984). "At the end of Wolfcamp deposition, the basin probably

was about 1,500 ft (450 m) deep, and large amounts of organic material were preserved" (Hills, 1984, 254).

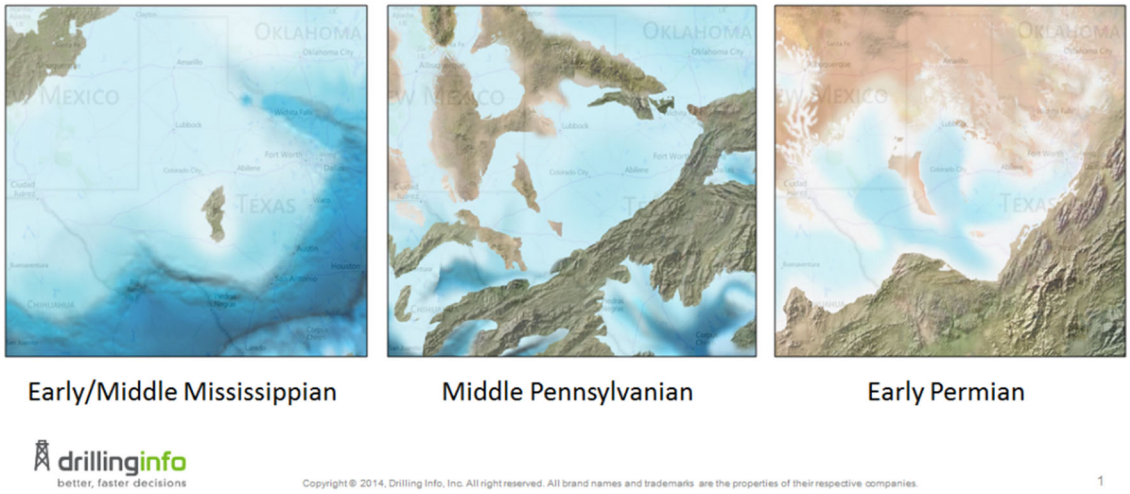

Figure 17: Paleogeographic evolution of the Permian Basin. Broad carbonate banks growing on the perimeter of Delaware Basin. Image taken from Enverus (2017).

2.2.2 Middle Permian Deposition

During the Leonardian, fine clastic sediment and thin sandstone beds continued to deposit in the basin center, but now were being interrupted by numerous carbonate wedges (from the basin margin/edges) and thin limestone beds (in the center of the basin). With compaction of the fine sediments, fluids inside the pores migrated into adjacent sandstones and limestones. At the end of the Leonardian the Wolfcampian beds were buried more than 3,000 feet and organic material began to convert to kerogen (Hills, 1984). Development of carbonate shelves increased along with the preservation of organic matter in the Bone Spring, Cutoff, and the previous Wolfcamp. The bottom waters of the Delaware Basin were generally anoxic owing to the basin

being restricted; however, three channels provide top water circulation into the basin (Crosby, 2015).

Through most previous studies, the Cutoff Formation has been included within the Bone Spring Formation, as the Cutoff Formation is thought to be both Leonardian and Guadalupian in age. It is only recently that the Cutoff Formation was actually named. Previous formation boundaries have defined the formations by major unconformities which correspond generally to second or third order global sea level cycles from highstand to highstand (i.e. Wolfcampian, Leonardian, Guadalupian). This division is significant, because the Cutoff Formation, in contrast, represents one sea level cycle from lowstand to lowstand. Recent advancements in technology have allowed more detailed analyses of these formations and their boundaries. Although this section of the thesis incorporates the deposition of the Cutoff Formation within the deposition of the Bone Spring Formation, it is important to mention that these different formations and their constituents, lithologies, processes, environments, and sequences will be divided and discussed in detail later on.

The Bone Spring Formation, along with the Cutoff Formation, is Early to Middle Permian in age, was deposited during the Leonardian for around 10 million years (282.5-272.3 Ma), is around 3,500 ft. thick on average, and is an alternating sequence of slope-to-basin siliciclastic and carbonate rocks that were the result of subaqueous deposition on a slope and basin (Hart, 1997; Montgomery, 1997; Henderson et al., 2012; Crosby, 2015). These carbonate and siliciclastic beds alternated, owing to reciprocal sedimentation, the result of relative sea level changes where carbonates are deposited during highstands and transgressions, while clastics are deposited during lowstands and regressions (Hart, 1997).

The sea level fluctuations are generally thought to have resulted in the deposition of six stratigraphic units, grouped in pairs, known as the 1st, 2nd, and 3rd Bone Spring. The units of focus in this study are ascending chronological order (Figure 5) are the 1st Bone Spring Carbonate (Sand, C, B, and A), the Avalon Complex (Bone Spring and Cutoff), the Upper Cutoff Formation, and the lower Brushy Canyon Formation. According to Montgomery (1998), previous studies suggested deposition was most likely not controlled by tectonics during the Leonardian, however, Montegomery (1998) proposed that the rate of subsidence was likely just as high as during the Wolfcampian and, thus, implying more structural control. Furthermore, most of the carbonates in the northern margins of the basin are the direct result of gravity debris flows caused, in part, by wave activity during highstands (Montgomery, 1998). In 1998, Hart explained and added how the low structures that formed during the tectonically active Pennsylvanian acted as sediment traps for turbidite and debris flow deposits during the Bone Spring (and Cutoff), therefore, controlling, or at the very least influencing, slope to basin depositional geometry (Hart, 1998; Crosby, 2015). The clastic deposits, although not really seen in Bone Canyon, are primarily the result of submarine fan and submarine channel mechanisms, however, aeolian strata are also present in the Bone Spring (Montgomery, 1998; Crosby, 2015).

During the Leonardian, the northern Delaware Basin consisted of numerous transgressive-regressive sequences and allowed the continued development of prograding shelf carbonates in a 'keep-up'style basin. Owing to the inherited topography from Wolfcampian shelf to slope deposits during this time, the first major Permian progradation in the Delaware Basin occurred (Silver and Todd, 1969; Crosby, 2015). As the carbonates continued to develop, they began to create barrier-like structures on the shelves. The barrier-like structures likely influenced oxygen levels within the ocean's top waters and also hindered sediment from reaching the basin.

Adams (1965) discussed how the northern margins of the Delaware Basin were less influenced by the built-up barriers allowing clatics to be deposited in channels within the barriers (Adams, 1965; Crosby, 2015). During lowstands, the channels provided pathways for basinal turbidites to be directed and deposited deeper in the basin. Bone Canyon is composed primarily of carbonate turbidite deposits; however, it also includes a few phases of gravity debris flow deposits. The Lower Cutoff Formation in the canyon represents one of these gravity debris flow deposits and is represented by more siliciclastic, or mud/shale-rich, deposits that include large carbonate litho-clasts inside a mud-matrix, referred to as megabreccia, and which also display slumping structures. The Middle Cutoff, however, represents a shale-rich deposit that drapes over the underlying sediment that corresponds to the transgressing sea level. Some Upper Cutoff deposits are seen on the southern wall of the canyon, but are channel bound and, therefore, are not laterally continuous throughout the canyon.

2.2.3 Post Middle Permian Deposition

2.2.3.1 (Guadalupian-Ochoan)

During the Guadalupian, the Delaware Basin was still slowly tilting to the East with sediments still compacting resulting in subsidence equaling the sedimentation rate. Fine and medium-grained clastic sediments continued to fill the basin and organisms thrived in the aerated surface waters (Hills, 1984). The Guadalupian marked a change in the basin floor deposition. Siliciclastics were primarily being deposited (Bell-, Cherry-, and Brushy Canyon) as opposed to the carbonate deposits of the Wolfcampian and the sequential carbonate and siliciclastic deposits in the Leonardian (Silver and Todd, 1969; Crosby, 2015). Adams (1965) explains the noticeable change in ocean chemistry or redox conditions during the Guadalupain, seen by a change from

dark grey or black basinal carbonates to light grey or tan slope carbonates (Adams, 1965; Crosby, 2015). This change can be seen in the Upper Cutoff Formation turbidite deposits below the contact with the Brushy Canyon Sandstone. Near the end of the Guadalupian, carbonate banks and reefs along the basin margin continued to grow and flourish. The reefs acted as barriers to sediments flowing into the central basin and decreased water circulation, causing evaporites to be deposited. The sediments that were able to accumulate in the basin were organic rich owing to the restricted circulation. At the end of the Guadalupian, the Leonardian (Bone Spring and Cutoff Formations) sediments underneath were buried several thousands of feet and were brought into the catagenic zone allowing the kerogen to mature and turn to oil and wet gas (Hills, 1984). The Wolfcampian sediments, underneath the Leonardian sediments, were now buried to depths up to 10,000 ft. and the hydrocarbons began to crack into light, gaseous molecules (Hills, 1984).

By the Ochoan, the carbonate reefs and banks were highly developed in the Delaware Basin and the continued restriction of water circulation gave way to the deposition of the thick (2,000 ft.) Castile subaqueous evaporites, which then acted as an impermeable layer. As these evaporites were deposited, the overburden pressure caused the underlying clastics to compact and fluids began to squeeze out and migrate. The migrating fluids contained minimal amounts of immature organic material. The fluids could not migrate vertically because of the impermeable evaporites and, although some fluids were trapped by different permeable layers within the basin, the majority of the fluids migrated laterally into the surrounding carbonate platforms and shelves or wherever there were traps (Hills, 1984). “Conduction of heat through the evaporite resulted in a longer interval of petroleum generation and a smaller proportion of gas in Upper Permian beds than might be expected from the burial depth” (Hills, 1984). The lack of sulfate in

the evaporites found in the basin suggests that these evaporites had less sulfur in the basinal oils than the platform oils. Though insufficient organics accumulated within the evaporites to produce petroleum commercially, but the calcite laminae found in the evaporites has a brown color indicating well advanced maturation in the seasonal varves (Hills, 1984).

Capping the Ochoans the Salado evaporites were deposited in a shallow, well circulated sea that resulted in little to no organic preservation, though still contributing to sealing the hydrocarbons and fluids below. Near the end of the Permian, the Salado Formation was being eroded and eventually the Rustler Formation that was composed of evaporites, dolomite, and few organics was deposited. The final formation, which was a part of the Dewey Lake red beds, added hundreds of feet of sediment to cap the Permian.

2.2.4 Post Permian (Mesozoic and Cenozoic)

Most of the petroleum generation that occurred during the Permian formed near the present source rock locations. For a long time after the Permian period the ocean retreated and the Dewey Lake and Rustler Formations were subaerially eroded while the Salado and Castile Formations were subjected to subsurface and subaerial solution, both resulting in the removal of hundreds of feet of Upper Permian strata (Hills, 1984). Continental red beds began to be deposited in the Permian Basin, and northeastern Delaware Basin within, by the end of the Middle Triassic. Jurassic and Cretaceous strata are not found within the Delaware Basin likely caused by extensive subaerial erosion of the strata and subsurface solution of the Upper Permian formations (Hills, 1984). The Jurassic and Cretaceous strata were likely deposited across the Delaware Basin in a shallow sea and represent a complete paleogeographic change from the

Triassic as there is no evidence of the Central Basin Platform or the Delaware Basin (Hills, 1984, Adams, 1940).

Although there is evidence of Late Cretaceous sediments on the western and northern Delaware Basin, Late Cretaceous deposition was minimized. As solution of the Upper Permian evaporite beds continued, along with slight tectonic activity, subsidence continued with it leading to the formation of enclosed basins that are currently filled with 1,600 ft. of Holocene sandstones (Hills, 1984). The subsidence also caused a solution basin from Pecos, Texas to Carlsbad, New Mexico and eventually became integrated into the Pecos River drainage. The Upper Permian evaporites are continually being dissolved by the Pecos River underflow causing the Pecos River to migrate downdip eastward (Hills, 1984; WTGS, 1964).

Cenozoic faulting has not had a great impact on the Delaware Basin, but in the Salt Flat, parallel faults have pushed the graben down against the western margin of the Delaware Basin and resulted in the Capitan reef being covered by the bolson fill. Cenozoic events have caused hundreds of feet of Upper Permian beds to be removed by solution, but an apron of Pliocene-Pleistocene gravels have offset the overburden loss from the solution of evaporites. Eventually, solution collapse of the evaporites created accommodation space for Holocene sands (Hills, 1984). “Because Paleozoic sedimentation in the Delaware Basin was fairly continuous, with few major interruptions, the rock record is fairly complete and uniform throughout the basin. Carbonate rocks predominate in the lower Paleozoic, with shales in the middle, and thick Permian evaporites at the top of the section” (Hills, 1984).

There have been three main source rocks identified within the Delaware Basin including the 1) Middle Ordovician shales and limestones, 2) Upper Devonian and Mississippian shales and shaly limestones, and 3) the basinal facies of the Pennsylvanian and Permian rocks (Hills,

1984). The main focus is on the source rocks of the Permian. During the Middle to Late Permian filling of the Delaware Basin with fine, organic rich sediments coupled with water circulation progressively restricting favored the preservation of organic material. Although the deposition of evaporites by increased salinity in the water causing decreased organic production, the maturation and reduction of organics within the older Permian beds continued (Hills, 1984). The hydrocarbons that were produced began to migrate into interbedded sandstone reservoirs within the basin and into carbonate reservoirs on the basin margins where they were trapped and eventually turned into medium-heavy high-sulfur crude oil "of the dolomite reservoirs" (Hills, 1984). The hydrocarbons that are found within the sandstone reservoirs are only found in moderate quantities compared to the large quantities of hydrocarbons found updip on the shelves where most of them had migrated to. During much of the Paleozoic, the slightly restricted circulation allowed the deposition of organic-rich shales that later formed source rocks (Hills, 1984). The Delaware Basin, as a whole, "is a good example of a long-lived, tectonically stable, confined basin with sedimentary environments very favorable for growth and preservation of organic matter and the generation and maturation of hydrocarbons" (Hills, 1984).

Chapter 3: Sequence Stratigraphy

Larry Sloss (1988) discusses the importance of sequence stratigraphy and emphasizes that the language and semantic structure of sequences and their surfaces are not what is important, but rather, "What does it all mean?" (Sloss, 1988). Figuring out what these surfaces are and what they mean provides a more complete depositional framework that shows the environmental controls on the surfaces and further delineates complicated periods through geologic time. The knowledge of such stratigraphic surfaces in the industry decreases well placement uncertainty (Crosby, 2015). This study aims to delineate important sequences through stratigraphic surfaces to gain a better understanding of the complex depositional history of Bone Canyon. As will be seen later, Bone Canyon is composed of more than just the Bone Spring Formation and by analyzing the outcropped strata, and the facies within them, the study will provide evidence showing that the Bone Spring in the subsurface actually contains more divisions than what is generally thought. The sequence stratigraphic surfaces outcropped in the canyon provide a more detailed, high-resolution look into the Bone Springs Formation, as well as the Cutoff and Brushy Canyon Formations.

Slatt (2006) defines Sequence Stratigraphy as the "study of sedimentary rock relationships within a chronostratigraphic or geologic-time framework that is based on the recognition of time surfaces throughout the rock record" (Crosby, 2015). Surfaces allocate rock units into certain cycles based on fluctuations in relative sea level, tectonic subsidence, and sediment supply (Slatt, 2006; Crosby, 2015). For example, unconformities bound supercycles into sequences. **Table 1 and 2** show the general orders of these sequence stratigraphic cycles and important features related to them (Slatt, 2006; Crosby, 2015). Sequence Stratigraphy is the

integral approach for interpreting sedimentary processes and geometries because of the easily recognizable surfaces (Catuneanu et al., 2011; Crosby, 2015).

Stratigraphic Cycle Orders			
Type	Terms	Duration (in Ma)	Cause
First Order	Supercycle	100 – 400	Major eustatic cycles caused by formation and break up of supercontinents
Second Order	Sequence	10 – 100	Eustatic cycles induced by volume change in spreading ridge system
Third Order	Mega Cycle	1 – 10	Ridge changes and variations in continental ice
Fourth Order	Major Cycle	0.4 – 1	Glacioeustatic cycles, astronomical forcing
Fifth/Sixth Order	Minor Cycles	≤ 0.4	Glacioeustatic cycles, Milankovitch cycles

Table 1: General sequence stratigraphic hierarchal orders with their terms, duration, and cause. Taken from Crosby (2015) and modified from Slatt (2006).

Stratal Unit	Definition	Bounding Surfaces	Temporal Order
Parasequence (Cycle)	A relatively conformable succession of genetically related beds or bedsets bounded by marine-flooding surfaces and their correlative surfaces; may be subtidal or peritidal, symmetric or asymmetric	Subaerial exposre features developed on peritidal facies; marine firmground or hardground (burrowed/bored); submarine erosion at wavebase; landward shift in facies across surface	4th-Order (0.1-1.0 m.y. period) & 5th-Order (0.01-0.1 m.y. period)
Parasequence Set (Cycle Set)	A succession of genetically related parasequences forming a distictive stacking pattern (landward-, vertically- or seward-stepping) and commonly bounded by major marine-flooding surfaces and their correlative surfaces may be coincident with systems tracts (landward-stepping or retrogradational parasequence set = TST, seaward steeping or progradational parasequence set = HST	Subaerial exposure features developed on peritidal facels; marine firmground or hardground; submarine erosion at wavebase; intraclsts/lithoclasts above boundary; landward shift in facies across boundary. Parasequence set boudaries typically display greater facies offset and/or bounding surface alteration than parasequence boundaries within parasequence set. Separate distinctive parasequence-stacking patterns, may coincide with sequence boudnaries or downlap surfaces	4th-Order (0.1-1.0 m.y. period) & 5th-Order (0.01-0.1 m.y. period); may be 3rd-Order (1-10 m.y. period)
Sequence, High-Frequency Sequence (HFS)	A relatively conformable succession of genetically relaed strata (parasequences and parasequence sets) bounded by unconformities and their correlative conformities	Subaerial exposure features developed on subtidal facies, possible submarine erosion of slope due to lowering of wave base and mass-wasting	3rd-Order (1-10 m.y.) & 4th-Order (0.1-1.0 m.y.); 5th-Order (0.01-0.1 m.y. in areas of high subsidence and sediment supply. 4th-Order more common during periods of glacial maxima and high-amplitude glacio-eustasy
Sequence Set, High-Frequency Sequence Set	A succession of genetically related sequences arranged in a distinctive progradational (HST and LST sequence sets), aggradational (HST or TST sequence sets), or retrogradational (TST) stacking pattern	Highstand sequence set bounded below by 3rd-Order maximum-flooding surface (regional downlap surface and condensed interval in many cases) and bounded above by composite sequence boundary (subaerial exposure features); transgressive sequence set bounded below by composite sequence boundary and above by maximum flooding surface; lowstand sequence set is bounded below by composite sequence boundary and above by 3rd-Order transgressive surface, which is restricted to basin	3rd-Order (1-10 m.y.) & 4th-Order (0.1-1.0 m.y.)
Composite Sequence	A succession of genetically related sequences in which the individual sequences stack into lowstand, transgressive and highstand sequence sets, although not all sequence sets may be well-developed	Widespread and well-developed subaerial exposure features developed on subtidal facies; basinwide subaerial unconformities with stratal truncation, karst and/or caliche development, associated regional aquifer and meteoric phreatic diagenesis (dissolution, cementation)	2nd-Order (10-100 m.y. period) & 3rd-Order (1-10 m.y.)
Supersequence	A group of sequences or composite sequences that successively reach higher positions of encroachment onto the underlying unconformity surface, followed by one or more sequences with lower positions of encroachment (Mitchum, 1977)	Major interregional unconformities	2nd-Order (10-100 m.y.)

Table 2: Hierarchal orders of sequence stratigraphy. The stratal units with their definition, bounding surfaces, and temporal order are shown. Modified from Slatt (2006).

Important sequence stratigraphic names, along with their meanings, are listed below and were taken from Crosby (2015) owing to the work's direct relation to the Bone Springs Formation in this study. These terms were modified from Catuneanu et al. (2011), McCullough (2014), Zhou (2014), and Pigott and Bradley (2014).

Parasequence – A relatively conformable succession of genetically related beds or bedsets bounded by sub-regional correlative surfaces.

Sequence – A succession of genetically related strata during a full cycle of change in accommodation or sediment supply.

Sequence Boundary (SB) – a regional surface that denotes the transition from one sequence to another, such as the surface marking the transition from lowstand siliciclastic deposition of the 1st Bone Spring Sand and the highstand carbonate deposition of the 1st Bone Spring Carbonate.

Transgressive surface of erosion (TSE) – First surface indicating the onset of a rise in sea level or transgressive systems tract and can be an indicator of the reactivation of carbonate deposition and signifies the end of basinal siliciclastic deposition.

Lowstand systems tract (LST) – Lower systems tract in a sequence denoting the lowest relative sea level and thus the deposition of basinal turbidites such as the 1st, 2nd, and 3rd Bone Spring Sands in the northern Delaware Basin.

Highstand systems tract (HST) – Upper systems tract signifying a decrease in the rise of and maintenance of the highest term in relative sea level. Marked by the deposition of extensive carbonates such as the 1st, 2nd, and 3rd Bone Spring Carbonates.

Transgressive systems tract (TST) – Marks the onset of sea level rise following the LST or HST and is marked by deposits filling erosional surfaces formed in previous systems tracts as seen in high order sequences in the 2nd Bone Spring Carbonate.

Regressive systems tract (RST) – Marks the onset of sea level fall following the HST or LST resulting in slope destabilization, toe-of-slope deposition, or erosion of the underlying strata. RSTs are associated with intrabasinal input and accompanying intrabasinal uplift. Sequence Boundary formation is possible due to erosional surfaces, however, can be less defined in deep-water settings where autocyclic erosional processes occur.

Figure 18, taken from Crosby (2015) and modified from Slatt (2006) and Slatt (2013) shows one full sea level cycle (highstand to highstand) through time and the associated system tracts and surfaces. Catuneanu (2009) discusses how fluctuations in eustatic and relative sea level, tectonic subsidence, sediment supply, climate, basin physiography, energy, and biota are the primary controls of sequence stratigraphy (Crosby, 2015). The type of sediment in the basin is likely controlled more by fluctuations in eustatic and relative sea level, while the sediment supply, is likely controlled more so by tectonic subsidence, climate, and environmental energy (Crosby, 2015). Crosby (2015) discusses how in highly cyclic, mixed-origin sedimentary environments, basin physiography, biota, and sediment supply are largely responsible for the

geometry and path of sediments within the basin. The Bone Spring and Cutoff Formations are prime examples of a highly cyclic, mixed origin sedimentary environment and because of this basin physiography, biota, and sediment supply are critical controls in this formation.

> "With that being said these commonly overlooked controls on sequence stratigraphy seem to play a crucial role in the prediction of sedimentary bodies in the subsurface, which in the author's opinion is the most critical product of sequence stratigraphy as it applies to practical, economic use in oil and gas exploration (or the exploration for any geological resource for that matter)" (Crosby, 2015).

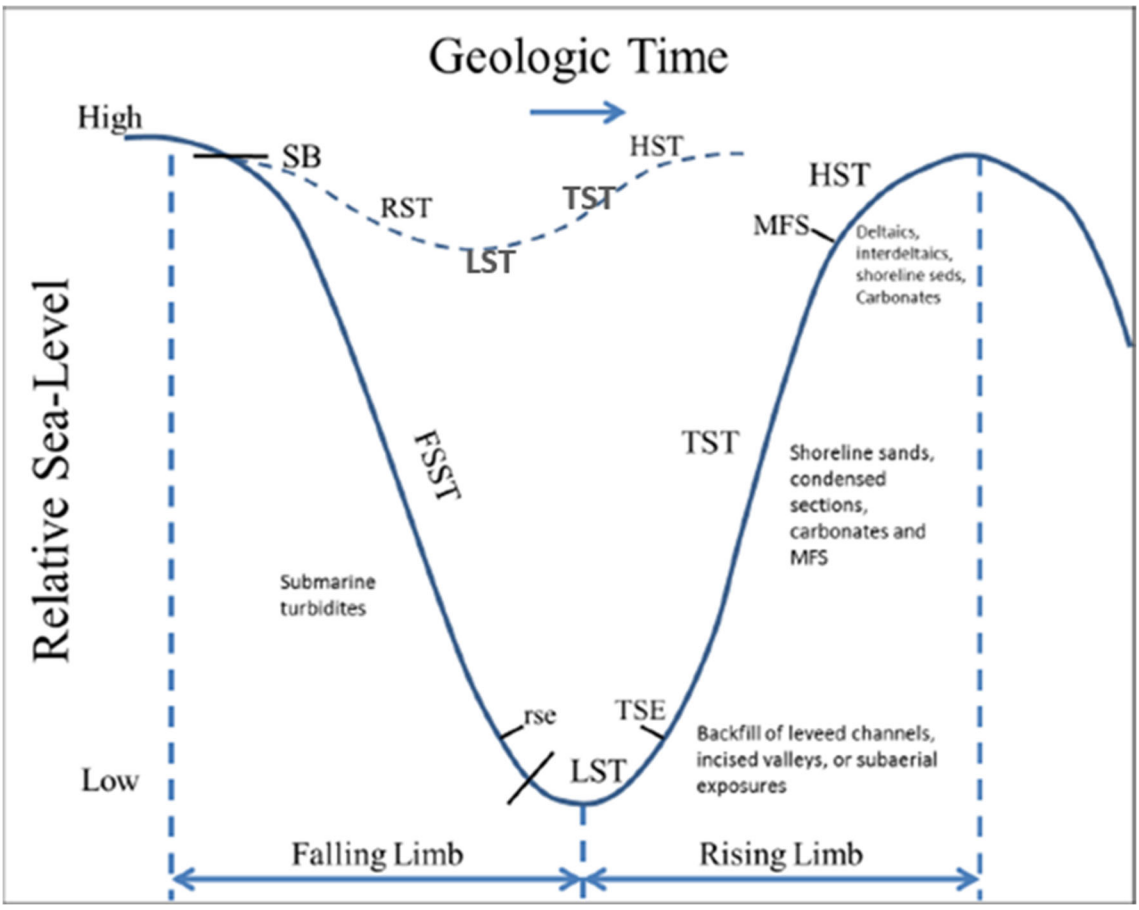

Figure 18: One complete sea level cycle showing associated systems tracts and surfaces. Vail Sequence Boundary (SB), Regressive Systems Tract (RST), Falling Stage Systems Tract (RST), Regressive Surface of Erosion (rse), Lowstand Systems Tract (LST), Transgressive Surface of Erosion (TSE), Transgressive Systems Tract (TST), Maximum Flooding Surface

(MFS), and Highstand Systems Tract (HST). Taken from Crosby (2015) and modified from Slatt (2006, 2013) and Pigott and Bradley, 2014.

3.1 Reciprocal Sedimentation

As previously mentioned, the Bone Spring Formation and Cutoff Formations are comprised of alternating units of carbonate and siliciclastic sediment- generally thought to correspond to 3rd order cycles of relative sea level. Carbonate deposition corresponds to highstands, whereas clastic/siliciclastic deposition corresponds to lowstands in sea level. This pattern of sedimentation, described from here on as *reciprocal sedimentation*, refers to alternating clastic and carbonated dominated depositional environments and their associated facies as controlled by changes in relative sea level.

Mullins and Cook (1986) further developed the study and classification of carbonate aprons versus submarine fans. The carbonate apron facies and their depositional environments are discussed in detail, but only the important findings that relate to this thesis will be discussed. The Bone Spring carbonate units were deposited in these apron environments as turbidite and debris flow deposits during the highstand times of the reciprocal sedimentation model during the Leonardian. Crosby (2015) explains how these carbonates exhibit the characteristics of the inner apron model described by Mullins and Cook (1986), which are made up of mud-supported debris flows and allochthonous packstones. Carbonate deposition during highstands was interrupted by clastic deposition during lowstands. The clastics were deposited as fine-grained sandstone and siltstone clastic turbidite channels and submarine fans (Crosby, 2015).

Reciprocal sedimentation can also cause alternating carbonate and siliciclastic depositional environments through time (Catuneanu et al., 2009; Crosby, 2015). The reciprocal sedimentation model is seen in the Leonardian series of deposition in wireline logs throughout

the Delaware Basin. Therefore, the reciprocal sedimentation model (**Figure 19**) is mentioned in this thesis as a help in understanding how the overall Bone Spring Formation is assembled. High resolution sequence stratigraphy and the development of depositional environments through geochemistry in Bone Canyon may aid in further refining this reciprocal sedimentation model.

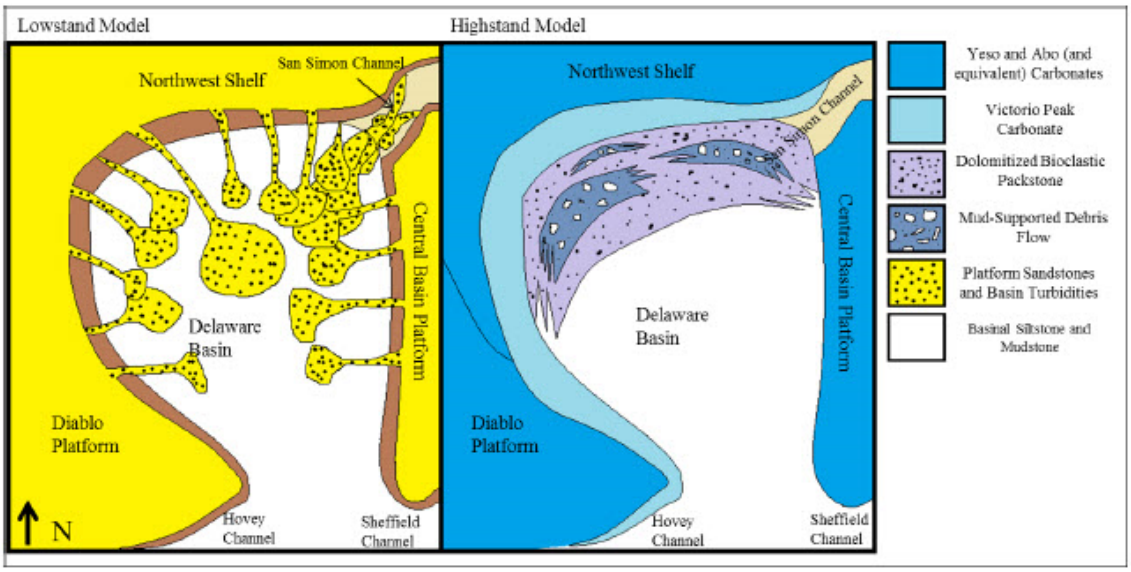

Figure 19: Reciprocal Sedimentation Model showing the facies and environments associated with sea level fluctuations. Clastic turbidite and aeolian sedimentation corresponds to lowstands and alternate with carbonate apron and debris flow sedimentation corresponding to highstands. This model resembles deposition of the Bone Spring Formation. Taken from Crosby (2015).

3.2 Permian Sequence Stratigraphy

The Permian strata fall within the 1st order Absaroka Sequence (Late Mississippian-Early Jurassic) of the North American Craton (Sloss, 1963; Crosby, 2015). Sloss (1988) further divided the Absaroka Sequence where the Leonardian strata are found within the greater sequence known as the Lower Absaroka II (Crosby, 2015). Ross and Ross (1995) discuss the differences between the division of the Absaroka in relation to frequency and amplitude of sea level

fluctuations. Absaroka I (Pennsylvanian-Early Permian) exhibits higher frequency and amplitude fluctuations of sea level than the overlying Absaroka II, but Absaroka II exhibits higher frequency and amplitude fluctuations of sea level than the overlying Absaroka III (Triassic-Early Jurassic) (Ross and Ross, 1995; Crosby, 2015). The supersequences are illustrated in **Figure 20**from Sarg (1999).

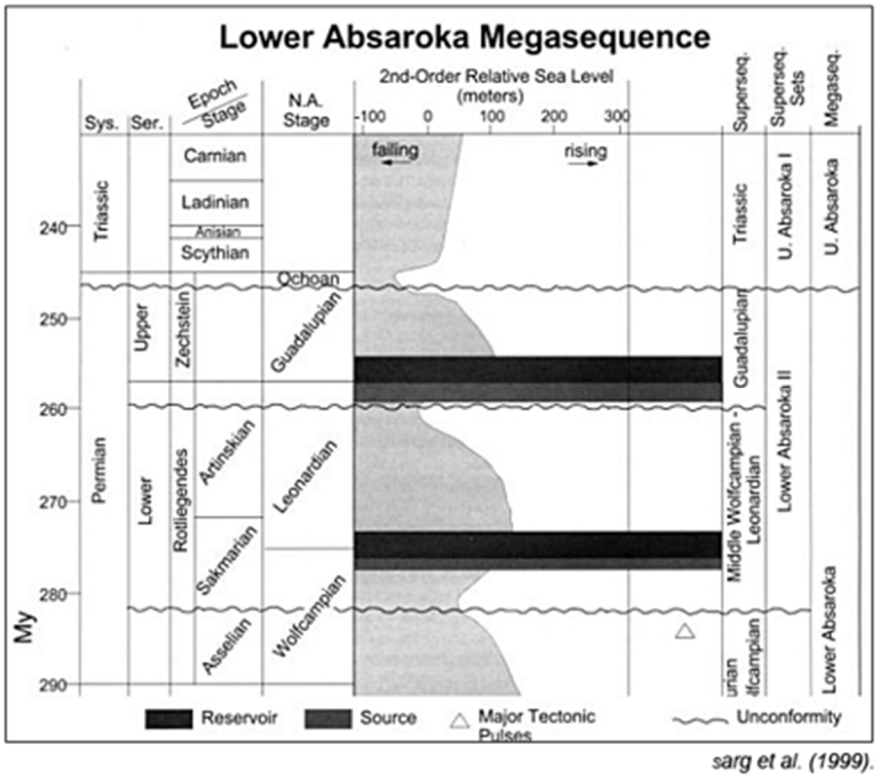

Figure 20: Lower Absaroka Megasequence showing Leonardian Strata within the bottom portion of the Lower Absaroka II. Taken from Sarg et al. (1999).

Ross and Ross (1995) show a 2nd order eustatic regression during the Permian portion of the Lower Absaroka II (Crosby, 2015). The Wolfcampian, Leonardian, Guadalupian, and Ochoan (Permian) represent cyclic fluctuations in sea level that are superimposed on this 1st or 2nd order regression. The Leonardian represents a slight transgression (Crosby, 2015).

Stratigraphy, in relation to lithology and biology, differ between these four series and, therefore, divide them. Differential fossil dating and fusulinid zonation are perhaps the best means of dividing the series (Adams et al., 1939; Ross and Ross, 1994; Montgomery, 1998; Crosby, 2015). Ross and Ross (1994) insist that these methods of biostratigraphy do not apply to the Ochoan, rather a significant change in lithostratigraphy (evaporites) divides the Ochoan from the previous Guadalupian (Crosby, 2015). Kerans (2016) used conodont biostratigraphy in order to correlate the outcrops in the Guadalupe Mountains to the subsurface. This resulted in the Lower Avalon Shale correlating to the L5 HFS of the Bone Spring Formation, the Middle Avalon (carbonate) correlating to the L6 HFS (lower half of Bone Canyon) of the Bone Spring Formation, and the Upper Avalon Shale correlating the L7-L8 HFS of the Lower Cutoff Formation.

The four series within the Permian contain 3rd order, and higher, sequences that are directly related to the depositional history, stratigraphy, and oil and gas exploration of the Delaware Basin (Crosby, 2015). Although sea level fluctuations (glacioeustacy) are the primary controls on Permian strata, tectonic subsidence, sediment supply, provenance and route, and biota are also considered to be critical controls in these series (Silver and Todd, 1969; Mack and Dinterman, 2002; Crosby, 2015).

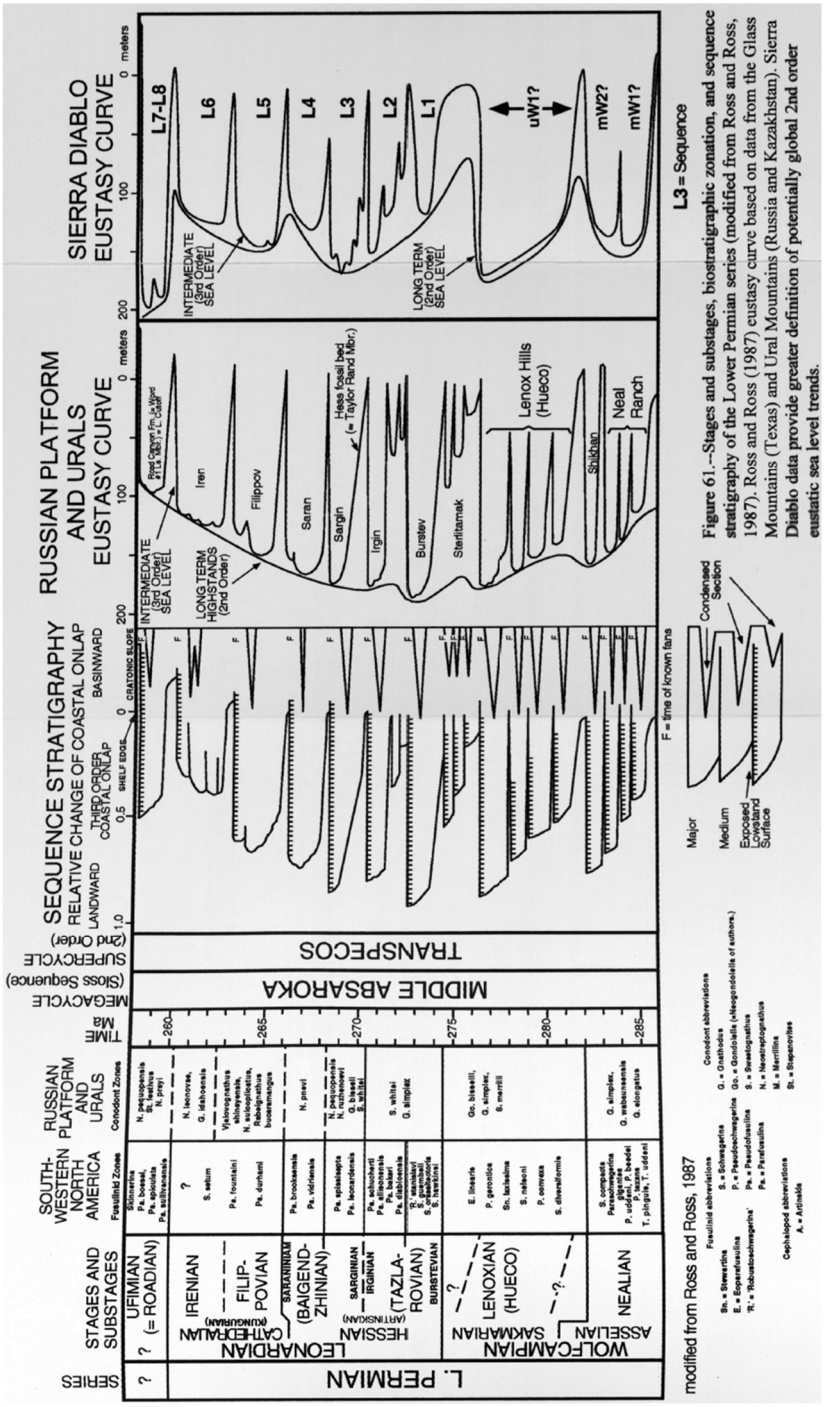

Figure 21: Permian Sequence Stratigraphy showing stages, cycles, coastal onlap, and eustasy curve. Taken from Fitchen (1997) modified from Ross and Ross (1987).

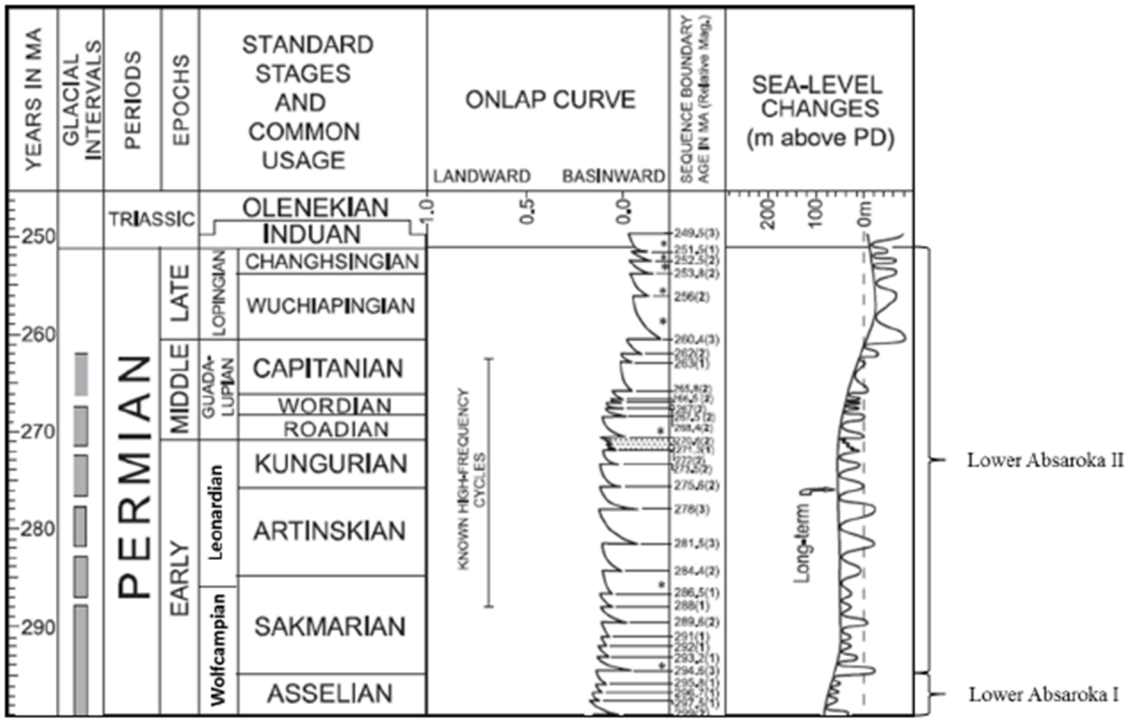

Figure 22: Geological time scale showing glacial periods, onlap curve, and high order fluctuations in sea level superimposed on the 2nd order cycle. The position of Leonardian strata in relation to these factors is also shown. Taken from Crosby (2015) and modified from Haq and Schutter (2008).

3.2.1 Wolfcampian

As discussed previously, many investigators believe that during the Wolfcampian and Early Leonardian the Delaware Basin was still tectonically active and because of this these two series provide insight into stratigraphic responses to tectonism and eustatic episodes. Small scale glaciation and relative sea level change are also factors (Crosby, 2015).

Four to five 3rd order sequences are designated within the Wolfcampian (Ross and Ross, 1994; Crosby, 2015). Crosby (2015) shows these 3rd order cycles on gamma ray motifs of the entire Permian (**Figure 23**). Veevers and Powell (1987) propose that the high frequency, relative sea level fluctuations during the Early Permian are the result of Glacioeustacy. They also go

further to say the Permian strata consist of 4th-6th order transgressions and regressions as the result of continental ice volumes on Gondwana (Crosby, 2015). Goldhammer et al. (1987) also suggests that these high order cycles are the product of glacioeustacy and Milankovitch cycles (Crosby, 2015).

3.2.2 Leonardian

Henderson et al. (2012) dates the Leonardian stage as between 282.5-272.3 Ma. Most sequence stratigraphy research on the Leonardian has been done on the shelf and shelf margin Clear Fork, Abo, Yeso Formations, rather than on the slope and into the basin Bone Spring and Cutoff Formations (Montgomery, 1998; Ruppel and Ward, 2013; Crosby, 2015). Owing to the fact that these shelf equivalent formations of the Bone Spring have been subjected to extensive analysis, one of the goals of this study is to provide more information about higher orders (3rd-5th) of sequence stratigraphy in the Bone Spring and Cutoff Formations in the basin.

The Leonardian Bone Spring Formation is bounded by the Wolfcampian Unconformity at the base and, in Bone Canyon, by the unconformable contact between the Upper Bone Spring Carbonate and the Cutoff Formation (Late Leonardian-Early Guadalupian). The Cutoff Formation lies above the Bone Springs Formation in Bone Canyon because of the erosion of the relic shelf that deposited material in paleotopographic cuts/canyons on the relic upper slope (Hurd and Kerans, 2014). The amount of 3rd order sequences found within the Leonardian is still subject to debate, however, Ross and Ross (1994) found four, Ye and Kerans (1996) and Sarg (1988) found seven, and Montgomery (1998) designated up to eight (Crosby, 2015). The results of this thesis, discussed later, are in agreement with eight 3rd order sequences within the Leonardian.

Ross and Ross (1994) discuss how, regardless of sequence number or order, each sequence is internally complex. As mentioned earlier, the Leonardian high frequency, cyclic sequences and all their complexities are the result of Milankovitch cycles and fluctuating ice volumes on Gondwana until the Early Leonardian (Veevers and Powell, 1987; Crosby, 2015). Ross and Ross (1995) discuss how the 3rd order sequences last longer in the Leonardian than in the Wolfcampian owing to increased carbonate production. Crosby (2015) confirmed that these higher order sequences (>=3rd) were of longer time duration during the Leonardian.

3.2.3 Guadalupian

The Guadalupian is comprised of five depositional sequences that are each just as complex as the Leonardian 4th and 5th order cycles (Ross and Ross, 1994). In 1998, Tinker was able to find at least nine 4th or 5th order cycles within the Guadalupian strata in the Guadalupe Mountains. Tinker (1998) focuses on the complexities of stratigraphic development seen in 3rd order, or higher, sequences within the Guadalupian.

3.2.4 Ochoan

The Ochoan was a time of extensive evaporate deposition within the Delaware Basin. These evaporates were deposited in four main phases of deposition. The four deposits making up the Ochoan are: Castile, Salado, Rustler, and Dewey Lake in ascending chronological order (Adams, 1944; Crosby, 2015). Owing to such a drastic change in lithology, the controls on the sequence stratigraphy of evaporates are different than the controls on the sequence stratigraphy of clastics or carbonates. “Evaporite sequence stratigraphy, in the authors understanding, is based

upon the combination of the physiochemical controls on the sequence of rocks deposited in a tectonically barred evaporite basin" (Crosby, 2015).

A large regression at the end of the Guadalupian led to a lowstand and a restricted basin. The alternating beds of carbonate and evaporites in the Castile Formation are evidence of small scale (4^{th}, 5^{th}, 6^{th} order) fluctuations in sea level and subaqueous precipitation of evaporites alternating with small scale deposition of carbonates (Crosby, 2015). The progradation of the terrestrial Dewey Lake red beds that were deposited at the end of the Permian ceased the Ochoan regression (Adams, 1944; Crosby, 2015). The Figures below show 3^{rd} order sequences through gamma ray motifs provided by Crosby (2015). The red arrows represent regressions, or coarsening upwards, and green arrows represent transgressions, or fining upwards trends. Crosby (2015) mapped the boundaries of the series within the Permian, as well as the 3^{rd} order sequences found in his study area, and then correlated them to the global sea level curve from Haq and Schutter (2008). It is worth mentioning that most previous subsurface work, as mentioned before, combines the Avalon and the Upper Bone Spring Carbonate into the Bone Spring Formation, however, in Bone Canyon, the Upper Avalon and the carbonate above will be considered to represent the Cutoff Formation.

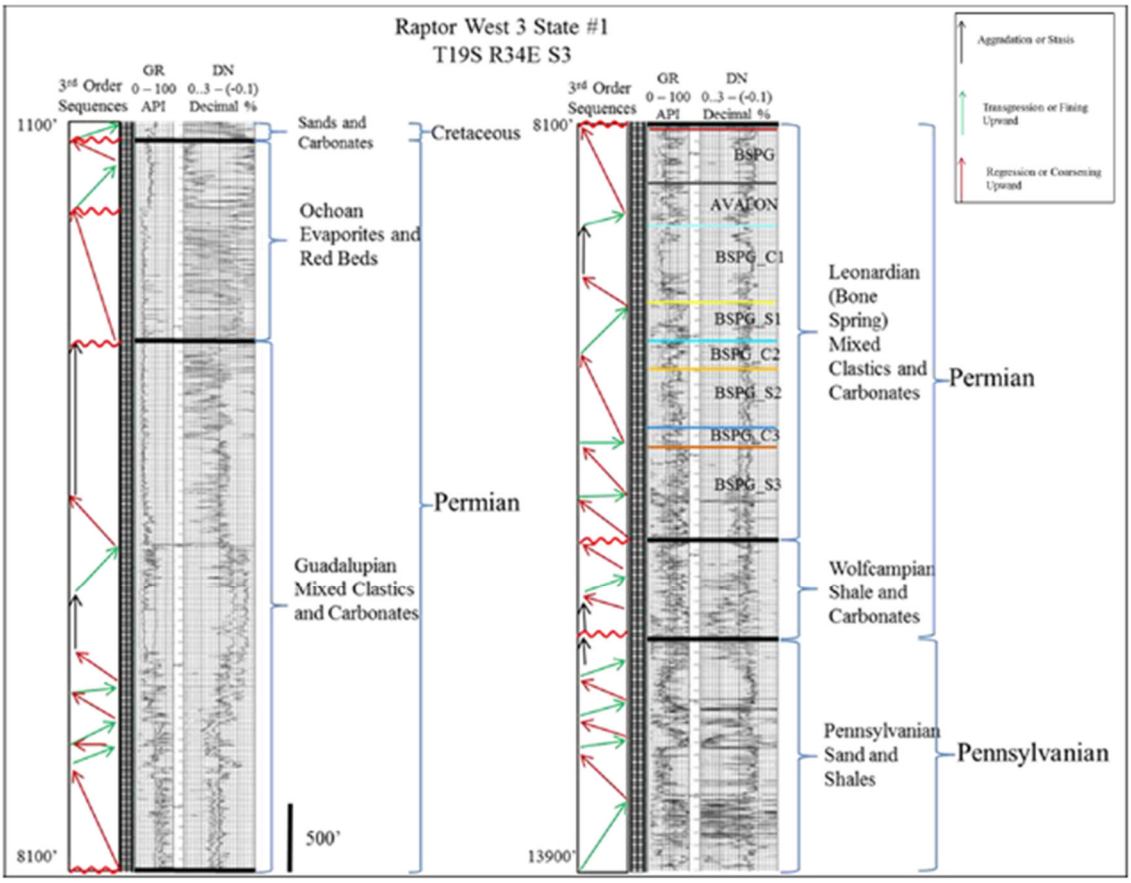

Figure 23: Crosby's (2015) interpretation of the major sequence stratigraphic trends during the Permian in the Raptor West '3' State #1 well found within the slope-basin transition in the Delaware Basin. Bounding units include major unconformities (wavy red lines) and individual Bone Spring Members are label within the Leonardian section. The Upper Avalon and Upper Bone Spring Members here are related to the Cutoff Formation in Bone Canyon. Taken from Crosby (2015).

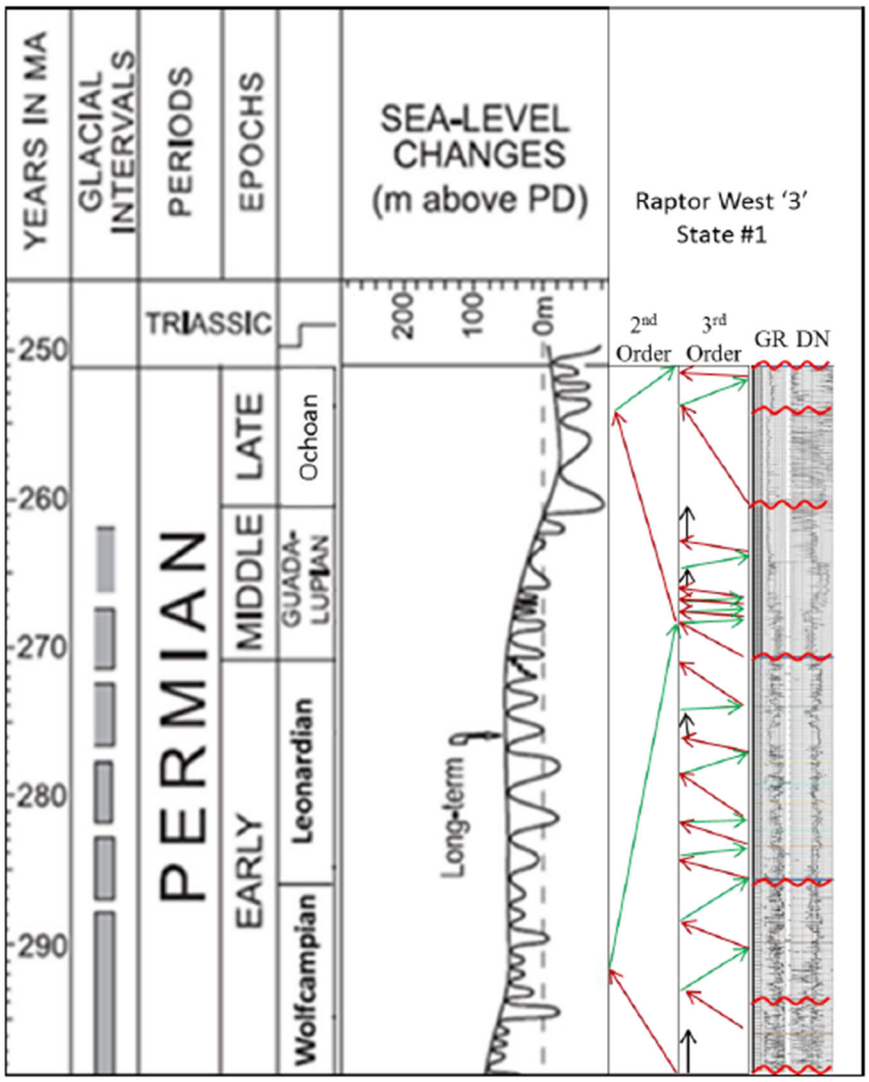

Figure 24: Crosby's (2015) interpretation of the correlation of the Raptor West '3' State #1 well to the global sea level curve taken from Haq and Schutter (2008). The Upper Avalon and Upper Bone Spring Members here are related to the Cutoff Formation in Bone Canyon. Taken from Crosby (2015).

Chapter 4: Methods

4.1 Field Methods

Field observations were taken throughout the entirety of Bone Canyon. Observations include pictures and descriptions of the general lithology, stratigraphy, thickness, dip, and sedimentary structures (if present) of the beds, as well as identifying unconformities and other important boundaries. The most important observations will be discussed in detail in the *Results* section below. The canyon was split into seven transects where the beds were best exposed and best to collect data. Two of the seven transects were labeled Detailed Sections (1-2) because of the thorough work that was done regarding each one. Detailed Section 2 corresponds to Transect 3 and Detailed Section 1 corresponds to Transect 4. All of the transects were used together for lower order observations while the detailed sections were used for high order observations. The geometry and locations of the 7 transects were measured with tape, a five-foot Jacob Staff, GPS coordinates, and a brunton compass depending upon the accessibility of the outcrops. For example, in some areas, the beds were either too challenging to access and measure or were covered, but in all cases measuring tape was used (perpendicular to bedding planes) along with GPS (measuring distances between points) for redundancies. A photo was taken at each measuring interval and provided a number for later reference.

GPS measurements were taken at the beginning and end of each transect as well as at each point data was collected within each transect. GPS measurements were taken with a Garmin Montana 650t and 680t. GPS measurements have a 3-meter horizontal accuracy to the measurement location. The main reason for using the GPS is because of how useful it is for visualizing the locations of each measurement. The GPS was also important for use in the

canyon when the terrain made it too difficult to get to, and measure, the beds. This allowed the GPS to track lateral movement within the measured section. Using the lateral measurement and the dipping angle of the beds, the true vertical depth (bed thickness) was calculated. However, the main (most accurate) method for measuring thickness was measuring tape that ran perpendicular to the beds with +/- one-inch resolution. In many cases the beds would be exposed on the North, or South, wall and then would get covered up-section. If beds on the opposite wall were a continuation of the beds from the north wall, the last exposed bed would be correlated to the opposite wall. GPS helped correlate beds from the North and South Wall. It could be said that measuring bed thickness in outcrop is a combination of art, science and tenacity.

Figure 25: Field image of Transect 4 (DS1) showing the main method of measurement. For scale, the human holding the white board is 5' 9" in height.

4.1.1 XRF

XRF data was collected in the field at each of the designated transects. A detailed technical account of the XRF methods are described later in the laboratory methods. Other than Detailed Sections 1 and 2 where the measurements are dependent on the distance between beds, the other transects have equally spaced measurements. No set or constant number of data points were made for all transects, but rather the number of points at each transect was determined by overall thickness of the transect, the availability of fresh and flat surfaces, and the position of the transect within the entire canyon. More points were collected at and below Detailed Section 1 (Transect 4) because of the factors above.

Transect 5 and 6 are composed of the same host as Transect 4, however, the formation of chert varies (discussed later). The purpose of collected points above Transect 4 is primarily to see and show the changes in chert. Above Transect 6 the Bone Spring Formation (focus of this study) ends. Unfortunately, no easily accessible and exposed beds were near the contact between the Bone Spring Formation and the Cutoff Formation (above Transect 6). Although no data points were collected until Transect 7 (contact between Cutoff and Brushy Canyon), field observations were taken to help determine the changes in stratigraphy above the Bone Spring Formation in order to create a more complete picture of the entire canyon. This difficulty is also the reason of collecting data at Transect 7- to provide a more complete (detailed) analysis of the stratigraphy in the entire canyon. The focus of the analysis remains on the Bone Spring Formation, however, examining and understanding the overlying Cutoff Formation, and the strata above provides important information regarding the depositional history of Bone Canyon and, therefore, the correlation of the units to the subsurface.

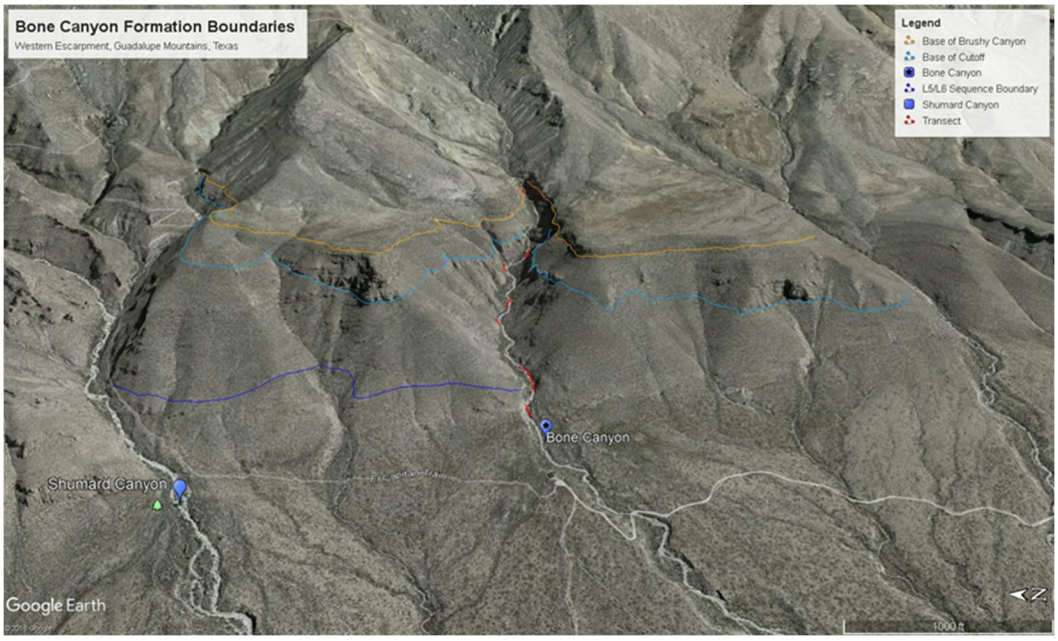

Figure 26: Google Earth image of Bone Canyon. The red lines in the creek correspond to the transects where XRF data was collected.

Figure 27: Field image showing the collection of XRF data at Transect 7. This transect shows the contact between the Cutoff and Brushy Canyon Formations.

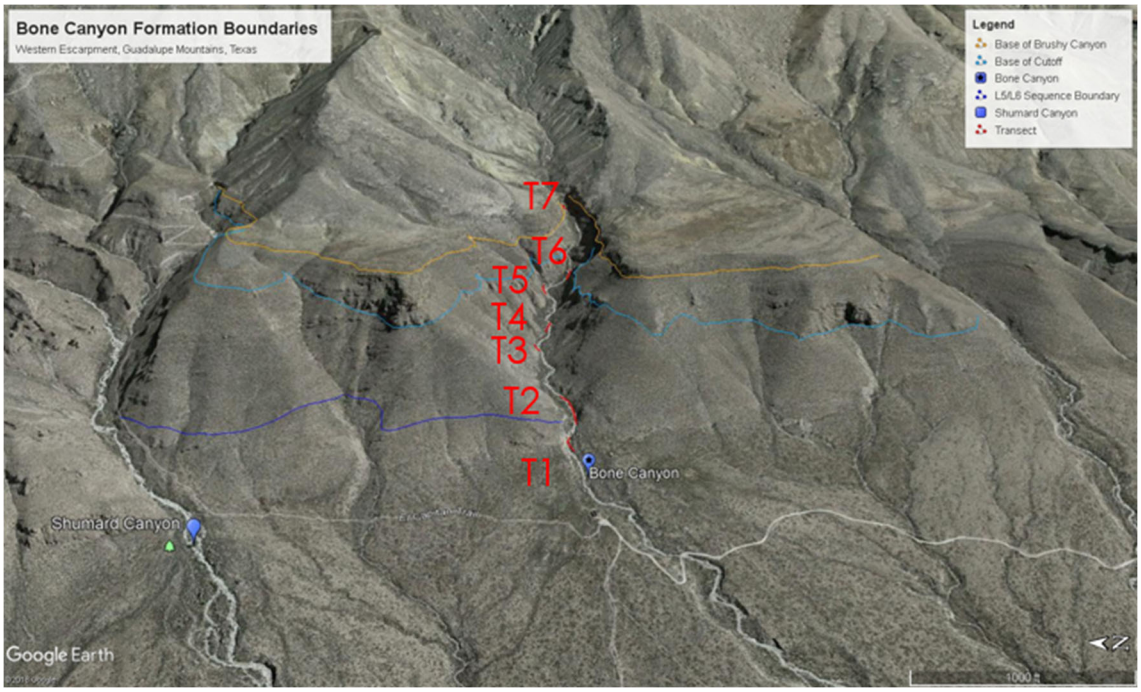

Figure 28: Google Earth image of Bone Canyon, Guadalupe Mountains, West Texas. Location and placement within the creek are shown in red.

4.2 Laboratory Methods

4.2.1 XRF

Recent developments in technology regarding inorganic geochemistry have proven to be useful tools for geologists. Equipment advancements, such as the hand-held XRF, have made determining lithology, trends, and depositional environments convenient. The data the XRF model used in this analysis were created from the Thermo Scientific Niton XL3t Ultra. The XRF measurement intervals at the "detailed sections" were dependent upon the spatial geometries of the beds within each transect, respectively. This increased sample resolution allowed for a more detailed look into the changes in lithology within each bed rather than the more common

approach of taking measurements at 1ft intervals like Rowe et al. (2012), Turner et al. (2014), and Treanton (2014), Crosby (2010)- ideas taken from Crosby 2010.

The x-ray fluorescence (XRF) is more so of a process that occurs, involving electrons and the energy released from these electrons that takes place between a device that provides energy and the rock sample rather than a device itself. During the fluorescence process (**Figure 29**) electrons are knocked from their unique, atomic orbital positions. Once an electron is displaced from its orbital position the atom is unstable and balance must be restored. An electron from a higher orbit moves in to fill the vacancy created from the knocked electron. The further an electron is from the atom the higher binding energy it has. Consequently, when an electron drops to a lower electron orbit closer to the nucleus, energy is released. The energy released is unique to that element thus measuring the amount of energy released can determine a given element (Bruker, 2018). An instrument or software must be used in order to determine the quantity of present elements. The fluorescence process occurs within fractions of a second. Measurements from an XRF are made within seconds to minutes dependent upon the sample and the level of interest. Measurements made within a few seconds provides high percentage levels, while measurements made within a few minutes provide levels in part-per-million.

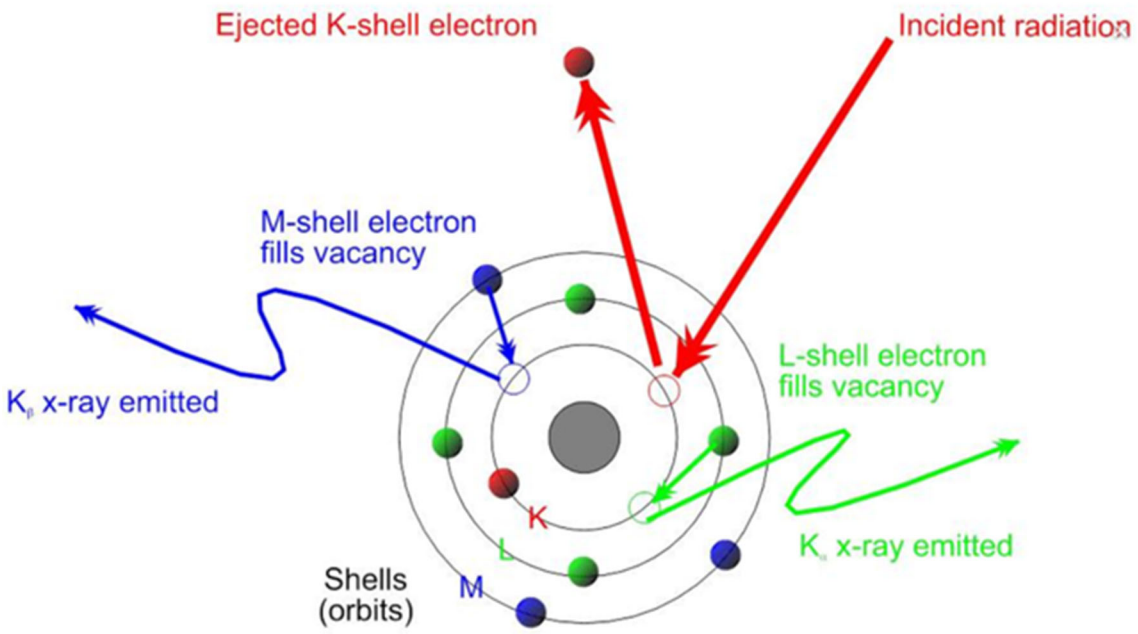

Figure 29: Illustration showing the XRF process. X-rays knock electrons out and cause electrons from a further orbit to fill the vacancy to restore balance. The energy released when this occurs is unique to every element and is recorded by the XRF. Taken from wikipedia.

Before using the XRF, the device must be calibrated to verify it is operating up to standards (Thermo Fisher Scientific, 2010). Each XRF measurement was measured using the TEST ALL GEO mode and had a sampling time of at least 210 seconds, however, did not exceed 215 seconds, to allow major and light elements to be picked up and to ensure the quality of each measurement. As mentioned above these measurements record part-per-million levels. The major elements were measured through three filter ranges known as the Main Range, Low Range, and High Range. The "Main Range" filter provides optimum sensitivity for elements from manganese (Mn) through bismuth (Bi), the "Low Range" optimizes titanium (Ti) through chromium (Cr), and the "High Range" from silver (Ag) to barium (Ba), respectively (Thermo Fisher Scientific, 2010). These filters each have a run time of 60 seconds. Another range, the Light Range, optimizes sensitivity to light elements not measured through the other filters and

has a run time of 90 seconds (Thermo Fisher Scientific, 2010). To insure accurate and reliable data, the SARM-41 standard provided by Thermo Scientific and the Post-Archean Australian Average Shale (PAAS) standard were used.

The results from the XRF scans were used to create a pseudo gamma ray profile and to show elemental concentrations vs. depth, similar to wireline log profiles, and were used as geochemical proxies for lithologic composition, paleoenvironmental conditions, and sequence stratigraphy by identifying high order chemostratigrphic subdivisions within the Bone Spring (revised from Crosby). Proxies, more often than not, consist of a single element or ratios of single elements. Geochemistry is a very important tool that geoscientists use to gain a better understanding of lithology and paleoenvironments. In this study, geochemical proxies were used throughout the canyon. The proxy analysis below provides a background for geochemical proxies and their interpretations in this report.

4.2.1.1 Geochemistry

Advancements in technology, especially in the field of inorganic geochemistry, has made data acquisition more affordable and efficient. A major advancement is the hand-held XRF, that was used in this study, which allows for time efficient and nondestructive ways to collect data in the field or in the lab. A major advantage in this field with this equipment is the ability to determine changes within rocks that are visually similar (grain size, structure, color) through large vertical intervals. Techniques using major, minor, and trace element abundances and ratios can enhance stratigraphic control within these “similar” vertical intervals (Smith and Malicse, 2010; Hornbuckle, 2015). Apparent homogenous rocks can actually be very heterogeneous and geochemical analysis of these rocks can identify the heterogeneities (Slatt and Rodriguez, 2012; Hornbuckle, 2015).

Certain elemental proxies can provide information about a rock's paleoenvironment, provenance, depositional history, and depositional processes making is useful for stratigraphy (Crosby, 2015). Nance and Rowe (2014) discuss how proxies become enriched or depleted during changes in sea level and because of this can be directly correlated with sequence stratigraphy.

The procedures and analysis conducted in this study are similar to that conducted by Crosby (2015). Crosby (2015)'s thesis focused on the Bone Spring Formation in the subsurface and because of that the lithologies and transportation mechanisms are the same. The elements listed below were used based on their reliability: silicon (Si), Iron (Fe), titanium (Ti), zirconium (Zr), aluminum (Al), potassium (K), phosphorous (P), calcium (Ca), strontium (Sr), magnesium (Mg), manganese (Mn), molybdenum (Mo), vanadium (V), cobalt (Co), nickel (Ni), copper (Cu), thorium (Th), and uranium (U) (Crosby, 2015; Hornbuckle, 2016).

The use of elements can be problematic because overprinting may occur. Turner et al. (2014) reported on using multiple proxies to reduce the risk of overprinting. In the report terrigenous and siliciclastic input is best analyzed with Si, Ti, Zr, and the Si/Al ratio. Ti and Zr are fairly immobile and are associated with terrestrial or continentally derived sediment. A decline in Ti and Zr likely would represent lateral retrograding, while an increase represents prograding deposits (Turner et al., 2015). Si is also an important element to use as a proxy, however, accumulations of Si may be related to detritus sediment or biogenic processes. To determine where the Si is coming from, the use of the Si/Al ratio is key. If the Si/Al ratio is high, meaning low Al input, the Si is likely biogenic in origin. If the Si/Al ratio is low, meaning high Al input, the Si is likely detritus in origin.

Pseudo Gamma Ray motifs were also created from the XRF. To do so U, Th, and K values were taken from each sample and were imputed into the following equation:

ϒ API = 4 Th + 8 U + 16 K (Crosby, 2015)

The results of the PsGR were used with K, Al, and Si/Al to be analyzed for the clay content throughout the canyon. Since Al is associated with terrigenous material, it must be used with other clay proxies, such as K (Treanton, 2014; Crosby, 2015; Hornbuckle, 2016). If the Pseudo gamma ray readings correlated to U, rather than K, then it is likely owing to sediment anoxia, organic matter, or a reduced paleoenvironment rather than a clay rich interval (Zhou, 2014; Crosby, 2015; Hornbuckle, 2016). Nance and Rowe (2015) discuss how clay rich intervals likely form with slow background sedimentation during the absence of turbidites.

The proxies P, Ca, Sr, Mg, and Mn are used in this study to determine carbonate influence. Treanton (2014) discusses the importance of using P, in association with Ca and Sr, because both Ca and Sr can be present in phosphate. Throughout the canyon, there is highly fluctuating levels of phosphate, but where present, there is an inverse relationship between phosphate and calcium, indicating the phosphate is not the source of carbonate accumulations. Owing to the concentrations of dolomite throughout the canyon, Mg is also an important proxy to include in the carbonate suite. Mg, however, dilutes the reliability of Sr as a proxy so Mn was included in the suite because of its covariance with Ca, Sr, and Mg (Crosby, 2015; Hornbuckle, 2016). Mn is very sensitive to redox conditions so Mn interpretations should be done carefully (Madhavaraju and Lee, 2009).

Paleoenvironment and Paleoredox conditions were analyzed by a suite of proxies, after K. L. Pigott et al. (2007) and Crosby (2015), containing Mo, V, Co, Ni, Cu, and Mn. Certain elements are more soluble under oxidizing conditions and, conversely, less soluble in reducing

conditions making certain elements enriched in oxygen-depleted sedimentary facies (Tribovillard et al., 2006; Hornbuckle, 2016). Variation in oxygen, basin restriction (sill development), and the cause of such variation can be observed with V, Cr, U, and Mo (Tribovillard et al., 2006; Smith and Malicse, 2010; Hornbuckle, 2016). Oxygen level is one of the main factors contributing to organic matter preservation. Best preservation potential comes from anoxic and euxinic conditions. These conditions occur when the supply of oxygen is less than the demand of oxygen or if water circulation, if restricted, prevents oxygen renewal (Tribovillard et al., 2006; Hornbuckle, 2016). Owing to Mo and V's immobility and independence from detrital fluxes, they are used to determine oxidizing or reducing conditions (Tribovillard et al., 2006; K. L. Pigott et al, 2007). Algeo and Rowe (2012) discuss how the "basin reservoir effect" must be considered with Mo and V concentrations. Lack of Mo and V can result because "increasing restriction results in low deep-water Mo concentrations as a result of Mo removal to the sediment in excess of resupply from ocean waters, not as a result of reducing conditions" (Hornbuckle, 2016). Owing to Cr and Co being susceptible to detrital fluxes, they are not suitable for paleoenvironment analysis (Tribovillard et al., 2006). Ni and Cu are associated with organometallic complexes resulting in high Ni and Cu concentrations correlating to high organic matter input (Tribovillard et al., 2006). U is also a good proxy for organic matter. McManus et al. (2005) and K.L. Pigott et al. (2007) found a good correlation with organic carbon content and U. Algeo and Maynard (2004) also found a direct correlation where high concentrations of U were associated with organic-carbon within anoxic facies. Brumsack (2006) shows Manganese correlates to suboxic and anoxic conditions owing to the fact that concentrations of Mn are high in the oxygen-minimum zone.

Madhayaraju and Lee (2009) discuss how Mn is highly sensitive to redox conditions and, because of a similar cycling pattern to Fe, has implications on paleoredox conditions. The relationship between Mn and Fe is seen in Crosby (2015)'s thesis that normalizes Fe and Mn to PAAS values by: $Mn^* = \log [(Mn_{sample} / Mn_{PAAS})/(Fe_{sample}/Fe_{PAAS})]$. Anoxic conditions correspond to lower values and oxic conditions correspond to higher values.

4.2.3 Thin Sections

Rock samples were randomly chosen at each transect to take back to the laboratory to be made into thin sections for mineralogical and diagenetic analysis. Mineralogical and diagenetic changes were seen throughout the canyon and aided in the understanding of chert appearance and depositional features. Thirteen thin sections were made and analyzed under a petrographic microscope in plain polorized optics (PPO) and cross polorized optics (CPO). The classic Dunham Classification scheme was used in order to determine mineralogy and lithology of the rock and thus the transect.

Chapter 5: Results

A number of different lithologic profiles created from XRF values, mentioned above, were analyzed throughout Bone Canyon in order to determine changes in lithology, depositional processes and environments, and to determine Leonardian-Guadalupian chronostratigraphic boundaries and the formation contacts within. The mapping of major units within the Leonardian and Guadalupian strata is crucial before delineating or subdividing the units further. The results of this investigation are intended to lay a foundation for more detailed analyses of further divided units, created here, of the Bone Spring Formation and to better understand the factors that influenced the variations of the strata in the divided units through high resolution investigations of Bone Canyon. The Late Permian stratigraphy is shown below with the interpreted stratigraphy of Bone Canyon, which crops out, in bold and displayed on Figure 30.

1. Brushy Canyon

2. Cutoff

- **A. Upper**
- **B. Middle**
- **C. Lower**
  - **1. Upper Avalon**

3. Bone Spring Formation

- **A. 1st Bone Spring Carbonate**
  - **1. A (bedded chert), B (nodular chert), C (mottled chert)**
    - **a. Middle Avalon**
  - **2. Carbonate Sand**
    - **b. Lower Avalon**

B. 1st Bone Spring Sand

C. 2nd Bone Spring Carbonate

D. 2nd Bone Spring Sand

E. 3rd Bone Spring Carbonate

F. 3rd Bone Spring Sand

Bone Canyon is comprised of the 1st Bone Spring Carbonate [Sand, FBSC A (bedded chert), FBSC B (nodular), and FBSC C (mottled chert)], the Cutoff Formation, and the Brushy Canyon Formation. The Avalon Shale is located within the canyon also, but it does not define a set of strata. Instead, the Avalon Shale refers to a petroleum play found within the FBSC. The Avalon Shale, depending on basinal position, is placed above, below, or amongst the 1st Bone Spring Carbonate. Bone Canyon is located in the northern Delaware Basin and represents the slope-to-basin transition. Here, the Avalon Shale correlates to the First Bone Spring Carbonate and the Lower Cutoff Formation, both Leonardian in age. This correlation will be further discussed later on.

This section will discuss the observations and results of the different methods used throughout Bone Canyon and, more specifically, at each transect where data was collected within Bone Canyon. Field Observations will be supported by XRF data, including geochemistry, and thin-section (where collected) analysis at each transect. Geochemistry is a very important tool that geoscientists use to gain a better understanding of lithology and paleoenvironments. In this study, geochemical proxies are used throughout the canyon. The proxy analysis discussed in the Methods section (above) provides a background for geochemical proxies and their interpretations in this report.

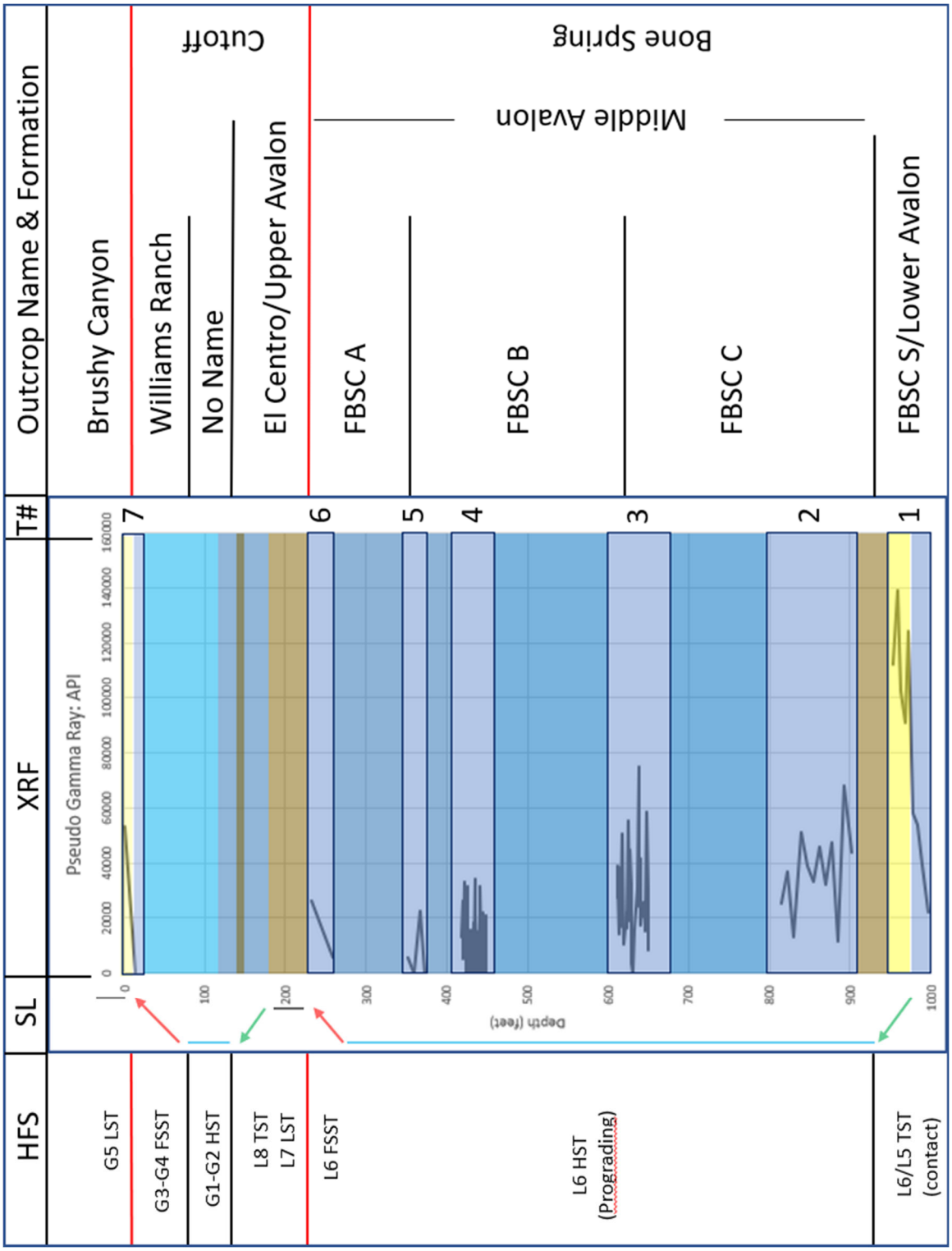

Figure 30: Summary of Results showing interpreted High-frequency Sequences (HFS), Relative Sea Level Curve (SL), Pseudo-Gamma Ray Log (XRF), Transect Number (T#), and Outcrop Name & Formation.

5.1 Field Work

Extensive research of the Western Escarpment stratigraphy was done prior to personally determining the lithology and stratigraphy found within Bone Canyon. This allowed the ability to hypothesize what could possibly be seen from the start of the Canyon and up-section until the Brushy Canyon Formation was reached. After a brief description of the observations seen at each transect, there will be an attempt to correlate the field observations in Bone Canyon to previous works done on the stratigraphy of the Western Escarpment, Guadalupe Mountains, West Texas.

Kerans et al. (1994, 95, 97) traced the transgressive boundary of L5 and L6 in the Western Escarpment until it is terminated in Shumard Canyon. This trace (**Figure 31**) implies that the strata in Bone Canyon likely are part of the L5 HFS. The L5 HFS (in Bone Canyon) would resemble toe-of-slope deposits (mudstone facies), while L6 HFS should more closely resemble upper slope deposits (crinoid and fusilinid packstone facies) (Fitchen, 1997). The L5 HFS is also defined by the presence of sand units found within carbonate facies. Just north, in Shumard Canyon, the base of the L5 sequence is defined by the oldest outcropped sand unit within the mudstone facies that is found at the mouth of the canyon (Kerans and Fitchen, 1995; Fitchen, 1997; Kerans, 2002). Similarly, the mouth of Bone Canyon contains an outcropped sand unit found within mudstone facies. Therefore, Transect 1 beds outcropped at the mouth of Bone Canyon have been placed within the L5 HFS.

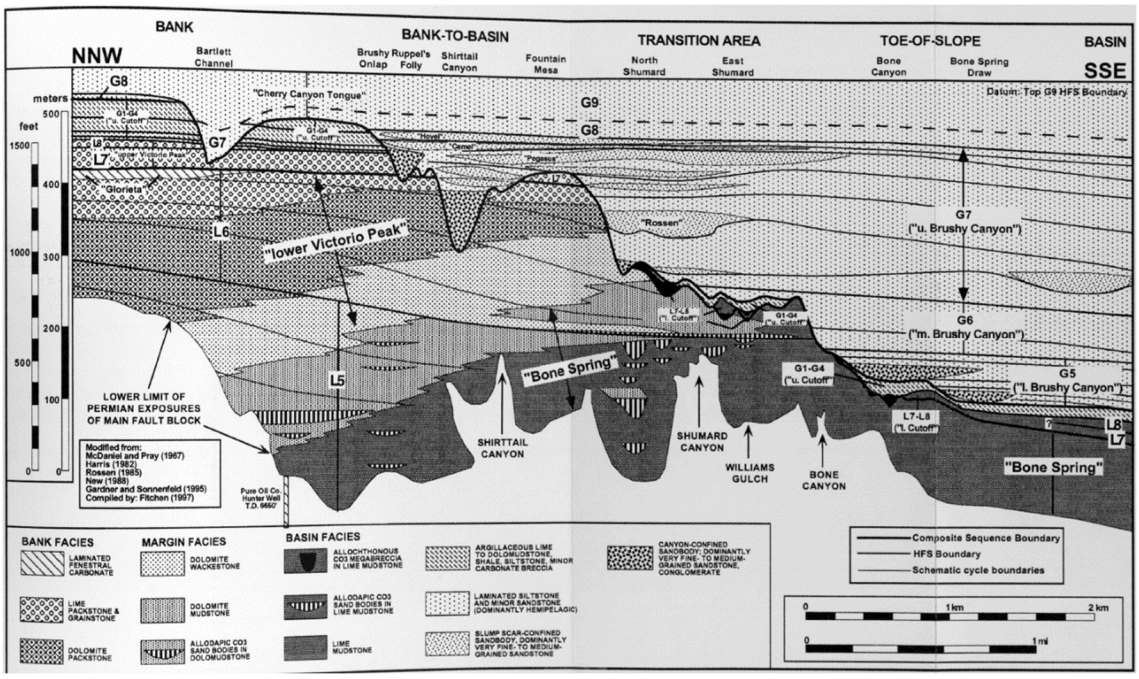

Figure 31: Stratigraphic cross-section of outcropped units in the Guadalupe Mountains. Bone Canyon is located on the toe-of-slope and is shown to likely represent the L5 HFS. Taken from Fitchen (1995).

Fitchen (1997) traced the top of the L5 HFS boundary from Apache Canyon to the Babb flexure and placed the L5/L6 sequence boundary 50m below the top boundary of King's (1965) Victorio Peak middle division. The Lower and Upper division of the Victorio Peak are middle and mostly outer shelf facies, while the Middle division is composed of inner shelf facies indicating that the Middle division represents a major progradation shift (Fitchen, 1997). "The L5 and L6 HFS exhibit ramp profiles with <1° to 5° ambient dip of strata. Higher angle dips within the outer shelf/ramp margin to lower slope/basin/distal ramp transition are related to filling of steep-sided "half channels" interpreted as slump scars. Facies tracts include inner shelf evaporites and dolomudstones, middle shelf peritidal carbonates and sandstones, outer shelf/ramp margin skeletal grainstones and packstones, and lower slope/basin/distal ramp wackestones and organic-rich mudstones. Within the L5 and L6 HFS the position of maximum

accommodation was in the outer shelf/ramp margin to lower slope/basin/distal ramp transition. The two HFS together exhibit a progradation/aggradation ratio of approximately 16, with at least 3.4 km of progradation and 220 m of aggradation" (Fitchen, 1997). Fitchen's (1997) work explains how the Bank-to-Basin, Transition Area, and Toe-of-Slope (Bone Canyon) were areas of maximum accommodation during deposition of L5 and L6 HFS. This accommodation allows the thickest deposits of L5 and L6 HFS to form.

Kerans' (2002) work defines many Composite, Formation, and HFS boundaries. The work also discusses how the L5 and L6 HFS boundary, undifferentiated in the Guadalupe Mountains, is the final outbuilding of the Leonardian platform. The subsurface equivalent to this platform is the uppermost Clear Fork and the Glorieta (basin-wide progradational event). The outcrop equivalent is found in the Algerita Escarpment and is composed of silty tidal-flat carbonates. The outer shelf-slope facies equivalent is the lower-middle Victorio Peak and Bone Spring Formations (Kerans, 2002).

Owing to the fact that a sand unit within a mudstone facies is seen at the mouth of Bone Canyon and that these sand units are not found within the L6 HFS; the oldest beds have been placed within the L5 HFS. The L6/L7 HFS boundary is located further into (up-section) the canyon. The base of the L7 HFS is defined by Kerans (1992), Kerans and Ruppel (1994), Kerans and Fitchen (1995), and Kerans (2002) as the appearance of megabreccia. This means that the contact between L5 and L6 is located somewhere in between these two boundaries and represents a progradation phase. The top portion of Transect 1, towards the top of location 2, and just above the sand unit is a thin shale unit. Above this shale unit, carbonate deposition continues. The change in facies from sand unit to shale unit to carbonate unit corresponds to a transition from a TST to HST, or progradational phase, and, therefore, has been defined as the

contact between the L5 and L6 HFS (**Figure 32**). Correlating these HFS to the subsurface results in the L5 HFS correlating to the lower Avalon Shale, the L6 HFS to the middle Avalon Shale, and the L7-8 HFS to the upper Avalon Shale (Hurd and Kerans, 2016). Although the Avalon is technically not a stratigraphic unit it may very well represent 4-6 HFS from L5-G2. The lower and upper Avalon are described as being "muddy" units, while the middle Avalon is described as a carbonate rich unit (Avalon Thesis, 2015; Kerans and Hurd, 2016). These descriptions match with the placement of the HFS boundaries defined in this work.

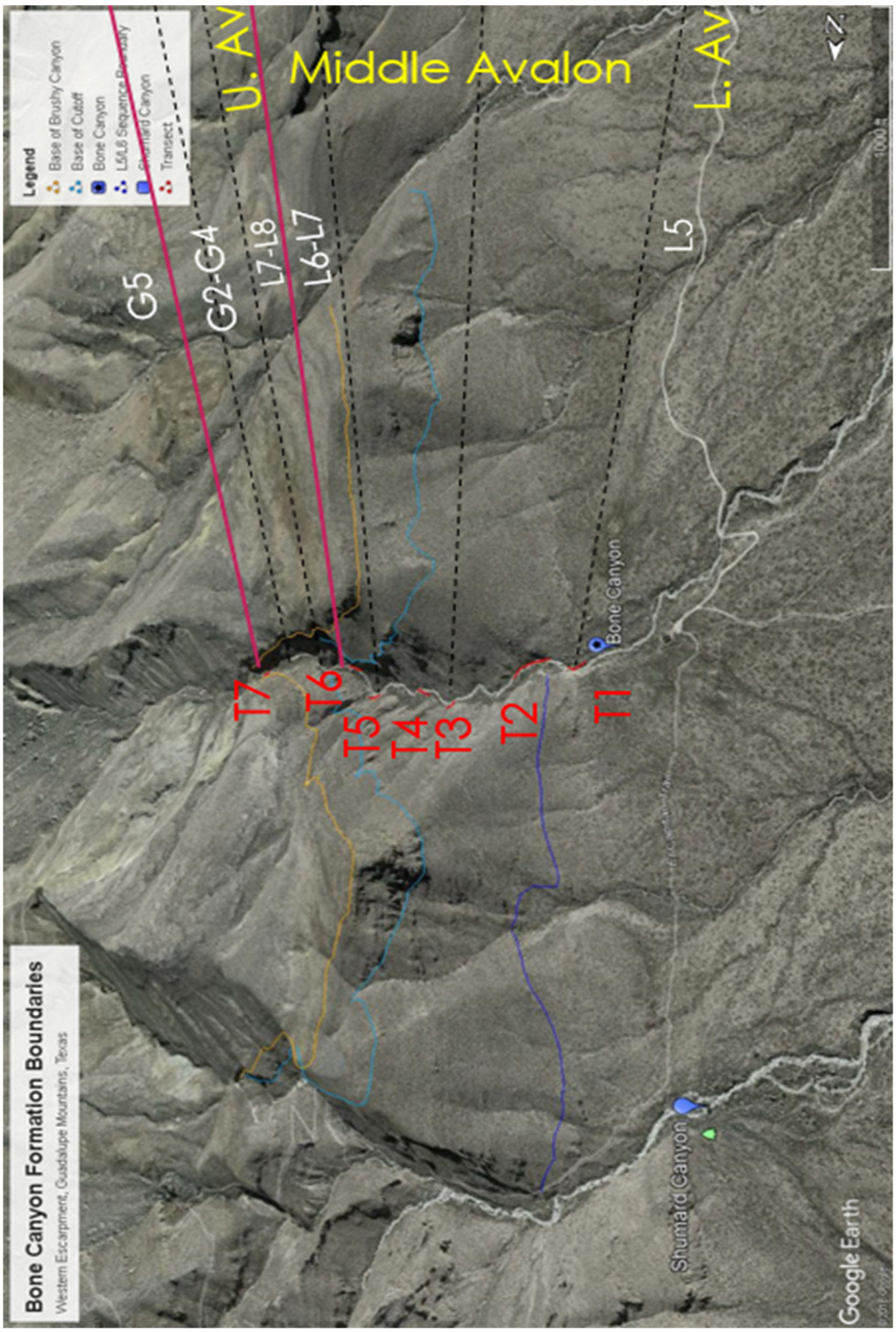

Figure 32: Google Earth image of Bone Canyon displaying Transect locations with their high-frequency sequence and relation to the Avalon Shale.

The L7 HFS is defined by megabreccias that overlie mudstone/wackestone facies and represent the Early Fall during L7 and Late Rise of L7. The fall in sea level caused erosion of much of the underlying L6 platform as well as created channel incisions on the slope-basin. As sea level began to rise at the end of L7, or doing the L8 HFS, it caused slope failure and debris flows composed on platform siliciclastic material were shed onto the slope and into the basin. These megabreccias represent this period of fall and rise. During the subsequent rise in sea level, mud-rich facies (Upper Avalon) were deposited above the megabreccia and represent the Shumard and El Centro Members of the Cutoff Formation that are Late Leonardian (L7-L8, respectively).

The L8-Early G2 HFS record an HST that is composed almost entirely of the El Centro Member of the Cutoff Formation. The younger part of the G2 HFS is composed of different facies. Conodont data shows the El Centro Member correlates to the Upper Avalon Shale (Hurd, 2016). As sea level begin to fall towards the end of G2, less mud is present, and deposition of a clean fenestral carbonate occurs. As sea level falls further, more erosion of the carbonate platform occurs and consequently sends MTDs full of course, conglomeritic, and mud debris onto the slope and into the basin.

Similar processes to L7 occurred to deposit the G3 HFS and therefore it is composed of similar material and deposits to that found in the L7 HFS. In the center of Bone Canyon on the south wall these G3 deposits are composed of megabreccias. Further east into the canyon, however, these deposits are more conglomeritic.

The G4 HFS represents a further fall in sea level and is composed entirely of the Williams Ranch Member of the Cutoff Formation. Although this unit can be seen on the South Wall of Bone Canyon (in center of canyon) it pinches out, or was eroded during G5 HFS, to the

east, south-east. This causes the G3 conglomerate deposit to be overlain by an unconformity that is overlain by the G5 LST sandstone deposits of the Brushy Canyon Formation. The subaqueous position of Bone Canyon during the time of deposition of the Brushy Canyon allowed for soft-sediment deformation within the G5 sandstone (seen at the top of Bone Canyon).

The results below provide evidence for the description above. Research was followed by field work, laboratory work, and then the results were analyzed. The results of each individual transect from the field and laboratory were analyzed then combined together for use as evidence for the conclusions. The field results of each transect will be discussed below, followed by laboratory results for each transect, and then these two work methods will be combined to show an analysis of Bone Canyon including its lithology, stratigraphy, and its correlation to the subsurface.

5.1.1 Transect 1

Transect 1 begins at the start of the canyon where bed layers start to become apparent. On the north wall, the oldest beds are lime-dolo-stone (**Figure 33**). Shortly up-section is a sandstone unit. At first look it was believed to be the contact between the 1st Bone Spring Sand and the younger 1st Bone Spring Carbonate. This hypothesis was later voided from Kerans' (2016) work regarding the sequence stratigraphy of the Guadalupe Mountains and then by thin section analysis of the unit that will be discussed later on. However, the characteristics seen here are similar to the units described by Hurd and Kerans (2014), in Shumard Canyon. Therefore, this siliceous mudstone was deposited during the L5 sequence, named in this work as the Bone Spring Carbonate Sand, which corresponds to the Lower Avalon Shale. Data points start where the biogenic-siliceous carbonate interval first appeared on the northern wall of the canyon

(**Figure 33**). Directly above the sand package is a mud-, shale-rich interval. It appears that there are two alternating sequences of a siliceous-mudstone with an overlying shale. The top of this unit, being mostly composed of shale (siliciclastic material), likely corresponds to the L5/L6 sequence boundary and marks the transition from outer shelf margin/upper slope facies at L5 to lower slope/basinal facies of L6.

Figure 33: Field image of Transect 1 showing the biogenic-silica-rich Sand and Shale units within the First Bone Spring Carbonate.

Transect 1 was measured to be 48 feet and nine equally spaced points were chosen throughout the transect. The spacing between each data point is approximately 5.33 feet. This

provided variations in lithology to be seen within the same transect with minimal data points. The lithology of the beds are as follows: 1a: limestone; 1b: chert; 1c: limestone; 1d: limestone; 1e: chert; 1f: biogenic-siliceous mudstone; 1g: biogenic-siliceous mudstone; 1h: shale; 1i: biogenic-siliceous mudstone.

The lithologies of Transect 1 are a combination of carbonate, chert, and shale. The older beds contain more carbonate, while the younger beds contain more very-fine grained quartz (silica) and clay minerals, before going back to mudstone dominated carbonate beds further up-section in the canyon. Carbonate beds are gray and chert beds are light-brown (tan) in color, perhaps suggesting more reducing conditions. The carbonate beds are thicker, with a general thickness around 4", while the chert beds are generally half that (2"). The chert appears to be within the carbonate beds, rather than being their own individual beds resulting in the chert appearing to be more like laminations than beds. It is not always laterally continuous and, sometimes, starts and ends throughout the host bed, creating mottled (splotchy) chert planes. Much of the chert seems to be on the bedding planes of the carbonate beds, dividing them, and become visible owing to differences in weathering and color. Chert that is not found on the bedding planes is found interbedded with the carbonate. Many horizontal and vertical fractures are present. The horizontal fractures seem to correlate to chert beds, but vertical fractures cut through both carbonate and chert beds. In some instances, the contacts between the carbonate beds and the beds above, or below, appear wavy. Ripple laminations are seen in some carbonate beds with chert replacing the ripples. Transect was is named the First Bone Spring Carbonate Sand (FBSC Sand) owing to the siliciclastic nature of the transect.

Above Transect 1, the interval is covered. This covered interval is likely a continuation of the shale interval below, as shales commonly cause 'covered sections' because of their

characteristics and often develop into gentle slopes in outcrops, and as this is a transition from the L5 to L6 HFS, the covered section is presumed to be shale.

Figure 34: Field Image of Transect 1, the FBSC Sand, with the oldest unit being a biogenic siliceous carbonate sand package. The top left of the image shows a small shale package that can be reached not so far up-section in the creek of the canyon.

5.1.2 Transect 2

Between Transect 1 and Transect 2, there is a covered section approximately 45’ thick. Transect 2 beds come into the creek bed for a distance of around 280’ (lateral distance). Transect 2 was measured and 12 data points were picked throughout the transect, equally spaced with, approximately, 7.83’ between points. Transect 2 begins at a depth of 909.35’ and tops out at a depth of 815.35’ making the transect 94 feet thick. The field image of this transect can be seen in **Figure 35**.

The beds found at Transect 2 alternate between carbonate and chert. Here, the chert beds are more pronounced than the previous transect, Transect 1. The chert beds are once again thinly bedded with the limestone beds, in general, being around 2-3 times thicker, however in some areas the carbonate beds are thinner and/or chert beds are thicker. The carbonate beds are, in general, around 2-4 inches thick while the chert beds are around .5-1.5 inches thick. Multicolor chert beds can be seen, usually where chert beds are thicker. These beds have black or dark brown chert on the outside with light tan chert in the middle. Owing to the bedded characteristics of the chert beds, this transect is named the First Bone Spring Carbonate A (FBSC A). The beds represented in Transect 2 continue up-section, however, most of the section is covered for so no data points were collected for, approximately, 140 feet until transect 3 (Detailed Section 2).

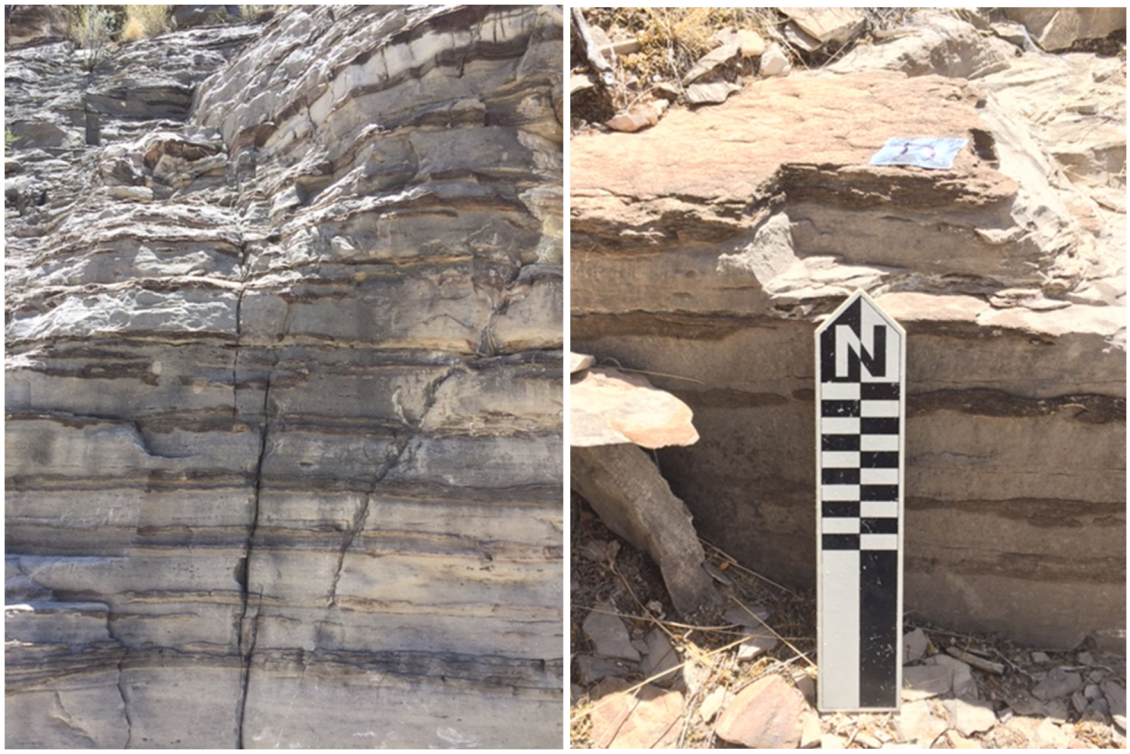

Figure 35: Field images of Transect 2 showing the alternating layers of limestone and chert. Transect 2 corresponds with FBSC A (bedded chert).

5.1.3 Transect 3 (DS2)

A covered interval between Transects 2 and 3 was measured to be, approximately, 140' starting at a depth of 815.35' and topping out at a depth of 675.35'. This covered interval is visually very similar to the Transects that bound it. The oldest portion of the covered interval closely resembles Transect 2, while the youngest portion of the covered interval more closely resembles the beds found at Transect 3. With this in mind, this covered interval is likely a transition interval between the transects (T2-T3).

Transect 3 is known as Detailed Section 2 (DS2), rather than Detailed Section 1 (DS1), because data was collected at Transect 4 (DS1) first, before going back down-section to create a second detailed section here at Transect 3. Transect 3 begins at a depth of 675.35 feet and tops

out at a depth of 611.85 feet, making it 63.5 feet thick. This section is exposed for 63.5 feet, however, only 39.67 feet was accessible, well enough, to collect data. At Transect 3 (DS2), the carbonate and chert beds are well pronounced. The beds in this transect outcrop in the creek (and north wall) and are seen on the walking path creating a stair-like pattern (**Figure 36**). The distance between points were dependent upon the thickness of each bed, allowing for a more detailed look into the individual beds. Owing to alternating beds of carbonate and chert, the data points collected generally alternate between carbonate and chert beds.

In Detailed Section 2, the chert beds are more apparent and continuous than previous transects, meaning the beds are now, more so of, their own bed, separate from the carbonate beds. The chert beds in previous transects now seem to be, more so, contained within the carbonate host rock, as opposed to being their own bed. The chert at Transect 3 is also more apparent owing to differences in weathering. However, a main difference in the chert beds from the previous transects can also be seen here. The chert is now a lighter shade of gray, or tan, as opposed to the previous, darker chert. The carbonate and chert beds at Transect 3 have very similar colors. The lighter color of these beds may suggest a more reducing environment. This transect is named the First Bone Spring Carbonate B (FBSC B), because of the bedded and nodular characteristics of the chert beds.

Many of the thicker chert beds are multicolored with a dark brown outside and a light tan middle. In many light-colored limestone beds, there are darker planar to wavy laminae running through the beds. Some chert beds thin and/or pinch out and, in many cases throughout the section, the chert forms into nodules with a radius of, approximately, 2-3 inches. Chert beds range in thickness from 2-4 inches and the carbonate beds range from 4-12 inches.

Figure 36: Field image of Transect 3 (Detailed Section 2) showing alternating beds of carbonate and chert. The chert beds are more pronounced as their own bed-forms with a different weathering pattern and a lighter shade of gray, or tan, than the carbonate beds, as well as previous transects. The differences in chert separate this transect from previous transects and, therefore, was given the name, First Bone Spring Carbonate B.

Figure 37: Field image with a broader view of Transect 3 (Detailed Section 2). T3 corresponds to FBSC B (bedded-nodular chert).

5.1.4 Transect 4 (DS1)

Between Transect 3 and Transect 4 is a covered interval approximately 146 feet thick. This covered interval was problematic when measuring. Beds on either wall are not easily accessible and because of this, the distance between these detailed sections had to be measured using Google Earth. This covered interval is similar in nature to the previous covered interval, in that it represents a transition between, the previous, Transect 3 and, the following, Transect 4. This conclusion was made owing to the visually similar characteristics observed at the beginning and end of the covered interval.

The exposure of Transect 4 (Detailed Section 1) is seen on the southern wall of Bone Canyon. This transect begins at a depth of 465.85 feet and tops out at a depth of 418.83 feet,

making DS1 47.02 feet thick. Of the 47.02 feet, 31.23 feet was used because of the accessibility of the exposure to collect data. It is worth mentioning that at near the beginning of the transect, there is a fault that cuts through the beds. The beds to the left of the fault onlap the fault plane, while the beds to the right terminate against the same plane.

As seen in **Figure 38**, DS1 shows alternating layers of carbonate and chert. In general, the chert beds appear thicker here, however, the carbonate beds are still thicker (1-2x). Similar to Detailed Section 2, the actual distance between data points was dependent upon the thickness of each bed. The chert in Transect 4 is thicker than in Transect 3 and some layers contain a black inside with the normal tan color on the outside. The carbonate beds, however, are a darker gray than the previous transect (T3). Some chert beds are multicolored with a light-tan outside and a dark-brown, or black, inside. For the most part the chert beds are continuous throughout this transect. Most chert beds are similar in thickness (6 inches). Moving up-section in this transect, the chert layers become less prevalent in the bedding planes and, once again, start to form into nodules. These nodules, however, are larger than the previous transect, with some around 8 inches thick and reaching 2 feet in length. Although these beds vary from the previous transect, their bed-forms are similar. Transect 4, similar to Transect 3, is also named the First Bone Spring Carbonate B (FBSC B) owing to the similarities in the bed forms.

Figure 38: Field image of Transect 4 (Detailed Section 1). DS1 correlates to FBSC B (bedded-nodular chert).

5.1.5 Transect 5

From Transect 4 to Transect 5 there is another covered section measured to be, approximately, 38 feet thick. Where beds are present, they show alternating layers of carbonate and chert. The chert is multicolored with dark brown in the middle and light tan on the outside. However, the frequency of large chert nodules appears to be increasing up-section and creates a discontinuity of chert on the bedding planes. Fractures in this interval are seen to be filled with chert.

Transect 5 was measured to be 29 feet thick starting at 351.83 feet and ending at 380.83 feet of the overall stratigraphic thickness of Bone Canyon, as it relates to this thesis. Transect 5 shows alternating beds of carbonate and chert, however, the chert beds are not always laterally continuous. In fact, similar to the observations from the previous covered interval, much of the chert has formed into giant nodules (**Figure 39**). Similar to the previous transect, this transect is named the First Bone Spring Carbonate B (FBSC B) owing to the bedded and nodular characteristics of the chert. The significance of the changes in chert, from bedded to nodular to mottled (Transect 6), will be discussed in more detail later.

Figure 39: Field images of Transect 5 showing nodular chert within limestone correlating to FBSC B (bedded-nodular chert).

5.1.6 Transect 6

Similar to before, there is another covered section between Transect 5 and Transect 6. This covered interval was measured to be 67.5 feet thick. Owing to the inaccessible nature of this interval, no data points were collected. Similar to before, although it is a covered interval, visual observations could still be made. These observations show the interval to be another transition between Transect 5 and Transect 6.

Transect 6 was measured to be 52 feet thick, starting at a depth of 232.33 feet and ending at a depth of 284.33 feet of the overall stratigraphic thickness of Bone Canyon, as it relates to this thesis. Transect 6 shows another variation in the characteristic of the chert beds. Here, the chert is mottled (splotchy) and is not laterally continuous (**Figure 40**). The chert, where present, is found on the bedding planes of, or between, carbonate beds. The chert likely would form beds, like those seen in previous transects, but as there was either not enough silica present in the system during deposition, or the system was affected by different syn-, or post-depositional, processes. This transect is named the First Bone Spring Carbonate C (FBSC C) owing to the different characteristics of the chert. Variations in chert will be discussed in more detail later.

Figure 40: Field image of the mottled/splotchy chert at Transect 6. This unit is named the First Bone Spring Carbonate C (FBSC C) owing to these characteristics.

Between Transect 6 and Transect 7

Above Transect 6 appears to be more enriched in siliciclastic, or mud-/shale-rich material. The textures of the beds appear to be more fissile/flakey. No data was collected on these beds; however, pictures and observations were still collected (**Figure 41-Figure 43**). This covered section is near the location named "the narrows" by P.B King and it is of significance because the unconformity seen there. Further up-section from Transect 6, and below Transect 7, there is a shale-rich interval that briefly crops out for, approximately, 50 feet thick.

The oldest portion of this muddy unit is massively deformed (**Figure 42**). Around 35 feet up-section from the base of the unit is an, approximately, 3 feet thick interval of mudstone filled with sub-rounded-sub-angular cobbles and litho-clasts (**Figure 43**). Directly above, appearing within the same unit, is an, approximately, 5 feet thick, shale-rich interval. The contact between

these varying lithologies is easily noticeable (sharp), however, it also has gradual characteristics. This suggests that this interval resulted from slope failure, causing, approximately, 50 feet of sediment to be transported down the slope and into the basin as a gravity debris flow deposit. This process is common throughout Bone Spring and Cutoff deposition and occurs after a shift in environment (SL fall/rise) that results in sediment on the shelf and slope to become unstable. Slope failure can happen during a RST or TST. In this case, the slumped interval was deposited during the RST, the layered unit of carbonate clasts in a mud matrix was deposited during the following LST, and the layered shale above during the following TST.

Figure 41: Field image above Transect 6 showing the more flakey/platey siliciclastic-rich carbonate interval.

Figure 42: Field image of the lower portion of the mud-rich interval above Transect 6.

Figure 43: Field image above Transect 6 of the shale-rich interval. Notice the base is a mudstone bed composed of large cobbles and litho-clasts. The shale above is flakey/platey. These beds appear to be a part of the same unit suggesting a debris flow-like deposit.

Further up-section, above the previously described interval and just below the Cutoff Conglomerate seen at the top of Bone Canyon, there is another change in depositional environment. This interval is a clean and layered carbonate mudstone (**Figure 44**). Visually the layers appear to be of 2 thicknesses, a thick bed followed by thinner bed(s). The thick beds are around 1 foot and the thinner beds are around <.5 foot. This suggests a turbidite depositional processes in which thicker (coarser) beds likely flowed into the basin and the thinner beds settled out on top. The thinner beds have a flakey texture and are more weathered than the thicker beds. Down-section, the beds were siliciclastic/shale-rich and now there is a clean layered carbonate, suggesting a continued rise in sea level from the last shale-rich interval, discussed briefly above

between Transect 6 and Transect 7, to the carbonate turbidites seen here. This change in deposition reflects the transition from a TST to an HST (L8-G2 HFS), which we be discussed further in the laboratory results.

Figure 44: Field image of the Upper Cutoff Formation just below Transect 7. The image shows bed couplets with a more resistant, thicker bed and a thin, less resistant bed. Overall, the unit becomes more resistant up-section likely deposited as turbidites.

5.1.7 Transect 7

Transect 7 (**Figure 45**) is the youngest, and stratigraphically highest, unit studied in this work in Bone Canyon. This transect was measured to be 30 feet thick starting at 0 feet and ending at 30 feet of the overall stratigraphic thickness of Bone Canyon in this thesis. One data point was collected on the lower carbonate and one on the higher sandstone unit. Transect 7 does not contain any chert, but it does represent a drastic change in the depositional environment from highstand carbonate deposition to lowstand clastic deposition. The lower bed is a massive carbonate conglomerate, likely deposited as a debris flow as a result of slope failure caused by

the falling sea level. No bedding features are seen in this unit and, therefore, could not have been deposited by the same process that occurred directly underneath it.

The unit above is a highly deformed (soft-sediment deformation) very fine-fine grained sandstone. Sandstones make their way into the basin by bypassing the carbonate platform. Through deposition of the Bone Spring and Cutoff Formations, the platforms were built-up and the basin was fairly restricted. Sandstones would need pathways to reach the basin. The Brushy Canyon Formation deposits were able to reach this paleo-area via incised channels and turbidity currents, created during LSTs (and RSTs). The end of the Leonardian marked a time of sea level fall. This eventually led to the creation of the necessary pathways for the sandstones. Transect 7 shows the RST transition from an HST to an LST. This unconformity is often called the Leonardian Unconformity. However, the canyon boundary correlates closer to the contact of the Late Cutoff (Early Guadalupian) and Brushy Canyon Formations (Guadalupian).

Field observations play a crucial role in understanding changes in lithology and/or strata and allow the ability to see, trace, and/or approximate formation, sequence, and environmental boundaries. Owing to similar lithologies, and weathering, many units look visually similar and no distinctions can be made. In order to determine variations in visually similar, but different units, XRF and thin-section data was collected. The XRF data was used to create pseudo-gamma ray and geochemical proxy curves, while the thin-section data was used to compliment XRF data regarding diagenetic processes. Below are the laboratory results from these methods.

Figure 45: Field image of Transect 7 showing the contact between the Cutoff and Brushy Canyon Formations. Sand unit displays lots of deformation.

5.2 Laboratory Results

Field work is very important for building a foundation for research. It helps to delineate major units through seeing variations in lithology. Of course, what is seen, or thought to be seen, must be validated. Recent advancements in technology provide the necessary tools to validate or dispute field research and hypotheses. Below are the Laboratory Results that are used in conjunction with the Field Results. A main difference between these results is that laboratory analysis provides the actual evidence for hypotheses created in the field. The laboratory also provides insight that would otherwise be unknown owing to the fact that it sees what can't be seen with the human eye alone. The results below will go through each transect, highlighting important features found through XRF, LiDAR, and Thin Section analysis. Before diving into these (higher-order) individual transects, it is important to understand the bigger (lower-order) picture of the entire canyon. So, without further ado, let us begin.

From the previous sections we have learned, in general, the major changes in lithology in the canyon. From there, locations for data collection were determined, pictures were taken, and boundaries were hypothesized. The main features found during the field investigation are shown below **(Figure 46** and **Figure 47)**. The Google Earth image shows the major formation boundaries with the red lines, show the location and the approximate extent of the transects, and the green numbers now included in the Google Earth image correlate to the photos shown in **Figure 47**. Transects 1-6 correlate to photos 1-6, photos 7-8 correspond to major changes in lithology seen in the field that do not have laboratory data, and photo 9 correlates to Transect 7.

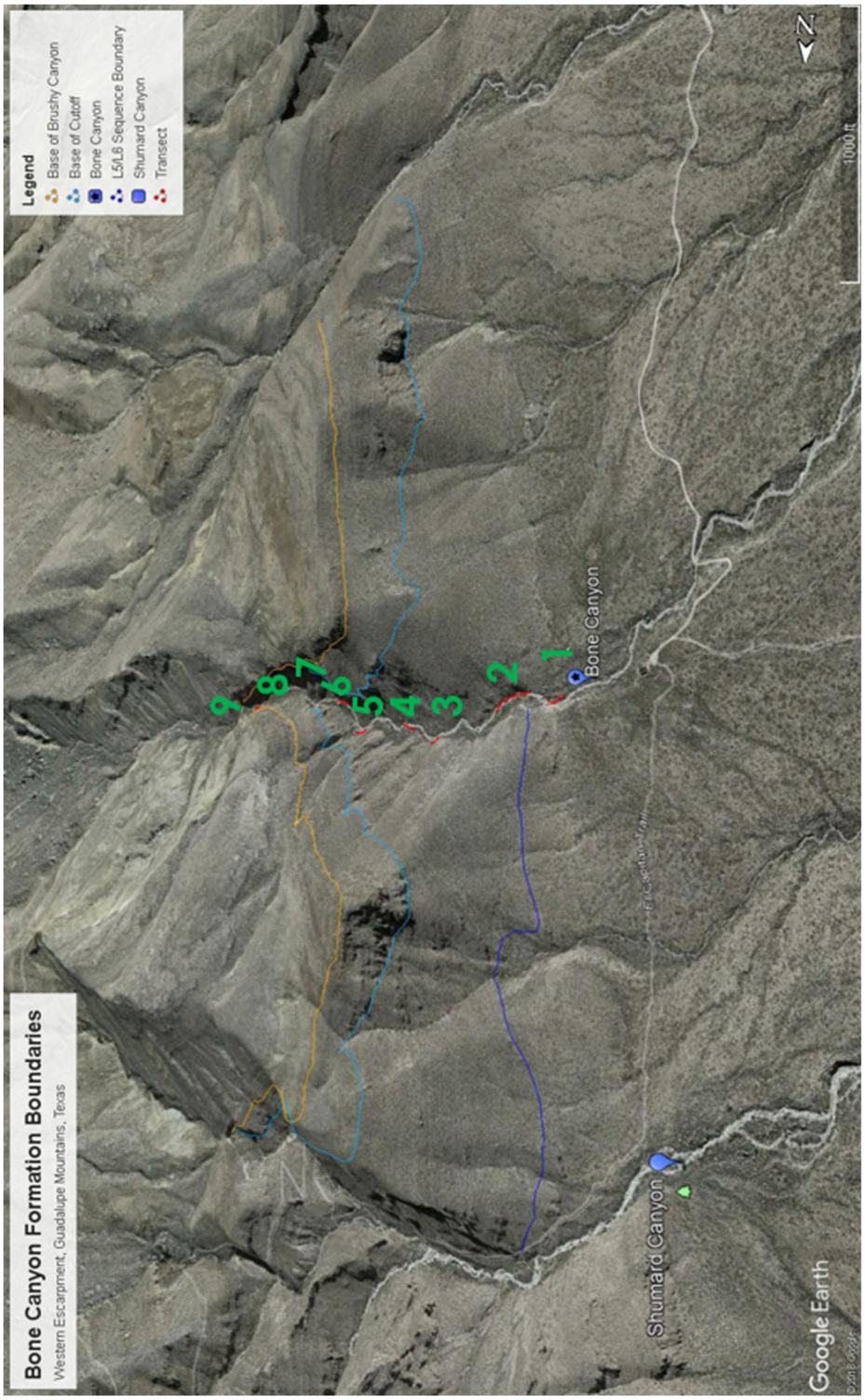

Figure 46: Google Earth image of Bone Canyon showing major boundaries, transect locations, and green numbers that correspond to the photos seen in the Figure below.

Figure 47: Field images of the major units within Bone Canyon. Location of each photo is seen in the Figure above.

The next processes, the purpose of this entire section, was the collection of XRF data through the entire canyon. As previously mentioned, U, Th, and K values were taken, converted to API, and made into a pseudo-gamma ray log seen below (**Figure 48**). By combining previous research, field results, and now XRF results, Bone Canyon was divided into its major units.

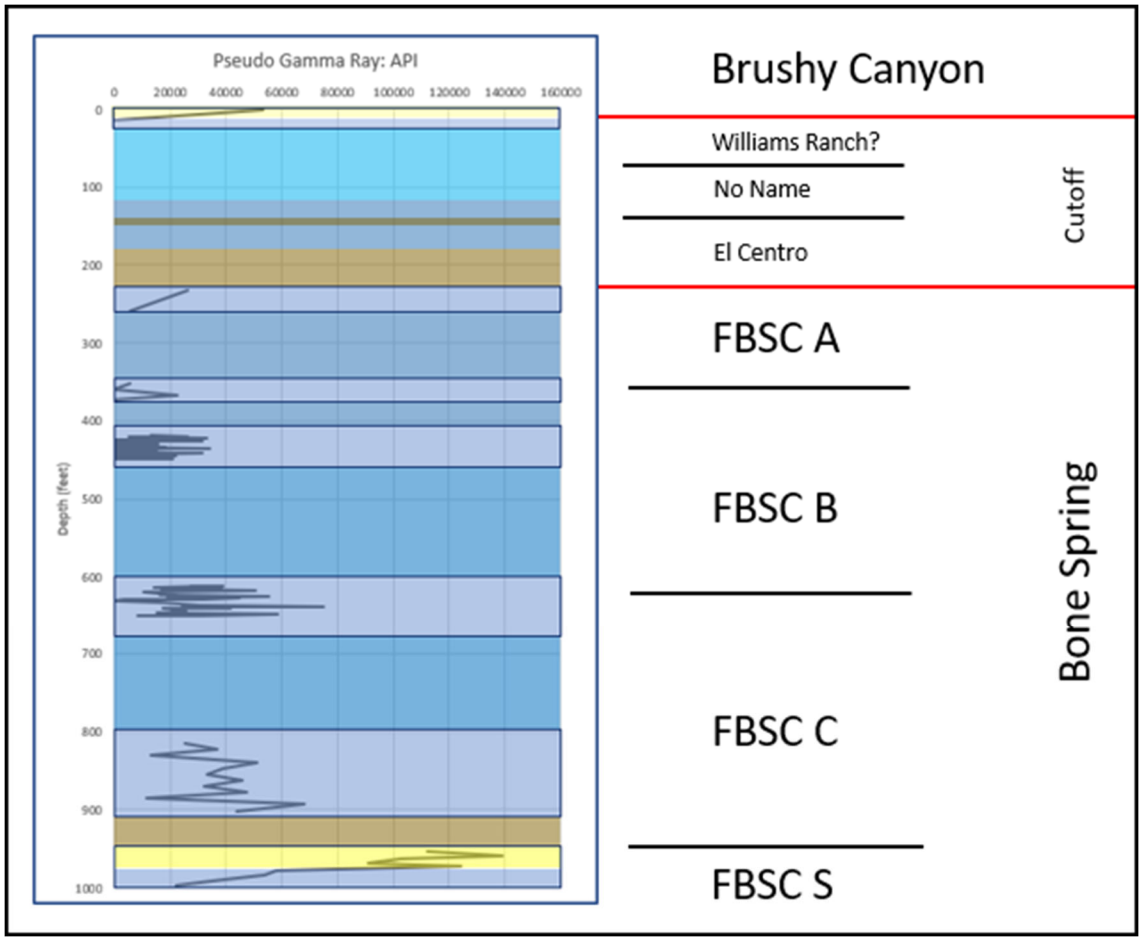

Figure 48: Bone Canyon Pseudo-Gamma ray Log displaying intervals with data (outlined with dark blue rectangles) and the units that make up the canyon.

As previously mentioned, it is important to get an overall understanding of the canyon before diving into each transect. This way the forest will be seen before getting lost in the trees. Bone Canyon represents ~ 4 Leonardian high-frequency sequences (L5-L8) and ~ 3-5 Guadalupian high-frequency sequences (G1-G4) depending on (lateral) position within the canyon. Position is an important factor because some HFS are channel bound, therefore are not present (laterally continuous) in certain areas of the canyon.

The Geologic Background and Sequence Stratigraphy sections of this thesis discuss trends that should be seen when looking at the bigger picture (lower-order) of the canyon. As

previously mentioned in these sections, the Bone Spring is the result of reciprocal sedimentation and is generally thought to represent eight 3rd order sequences deposited during a 2nd order regression, or perhaps a slight stasis. Bone Canyon outcrops do not show the entire extent of the Bone Spring Formation. Instead, the canyon begins within the First Bone Spring Carbonate, contains the Cutoff Formation (Leonardian-Guadalupian), and ends at the top of the canyon (relative to this thesis) with the earliest sands of the Brushy Canyon Formation.

Thus, from the explanation above, the Bone Canyon rock record contains the strata which include two 3rd order sequences of the Bone Spring Formation, which are the First Bone Spring Carbonate Sand and the First Bone Spring Carbonate (L5-L6), and four-six 3rd order sequences of the Cutoff and Brushy Canyon Formations (L7-G4), which contain several higher (4th-6th) order sequences. However, since there is not enough continuous data here to support interpretations of higher order depositional sequences, the interpretations from the data will be focused on the 3rd order sequences, though the higher order (4th-6th) cycles could be referred to and discussed. As previously mentioned, at the 3rd order depositional sequence scale, the Bone Spring Carbonate was deposited during a highstand in sea level. Subsurface work done on this formation often blend the sequences at the top of the formation, which is likely the result of seismic quality and/or interpretation. Outcrop investigation performed on this formation, however, provides true and precise lithological characteristics of the rocks. As seismic stratigraphy has improved through recent years, the results mentioned in this work have become more apparent. **Figure 49** shows the pseudo-gamma ray log for Bone Canyon in its entirety (as it relates to this thesis). From previous, recent research done on the Western Escarpment (Kerans (2016), Hurd and Kerans (2014), Kerans and Kempter (2002)), the field data collected in this

work, and now with the addition of laboratory work (i.e. XRF), a 3rd order sea level curve can be seen (left side of **Figure 49**).

Based upon previous works, the variations in lithology previously mentioned in the field results, a purposed sea level curve was created. The laboratory results will aid in confirming sea level cycles, depositional processes, and paleoenvironmental controls. Sea level fluctuations may have potentially caused the main variations in lithology. With this designated 3rd order sea level curve and the geochemical analysis, the 3rd-4th order high-frequency sequences can be determined. The correlation to this sea level curve will become more apparent, and corroborated, in the analysis below.

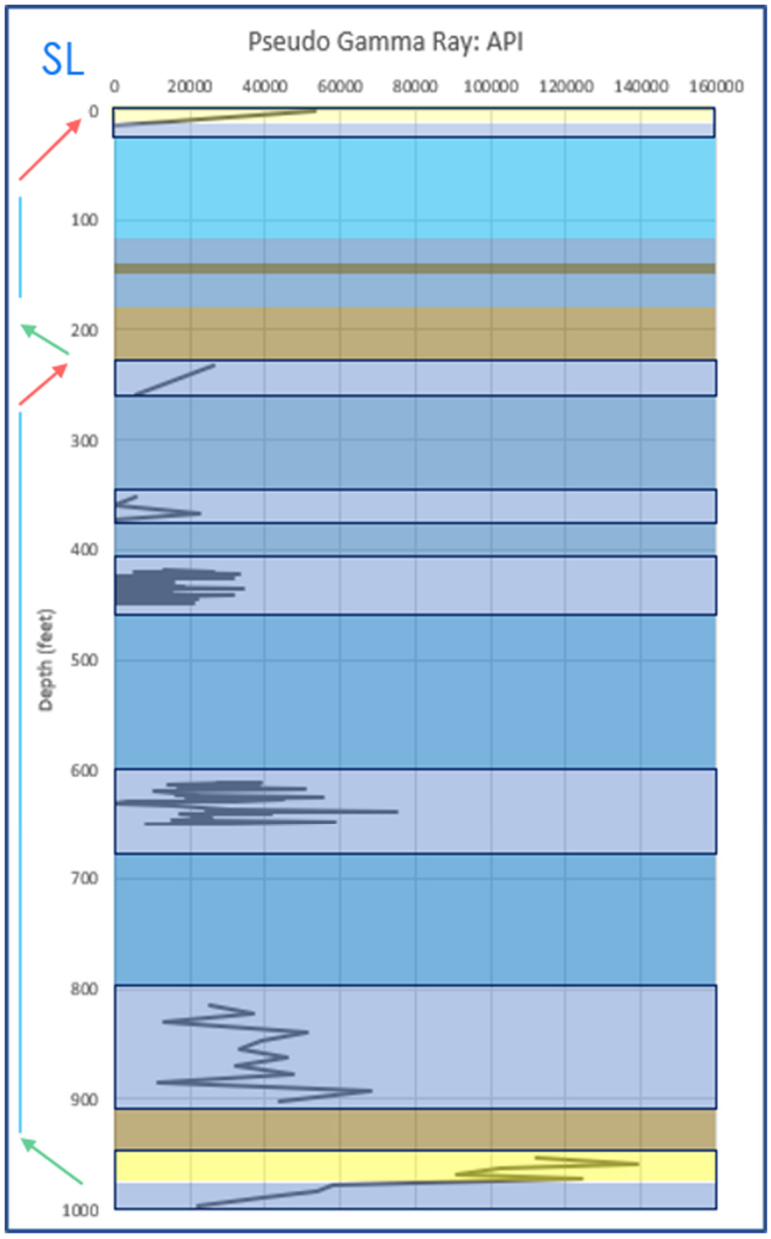

Figure 49: Bone Canyon Pseudo-Gamma Ray Log displaying general 4th order trends of relative sea level (left). Green arrows represent TST, red arrows RST, and blue arrows HST respectively.

From previous research in the area immediately to the north of Bone Canyon, as well as information in Bone Canyon, the L5 HFS of the Bone Spring Formation represents a TST and the L6 represents an HST (Kerans and Kempter, 2002). An important feature must be present at

Transect 1 for this to be the contact between the L5 and L6 high-frequency sequences. This feature, previously defined, is interpreted as a maximum flooding surface (mfs) and marks the furthest, landward position of sea level. This surface is a great correlating surface owing to its high API (pseudo-gamma ray) value and can be identified in the field because it is a mud/shale-rich interval that drapes over the underlying strata.

The L5 HFS is also identifiable, in close proximity to Bone Canyon (Shumard Canyon), by sandy units within a carbonate host-rock. The mouth of Bone Canyon contains a sandy unit, similar to the mouth of Shumard Canyon, further suggesting that this unit correlates to the L5 HFS. Immediately above, and seen in the pseudo-gamma ray, is a shale-rich interval that is from here on referred to as the mfs and is shown to separate the L5 from the L6 HFS. In some areas (Sierra Diablos), the L5 and L6 HFS are not easily differentiated. However, this mfs, along with geochemical analysis, provides further evidence of these two sequences.

The L6 HFS is observable throughout the Guadalupe Mountains and, specifically, the Western Escarpment. The L6 HFS corresponds to the maximum progradation of the Leonardian carbonate platform margin. Previous studies (Kerans and Kempter, 2002) show the platform margin extending (NW to SE) along the northwestern portion (relative to Bone Canyon) of the Western Escarpment and terminating somewhere near Shumard Canyon to the north. The location of Shumard Canyon, and specifically Bone Canyon, is extremely important. This slope-to-toe-of-slope location was subjected to numerous subaqueous erosional processes (i.e. debris flows and channel-cut routes bypassing the platform) causing underlying strata to be stripped from the record and, more importantly, the termination of the L6 platform margin. With the results from this thesis, the basinal portion of L6 HFS is shown to extend into Bone Canyon.

Depending on the research and order of investigation, the following phase is identified as the end of the L6 HFS (4th order) and is marked by a late regression, or is identified as the L7 LST (3rd order), however, occasionally research combines the L7 and L8 HFS into a 3rd-order TST. Regardless of where the fall in sea level is identified within an HFS, the important aspect of this time is that sea level fell. The work done in this study has determined this fall in sea level to be marked as the L7 HFS.

The L7 HFS is composed of megabreccia blocks inside of a carbonate-rich mudstone suggesting it was transported into the basin via debris flows. The resulting relative rise in sea level during the L8 HFS draped a mud/shale-rich unit over this megabreccia debris flow and is seen within Bone Canyon just above Transect 6. It is important to mention that the L7 and L8 HFS contact represents an intraformational contact within the Cutoff Formation, not the Bone Spring Formation. The L7 HFS is named the Shumard Member and the L8 (through G1.5) HFS is named the El Centro Member of the Cutoff Formation (Kerans and Kempter, 2002; Hurd & Kerans, 2014).

The G1 HFS (El Centro Mbr.) corresponds to a 3rd order highstand in sea level. This 3rd order highstand in sea level is considered to roll over into the G2 HFS, however, the G2 member has a lower 3rd order sea level than the G1 HFS, but with a relative 4th order highstand resulting in similar depostion. Hurd & Kerans (2014) separate the G2 member into two units. The lower half is related to the G1 HST and is therefore named the El Centro Mbr. The upper half of the G2 HFS, where (3rd and 4th order) sea level begins to fall ever so slightly, does not have a name other than "No Name". For the purpose of this study, this unit will, from hereon, be referred to as the "Pigott-Brown (PB) Mbr". The PB Mbr. of the G2 HFS (**Figure 50**) is seen just below Transect 7 in Bone Canyon as a clean carbonate mudstone. In Bone Canyon this unit displays

numerous bed couplets with a thick, less weathered bed followed by a thin, platy weathered bed. The overall weathering trend of this unit becomes less weathered up-section. These characteristics imply another interval of turbidite deposition.

Figure 50: Field image of the G2 "PB" clean, carbonate turbidites displaying numerous bed couplets (thick, less weathered and thin, weathered) becoming more resistant up-section. A meter stick is held by Dr. Pigott for scale.

As sea level continued to fall during the RST of the G3 HFS (not yet low enough for sediment bypass and clastic deposition), the slope and the carbonate platform margin once again became unstable. This instability lead to slope failure, causing large amounts of platform margin sediment and material, mixed with slope and basinal sediment, to be thrown onto the deeper

portions of the slope and into the basin. This debris flow, filled with unconsolidated, poorly sorted carbonate material and lithoclasts found its resting place near the toe-of-slope and, consequently, is seen at the lower half of Transect 7 as yet another conglomerate/megabreccia unit. This G3 HFS is combined with the upper half of the G2 HFS (RST) and, similar to the upper portion of the G2 HFS, the G3 HFS has no name so it is now named the PB Mbr.

The G4 HFS of Hurd & Kerans (2014), known as the Williams Ranch Member, is channel bound within the canyon and can be seen on the southern wall of Bone Canyon **(Figure 51)**. Since data was collected moving up-section in the canyon, rather than drilling a vertical well closer to the mouth of Bone Canyon's southern wall, this channel was not seen further to the south-east in the canyon's creek. Instead, the G5 HFS, now called the Brushy Canyon Formation, lays unconformably on the "PB Mbr." of the Cutoff Formation. The G5 HFS represents the early stages of an LST, in which sediment was able to bypass the carbonate platform margin, via subaqueous channels previously eroded from gravity flows of the G3 HFS, resulting in deposition onto the toe-of-slope and into the basin. The transport mechanism for the G5 HFS is determined to be subaqueous in origin owing to the large amounts of deformation seen within the very fine-fine grained sandstone in the top half of Transect 7 **(Figure 52)**. Briefly looking above this sand appears to be alternating units of sandstone and carbonate deposited by a higher-order (4^{th}-5^{th}) process of reciprocal sedimentation. These alternating units represent the high-frequency sequences of the Brushy Canyon Formation (G5-G8).

Now, with a good understanding of the "forest" (entire canyon: 3^{rd}-4^{th} order) in Bone Canyon, the "trees" (individual transects: 5^{th}-6^{th} order) can be seen clearly, analyzed in detailed, and well-understood. The goal while discussing each individual transect is to provide further evidence that supports the lower order sequences discussed above, to provide information

regarding higher order sequences within the Bone Spring Formation, and finally to correlate Bone Canyon to the subsurface. All of the results will then be combined in the conclusions to highlight the important features of Bone Canyon.

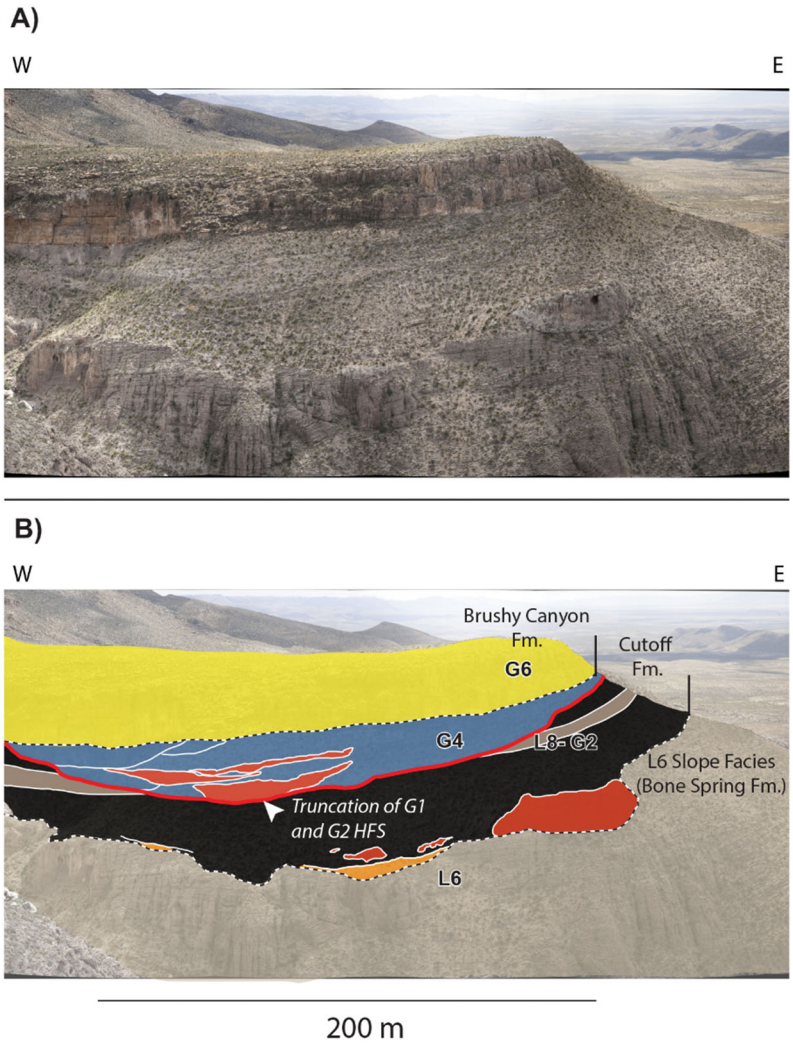

Figure 51: Image showing the stratigraphic interpretation of the L6-G6 HFS. The G4 HFS is channel bound on the southern wall in Bone Canyon. Taken from Kerans (2016).

Figure 52: Field image of the G5 HFS known as the Brushy Canyon Formation.

5.2.1 XRF

5.2.1.1 Transect 1 XRF

Figure 53 and **Figure 54** show the location of Transect 1 and the beds within it. The lithology log created from the XRF of Transect 1 is shown in **Figure 55**. This transect shows an important time during Bone Canyon deposition, which is composed of biogenic-silica-rich carbonate and is of interest because of its high clay and quartz content, which gives this unit the highest API, and terrestrial proxy, values seen in the canyon. The first 7 beds within this unit contain 35-50% dolomite, 40-50% clay, and 5-15% quartz/chert. Although the quartz concentration fluctuates, it is, in general, seen to gradually increase up-section. The same is true for clay concentration. Similarly, but opposite, dolomite concentration is seen to decrease up-

section. The high API values correspond to the increases in clay and quartz. This suggests that there is a change in depositional processes occurring here. This increase in clay and quartz, represented through an increase in API, suggests that sea level is changing (i.e. falling or rising).

In general, the API increases throughout transect 1. This suggests that the lower portion of the transect is primarily carbonate material with some siliciclastic influence. As sea level transgressed then fell during L5-L6 HFS, more siliciclastic material was brought into the basin via MTDs and debris (gravity) flows owing to an unstable slope. This is reflected in the pseudo gamma ray motif (increase in API) towards the top half of the transect. It is important to mention that the shale unit immediately above the siliceous package has the highest API readings. The transition from the TST to the HST resulted in a slight relative fall, however, sea level was still high, resulting in high siliciclastic material found within the carbonate-rich unit.

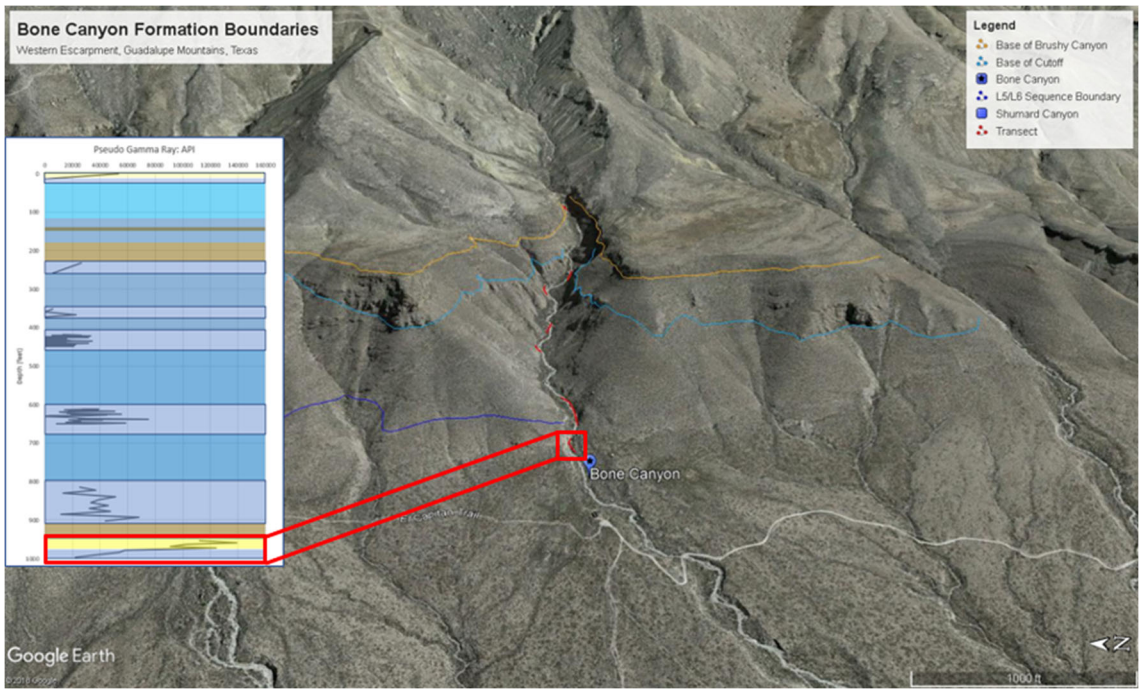

Figure 53: Google Earth image of Transect 1 location in Bone Canyon.

Figure 54: Field images of Transect 1 showing siliceous mudstone and shale units.

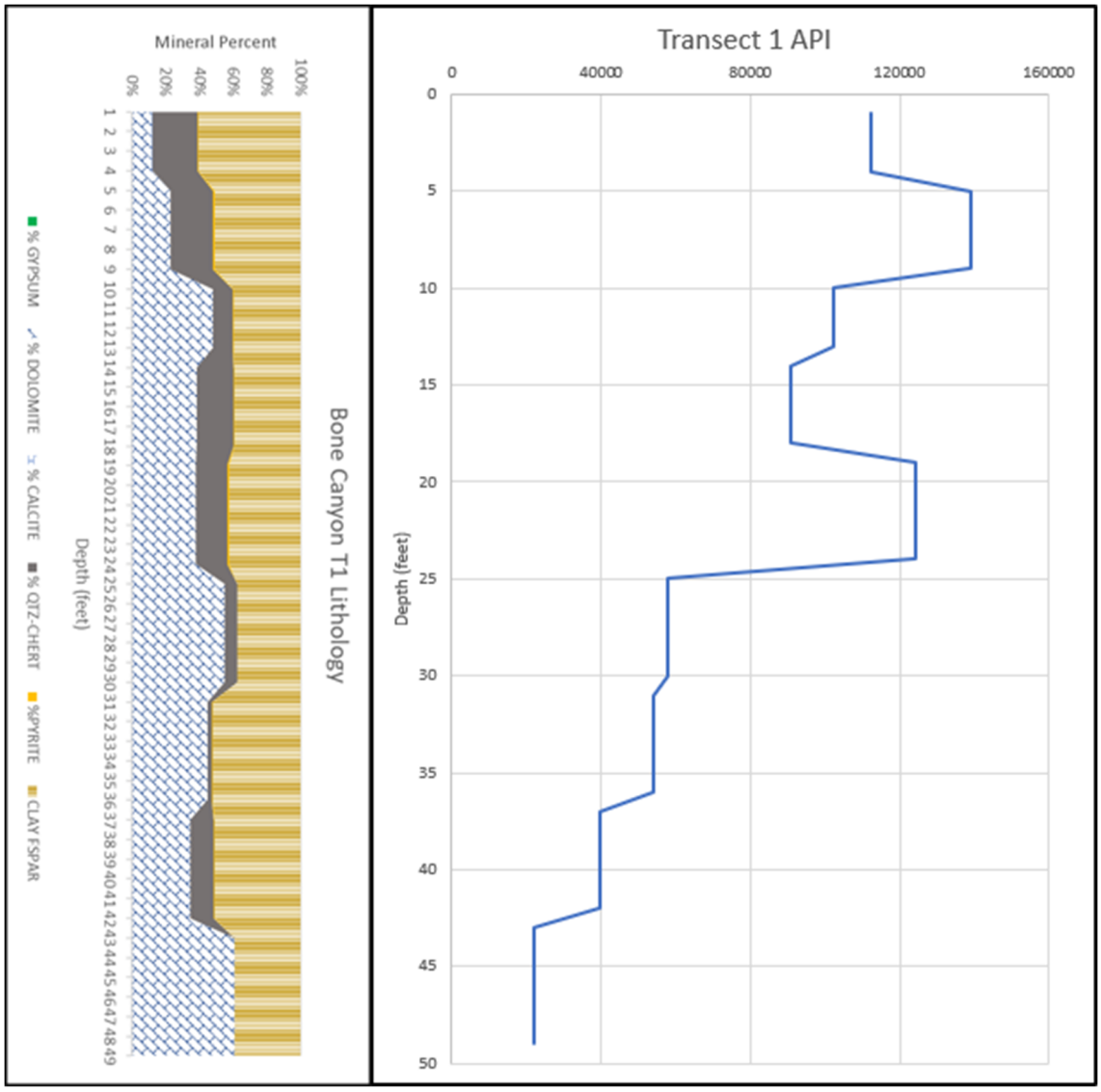

Figure 55: Transect 1 Lithology Log (left) and Pseudo-Gamma ray Log (right) generated from the XRF. T1 is from 954.35 to 1002.4'. T1 is 49' thick with 9 data points ~ 5.333' between points. Both logs were made using 1-foot intervals. T1 corresponds to the FBSC Sand and represents the Lower Avalon Shale and the transition from the TST of the L5 HFS to the HST of the L6 HFS.

5.2.1.1.1 Transect 1 Geochemistry

Advancements in technology, such as the hand-held XRF, has made data acquisition more affordable and efficient, especially in the field of inorganic geochemistry. A major advantage of the XRF is the ability to determine changes within rocks that are visually similar

(grain size, structure, color) through large vertical intervals. Using major, minor, and trace element abundances and ratios can enhance stratigraphic control within these "similar" vertical intervals (Smith and Malicse, 2010; Hornbuckle, 2015). Geochemical analysis of these rocks can identify the heterogeneities in rocks that appear homogenous (Slatt and Rodriguez, 2012; Hornbuckle, 2015).

Certain elemental proxies can provide information about a rock composition's paleoenvironment, provenance, depositional history, and depositional processes making it useful for stratigraphy (Crosby, 2015). Below are the geochemical proxy results from each transect. Conclusions of the results are made for each transect first and then are combined together for the overall conclusions of Bone Canyon.

Figure 56 shows API, U, Th, and K curves taken from Transect 1. These proxies used together show the sources of radioactivity. The spikes seen in the total pseudo gamma ray curve closely correlate to the spikes seen in the K curve. The trend in both curves is increasing upward. From point 9 to point 7, all curves show a positive covariance, however, API, U, and K are more positive. From 7-6, U and Th remain with a positive covariance, but are both negatively covariant with API and K. From 6-5 U joins back into the positive covariance with API and K, while Th is negative. From 5-3, all values display a positive covariance once again. From 3-2, U and Th remain with a positive covariance, but are both negatively covariant with API and K. From 2-1, Th joins back into the positive covariance with API and K, rather than U (as seen in 6-5). The trend that can be seen here is 1) all positive, 2) Th and U negative covariance with API and K (positive with each other), 3) Th is negative with all, 4) all positive, 5) Th and U negative covariance with API and K (positive with each other), 6) U is negative with all. If Th had been negative at the top of the section, instead of U, the trend would be cyclical. Instead, the trend

changes, however, it is still somewhat cyclical. The last part of the cycle, however, alternates with a positive covariance of API, K, and U or API, K, and Th. This means that the influence of U and Th alternate at the end of each cycle. U is more influential in the older beds and Th is more influential in the younger beds.

API and K are more positive with U until point 7. API and K are only positive, together, at point 6. From 7-6, both API and K values seem to slightly increase, but at a much lower rate than previously. The lower rate of increase in API and K likely corresponds to the drop in Th and U values. U has a drastic fall while Th slightly falls. Although API and K increase, perhaps they are more influenced by Th from 7-6, instead of U, and therefore API and K values do not spike. From 6-5 API and K return to being influenced more by U and therefore show an increase. Although subtle, Th values have a greater fall from 5-4 than U, which is then reflected by a drastic fall in API and K. From 4-3 Th increases and, while U increases as well, it does not increase as much, which closer resembles the slight increase in API and K. From 3-2 API and K show negative covariance with both U and Th. From 2-1, API and K show positive covariance with Th. then more positive with U from 6-5. API and K show positive covariance with both U and Th from 5-3, then negative covariance from 3-2. From 2-1, Th shows positive covariance with API and K. from 6-than Th (Th shows more negative covariance). The shale interval has the highest values of API and K, but lower U and Th values. Overall, U and Th have a positive covariance and API and K have a positive covariance.

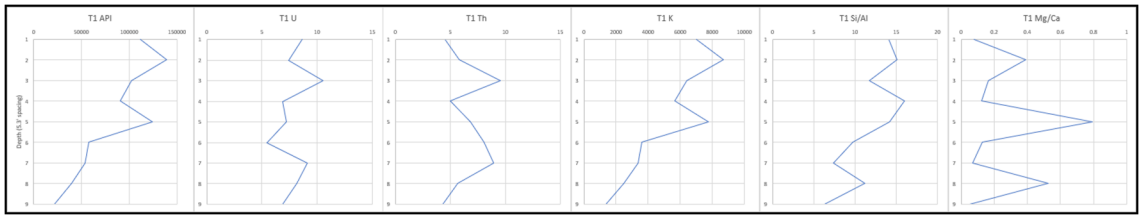

Figure 56: Transect 1 total pseudo gamma ray (far left) for the Bone Canyon. Sources of radiation seen in U, Th, and K curves from left to right. Si/Al and Mg/Ca ratios are also provided, respectively. 5.333 ft spacing. Element concentration in PPM.

The clastic proxy suite for Transect 1 **(Figure 57)** is very significant. Transect 1 represents a carbonate and siliciclastic rich unit. Ti, Zr, Si/Al, and K are generally seen to be gradually increasing. Si and Al appear to be fairly stable, however, Al appears to be slightly decreasing. Ti increases from 8-5, while Al decreases. Si, Ti, and K show increasing spikes at point 5. From 5-3, Zr has a large increase, while Ti, Si, Al, and K generally decrease. Si/Al appears to be increasing meaning that the Si is most likely biogenic, or at least becoming more biogenic. An increase in the terrigenous proxies indicates an increase in terrigenous sediment. An increase in terrigenous proxies alongside an increase in biogenic silica suggests a process that brings in terrigenous proxies during an increase in carbonate pelagic production. Carbonate production, in this case, may be accompanying a nutrient increase when sea level and clastics were introduced.

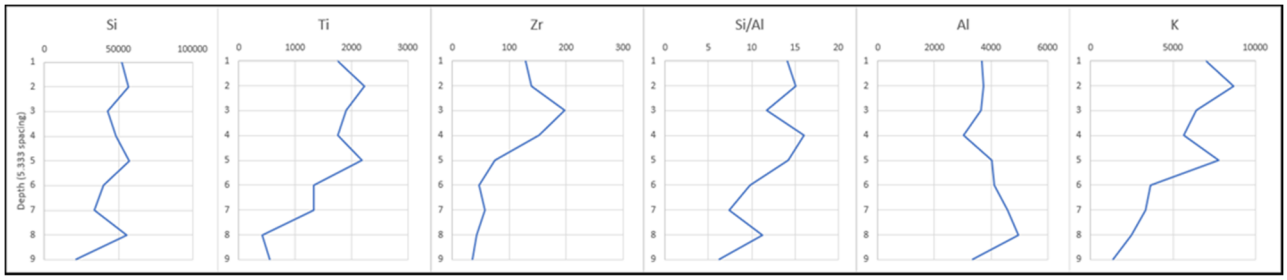

Figure 57: Clastic, clay composition, lowstand proxy suite for the Bone Canyon Transect 1. Outcrop displaying Si, Ti, Zr, Si/Al, Al, and K curves generated from the XRF from left to right. 5.333 ft spacing. Element concentration in PPM.

The carbonate proxy suite for Transect 1 is shown in **Figure 58**. P and Ca almost mirror one another (negative covariance), however, display some differences, but they both show decreasing trends. P and Ca show positive covariance at 7-6 and 4-3. It appears Ca and Sr have a positive covariance until the last interval (2-1). So, P, Ca, and Sr, are positive at 7-6 and 4-3. Mg shows positive covariance with Ca and Sr from 9-7, 6-5, and 4-2. From 7-6 Mg has a spike increase with the only other increase (although small) being Mn. Mn shows a positive covariation with P except at 7-6 (positive with Mg) and 2-1 (positive with Ca). The highest peak in Mn corresponds to a high in P and a low in Ca. Ca and Mg appear to show the greatest decrease throughout transect 1. P and Sr are both decreasing, but not much. Mn appears to be increasing to point 5, then a large decrease from 5-4, but then starts to slightly increase again from 4-1 Ca, Sr, and Mg show positive covariance.

The main aspect is that P, Ca, Sr, and Mg gradually decrease upwards. Mn is the only proxy that has a general increasing trend.

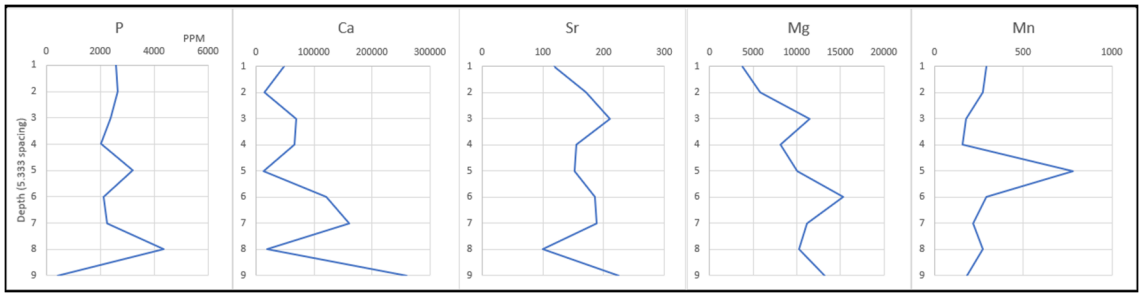

Figure 58: Carbonate, composition, highstand proxy suite for the Bone Canyon Transect 1. Outcrop displaying P, Ca, Sr, Mg, and Mn curves generated from the XRF from left to right. 5.333 ft spacing. Element concentration in PPM.

The paleoredox, basin restriction, and paleoenvironment proxy suite is shown in **Figure 59**. Mo and Cu steadily increase to point 7, but then fall to point 4, increase to point 3, and then decrease to point 2 showing a positive covariance except from 2-1. Ni has a very similar trend to Mo and Cu, however, changes in Ni seem to precede the same changes in Mo and Cu except at point 1 where Ni has a positive covariance with Mo. Cu and U show positive covariance, however, when Mn* spikes at point 5, U increases as Cu decreases (negative covariance). At point 6, Mn* causes U to have negative covariance with Mo and Cu. From 3-2, all decrease except V and Mn*. Mo, Cu, and U are positive except at 5 (U negative) and 1 (Mo negative). Ni is affected by Mn* at 8-7. Mn* affects U from 6-3. Overall, U and Mn* are generally increasing, while Mo, Ni, and Cu decrease.

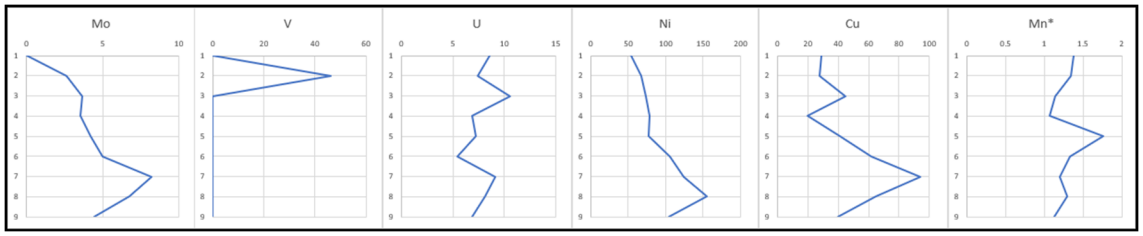

Figure 59: Paleoredox, basin restriction, and paleoenvironment proxy suite for the Bone Canyon Transect 1. Outcrop displaying Mo, V, U, Ni, Cu, and Mn curves generated from the XRF from left to right. 5.333 ft spacing. Element concentration in PPM.

At this scale, these observed changes reflect high orders (5^{th}-6^{th}). Unfortunately, without having the full L5 HFS in outcrop, it is impossible to know the amount, and extent, of sequences for sure. The top of Transect 1 may reflect one 5^{th}-order sequence that corresponds to the relative, and relatively rapid, fall in sea level that marks the L5 and L6 HFS boundary.

5.2.1.2 Transect 2 XRF

For reference, the location of this transect in Bone Canyon and within the overall pseudo-gamma ray log is shown in **Figure 60** with the lithology and pseudo-gamma ray log for Transect 2 shown in **Figure 61**. At Transect 2 the beds alternate between limestone and chert. This is another indication of the Middle Avalon. The Transect 2 beds, 9-7 are chert and 6-5 are limestone, other than that they alternate.

This transect displays low-to-moderate PsGR values with no distinct vertical trends, however, not seeing vertical trends is likely owing to the lack of available data. The highest value at Transect 2 is 68429 API at 11’ with the lowest value reaching 11468 API immediately following at 10’ showing a difference of 56,960 API. The average API at Transect 2 is 37,344 API- about 45,000 API lower than (older) Transect 1 and about 10,000 higher than (younger) Detailed Section 2 (Transect 3). It is important to note that in these carbonate rich deposits it is still possible to see interbedded facies in logs owing to the high contrast in the PGR values.

Limestone beds correlate to lower API readings while the chert beds correlate to, in general, higher API values. In general, when moving up-section in T2, the pseudo gamma ray readings for the chert beds are decreasing. This causes an overall general decrease in API throughout the transect. In general, the chert beds also contain higher concentrations of dolomite, k-spar, and clay minerals. In contrast, the limestone beds contain lesser concentrations of dolomite, k-spar, and clay minerals. Points 9-7 are chert beds, however, owing to a decrease in dolomite (slight decrease in k-spar and clay minerals) at point 8 there is a decrease in API. A similar, opposite, observance can be made in the limestone beds of points 6 and 5. Although they are both limestone beds, an increase in dolomite, chert, and clay minerals causes the bed of point 5 to show an increase in API. It is important to mention that overall API values seem to be decreasing up-section, or are reaching lower values. As we move up-section the chert beds are becoming more pronounced.

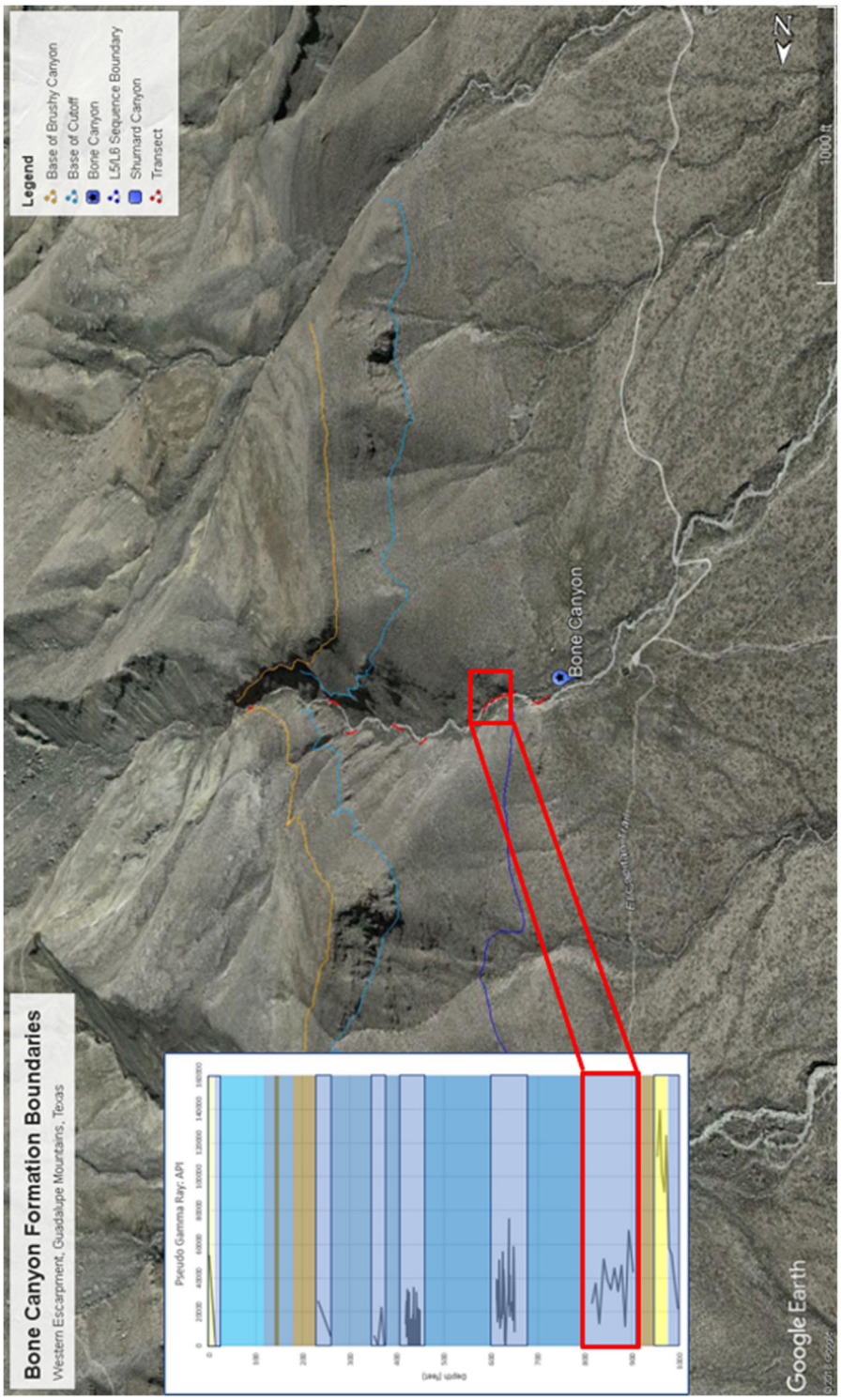

Figure 60: Google Earth image of Transect 2 location within Bone Canyon.

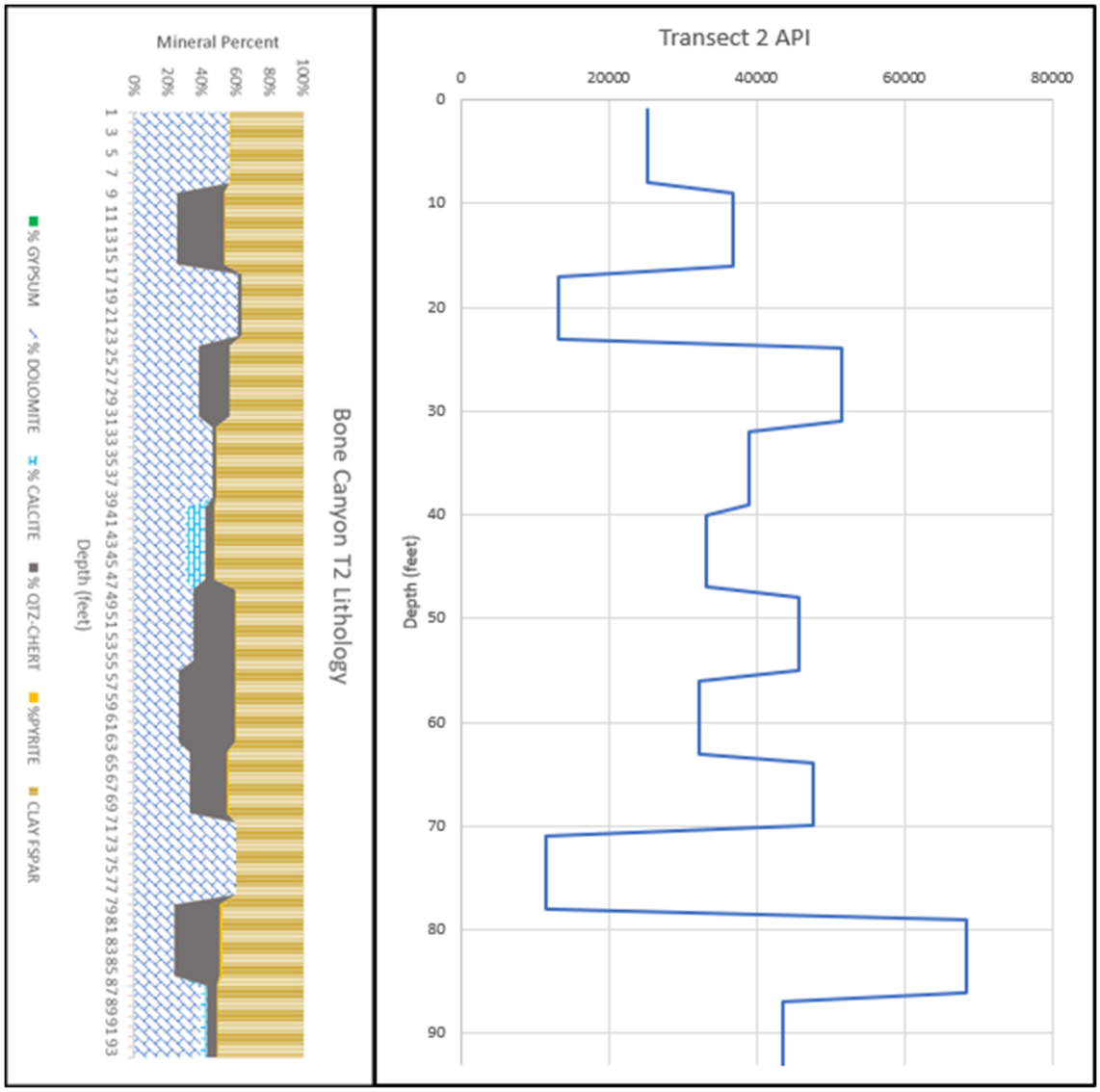

Figure 61: Transect 2 Lithology Log (left) and Pseudo-Gamma ray Curve (right). T2 is from 909.35'-815.35'. T2 is 94' thick with 12 points ~ 7.833' per point. T2 corresponds to the HST of the L6 HFS, the FBSC A, and the Middle Avalon (carbonate).

5.2.1.2.1 Transect 2 Geochemistry

The figures below **(Figure 62-Figure 65)** show the various proxy suites used in this work for Transect 2. The first proxy suite includes API, U, Th, and K to determine sources of radiation. The Second suite displays the clastic/terrestrial proxies including Ti, Zr, Si, Si/Al, Al, and K. The third suite contains the carbonate proxies including P, Ca, Sr, Mg, and Mn. The final

suite displays the paleoredox proxies including Mo, V, Ni, Cu, U, and Mn* (normalized with Fe- see Geochemistry methods). In general, the low spikes correlate to limestone beds while the high spikes correlate to chert beds.

API displays a positive covariance with U until point 9, then API is positive with both U and Th from 9-7. API is only positive with K from 7-6. API shows positive covariance with Th from 6-5, then U from 5-4, then both U and Th from 4-3, then only Th from 3-2. From point 2-1, API is only covariant with K. API, always positively covariant with K, alternates positively with U and Th. The positive covariance with API seen here is with (from oldest to youngest) 1) U, 2) Th and U, 3) K, 4) Th, 5) U, 6) U and Th, 7) Th, 8) K. Although not cyclical, a pattern can still be somewhat seen. Beds alternate with main sources of radiation. All beds reflect K values; however, some reflect U and Th, separately and together, more than others. Beds either show radiation from only U (and K), U and Th (and K), only K, only Th (and K). As previously mentioned, K has the biggest influence on API values, however, U and Th add to the influence in various forms. U is covariant with both Si/Al and Mg/Ca ratios.

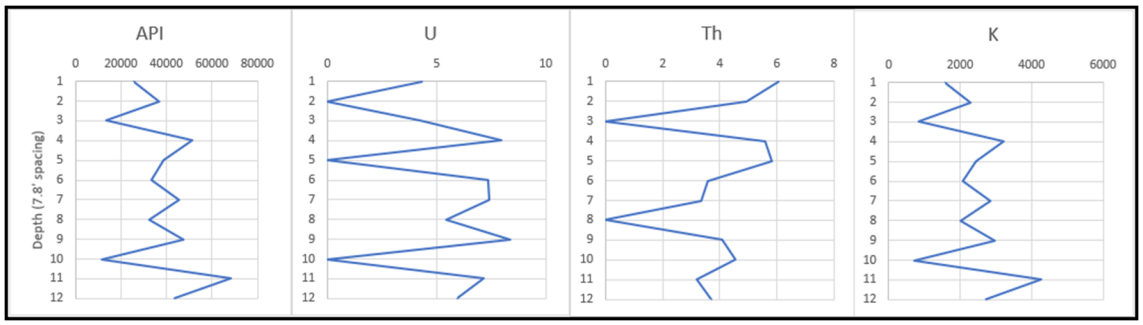

Figure 62: Transect 2 Radiation Proxy Suite. API curve is shown on the left with the sources of radiation (U, Th, and K) to the right, respectively.

Figure 63 illustrates the clastic proxy suite for Transect 2. Ti and Zr show positive covariance at 12-10, 8-6, and 3-1. Ti and Zr do not fluctuate as much as the other clastic proxies. Overall, it appears that clastic proxies are decreasing. Si and K are positive except from 9-7. Si and Al have a positive covariance from 7-5 and 4-2.

Ti, Zr, and Si display decreasing upward trends. Si/Al and K are fairly constant throughout. Al remains constant during the lower half of the transect, but then increases upward from 6-5, and eventually decreases after 5. This transect displays a fairly constant concentration of terrigenous proxies; however, they appear to be decreasing overall. The terrigenous proxies are lower, overall, than the previous transect.

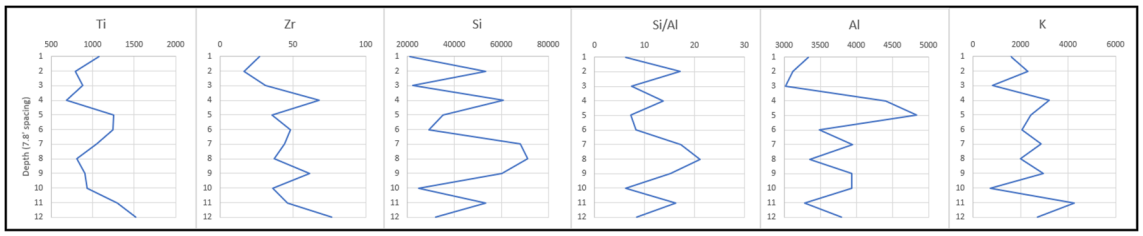

Figure 63: Transect 2 Clastic Proxy Suite displaying concentrations of Ti, Zr, Si, Si/Al, Al, and K, respectively.

Figure 64 reveals the carbonate proxy suite for Transect 2. Similar to the previous transect, P and Ca appear to mirror each other (negative covariance). From 12-9 and 7-1, Ca and Sr have a positive covariance. Mg and Mn show a negative covariance from 12-9, a positive covariance from 8-7, then have a negative covariance from 7-1. Si/Al and Mg/Ca have a high positive covariance except at point 7 when Si/Al decreases and Mg/Ca increases (negative covariance).

The trend in the Ca carbonate proxy appears to be more increasing. Sr and Mg fluctuate, but seem to remain fairly constant. Mn appears to be increasing overall, but remains fairly constant here as well. P is unique in that, although it remains fairly constant, it shows a decreasing trend overall.

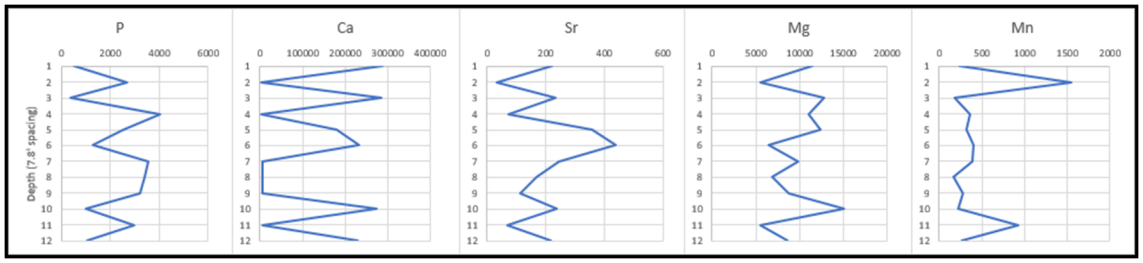

Figure 64: Transect 2 Carbonate Proxy Suite displaying concentrations of P, Ca, Sr, Mg, and Mn, respectively.

Figure 65 displays the paleoredox proxy suite for Transect 2. The results below are similar to the previous transect. Cu and Ni are positive from 12-9, then Cu is similar to U and Mo. Ni seems to precede changes in Cu in some cases. From 5-1 Cu and Ni and Mo are positively covariant. Mn* is pretty constant throughout with two main spikes at 11 and 2. U and Mo have a strong positive covariance from 12-3. V shows a positive relationship at point 4 with U. Transect 2 paleoredox proxies fluctuate, but overall, they remain fairly constant overall.

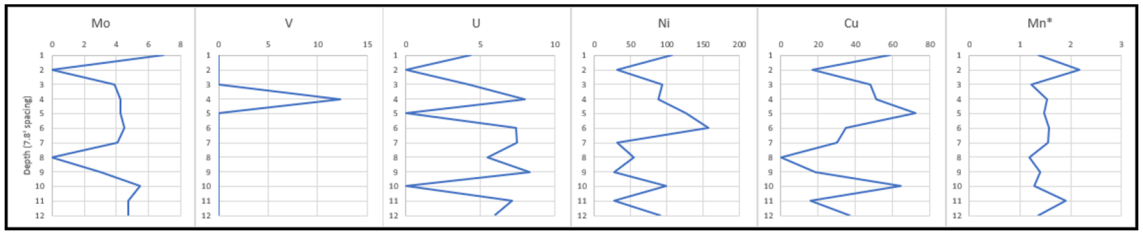

Figure 65: Transect 2 Paleoredox Proxy Suite displaying concentrations of Mo, V, U, Ni, Cu, and Mn*, respectively.

The fact that more data was collected at Transect 2 allows a better look, than before, into possible higher order sequences. API values, although overall decrease, appear to show two higher-order (5^{th}-6^{th} order) sequences. In comparison to Transect 1, Transect 2 values appear to be in par with the lower portion of Transect 1. It is possible that after the transition from the L5-L6 HFS, similar depositional patterns would resume.

5.2.1.3 Transect 3 (Detailed Section 2) XRF

Figure 66 is a Google Earth image of the location of Transect 3 and its location within the overall pseudo-gamma ray log. **Figure 67** shows the Pseudo-Gamma ray Log in feet, while **Figure 68** includes the Lithology Log at 1-foot intervals. Similar to Transect 2, the beds show alternating beds of limestone and chert. As throughout the canyon, the carbonate beds are thicker than the chert beds. Here, the chert beds appear to be more weathered than previous transects. Similar to the profiles before, the carbonate beds contain high concentrations of dolomite. When chert is the primary component, quartz is more prominent. In general, where calcite is present in the carbonate beds, there appear to be higher concentrations of clay minerals. It is also important to note that the chert beds, in general, contain a larger percentage of feldspars and clay minerals compared to the dolomite-rich carbonate beds, which is likely the reason the beds were subjected to more weathering. Calcite, although only appearing a few times, appears to be increasing. Calcite concentration is highest around 16 feet.

When looking at the PGR profile, four 5^{th} (or 6^{th}) order cycles can be seen. Each cycle begins with a “stair-stepping” spike in API followed by a pretty drastic “stair-stepping” decrease in API. API values in DS2 reach much lower values than the previous transects (>10,000). The

maximum value is 75,180 API at 27.42’ and following it in the “stair-stepping pattern” is the minimum value reaching 3,527 API at 19.83’ showing a difference of 71,654 API. The average value for DS2 is 27,887.5 API- about 10,000 API lower than (older) Transect 2 and about 16,000 API higher than (younger) Detailed Section 1 (Transect 4).

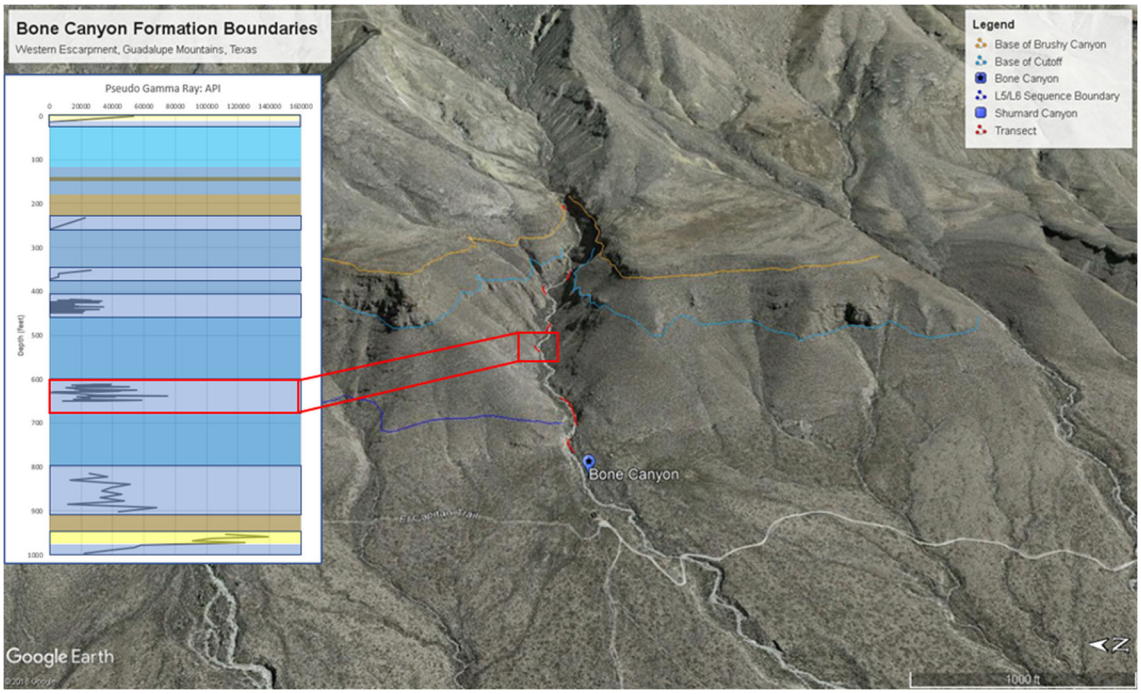

Figure 66: Google Earth Image showing Detailed Section 2 (Transect 3) Location and Pseudo-Gamma Ray.

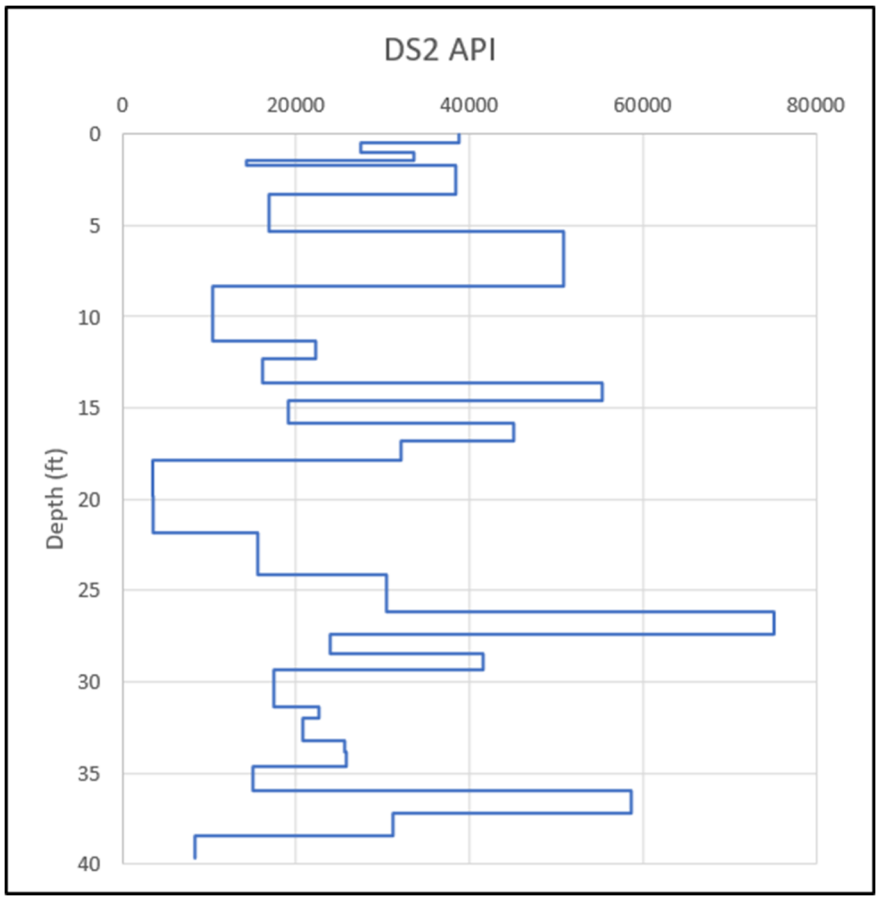

Figure 67: Transect 3 (DS2) Pseudo-Gamma Ray curve created from the XRF. DS2 is from 611.85' to 675.35'. Only 39.67/63.5' measured was accessible enough to collect data. Y-axis displaying bed thickness and individual transect depth. DS2 corresponds to the HST of the L6 HFS, the FBSC B, and the Middle Avalon (carbonate).

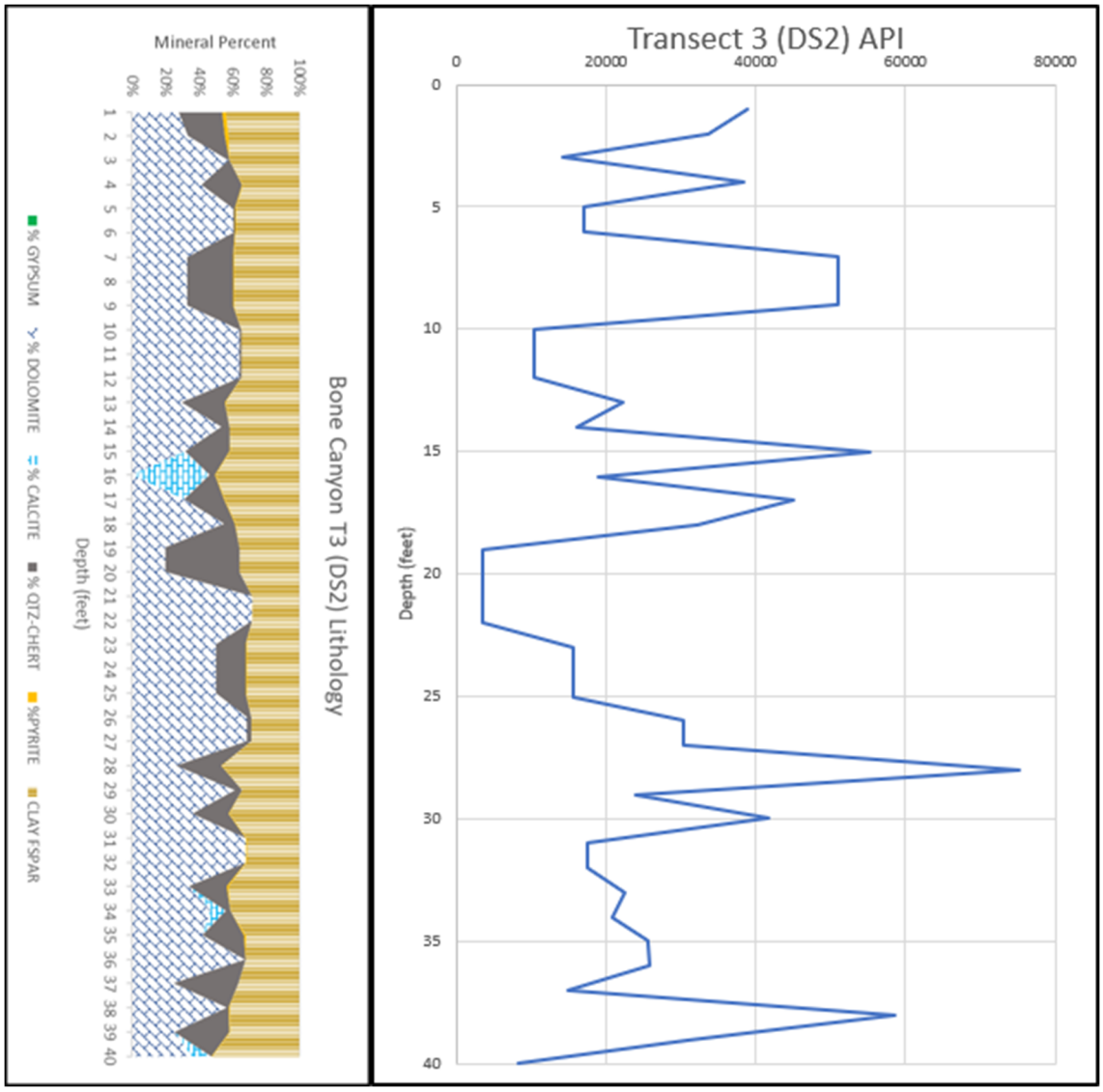

Figure 68: Transect 3 (DS2) Lithology Log (left) and Pseudo-Gamma Ray Log (right). T3 shows alternating beds of carbonate and chert deposited as carbonate turbidites that correlates to the HST of the L6 HFS, the FBSC B, and the Middle Avalon (carbonate). Log depths were converted to 1-foot intervals for visual and correlation purposes.

5.2.1.3.1 Detailed Section 2 (Transect 3) Geochemistry

Figure 69-Figure 73, as well as Appendix A, display the various proxy suites used in this work for Transect 3 (Detailed Section 2). The first proxy suite includes API, U, Th, and K to determine sources of radiation. The Second suite displays the clastic/terrestrial proxies including Ti, Zr, Si, Si/Al, Al, and K. The third suite contains the carbonate proxies including P, Ca, Sr, Mg, and Mn. The final suite displays the paleoredox proxies including Mo, V, Ni, Cu, U, and Mn* (normalized with Fe- see Geochemistry methods).

Overall, API is lower than the previous two transects. This is interesting because Transect 3 Th concentrations reach higher levels than any other transect. Also, U concentrations reach higher levels than the previous transects. Average U values increase from the previous transect, but are still lower than Transect 1. Average Th values here actually decrease from the previous two transects, but only slightly vary from Transect 2. Average K values continue to decrease from both Transect 1 and Transect 2. Average U concentrations increase from the previous transect, average Th concentrations slightly decrease, and average K concentrations decrease. From T2-T3, in general, U and Th alternate between positive and negative covariance. The large spike increase in U has a negative covariance with Th, but a positive covariance with K. The large spike increase in Th has a negative covariance with U, but a positive covariance with K and API. API and K concentrations between Transect 2 and Transect 3 are fairly similar, however, concentrations of U and Th at Transect 3 are closer to the following transect (Transect 4). After Transect 2, U, Th and K visually appear to increase. It is important to mention that, although they all visually increase, U on average, only increases.

Average Si concentrations at Transect 3 continue to decrease from the previous transects. Similarly, average Ti, Zr, and Al concentrations also continue to decrease from the previous transects. The average decreases in Al concentration, along with the decrease in Si concentration,

effect the change in the Si/Al ratio. From T1-T3, average Si/Al increases. This is important because Si/Al suggests the source of silica. From T1-T3 the system shows an increase in biogenic silica, suggesting high carbonate production. It is interesting to mention that at Transect 4 (and to Transect 5) the biogenic silica decreases. Other than Transect 6, Transect 3 has the highest average Si/Al ratio. It is possible that Transect 5 and Transect 6 may also represent a decrease from Transect 3 and Transect 4, but because the amount of data collected at Transect 5 and Transect 6 is much less than T3-T4, the results may be slightly skewed.

Average P concentrations continue to decrease from Transect 1 and until the following Transect 4. Average Ca concentrations continue to increase from Transect 1 and until the following Transect 5 (T1-T5). Average Sr concentrations increase from Transect 1 to Transect 3. It is important to mention that average Sr concentrations decrease from Transect 3-Transect 5 (T3-T5). Average Mg concentrations decrease from Transect 1 to Transect 3, but then increase at Transect 4. Average Mn concentrations increase from Transect 1-Transect 2 and then gradually decrease from Transect 2 until Transect 5. The average Mg/Ca ratio increases from Transect 1-Transect 2, decreases from Transect 2-Transect 3, then increases from Transect 3-Transect 4.

In general, Si, Si/Al, Ca, Mg, and Mg/Ca gradually increase from Transect 1-Transect 3. General decreases from Transect 1 to Transect 3 are seen in API, K, Ti, and Zr. Proxies that may show a slight trend, but in general remain fairly constant from Transect 2 to Transect 3 are U, Th, and K. U and Th originally decrease from T1-T2, but slightly increase from T2-T4. A unique variation at Transect 3 is shown in the Si/Al ratio, which contains the highest values reached. API and K values also reach higher values than all other transects, except for Transect 1.

Transect 3 is similar to Transect 4 although some proxies slightly increase and decrease between the two transects. This suggests that Transect 1 was uniquely deposited compared to all

other transects, however, the overall depositional environment was similar to that of Transect 2. Furthermore, Transect 3 and Transect 4 were likely deposited in a similar environment. From the proxies, especially API, U, Th, K, Ti, Zr, Ca, Mg, Mg/Ca, Si, Al, and Si/Al, it is seen that the environment of deposition from T1-T3 was fairly similar, however, different processes were occurring within that environment. The environment between T1-T3 is associated with a relatively high sea level (highstand). The depositional processes vary owing to fluctuations within this highstand. At Transect 1, the slope became unstable and caused gravity flow processes that likely caused more siliciclastic material to reach the basin. This siliciclastic material caused significant increases in radiation and terrigenous proxies; however, it does not imply that the sea level was low during this time. During the ensuing highstand, carbonate production was high, which provided enough carbonate sediment to allow the system to prograde basinward. This progradational phase is seen by the gradual changes in, primarily carbonate, proxies. In general, carbonate proxies gradually increase, while terrigenous proxies generally decrease.

Progradation causes Si/Al concentrations to reach higher values at Transect 3, but the high values are fairly constant compared to Transects 2 and 4. Transect 3 also reaches higher concentrations of Ca and Mg than the previous transects. The Mg/Ca ratio at Transect 3 is similar to Transect 2 and Transect 4, however, it is lower than both transects. The combination of higher Ca, Mg, Si, and Si/Al with a lower Al, Ti, Zr and API suggests Transect 3 represents a continuing progradation from the previous transects.

When looking at the API (pseudo-gamma ray curve) in **Figure 69**, four 5^{th} (or 6^{th}) order cycles can be seen. Each cycle begins with a “stair-stepping” spike in API followed by a pretty drastic “stair-stepping” decrease in API. As is the case throughout Bone Canyon, API has a

strong positive covariance with K (mimicking one another). API values in DS2 reach much lower values than the previous transects (>10,000). The maximum value is 75,180.8 API at 27.42' and following it in the "stair-stepping pattern" is the minimum value reaching 3,527.04 API at 19.83' showing a difference of 71,654 API. The average value for DS2 is 27,887.5 API- about 10,000 API lower than (older) Transect 2 and about 16,000 API higher than (younger) Detailed Section 1 (Transect 4). Similar to API, U, Th, and K also display high-order sequences.

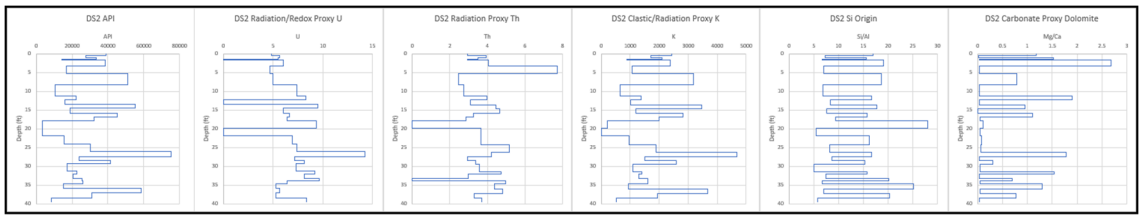

Figure 69: Transect 3 Radiation Proxy Suite displaying API values and the sources of radiation (U, Th, K) to the right. The Si/Al and Mg/Ca ratios to the right of sources of radiation are also shown to aid in understanding the depositional processes.

Figure 70 illustrates the clastic (terrigenous) proxy suite for Transect 3 (Detailed Section 2). The curves have been altered so that they display the individual bed thickness of each bed and the concentrations of each elemental proxy contained within the bed. Ti and Zr show a positive covariance throughout the transect with some minor variations. The lower part of this transect shows a positive covariance with Ti and K, while the upper part of this transect shows more of a positive covariance between Zr and K. Overall Ti displays an increasing trend, not only within the chert beds, but also in the carbonate beds, which results in an overall increase throughout. Zr is shown to have a gradual increasing trend during the bottom (first) third, a sharp decrease and increase in the middle, and then an overall decreasing trend in the last third. Al shows an

opposite gradual decreasing trend upward for the first half and then it begins to decrease in the last half. The same is true for Si. Si/Al, however, is fairly constant throughout with a subtle decrease and then a subtle increase after the spike increase. The large spike increase in Si/Al reflects a moderately high Si concentration and a very low Al concentration, thus high Si/Al. Cyclical decreasing (bottom half) and then increasing trends (top half) of the section are seen in Si/Al, Si, Al, and K. Reversely, cyclical increasing and then decreasing trends are seen in Zr and K.

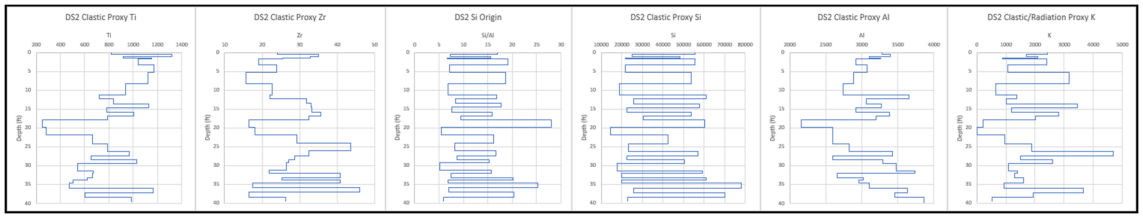

Figure 70: Transect 3 Clastic Proxy Suite displaying Ti, Zr, Si/Al, Si, Al, and K, respectively.

Figure 71 displays the carbonate proxy suite for Transect 3. From left to right, the proxies used for this suite are as follows: Mg/Ca, Ca, Mg, P, Sr, and Mn, respectively. Mg/Ca is gradually increasing in the carbonate beds, while the silica-rich beds contain none. Ca is shown to gradually increase and then decrease in carbonate beds. This is also true within the silica-rich beds. Mg appears to slightly increase, then decrease (top 7/8ths). P is shown to decrease the first (bottom) half and then increases. Sr in the silica beds and, in general, the carbonate beds shows a gradual decrease throughout. Mn displays a negative covariance with Sr, except positive with the spike increase and the earliest stages of the top half, and shows a gradual increase throughout.

Bed thicknesses appear to vary, but also show a cyclical nature. Thicker beds are followed by many numerous thinner beds. This is best seen when looking at Ca concentration.

Thick beds followed by thin beds suggests a depositional process similar to turbidite (bouma) deposition.

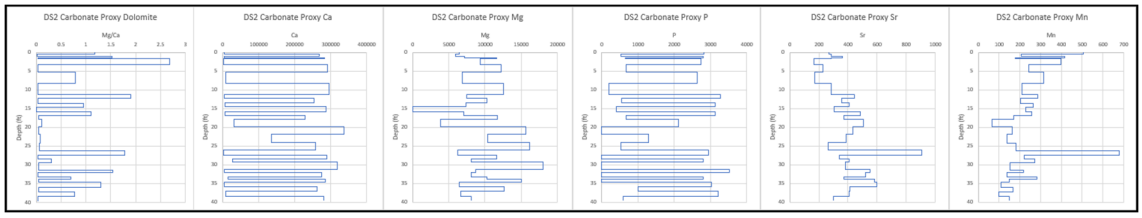

Figure 71: Transect 3 Carbonate Proxy Suite displaying Mg/Ca, Ca, Mg, P, Sr, and Mn, respectively.

Figure 72 reveals the paleoredox proxy suite for Transect 3. From left to right, the proxies used for this suite are as follows: Mo, V, Ni, Cu, U, and Mn*, respectively. Mo is fairly constant throughout with a decreasing trend and spike in the lower third and then a large increasing spike at the top of the section. V displays an increase at the bottom and very top of the section. Ni and Cu have a positive covariance until the upper third of the section where Cu remains at zero for an extended period of time, but when Ni increases once again in the top portion, the proxies become positive once again. U is positive with Cu and Ni at the bottom, but then becomes negative with Ni and Cu until the extended low concentration towards the top, where it remains positive with Ni, then negative at the very top with both Ni and Cu. Mn* varies in covariance. Mn* is mostly positive with U in the bottom third, then positive with Cu, then negative with everything, except at the very top when it becomes positive with U.

Mo is the most constant in this section. Ni is fairly constant, but fluctuates, and, in general, increases in the bottom half and then decreases in the top half. Cu decreases and is low in first third, increases and remains high in second third, and, in the final third, Cu in the

carbonate beds remains high, but drops to zero in silica-rich beds. U, in general, decreases throughout. Mn* increases in bottom third, increases in second third, and decreases in final third.

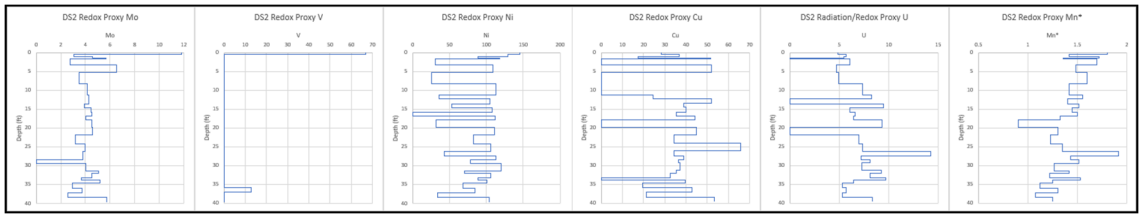

Figure 72: Transect 3 Paleoredox Proxy Suite displaying Mo, V, Ni, Cu, U, and Mn*, respectively.

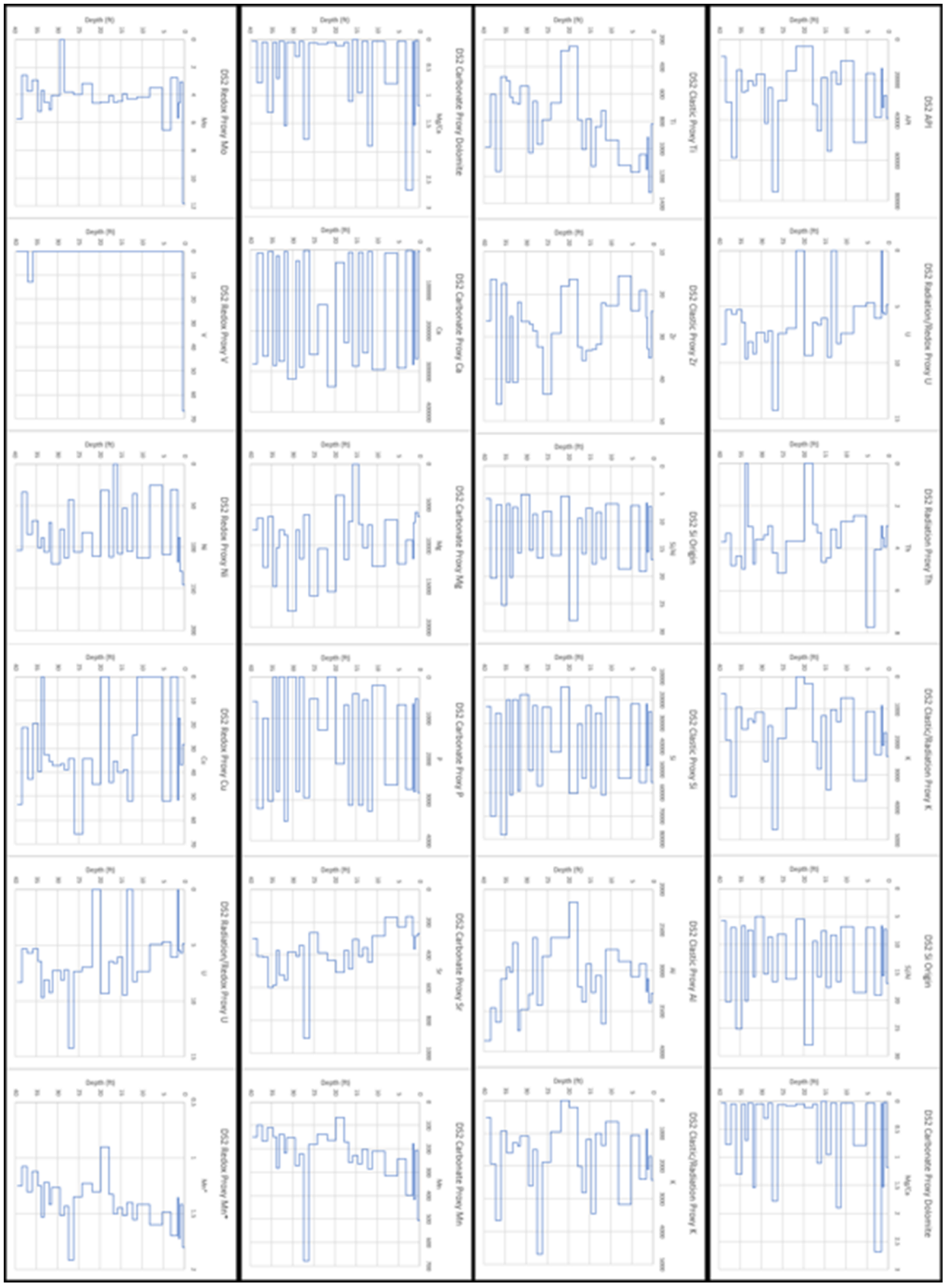

Figure 73: Transect 3 (Detailed Section 2) geochemical proxies obtained from the XRF.

5.2.1.4 Detailed Section 1 (Transect 4) XRF

Figure 74 is a Google Earth image of the location of Transect 4 (Detailed Section 1) along with its location within the total pseudo-gamma ray log in Bone Canyon. **Figure 75** shows the Pseudo-Gamma ray Log in feet, while **Figure 76** includes the Lithology Log at 1-foot intervals. In the carbonate beds, feldspars and clay minerals make up less of the overall lithology of the bed. Quartz/chert concentration is not seen at all in the carbonate beds. In contrast, in the chert beds, quartz, feldspars, and clay minerals make up a larger percentage of the overall bed. The chert beds are composed primarily of quartz/chert and the carbonate beds are composed primarily of dolomite, clay, and calcite. Calcite is shown with low concentrations in most of the carbonate beds. Where calcite is present, except in the oldest bed, clay content appears to increase. The frequency of calcite appearing in beds is increasing from the previous transects.

Spikes in the pseudo-gamma ray profile generally correlate to the chert beds, while lower API readings correspond to the carbonate beds. 3-4 cycles can be seen in the pseudo-gamma ray profiles. Starting at the bottom, 3 spikes are seen followed by 1 larger spike (~20,000-35,000) in API. This increasing trend is generally seen moving up-section, which gives this transect an overall increasing trend. Stolz's (2014) thesis on the Avalon Shale discusses the relationship between carbonate concentration and clay and quartz, as well as the relationship between clay and quartz and porosity. **Figure 77** shows that, in general, clay and quartz increase with a decrease in carbonate. **Figure 78** shows that, in general, increases in clay and quartz also results in increased organics and porosity, while increases in carbonates are associated with a decrease in porosity (Stolz, 2014).

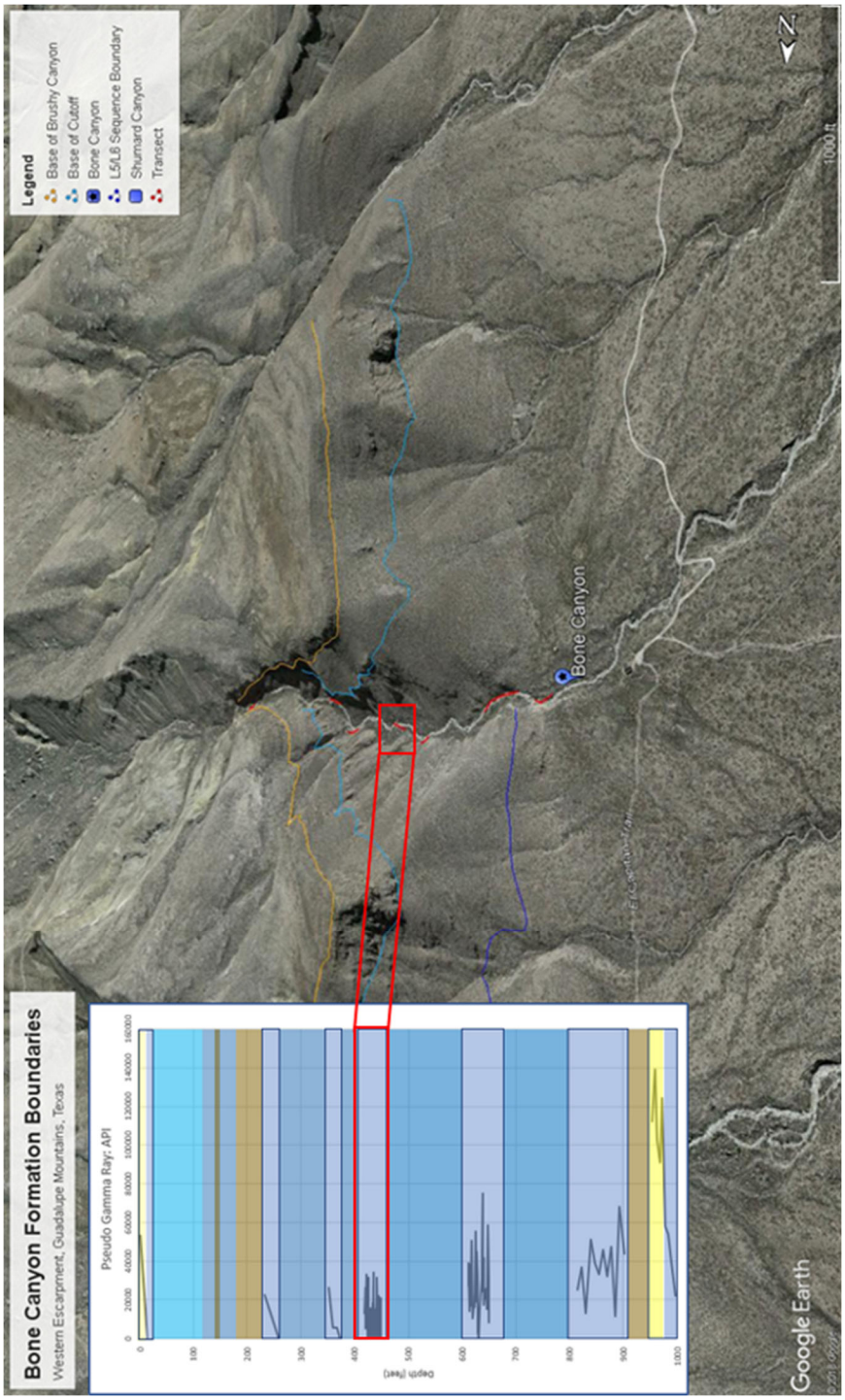

Figure 74: Transect 4 (Detailed Section 1) Google Earth image showing location within Bone Canyon and the total API curve.

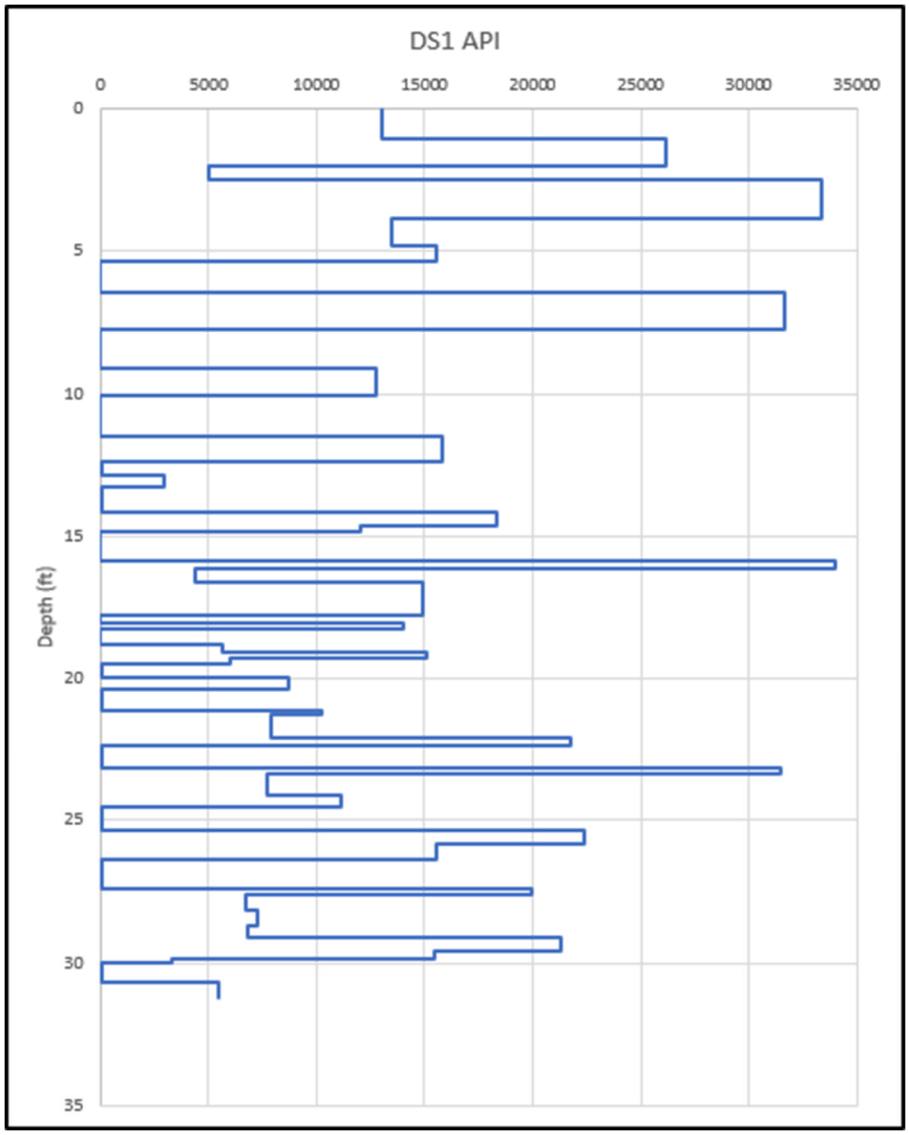

Figure 75: Transect 4 (DS1) Pseudo-Gamma ray Log. T4 corresponds to the HST of the L6 HFS, the FBSC B, and the Middle Avalon (carbonate). Y-axis corresponds to bed thicknesses and individual transect depth (feet).

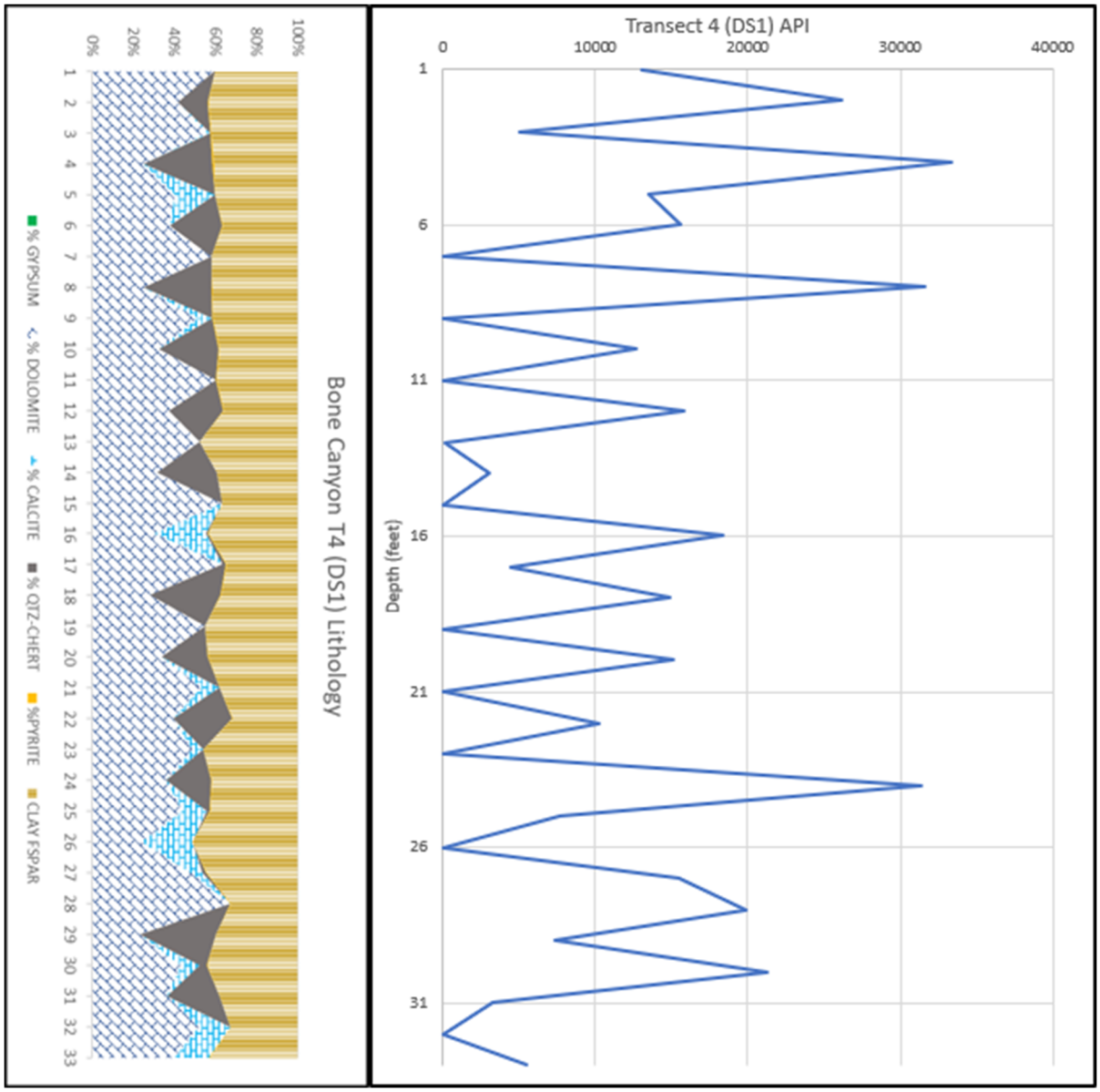

Figure 76: Transect 4 (DS1) Lithology Log (left) and Pseudo-Gamma Ray Log (right). T4 is from 418.83' to 465.85'. Only 33'/47.02' measured was accessible enough to collect data. T4 shows alternating layers of carbonate and chert deposited as carbonate turbidites. T4 corresponds to the HST of the L6 HFS, the FBSC B, and the Middle Avalon (carbonate). Y-axis shown as 1-foot intervals.

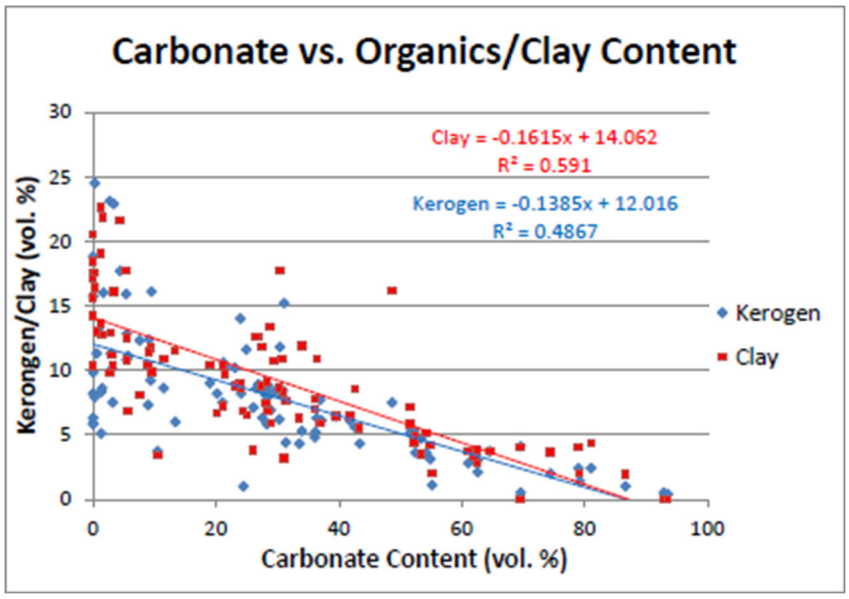

Figure 77: Cross plot showing carbonate concentration vs. organics/clay content. Image taken from Stolz (2014).

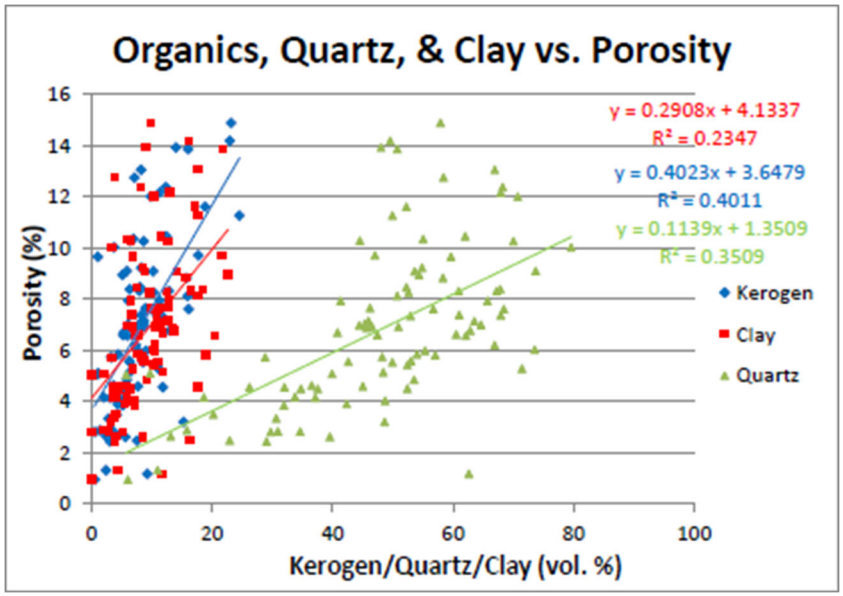

Figure 78: Cross plot showing Organics, Quartz, and Clay vs. Porosity. Image taken from Stolz (2014).

5.2.1.4.1 Detailed Section 1 (Transect 4) Geochemistry

Figure 79-Figure 82, below, illustrate the various proxy suites used in this work for Transect 4 (Detailed Section 1). The first proxy suite includes API, U, Th, and K to determine sources of radiation. Si/Al and Mg/Ca are also included in the first suite showing the influence of the origin of silica and dolomite. The Second suite displays the clastic/terrestrial/terrigenous proxies including Ti, Zr, Si, Si/Al, Al, and K. The third suite contains the carbonate proxies including P, Ca, Sr, Mg, and Mn. The final suite displays the paleoredox proxies including Mo, V, Ni, Cu, U, and Mn* (normalized with Fe- see Geochemistry methods).

Overall, API is lower than the previous transects. This is interesting because Transect 4 U concentrations reach higher levels than any other transect. However, average U values are the second lowest in the canyon (Transect 2 has lowest). Th values here are generally higher than any other transect and, other than Transect 1, have the highest average Th. Th concentrations reach higher values compared to other transects, except for Transect 3, however, T3 Th concentrations barely reach higher values and only in one bed. K values, however, are generally lower here than the previous transects, but higher than the following two transects. Average U concentrations decrease from the previous transect, average Th concentrations increase, and average K concentrations decrease. From T3-T4, in general, U and Th show a negative covariance, however, U is positive with K and API. However, from T4-T5 U and Th show a generally positive covariance, both together, and with K and API. After this transect (T5), U, Th, and K all appear to decrease from Transect 4. It is important to mention that, although they all visually decrease, Th on average, actually increases.

Average Si concentrations at Transect 4 continue to decrease from the previous transects. Similarly, average Ti and Zr concentrations also continue to decrease from the previous transects. Average Al values decreased from T1-T3, however, instead of continuing to decrease at Transect 4, Al concentrations actually increase. The average increases in Al concentration, along with the decrease in Si concentration, effect the change in the Si/Al ratio. From T1-T3, average Si/Al increases, but at Transect 4 the average Si/Al ratio decreases. This is important because Si/Al suggests the source of silica. From T1-T3 the system shows an increase in biogenic silica, but at Transect 4 (and to Transect 5) the biogenic silica decreases.

Average P concentrations continue to decrease from Transect 1-Transect 4. Average Ca concentrations continue to increase from Transect 1-Transect 4 (and again at Transect 5 (T1-T5)). Average Sr concentrations, increase from T1-T3, but decrease from Transect 3-Transect 4 (and again at Transect 5 (T3-T5)). Average Mg concentrations decrease from Transect 1-Transect 3, but then increase at Transect 4. Average Mn concentrations increase from Transect 1-Transect 2, then decrease from Transect 2-Transect 4. The average Mg/Ca ratio increases from Transect 1-Transect 2, decreases from Transect 2-Transect 3, then increases from Transect 3-Transect 4.

In general, Si, Si/Al, Ca, Mg, and Mg/Ca gradually increase from Transect 1-Transect 4. General decreases from Transect 1-Transect 4 are seen in API, K, Ti, and Zr. Proxies that may show a slight trend, but in general remain fairly constant from Transect 1-Transect 4 are U and Th. U and Th originally decrease from T1-T2, but slightly increase from T2-T4. A unique variation at Transect 4 is shown in Al concentrations.

Transect 4 is similar to Transect 3 although some proxies slightly increase and decrease between the two transects. This suggests that Transect 1 was uniquely deposited compared to all

other transects, however, the overall depositional environment was similar to that of Transect 2. Furthermore, Transect 3 and Transect 4 were likely deposited in a similar environment. From the proxies, especially API, U, Th, K, Ti, Zr, Ca, Mg, Mg/Ca, Si, Al, and Si/Al, it is seen that the environment of deposition from T1-T4 was fairly similar, however, different processes were occurring within that environment. The environment between T1-T4 was a relatively high sea level (highstand). The depositional processes vary owing to fluctuations within this highstand. At Transect 1, the slope became unstable and caused gravity flow processes that likely caused more siliciclastic material to reach the basin. This siliciclastic material caused significant increases in radiation and terrigenous proxies; however, it does not imply that the sea level was low during this time. During the ensuing highstand, carbonate production was high, which provided enough carbonate sediment to allow the system to prograde basinward. This progradational phase is seen by the gradual changes in, primarily carbonate, proxies. In general, carbonate proxies gradually increase, while terrigenous proxies generally decrease.

Progradation causes Mg/Ca and Si/Al concentrations to reach higher values at Transect 4, but the high values are fairly constant compared to Transects 2 and 3. Transect 4 also has higher concentrations of Ca and Mg than the previous transects. The combination of higher Ca, Mg, Mg/Ca, and Si/Al with a lower API suggests Transect 4 represents a continuing progradation.

5^{th}-6^{th} order:

In the radiation proxy suite, U and Th show a negative covariance until 25 feet, positive covariance between 25-15, negative covariance around 15 feet, and positive from 10-0 feet. This provides us with a trend that shows U and Th alternating covariance approximately every 10 feet. API also alternates covariance between these two proxies (U and Th). API starts positive with Th

for first couple feet, then positive with U around 27.5 feet, then Th around 25 feet, then U until around 22 feet, negative around 20 feet, positive with U around 17.5-14 feet, then Th around 12.5 feet, then both from around 12.5-9 feet, then U from 9-5 feet, then both around 5 feet, neither until 2.5 feet, and finishes positive with U from 2.5-0 feet. Both proxies begin with a gradual decrease then begin to gradually increase around 17 feet, then decrease around 12.5 feet, and then increase from 5-0 feet. This alternative influence of U and Th on API is similar to the previous transects. API and K, similar to previous transects, also show the strongest positive covariance (mimicking one another). API, K, Si/Al, and Mg/Ca show a strong positive covariance.

The trend seen in API is generally seen to increase to around 22.5 feet, a sharp decrease to 20 feet, a sharp increase to around 16 feet, a gradual decrease from 16-10 feet, and then increases from 10-0 feet. The trends observed in U and Th are generally seen to decrease until around 17 feet, increase to around 12 feet, decrease to around 5 feet, and then increase to the top of the section.

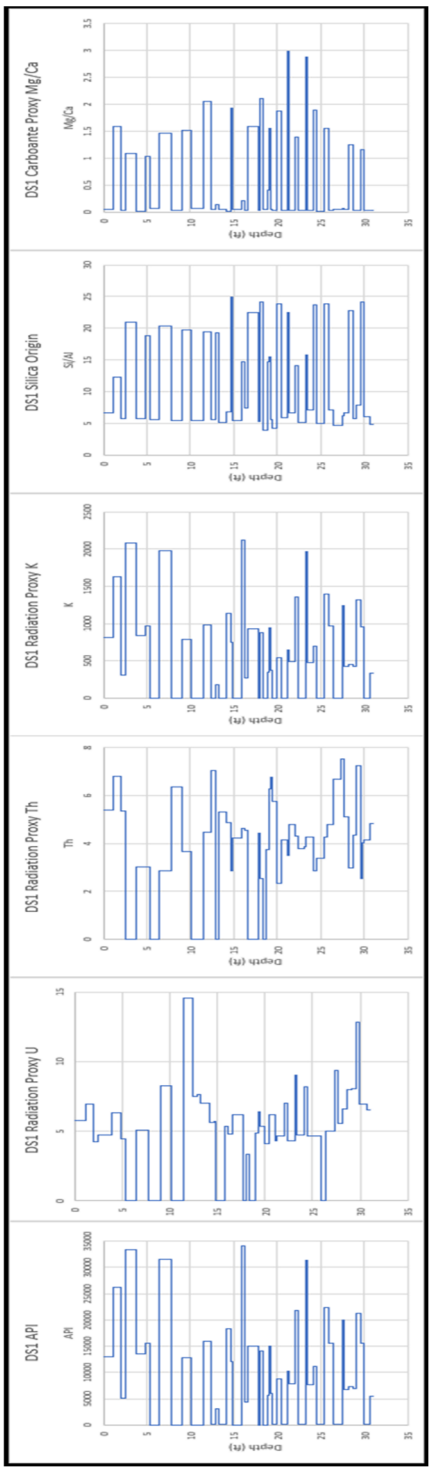

Figure 79: Transect 4 Radiation Proxy Suite displaying sources of radiation (U, Th, and K) with the ratios for Origin of Silica (Si/Al) and Dolomite (Mg/Ca), respectively.

In the terrigenous/clastic proxy suite **(Figure 80)**, Ti and Zr show a negatie covariance throughout the bottom half of the transect until around 15 feet, then show a positive covariance from 15-5 feet, and then show a negative covariance again from 5-0 feet. Ti is fairly constant through the bottom half, but has a subtle decrease and then increase. Above 15 feet, Ti shows a gradual increase. Zr shows a gradual increase in the bottom third, a quick decrease and gradual increase again in the second third, and then a gradual decrease in the top third. Ti and Zr show similar trends in the middle, both showing an increase. The bottom third, Ti decreases and Zr increases and then in the top third, Ti increases and Zr decreases. Overall, Ti decreases and then increases and Zr decreases and then (restarts) decreases again.

Si has a high fluctuation owing to the alternating beds of carbonate and chert. Carbonate beds appear to have a subtle decrease to around 20 feet, then a subtle increase to around 10 feet, and then fluctuates making it appear to remain constant, but it appears it may decrease overall. The Si in the chert beds appears to first increase to around 20 feet, a slight decrease to around 12.5 feet, then increases to around 5 feet, and then decreases. Al, overall, has an increasing trend upward. Interestingly, between 17.5-5 feet, Al appears higher in carbonate beds (Al has negative covariance with Si). However, in the bottom half, as the Si in carbonates decrease, Al increases. Si and Al, overall, remain constant in the bottom half, but both increase in the top half. However, Si does seem to fall again at the end. Si/Al highly fluctuates, which is expected owing to the fluctuations in Si and even in Al. It is hard to see trends in Si/Al in the bottom half of the section owing to fairly constant values of both proxies (individually), but if anything, it is increasing. In the top half, Si/Al shows an increasing trend before falling at the top.

API and K mimic one another, similar to previous transects. K shows a positive covariance with Zr until around 16 feet. Just above 16 feet, K has a large spike decrease (after its

large increase) giving it a negative covariance with Zr and Ti. Around 15, or just above, K is positive with Ti and negative with Zr. Just below 13 feet, K becomes positive again with Zr. Around 12-6 feet, K becomes positive with both Ti and Zr. Around 5-0 feet, K is only positive with Ti (negative with Zr). U and Ti are positive from 2.5-0. From 5-2.5, U is positive with Zr. From 14-5, U is positive with Ti and Zr. From 17.5 U is positive with Zr.

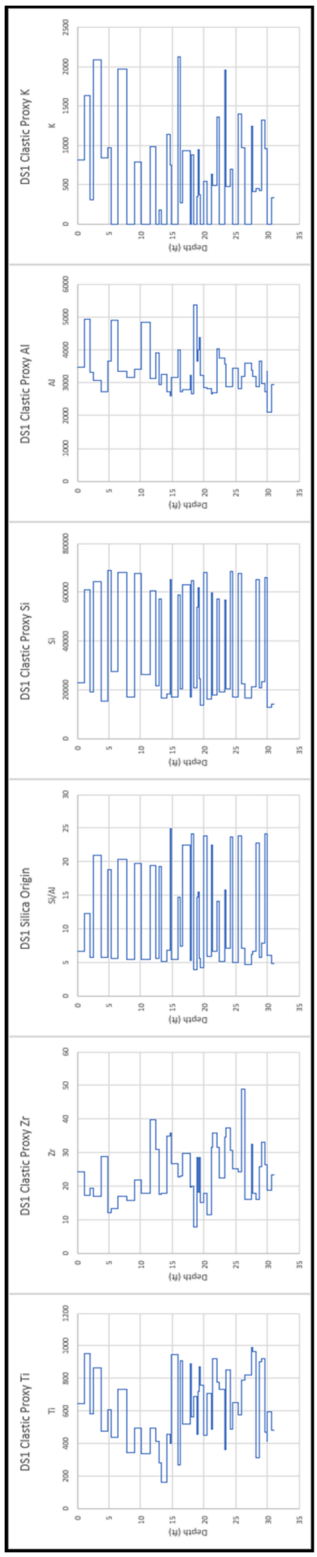

Figure 80: Transect 4 Terrigenous Proxy Suite displaying Ti, Zr, Si/Al, Si, Al, and K, respectively.

In the carbonate proxy suite **(Figure 81)** Ca highly fluctuates owing to alternating layers of carbonate and chert, similar, but opposite, to Si. Ca appears to gradually increase to around 20 feet. Ca then drops quickly and slowly increases, almost constant, from 20-15 feet. Ca decreases from 15-10 feet. Above 10 feet, Ca fluctuates, but slightly increases until around 4 feet and then decreases to 0 feet. The amount of Ca in the chert beds is extremely low and remains constant throughout the section.

Mg/Ca, overall, increases and then decreases. Mg increases from the bottom to around 12.5 feet and then decreases to around 5 feet, before it starts to increase again at the top. Large spikes in Mg/Ca are seen between 25-20 feet. Mg in the chert beds increases in the bottom third, remains fairly constant in the middle third with, perhaps, a slight decrease, and then decreases in the top third. Mg in the carbonate beds is high around 27.5 feet. From 25-10 feet, Mg (in carbonate beds) increases and then starts to decrease overall.

Overall, P shows a negative covariance with Ca. In the chert beds, P is fairly constant in the bottom half of the section, but eventually gradually increases in the top half. Sr, overall decreases throughout the section. From the bottom to around 27 feet Sr is negative with Ca. From 27-15, Ca and Sr have a positive covariance. 15-10 feet, Ca and Sr have a negative covariance. From 10-0, Ca and Sr have a positive covariance.

Mn, overall, increases to around 17 feet, decreases to around 10, and then increases. Mn appears negative with Ca until around 16 feet and then becomes positive, but quickly becomes negative again. From 17-12.5 Mn appears positive with Mg. Mn appears higher in chert beds. Mn follows a similar trend with Mg/Ca until around 10 feet, increasing and then decreasing. Mn then follows P until around 2.5 feet.

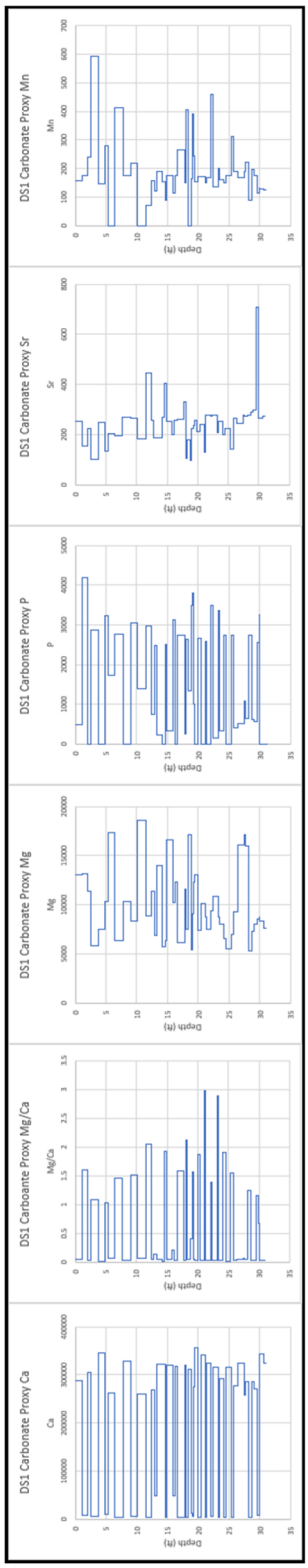

Figure 81: Transect 4 Carbonate Proxy Suite displaying Ca, Mg/Ca, Mg, P, Sr, and Mn, respectively.

In the paleoredox proxy suite **(Figure 82)** Mo, in general, decreases in the bottom half and then increases in the top half. V is low (zero) throughout the section. Ni appears to be increasing throughout the section. Cu fluctuates quite a bit, but has a slight decrease in bottom third and then increases. U decreases in the bottom half, quickly increases, then decreases, and finally increases at the top. Mn is fairly constant throughout the section, especially in the bottom third, then slightly decreases, and finally increases to the top.

Except at the lowest point and briefly just above 5 feet, Ni and Cu have a strong positive covariance. U starts positive with Cu, then is negative around 30, then positive to around 25 feet, then has a negative covariance with Ni and Cu from 25-22, positive from 22-20, negative from 20-5 feet. Just above 5 feet U is more positive with Ni than Cu. Around 2.5-2 feet U is negative with Ni and Cu then becomes positive with them both to the top. Mn primarily shows a positive covariance with U. From 10-5 feet, Mn* is positive with U, but it is negative with Ni and Cu. The decreasing spikes in Mn* correlate positively with U and negatively with Ni and Cu.

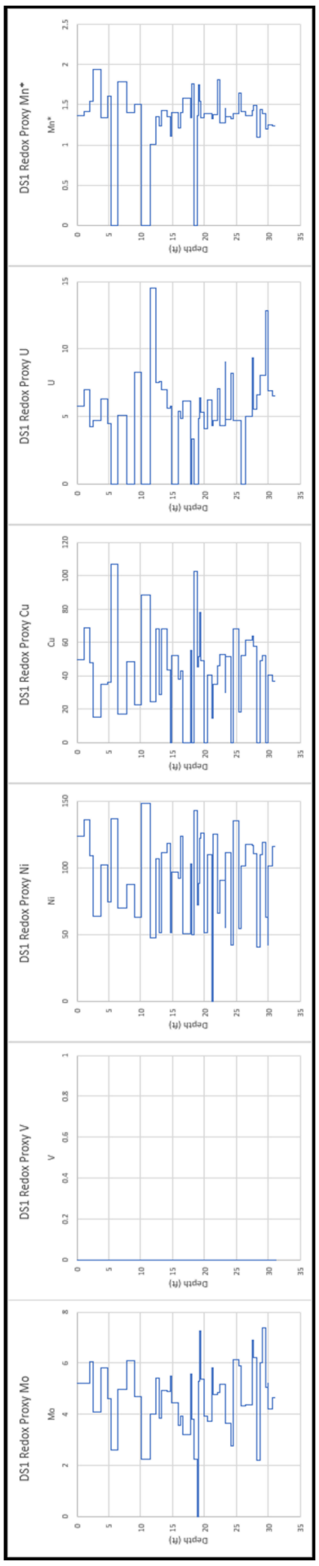

Figure 82: Transect 4 Paleoredox Proxy Suite displaying Mo, V, Ni, Cu, U, and Mn*, respectively.

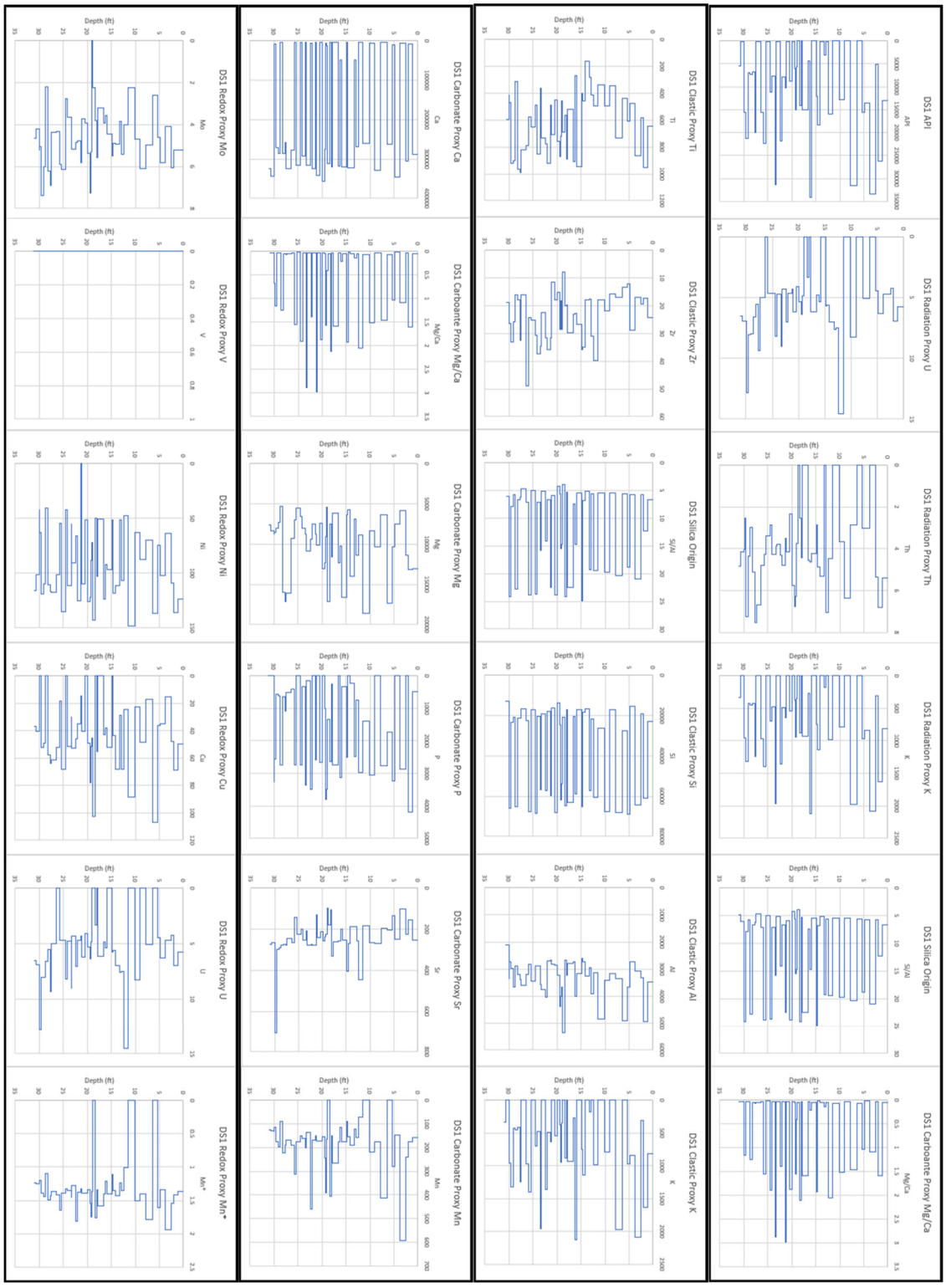

Figure 83: Transect 4 (Detailed Section 1) geochemical proxies obtained from the XRF.

5.2.1.5 Transect 5 XRF

The location of Transect 5 within Bone Canyon and within the total pseudo-gamma ray log is shown in **Figure 84**. The Transect 5 lithology log and pseudo-gamma ray log are shown in **Figure 85.** Transect 5 corresponds to the upper portion of the L6 HFS and is grouped in the FBSC B (bedded-nodular chert). API values are roughly half that of the previous transect (T4). The beds in Transect 5 alternate between limestone and chert. The chert here is not always laterally continuous and chert nodules, although mostly seen on bedding planes, are becoming more apparent. Therefore, this transect is grouped within the FBSC B. These layers appear to be shaley, flaky, fissile and thin.

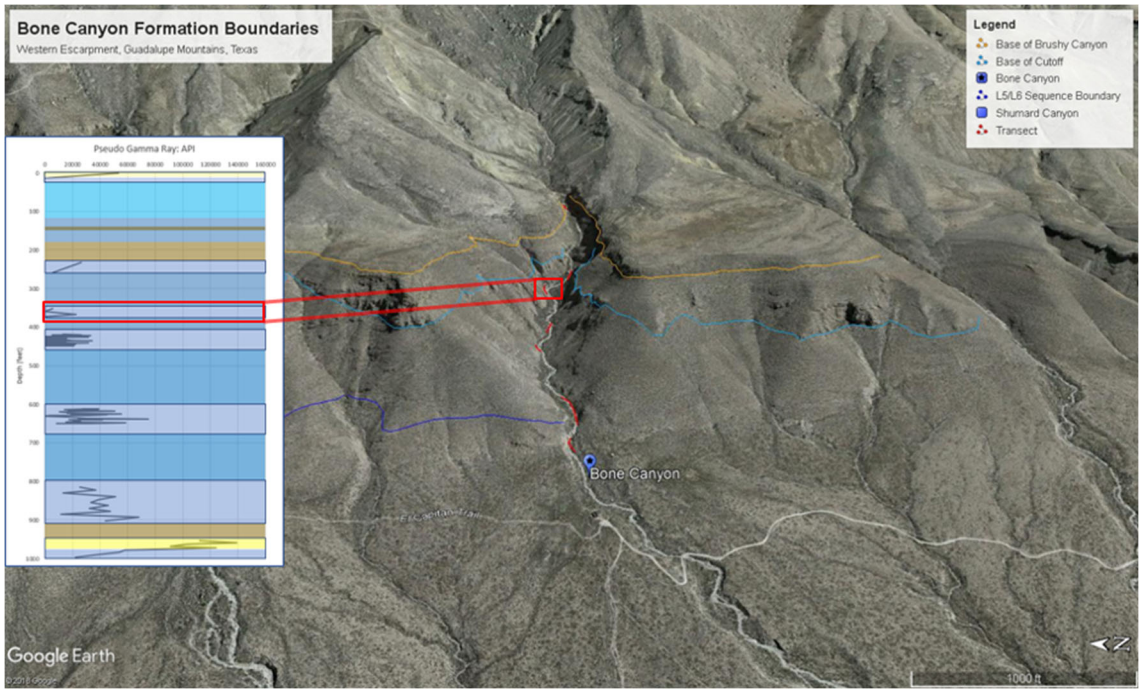

Figure 84: Google Earth image showing the location of Transect 5 within Bone Canyon and within the overall API curve (left).

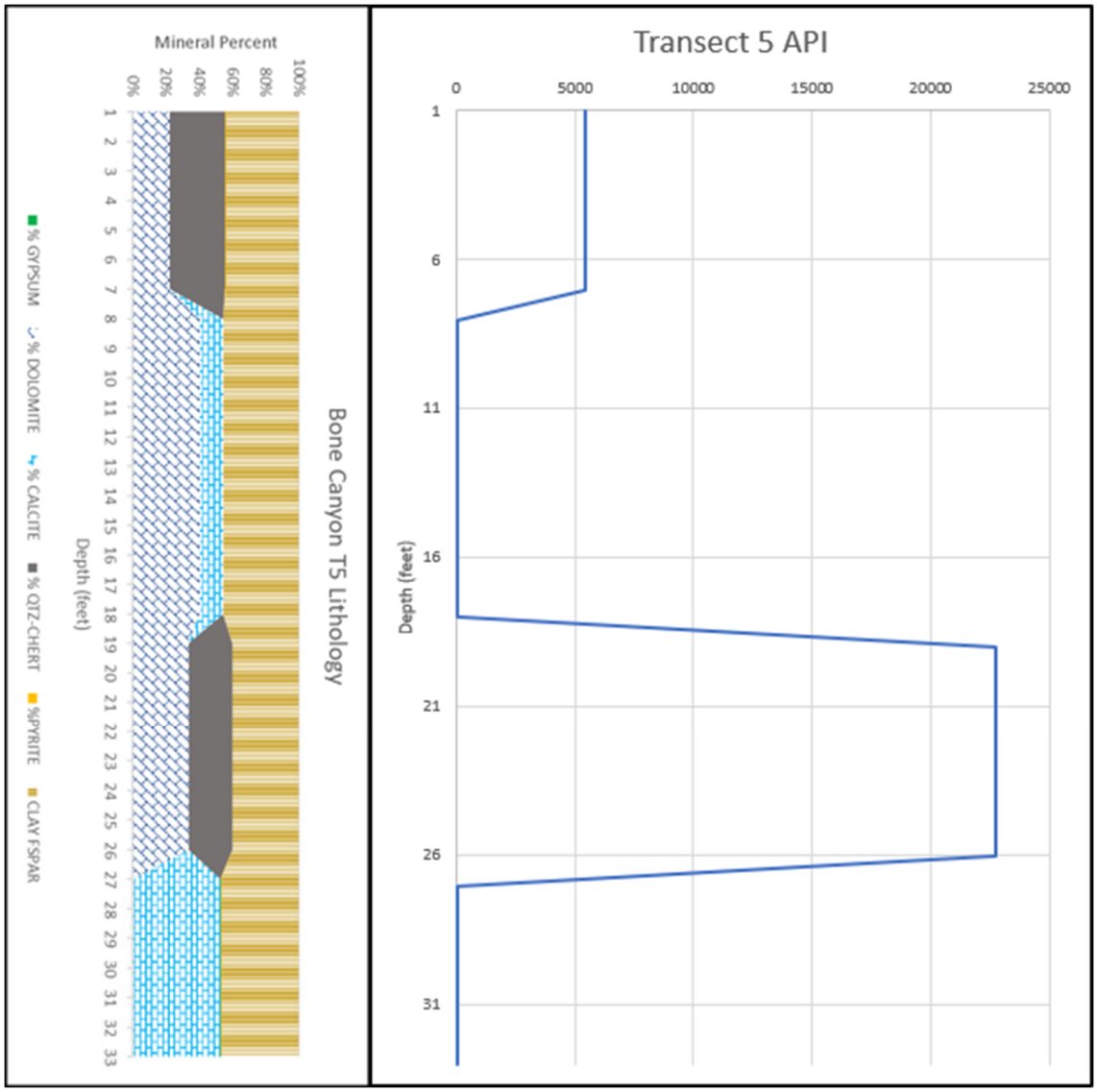

Figure 85: Transect 5 lithology lof (left) and pseudo-gamma ray log (right) generated from the XRF.

5.2.1.5.1 Transect 5 Geochemistry

Figure 86 shows the Geochemical proxy results for Transect 5. As previously mentioned, the beds alternate with limestone and chert and is now shown in the proxy suites below. The oldest (limestone) bed contains calcite and no dolomite unlike the third (limestone) bed that contains mostly dolomite with some calcite. The oldest chert bed

(bed two) contains around 20% chert and ~30% dolomite and the youngest (chert) bed contains around 20% dolomite and ~30% chert. Clay percent (45-50%) is consistent throughout this transect. It is important to mention that although the older chert bed contains less chert (more dolomite) compared to the younger chert bed, it has a significantly higher API value (~22,500). Both carbonate beds, between the chert beds, have API values of 0. As is the case throughout the canyon, Potassium (K) has the greatest effect on API.

Within the API curve for Bone Canyon, Transect 5 stands out because, in general, it contains the lowest API values. From Transect 1 to Transect 5, The API curve has an overall decreasing trend. After Transect 5, at Transect 6, the API values begin to increase and (likely) continue to Transect 7. This transect's geochemistry must contain valuable information as to why its values are so low.

Geochemical analysis of Transect 5 provides important details regarding the paleoenvironment at the time of deposition. Looking at elemental concentrations of calcium (Ca), Transect 5 displays the highest Ca concentrations (~ 362,168 ppm) in Bone Canyon. From Transect 1 to Transect 5, Ca concentrations gradually increase. Following Transect 5, Ca concentration is shown to decrease at Transect 6.

The Si/Al ratio, used for determining the origin/type of silica, decreases from the previous Transect 4. After Transect 5, Si/Al is shown to remain the same or slightly increase at Transect 6. Lower Si/Al values correspond to more terrestrial influenced silica. Previous transects, together, show an increasing trend in this ratio that likely corresponds to high carbonate production. In other words, from Transect 1 to Transect 4, the silica in the system is more, or becoming more, biogenic. This means that the silica

within the sediment is coming from organisms like sponges and radiolarian rather than being transported from terrestrial sources (i.e. beaches and rivers). For carbonate production to be high, the sea level must be relatively high, because carbonates correspond to highstands in sea level. Therefore, a drop in Si/Al ratio is related progradation and more terrestrial influence, overall. Transect 5 is within the L6 HFS that has a positive progradation ratio (Fitchen, 1997). When carbonate platforms prograde during highstands, it means that there is a high sedimentation rate. This sedimentation rate eventually changes the facies in the same, or similar, way a regression in sea level would. Owing to the fact the Ca is highest here, there is still lots of carbonate productivity. This leads to the fact that Transect 5 is likely the maximum progradation (in regards to the data acquired for this study) of the carbonate system.

Mg/Ca concentrations at Transect 5 further explain this. Both Ca and Mg increases with carbonate production. If the system is prograding, then Ca and Mg will be increasing in the once, more basinal position (Bone Canyon). This is reflected in the Mg and Ca concentrations from T1-T4. At Transect 5, however, Ca continues to gradually increase while Mg drastically decreases, likely suggesting a change in post-depositional processes.

The Mg/Ca ratio can also be used to distinguish dolomite from calcite. In Bone Canyon, Mg and Ca show a positive covariance from Transect 1 to Transect 4- the main transects that represent the prograding system during the HST. At Transect 5, the Mg concentration and the Mg/Ca ratio, and therefore dolomite, decreases drastically. Mg and Ca display a negative covariance at this transect- Ca increases while Mg decreases. If the same processes as before (previous transects) were occurring, Mg would increase with

Ca, but this is not the case, suggesting post-depositional diagenetic influence on Mg and Mg/Ca.

The prograding system eventually comes to halt, but is it here or at the next transect? Ca content continues to increase here. Si/Al decreases here likely from the shoreline moving basinward, resulting in more Al. The API curve continues to decrease here. This leads to the conclusion that Transect 5 is the maximum extent of the progradational phase, further supporting the fact that dolomite is more related to post-depositional, or diagenetic, processes.

Dolomite likely formed during early diagenesis when the deposits began experiencing overburden pressure from the sediments above. Although progradation continues in this transect (Transect 5), it does not continue after it. Meaning there was insufficient sediment deposited on top of (after) this unit to compress/load/compact the underlying deposits. This process can be viewed similar to the process of chert formation in the canyon. Similar to the silica, the magnesium is deposited within the unit. Through time, the Mg migrates upward in the interstitial fluids, looking to escape back into the water column. When sediment supply is high, this silica- and magnesium-rich interstitial fluid migrates up through permeable layers until it reaches an impermeable (impenetrable) layer. Fluids migrate to avoid areas of high pressure and, especially, if their contents are less dense than the surrounding material. This concept is critical in the oil and gas industry because hydrocarbons go through the same process. Since the fluid cannot escape, it moves laterally within the underlying, more permeable layer. Dependent upon the concentration (and even location within the system) of Mg, or Si, the fluid will migrate laterally and interact with whatever it comes into contact with. The higher the

concentration, the more likely it is for it to form beds. The lesser the concentration, the more likely it is to form nodules or replace more unstable elements/minerals. The lithology of the host rock, in which the fluid travels through, is important because if the host rock contains unstable minerals, the fluid will try to stabilize it by replacing the minerals or by filling in vacancies.

Although the following transect (T6) shows a slight increase in Mg, Mg/Ca, Si/Al, and API, it shows a slight decrease in Ca. Rather than the system prograding basinward owing to sediment supply and rate, the system is likely adjusting to less sediment and/or the early stages of the late L6 regression. The sea level eventually falls during the (late L6) L7 LST and quickly rises again during the L8 TST (Kerans, 2014). This change in environment, especially at such a quick rate, causes various degrees of deposition (and erosion). Important to this understanding is the fact that during the L7-L8 HFS, large quantities of sediment flowed into the basin via gravity (debris) flows filled with material from the shelf and upper slope. These units are deposited rather quickly, resulting in the underlying sediment being quickly buried. Burial is owing to a different process at this point (compared to the burial of previous transects), but nonetheless it provides the ideal circumstances for diagenetic processes to create dolomite and biogenetic silica-rich chert.

This is another indication of the system reaching its maximum progradation and shallower depths at Transect 5. Earlier transects reflect deeper depths, more accommodation space, higher sedimentation rates during deposition, and higher overburden pressure/loading, which results in more dolomite. As the Ca-rich carbonate platform progrades further into the basin, more calcium is being supplied to the deeper

portions of the basin. This appears to be the same case for Mg, except at this transect. This differentiation gave credence to the fact that Mg was more associated with post-depositional processes. It still makes sense that Mg would increase with Ca as the carbonate system prograded into the basin, because both Mg and Ca are carbonate minerals.

Progradation continues through Transect 5, but stops soon after. Through progradation, Bone Canyon reached shallower depths, resulting in more dolomite than before when it was at deeper depths. Now, at shallower depths, dolomite continues but is less, Si/Al is lower because shallower areas receive more terrestrial influence, and Ca concentration is high because the platform is further basinward (closer to Bone Canyon). This explains the changing chert characteristics. Si is now not being buried quick enough and the Si is escaping back into the water column (no chert beds). As progradation stops, the sea level begins to fall (after T5, during T6 or possibly shortly after). As sea level falls, for a short period, the facies realign themselves as they were during Transect 4 because the system balanced itself out basically.

Transect 6 contains similar things to those previously seen in T4 (API, Ca, Mg/Ca, Si/Al), possibly making Transect 5 a turning point. After Transect 5, sea level began to fall, depositing Transect 6 in a similar fashion to T5, but owing to sea level falling instead of progradational processes, resulting in similar, but different, facies. Similarly, Transect 6 was quickly buried, but not by the same processes (debris flows after T6). These different processes created similar depositional, and post-depositional, environments between T5 and T6.

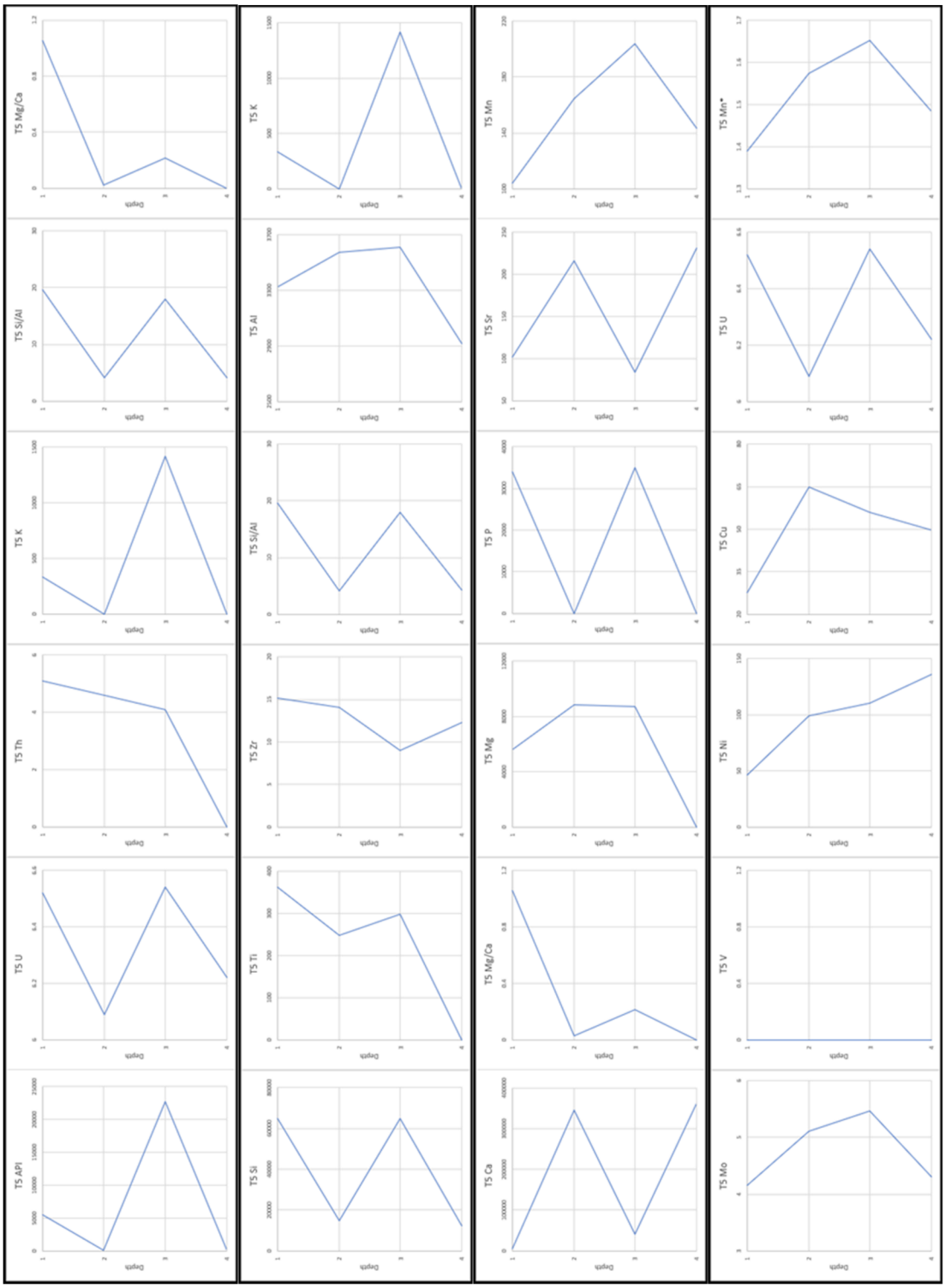

Figure 86: Geochemical proxy results of Transect 5. Proxy suites from top to bottom show Radiation Proxy Suite, Clastic Proxy Suite, Carbonate Proxy Suite, and Paleoredox Proxy Suite, respectively.

5.2.1.6 Transect 6 XRF

Transect 6 is likely a continuation of the transitional phase started at the end of Transect 5. Although there is a covered section between the two, the units are similar. The chert beds in Transect 6 are not laterally continuous and are barely bedded or nodular. Instead, the chert beds here display a mottled/splotchy texture. As such, this transect is grouped in the FBSC C (mottled/splotchy chert). The oldest bed here is a carbonate bed and is composed primarily of dolomite (~40%), clay (~40%), and some calcite (~20%). The youngest bed is similar, composed primarily of dolomite (~40%) and clay (~40%), but contains some chert (~20%) rather than calcite (0%).

The XRF data from Transect 6 is important because this transect is just below the contact with the Cutoff Formation. Depositional processes directly after transect deposition play an important role, which is seen in the geochemistry analysis of Transect 5. This stratigraphic position implies that the geochemistry of the strata should and will show a transition from the L6 highstand (Bone Spring Fm.) to the L7 lowstand (Cutoff Fm.).

Ca is associated with lower sea levels than dolomite, so a lower Mg/Ca ratio likely suggests a regression in sea level. Si/Al is an important ratio because it determines the origin of the silica. Did the silica come from a terrestrial source (river, beach) or did it come from a more biogenic source (sponges, radiolarian)? Silica, itself, cannot determine paleoenvironments, however, dividing silica by aluminum (Si/Al) provides the answer needed. High Si/Al usually reflects a higher sea level because there are more organisms (production) in the system. Low Si/Al usually reflects a lower sea level because Al is a good terrestrial indicator so the more Al, the more terrestrial sourced silica.

Certain geochemical curves like API and Mg/Ca help show trends throughout the canyon. The previous transects have shown certain proxies gradually increasing or decreasing reflecting the changes in the environment during deposition. Transect 6 is the stratigraphically highest and youngest Bone Spring interval with data in the canyon. The previous transects have shown the progradation of the L6 carbonate platform margin during a relative highstand in sea level. Towards the end of the L6 HFS there is a regression in sea level (Hurd and Kerans, 2014).

As sea level changed and fell, so did the environment. Although carbonate mudstones being deposited via turbidity currents continued, the location of certain facies shifted basinward. Rather than staying in a place with high carbonate production, with sponges and radiolarians (high Si content), and early diagenetic processes (quickly buried and compressed), Bone Canyon was now in a place with less carbonate production and less early diagenetic processes. The sediments during the late stages of the L6 HFS were not buried fast enough, which allowed the biogenic Si (high Si/Al) to escape into the water column rather than traveling vertically upwards and spreading laterally in permeable layers before being trapped by already deposited and less permeable layers.

The basin is an area with, in general, high accommodation space. This is especially true when comparing the basin to the shelf or slope. Before drawing conclusions, it is important to mention factors relating to changes in paleoenvironments. Changes in facies reflect changes in paleoenvironments. Changes in facies can be the result of a few various, but equally important, processes. Major processes effecting facies shifts are 1) changes in sea level (transgression or regression), 2) changes in accommodation space (uplift or subsidence), and 3) sediment supply (progradation or retrogradation). These processes, although very different in origin, cause the same (or very similar) shifts in facies. For example, chert abundance, size, and shape are

influenced by its position relative to the bank-basin. In general, within the Delaware Basin's basin, chert is very abundant, thin, elongated, bedded, and laterally continuous. In contrast, on the carbonate platform bank, chert is less prevalent, more rounded (circular), mottled/splotchy. Between these two ends is the carbonate platform margin, which can display a variation of abundance, nodular-bedded, rounded-elongated edges, mottled-laterally continuous.

Bone Canyon deposition began (Transect 1-2) in a more basinal (toe-of-slope) environment and, therefore, displays laminated beds, high chert abundance, and more lobate and laterally continuous chert beds or nodules. At the time of deposition-early diagenesis for Transect 6, the chert was now closer to resembling that of a carbonate platform margin, or even more so, a carbonate platform bank. So, what made the facies shift from a more basinal facies to a more carbonate margin, or bank, facies?

The L6 carbonate platform is shown as a prograding sequence (Fitchen, 1997; Kerans and Kempter, 2002; Hurd & Kerans, 2014) owing to its high carbonate production and sedimentation. Prograding sequences often have similar facies to sequences controlled by regressions in sea level. Transect 6 is the point of maximum progradation of the L6 HFS. As this point is reached, the sea level begins to fall, possibly a forced regression owing to the prograding platform. When progradation slowed and the sea level fell, the facies shift remained because these two processes give the same result. However, because progradation slowed and eventually stopped, sediment was not being buried as fast regardless of the sea level. This change (decrease) in sediment supply and rate resulted in more time each bed was exposed to the water column above. Silica within the deposits and interstitial fluid migrated vertically as usual, but instead of depositing itself in the highest permeable layer and unable to escape further because of a recently

deposited, non-permeable layer, the silica was now able to escape back into the water column. This process is seen at Transect 6 with a mottled/splotchy chert.

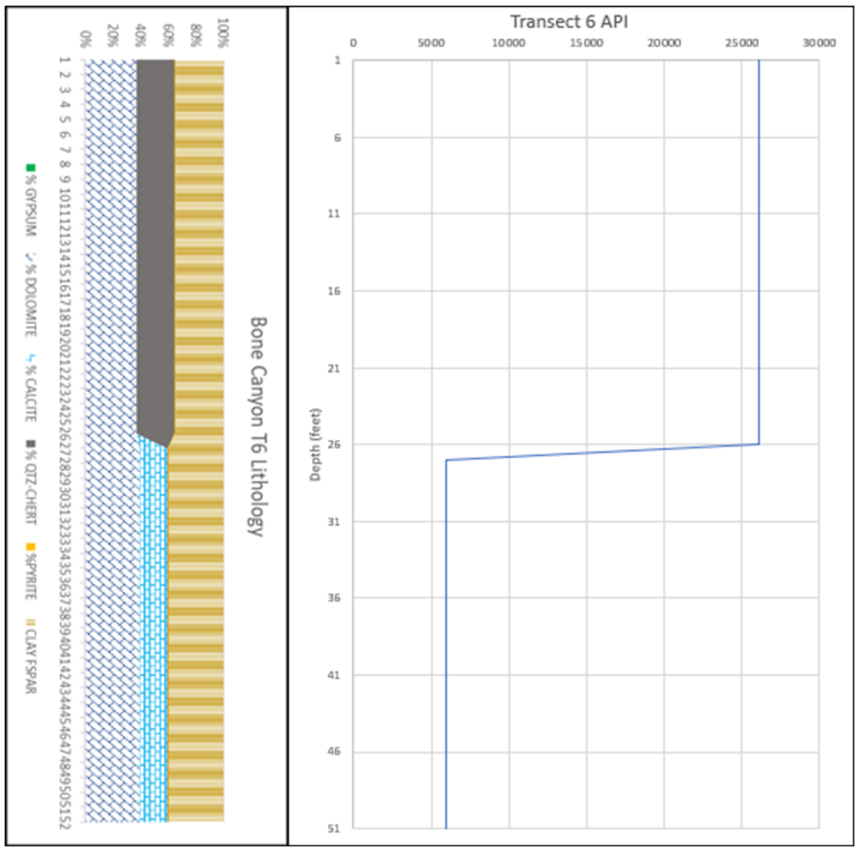

Figure 87: Transect 6 lithology log (left) and pseudo-gamma ray log (right). Bottom half corresponds to the Cutoff Conglomerate (G3 HFS) and the top half to the Brushy Canyon Formation (G5 HFS).

5.2.1.6.1 Transect 6 Geochemistry

Transect 6 differs from the previous sections because of its lack of chert and post depositional processes. Previous transects in the canyon have contained bedded or bedded-nodular chert beds alternating with carbonate-rich beds. At Transect 6, there is either not enough silica present during deposition or the beds were not buried quickly enough- allowing silica to

escape into the water column via interstitial fluids. Visually, and technically, this transect marks a change in depositional environment. The geochemical proxy results are shown in **Figure 88** below. Some differences in major proxies, compared to previous transects, can be seen.

The main proxies that have been used in the previous transects help explain the environment and processes associated with this transect. API, Mg/Ca, Si/Al, and Mg increase, while Ca decreases here (T6). The fact that Ca decreases rather than continuing to gradually increase, as it does throughout the previous transects, suggests a change in depositional processes. As previously mentioned, this likely represents the falling stage in sea level during the L6 HFS, or at least, the transfer of depositional controls from primarily being controlled by the sediment supply/rate to primarily controlled by sea level fluctuation- in this case, sea level fall.

At Transect 6, in general, the proxy values have rebounded back to values associated with Transect 4, but with some minor variations. Specifically, API, Ca, Si/Al, and, in part, Mg/Ca (to a lesser degree) values match those of Transect 4. Mg concentration does rebound back (towards values from T4), however, not near as much, or as close to T4 values, as the other main proxies. So, why doesn't Mg concentration return to T4 values as closely as the other proxies do? A change in depositional processes and, consequently, diagenesis.

Owing to the results of the other proxies observed, Transect 6, at first, appears to display a transgressive trend. When looking at the sea level curve, as well as lithology, the sea level is now regressing, not transgressing. An important concept is that, although Bone Canyon was primarily deposited during an HST, there is still an overall 2nd order regression. So, is this time likely primarily influenced by the amount of sediment, and carbonate production, within the system?

When sea level begins falling (especially seen in the strata above Transect 6), the slope becomes unstable. Slope instability is a crucial process to understand further. Instability occurs during both TSTs and RSTs, resulting in large quantities of sediment being deposited further into the basin because of the force of gravity. The falling sea level at the end of L6 appears to be a (geologically) quick fall. This would result in the deposits of Transect 6 being buried quickly from the gravity flow deposits, resulting in similar diagenetic processes that occurred in the previous transects. Regardless of how the sediment of Transect 6 was buried, it was buried nonetheless and with similar sediment.

The (newly, previously) prograded sediment was a part of the sediment gravity deposit. Transect 6 is a time period reflecting an adjustment phase. Sediment supply and rate slowed and sea level began to fall. The decrease is sediment supply would likely cause the system to appear to retrograde, but falling sea level would cause the opposite effect (prograde), unless the system did not have enough sediment to do so. This leads to the conclusion that sediment supply was still the primary influence and caused the system to become more aggradational-retrogradational. However, the fall in sea level did not allow for the system to continue to gradually retrograde. The fall in sea level, however, did cause instability and therefore more sediment was introduced via gravity flows and buried the Transect 6 deposits. The gravity flow must have been large enough to compress the underlying sediment quickly and without letting certain elements and minerals to escape.

Transect 5 and Transect 6 went through pretty similar processes. They both were not buried the same as the previous transects. Perhaps Transect 5 is still dominantly prograding (the end of prograding), however, Transect 6 becomes more aggradational. If sea level would not have fallen during, or shortly after this time, the system would continue to aggrade and

eventually retrograde. Since it fell, Transect 6 became the point in time that reflects this fall. The Mg (Mg/Ca) increases again because of the fall (causing a similar prograding response in the data) and dolomitization occurred within the sediment during early diagenesis because of the gravity flow deposits seen stratigraphically above Transect 6 (the flow deposits buried the sediment and created the necessary environmental factors for dolomitization). A fall in sea level at this time should cause the Si/Al ratio to decrease, however, it increases but it is still less than during the previous HST (T1-T4). Perhaps the ceasing of progradation at Transect 5, began closer to Transect 4.

Through this rational, Transect 6 is believed to be aggradational rather than progradational. This aggradational period results in the sediment below being buried differently than if it was progradational- that's why we see T5 with less dolomite as the previous sections. T6 increases in dolomite, not because the system returns to progradational, but only because this unit was buried quickly after deposition (the gravity flow deposit just above Transect 6- slump deposits- muddy/shaley- cobble base).

Ca concentration decreases from Transect 5 (and T4 in general). The Mg/Ca ratio, used to identify dolomite, increased from Transect 5, however, the ratio is, in general, lower than Transect 4, 3, and 2 forming an overall decreasing trend starting at Transect 2. The Si/Al ratio is another important proxy, which reflects the type of silica (authigenic or biogenic).

Si/Al has an increasing trend from Transect 1 to Transect 3, then begins to generally decrease from Transect 3 to Transect 7. The Si/Al ratio at Transect 6 is lower than Transect 3 and Transect 4, is roughly the same as the previous Transect 5, but is higher than the following Transect 7. This gives a general decreasing trend in the Si/Al ratio, meaning that the Si content is becoming more terrestrial (low Si/Al) rather than biogenic (high Si/Al). In general, low Si/Al

values correspond with lower sea levels or extensive progradation, while high Si/Al values correspond with higher sea levels or retrogradation. Both high and low Si/Al values can represent higher energies, however, owing to the opposite characteristics within carbonate and clastic systems. As previously mentioned, this transect reflects the transition from an HST to an LST (above T6), which is now seen through the Si/Al ratio.

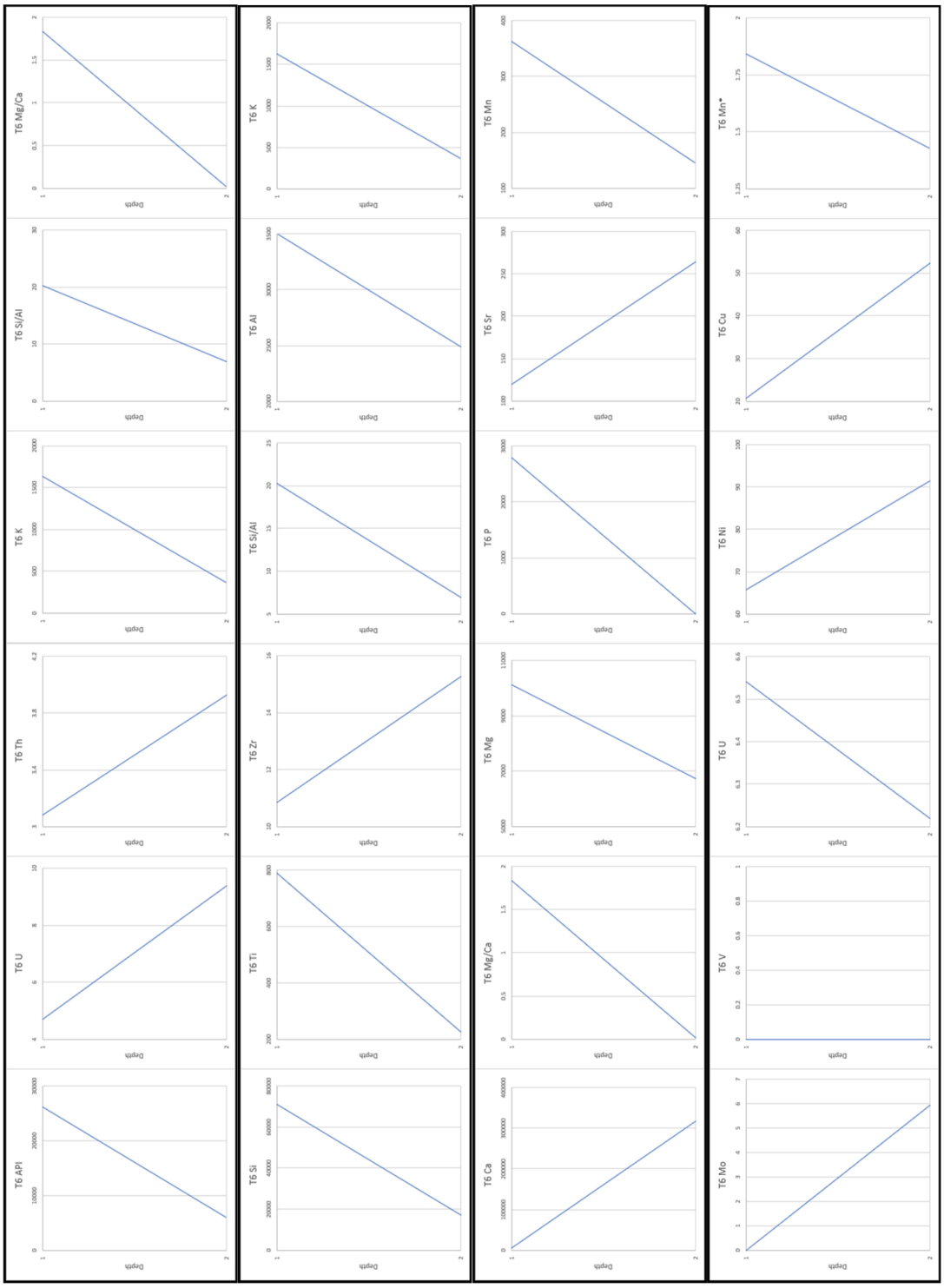

Figure 88: Transect 6 geochemical proxy results showing, from top to bottom, Radiation Proxy Suite, Clastic Proxy Suite, Carbonate Proxy Suite, and the Paleoredox Proxy Suite, respectively.

5.2.1.7 Transect 7 XRF

Transect 7 represents the contact between the Cutoff Formation, which is seen here as a massive conglomerate, and the Brushy Canyon Formation. **Figure 89**, below, shows the location of Transect 7 within Bone Canyon and within the total pseudo-gamma ray curve (left). The lithology log and pseudo-gamma ray log for Transect 7 are shown in **Figure 90**. The bottom half (oldest) of Transect 7 corresponds to the "No Name" Member of the Cutoff Formation and the top half (above 16') corresponds to the Brushy Canyon Formation. The Cutoff conglomerate was deposited during the G3 HFS as sea level began to fall. The regressing sea level caused instability in the slope causing gravity to bring down large volumes of sediment sourced from the platform, shelf, and slope. The debris flow is composed of large lithoclasts inside of a carbonate mud-rich matrix.

The Brushy Canyon Formation (BCF) lies directly above the Cutoff (conglomerate) Formation at Transect 7 and is the youngest and stratigraphically highest bed within Bone Canyon as it relates to this investigation. The BCF is a very fine-fine grained, well-sorted, and highly deformed sandstone. The fact that this unit was deposited subaqueous provides an explanation for the characteristics seen here. For example, the lithology log shows that the BCF is around ~ 40% clay, ~ 30% chert, and ~ 30% dolomite. The presence of dolomite may be an indicator of subaqueous deposition unless it was transported. Furthermore, the presence of soft-sediment deformation throughout this unit means that shortly after, or during, deposition the sediment was loose and not consolidated enough- to the extent at which sediment becomes a rock. An actual solidified bed at this scale cannot undergo deformation in the way that is seen here. The contact itself may help to further explain this.

The BCF cut (eroded) through the underlying carbonate via subaqueous channel(s). This is determined by the contact surface. The BCF erodes more of the underlying unit in certain areas, which in this case is the center, axial part of the unit. Lateral movement away from this center axial part, in either direction, shows less erosion of the underlying unit, resulting in a channel-form, sandstone unit. This helps clarify the paleoenvironment and the depositional processes that took place. When the sea level regressed, siliciclastic/clastic sediment from the shelf/platform was able to bypass the shelf. This coarser sediment carved through the underlying beds, which resulted in channel form surfaces in the slope and into the basin. These erosive channel-form surfaces then became conduits, or channels, for sediment to flow into and travel through. Bone Canyon's position was the perfect place for soft-sediment deformation processes because of its slope angle and geometric structure. As the sediment came to rest and as another (carbonate) unit was deposited on top of it, the differential compaction and loading of sediment caused deformation within the sediment below. As the edges of the channel had less sediment than the center axial portion of the channel, the degrees of compaction varied spatially across the unit.

This major unconformity (sandstone on top of carbonate) is an important surface when correlating units throughout the Guadalupe Mountains and in the subsurface. Second order unconformable surfaces are usually easy to identify (both in outcrop and subsurface) because visually the lithologies above and below the surface (contact) greatly contrast each other making them 'pop-out'. Similarly, in the subsurface, the beds above and below have a drastic contrast in API and elemental concentration. This makes unconformities a good "place marker" for determining location, and age, within certain strata.

Above Transect 7, although not the focus of this study, is an example of the entire Bone Spring Formation, just at a much smaller (higher order) scale. Sandstone units alternate with carbonate units, which resemble reciprocal sedimentation. The main difference here is scale, however, it is possible this process was confined to the channel in which it was deposited. Further work in this area will aid in the better understanding of higher order reciprocal sedimentation.

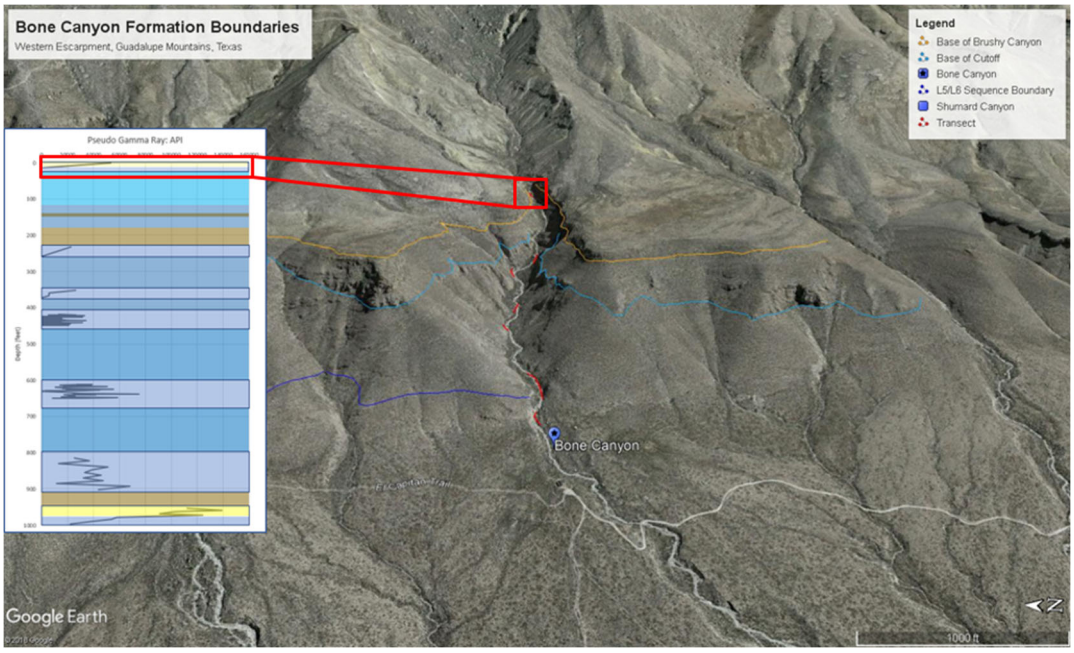

Figure 89: Google Earth image showing the location of Transect 7 within Bone Canyon and within the total pseudo gamma ray log (left).

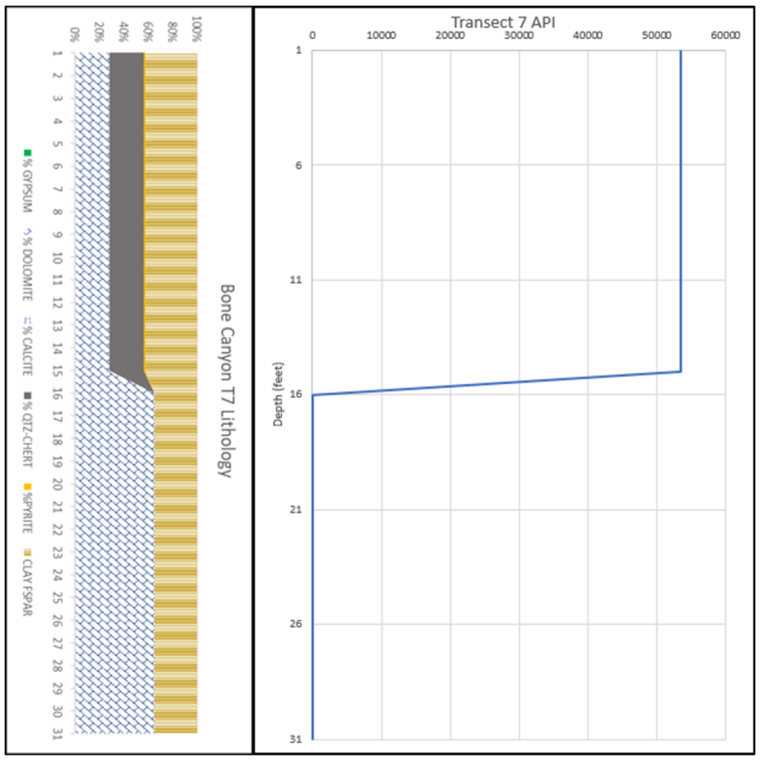

Figure 90: Transect 7 lithology log (left) and pseudo-gamma ray log (right). The Cutoff (conglomerate) Formation corresponds to points 16-31 and the Brushy Canyon Formation corresponds to points 1-16.

5.2.1.7.1 Transect 7 Geochemistry

Figure 91 displays the geochemical proxy results for Transect 7. The bottom half (oldest) of Transect 7 corresponds to the "No Name", or "Pigott-Brown" Member of the Cutoff Formation and the top half (above 16') corresponds to the Brushy Canyon Formation. The Cutoff conglomerate was deposited during the G3 HFS as sea level began to fall. The lowering of sea level caused instability in the slope causing gravity to bring down large volumes of sediment sourced from the platform, shelf, and slope. The debris flow is composed of large lithoclasts inside of a carbonate mud-rich matrix.

The Cutoff Carbonate, a fairly massive unit, is composed of ~ 60% dolomite and ~ 40% clay. This carbonate unit was likely sourced with a combination of material from the shelf (calcic

cobbles) and slope. The Brushy Canyon Sandstone, a highly deformed, channel-form unit, is composed of ~ 45% clay, ~ 30% qtz/chert, and ~ 25% dolomite. The higher concentration of finer, softer material allowed for more compaction and soft-sediment deformation.

The (stratigraphically) lower carbonate unit, compared to the higher clastic unit, displays low values of API (0), U, Th, K, Si/Al, Mg/Ca, Ti, Zr, K, P, Mn, and Mo. High values of Al, Ca, Mg, Sr, Ni, Cu, and Mn* are also observed. These high and low values are reversed for the higher unit. The proxies here show, and exemplify, the changing lithologies and therefore the change in depositional processes. Although the base level curve (2^{nd} order sea level) has been falling since the late G1 HFS, the sea level was not low enough for clastic sediment bypass, even during times of extensive relative sea level fall (3^{rd} order sea level), until now.

After the G4 HFS (possibly as early as G3 HFS), the base level curve reached and remained as low, and lower, as it was during the L7 HFS. The main difference between the LST at L7 and the LST after G3-G4 is that the L7 LST did not remain low for long at all. The LST (starting) at G3-G4 remained in this tract even after the end of the Permian (Guadalupian 8 HFS). This long lasting, low order LST allowed the bypass and deposition of clastic sediment into the basin. Relative, higher (3^{rd} - 4^{th}) order sea level fluctuations allowed carbonate deposition to occur, however, only during relative highstands, or latest transgressions-earliest regressions, in sea level. This process is seen just above the stratigraphically highest unit of (importance) this investigation. With the sea level low overall, clastics were now primarily being deposited in the deeper portions of the slope and basin and only when relative sea level rose high enough could carbonate deposition occur.

Furthermore, the opposite of this process is true. During times of lower order highstands in sea level, clastic bypass and deposition can only occur during relative lowstands in sea level in

which the sea level regresses low enough for it to occur. Bone Canyon is interesting because it contains at least two low (2^{nd}-3^{rd}) order sea level fluctuations. Bone Canyon begins within the first (1/2) lower order sea level highstand and ends within the second (2/2) lower order sea level lowstand. Within these lower order fluctuations are numerous higher order fluctuations. The actual amount of higher order fluctuations in Bone Canyon is, unfortunately, still unknown. This will be discussed later in the combined results and in the recommendations for future work.

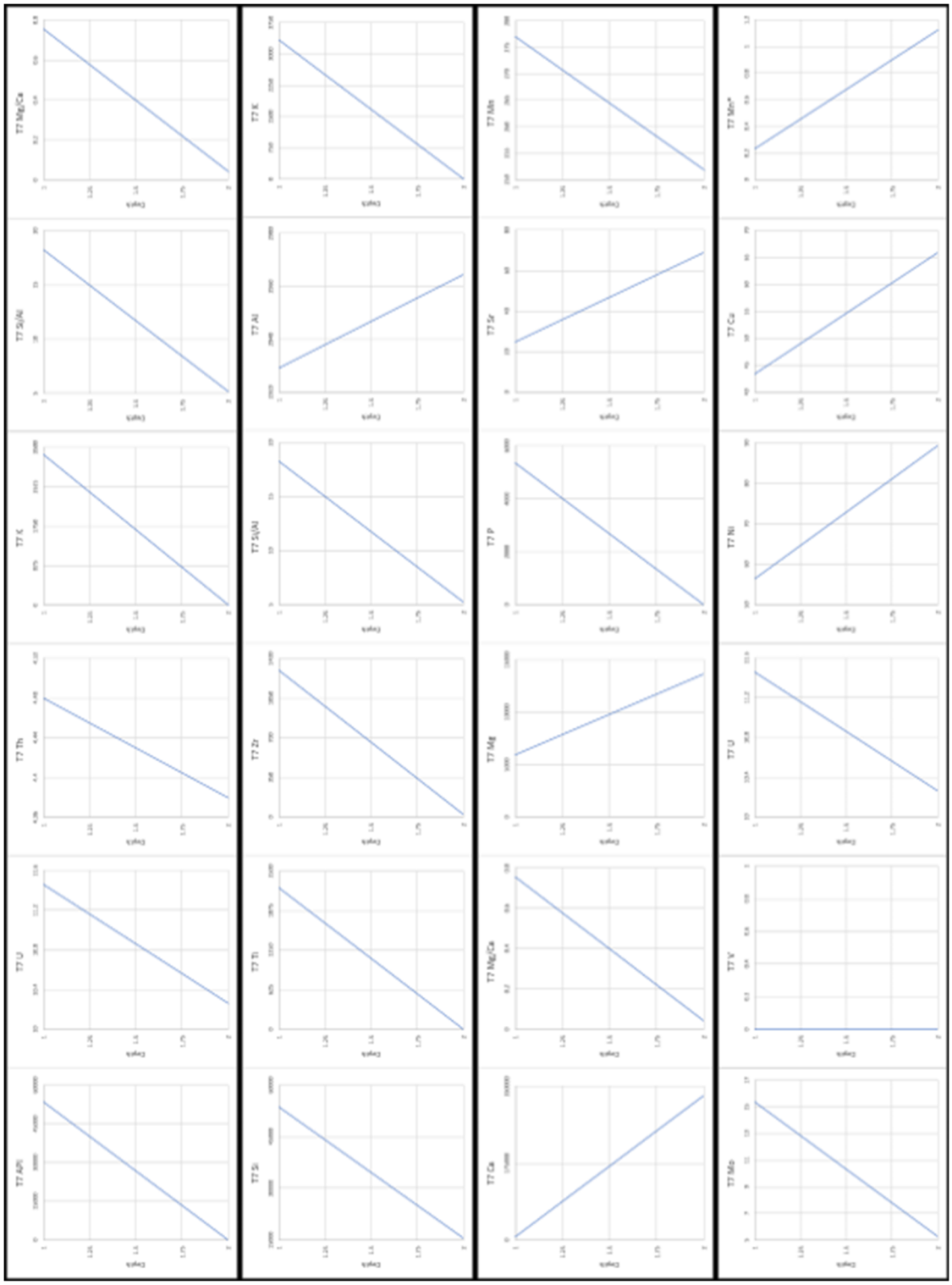

Figure 91: Transect 7 geochemical proxy results showing, from top to bottom, Radiation Proxy Suite, Clastic Proxy Suite, Carbonate Proxy Suite, and Paleoredox Proxy Suite, respectively.

5.2.2 Thin Sections

Hand samples were taken throughout Bone Canyon in key areas so thin sections could be made and analyzed. Thin sections of Transect 1 were made from the carbonate unit and the sand unit within in order to see the mineralogy and petrography. **Figure 92, (photo A)** shows that the carbonate unit in Transect 1 is a wackestone composed of radiolarian, benthic foraminifera, and bivalve skeletal fragments. Trilobite fragments are also present, but rare. There are trace amounts of biogenic silica and here the cement is composed of sparry calcite cement and kerogen-rich fibrous layers. The amorphous pore space suggests that dissolution dominated diagenesis. That this is a wackestone may suggest, if pervasive as a facies, a depositional regime shallower (shelf margin-slope) than a mudstone (slope-basin). The sand unit within is a siliceous mudstone dominated by biogenic silica. The section has undergone partial dolomitization. Dolomitization commonly can exhibit a euhedral, planar-rhombic structure, cloudy centers, or hypotropic-mosaic textures (Plemons, 19). Radiolarians and sponges are common. Calcic spears show sweeping extinction and show low mg calcite replacing aragonite. Very fine to fine silica grains occur in a spar-dimicrite matrix which may indicate an eolian source.

The paleoenvironmental facies of Bone Canyon at the time of deposition was at the toe-of-slope. This area is dominated by carbonate mudstones that were deposited as turbidites, carbonate aprons, and debris flows. The wackestone properties (A) followed by younger mudstone properties (B) may suggest an increase in sea level or a transgression. The earliest sediment of Transect 1 corresponds to a lower sea level and could suggest that the carbonate platform and slope failed, resulting in erosion and causing gravity flows and/or debris flows that carried more terrestrial material onto the slope and into the basin. The more siliciclastic-clastic-rich unit seen here is determined to be one of those deposits, which is overlain by a more shale-

rich unit that may correspond to a TST. This is further proof of the explanations provided in the analysis of Transect 1.

The next thin section was taken from Transect 2, which corresponds to the carbonate turbidite deposits that resulted in bedded, and alternating, deposits of carbonate and chert. As mentioned before, Transect 2 is composed of alternating beds of limestone and chert. The thin section (C) shows a chert/chalcedony dominated wackestone. Crinoids and ooids are present. Crinoids have kerogen-filled centers and a sparry calcite perimeter. Radial ooids were likely transported from the shelf. Chert beds contain high concentrations of chert/chalcedony cement and contain around 15% allochems. An important aspect of this thin section is that it is a wackestone.

Transect 1 was deposited via gravity flows during a TST and, therefore, contains shelfal material. If Transect 2 was a continuation of Transect 1, it is likely that the deposits would be more mud-rich. Instead, this wackestone suggests that the system is in a highstand environment rather than a system in a transgressive environment. Owing to the fact that during turbidite deposition the beds get buried quickly, Transect 1 and through Transect 4-5, the beds were quickly buried. This resulted, and promoted, early stages of diagenesis. During early diagenesis, the biogenic-silica could not escape into the water column. Instead, the silica migrated up to a more permeable layer, where it was trapped by a less permeable bed, and then spread laterally forming biogenic-silica-rich beds. It is important to mention that carbonate turbidite deposition in Bone Canyon usually follows the buoma sequence deposition and alternates back and forth between two main phases of the sequence. This alternating pattern results is one bed being thicker, less permeable and the other bed being thinner, more permeable.

Thin section D was taken from Transect 6, which is known in this work as Carbonate A and represents mottled chert. This thin-section is a kerogen rich siliceous mudstone with trace amounts of biogenic silica, suggesting the silica is less biogenic than the previous transects. This matches the analysis previously given of Transect 6. Chert is replacing allochems and crinoid centers subjected to dissolution. The matrix is dominantly micrite rather than the sparry-dimicrite common in the lower (older) carbonate units. Transect 6 was likely deposited in a similar manner to the previous transects, however, the depositional processes after Transect 6 were different. Sometime around the deposition of Transect 6, either shortly before or shortly after, the sea level began to regress and, therefore, caused the Transect 6 sediment to be buried in a different manner than the previous transects. As mentioned early, the sediment above Transect 6 was deposited during the LST of the L7 HFS. As seen in the field, this sediment was deposited as gravity debris flows when the slope became unstable during the RST. The debris flow was not deposited directly after Transect 6, but rather lagged compared to the rate of deposition of the carbonate turbidites in the previous transects. This slight lag allowed silica to escape more so than before. Also, the change in depositional processes effected the type of silica. Shortly after, when the slope became unstable enough, the gravity debris flow process occurred. This deposition is generally thought to occur relatively quickly. The quick deposition of large quantities of shelf-slope sourced sediment resulted in quick burial of Transect 6. This created a similar environment to the previously deposited and buried transects and, therefore, similar processes are seen at Transect 6, but slightly vary owing to the short lag in deposition.

Figure 93 displays the thin sections created from both the Cutoff Conglomerate (A) and the Brushy Canyon Formation (B) at Transect 7. The Cutoff is shown as a calclithite that is dominated by sparry-calcite cementation. The image shows rounded-sub-rounded and poorly

sorted clasts contained in a calcitic and partially dolomitized matrix. The Cutoff cobbles are rich in allochems and calcite that were likely sourced from the shelf. This provides further evidence that this unit was deposited during a late HST or early RST, which matches the evidence previously discussed. The image also shows two generations of isopachous cementation, which likely first formed during an early stage in marine cementation and then a phase of calcic spar isopachous cementation that formed rings. The spars in the second stage of cementation indicates a marine-vadose cementation. The thin section also shows a cloudy intra-clastic microcrystalline dolomitization and is very fine-grained.

The Brushy Canyon Formation thin section shows a subarkose containing calcite and partially dolomitized cement. The quartz grains are very fine-grained and angular to sub-angular. This unit only has a trace amount of feldspars (< 5%) and lacks fossils. The lack of trace fossils and replacement features indicates a more detrital/terrigenous source of silica. The silica differs from Transect 1 where the silica is more biogenic-rich. The outcrop displays a lot of soft sediment deformation implying subaqueous deposition. These characteristics also indicate this unit was deposited during a late RST and/or LST. This matches the evidence discussed in the previous sections.

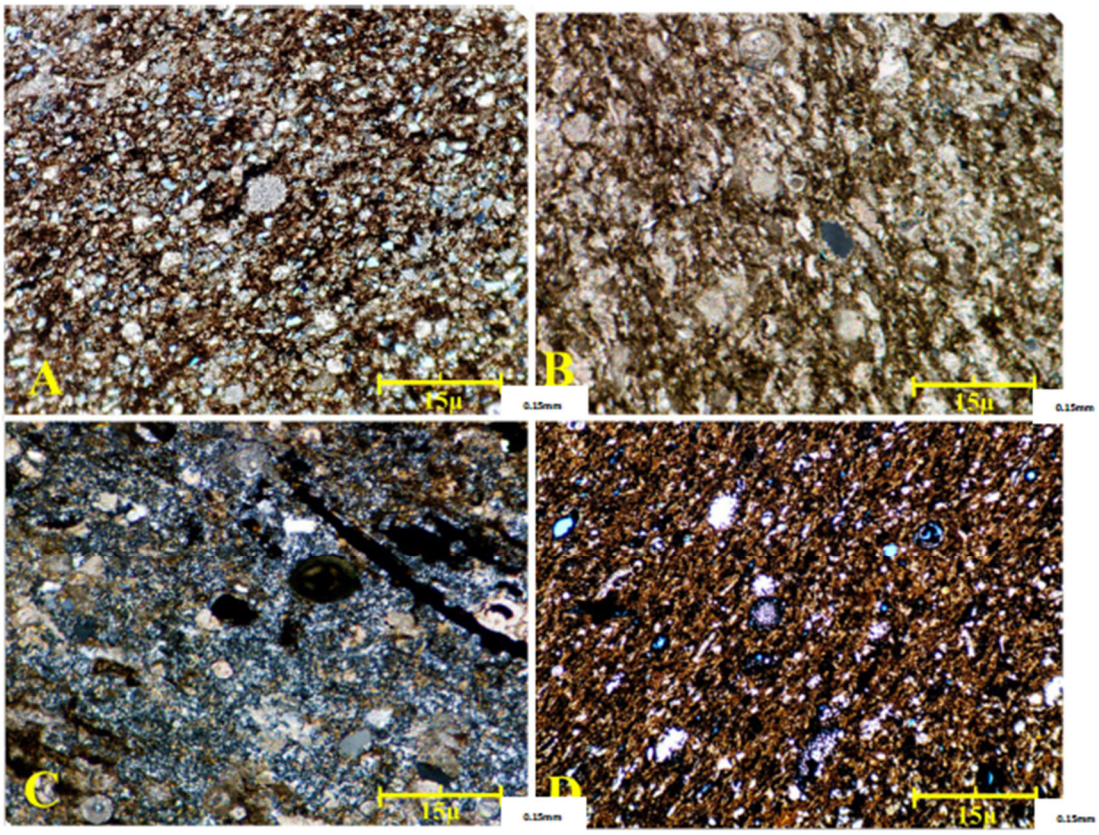

Figure 92: Thin-section images taken from Bone Canyon. A) corresponds to Transect 1, B) corresponds to Transect 2, C) corresponds to Transect 3, and D) corresponds to a chert bed from Transect 6. Taken from Plemmons (2019).

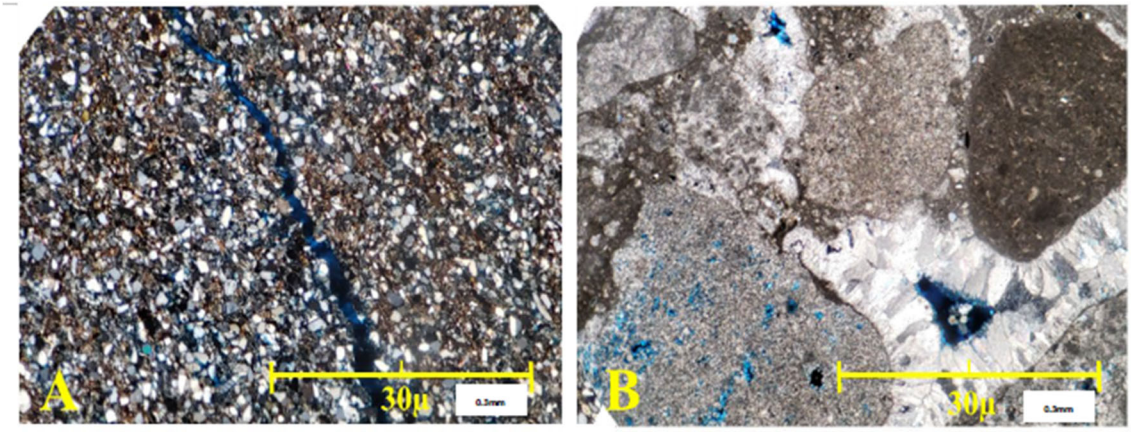

Figure 93: Thin-section images taken and created from Bone Canyon. A) corresponds to the Cutoff Conglomerate of Transect 7 and B) corresponds to the Brushy Canyon Formation at Transect 7. Taken from Plemmons (2019).

5.2.3 Subsurface Correlation

Finally, it is instructive to compare the Bone Spring pseudo-spectral gamma ray results with that of the subsurface interpreted by Crosby (2015). One well which Crosby (2015) used as a Bone Spring model for the subsurface is the Raptor West 3, State #1, which is located approximately 80 miles to the North East and essentially along strike. **Figure 94** illustrates the Upper Bone Spring gamma ray log of the Raptor Well and at the identical scale, the Bone Canyon analysis. For the Bone Canyon, the majority of the covered intervals are assumed to be hot sand to shales. For the Raptor, from the top of the Bone Spring Carbonate (BSPG_C2) to the top of the Bone Spring First Sand (BSPG_S1), the high gamma ray corresponds almost exactly to the top of the interpreted First Bone Spring Carbonate Sand (FBSC S) of Bone Canyon. For BSPG_C1 of Raptor, there are three major carbonate cycles which correlate to three major carbonate cycles in C and B of the First Bone Spring Carbonate of Bone Canyon (FBSC C and FBSC B, respectively). The top of the Avalon in the Raptor well has two major carbonate cycles interspersed with two major sand/shale units and correspond to those in the outcrop. Finally, the two carbonate units of the uppermost Bone Spring Sand (BSPG) of the well appear to match that of the El Centro and Williams Ranch members of Bone Canyon.

These results, while by no mean as rigorous as using a paleontologic or absolute time correlation, may be viewed as supportive of an approximate correlation of the outcrop in Bone Canyon to the subsurface, and moreover conformational of a regional significance of the sequence stratigraphy.

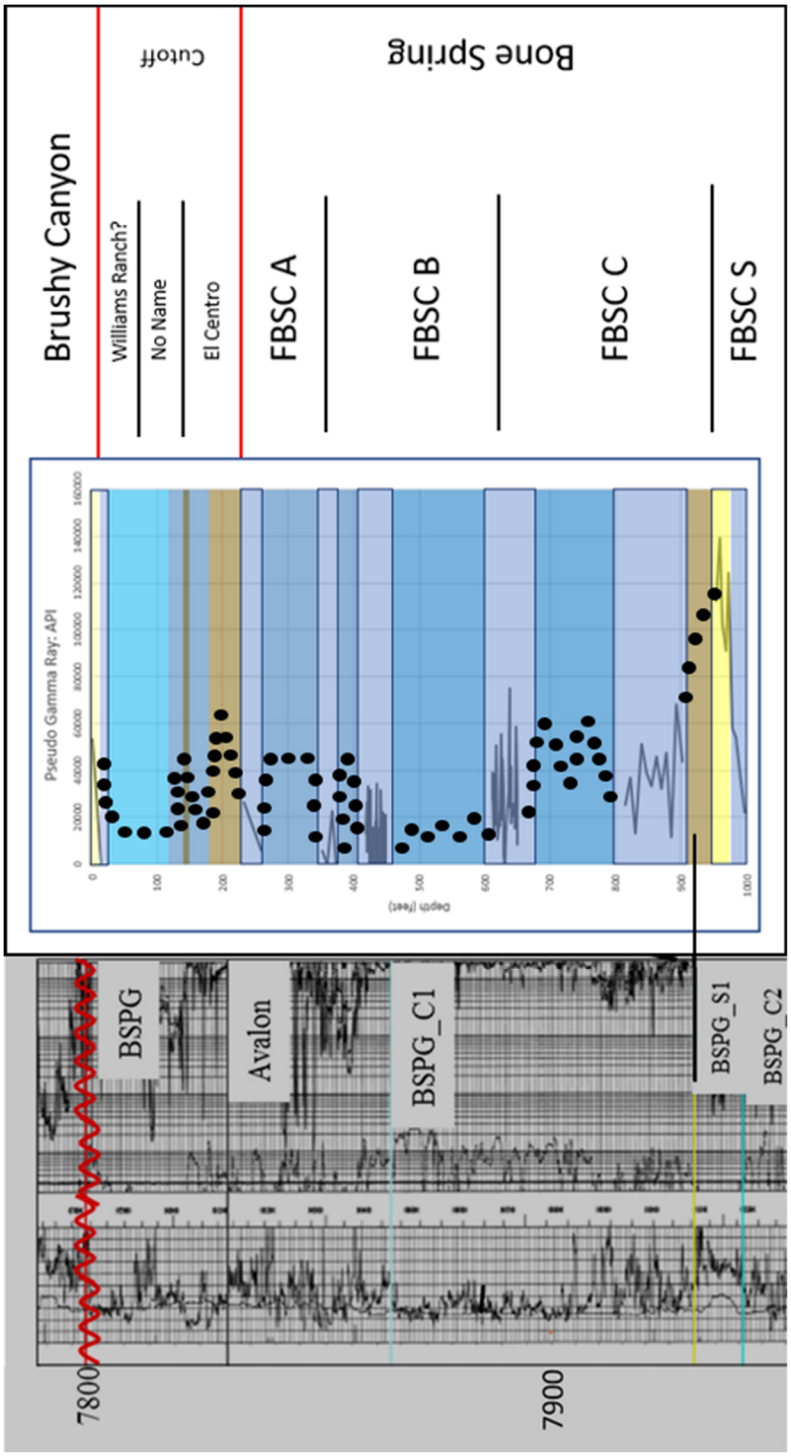

Figure 94: Outcrop to subsurface correlation of Bone Canyon to Crosby's (2015) interpretation of the Raptor West 3 State #1 Well.

Chapter 6: Discussion

Integration and Interpretation

Analyzing finer scale, high-order (individual transect) variations using outcrop observations, petrography, and XRF is important because it allows the ability to determine controls such as relative sea level, provenance, biota, and test for higher frequency sea level cycles i.e. Milankovitch Cycles. However, a more important question is, what does this all mean within the bigger picture? **Figure 95** shows the pseudo gamma ray curve generated for Bone Canyon. This image provides the ability to see significant changes in API throughout the canyon and, therefore, provides evidence of changes in depositional environment that correspond to several 3rd order high-frequency sequences.

The dark blue outlined intervals correlate to the transects with data (field and lab) in the canyon. Intervals not outlined are covered intervals where no data could be collected other than field data (pictures and notes) of the strata and lithology. In general, blue represents carbonate strata, yellow is clastic strata, and brown is shale strata. Dark blue areas between transects represent covered carbonate intervals and the light blue interval represents a clean, thinly layered carbonate mudstone. Yellow represents siliceous-rich or more terrestrial sourced strata (mudstone-vf sandstone). The thicker brown intervals represent shale intervals and the thin brown interval within the blue interval symbolizes a shaley-mudstone interval. Transects contain different occurrences of chert so the lower transects are connected with a darker shade of blue because of their similar occurrences of chert. Similarly, the middle-upper transects are connected with a darker blue because of their similarities of chert.

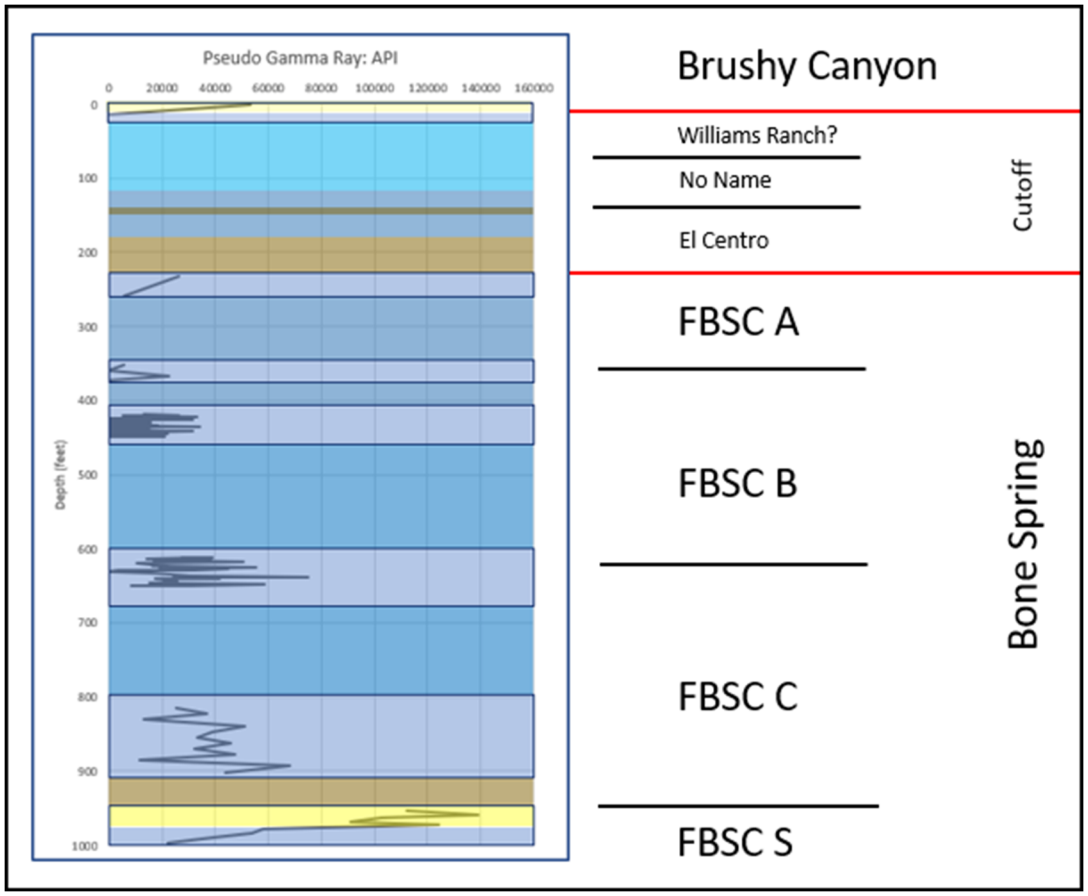

Figure 95: Bone Canyon's Pseudo-Gamma Ray Log displayed with unit names. In general, blue represents carbonate strata, while yellow and brown represent siliciclastic-clastic strata.

Transect 1 is significant because of the high API values, as well as the higher terrigenous proxy values, previously mentioned, compared to the rest of Bone Canyon. Comparing Transect 1 to Transect 2, a significant change in depositional processes occurs. Transect 1 begins with fairly high carbonate proxies such as Mg and Ca. Moving up-section in Transect 1, Al, Th, Ca, and Mg decrease, while API, Si, Ti, Zr, U, K, and the Si/Al ratio increase. The Mg/Ca ratio in Transect 1 increases and then decreases. Although some terrigenous proxies increase, it is important to mention that others do not, and in fact, some decrease (Al). It is also important to mention that Si/Al increases, suggesting more biogenic silica is coming into the system.

Increases in biogenic silica may represent pelagic deposits containing radiolarian. The influence of terrigenous sediment within a carbonate host, or vice versa, can actually occur during times of both TST's and/or RST's (transitional periods of sea level). In order to determine whether or not this transect, which contains higher concentrations of terrigenous proxies compared to the other transects, was deposited during an overall 3rd order HST or LST, previous work in the area, along with other proxies, and interpreting subsurface correlation is crucial. With this in mind, the Transect 1 may represent a sea level lowstand. It is possible that the first interval of carbonate below the sand represents the top portion of the Second Bone Spring Carbonate. The top of Transect 1 would therefore correlate to a TST. The increase in terrigenous proxies was likely the result of an unstable slope during the transition from the L5 to the L6 HFS.

The Leonardian 5 HFS (L5 HFS) was deposited during a LST-TST and the L6 HFS, immediately above, was deposited during an HST (Hurd and Kerans, 2014; Kerans and Kempter, 2002; Fitchen, 1997; Kerans, 1995). Their work in Shumard Canyon, just north-northwest of Bone Canyon, discusses the L5 and L6 HFS. The L5 HFS is a mudstone-wackestone with intervals of siliciclastic-clastic-terrigenous material occasionally found within it. This type of deposit is seen at the mouth, as well as in other areas, of Shumard Canyon. They determined that the material was shed (sourced) from the Victorio Peak platform and made its way onto the slope and into the basin via gravity debris flows from a failing shelf, shelf-slope. Debris flows occur on the slope (and shelf-slope) when sediment becomes unstable after fluctuations (rise or fall) in sea level.

Transect 1 is determined in this work to represent the TST of the L5 HFS. Immediately above the clastic/terrigenous-rich mudstone unit is a shale unit. Above this shale, the beds become covered (with a classic shale slope profile seen in the field) until Transect 2, where the

beds are mudstone interbedded with chert. After a TST, and before an HST, there is a maximum flooding surface (mfs) that is represented as a shale. After a TST, the sea is forced to regress just before the HST and similar sediment to that being deposited before the relative fall (before slope failure) is deposited once again. Slope failure can occur during the actual TST or during the slight and brief fall in sea level that moves the system into an HST. *How can I use paleoredox proxy suite here?

Fitchen (1997) did a detailed analysis on the Lower Leonardian high-frequency sequences and the strata that comprise them. The work explains how the L3, L4, and L5 HFS were defined during times of sea level rise (TST) and because of this, they all showed similar vertical successions of facies. During TST's, facies display a common vertical succession going from sandstone, to silty sandstone, to sandy siltstone, to silty carbonate- reflecting an increase in water depth (Fitchens, 1997). These basal sandstones and siltstones display thin-thick beds, recessive weathering, "and form the base of carbonate-capped shelf/ramp cycles…" (Fitchens, 1997). Through field observations and the pseudo-gamma ray curve, the facies shift from Transect 1 to Transect 2 is from carbonate, to siliciclastic-rich debris flow, to carbonate. Therefore, it has been identified as the transition from the L5 TST (Transect 1) to the L6 HST (Transect 2). Fitchens (1997), Pray (1988), and McDaniel and Pray (1967) further support this by placing the top of the L5 HFS at a major shift basin-ward of dolomite mudstone and wackestone facies in which they placed at a transition from outer shelf/ramp margin facies to lower slope/basin/distal ramp facies tracts (Fitchens, 1997). As is seen above at the top of Transect 1, and which will be seen and discussed later on above Transect 6, "This basin-ward shift is succeeded by a shelf-ward encroaching tongue of mudstone facies." (Fitchens, 1997), which corresponds to the contact between L5 and L6, as well as the Cutoff Formation in Bone Canyon.

Before the shelf-ward encroachment of the Cutoff Formation occured, the shift mentioned above is similar to what is seen from Transect 1 to Transect 2. Fitchens (1997) goes further to say that beds in low-angle toe-of-slope settings, like that of Bone Canyon strata in the Lower Permian, have high lateral continuity and sheet-like geometry. This is proven true in the older, lower strata of Bone Canyon where interbeds of limestone and chert are seen to be laterally continuous. Dolomite starts to increase in Transect 1, resembling Fitchens description, and then decreases in the top facies that resembles the shale-rich unit. All of this complimentary data provides a confident conclusion, in which the contact between L5 and L6 HFS is located at Transect 1 and up to Transect 2. It is important to mention that before the shale unit towards the top of Transect 1, the proxy values are fairly similar to the following transects.

Table 3 shows the maximum, minimum, the difference between them, and the average API values for each transect in Bone Canyon. The number of data points collected per transect is included because the number of data points has significant influence on the outcome and the conclusions that can be drawn. Transect 2 and Transect 3 (Detailed Section 2) have average values of 37344.38 and 27887.5 API, respectively. This is a decrease in average API from Transect 1 by 45,127.93 API (Transect 2). From Transect 2 to Transect 3 the average value only decreases by 9,456.88 API. The drastic change in average API between Transect 1 and both Transect 2 and 3 (DS2) is evidence of a change in depositional processes.

Main changes from Transect 1 to Transect 2 are seen in many of the proxies, especially, but not limited to, terrigenous proxies. Overall, at Transect 2 average API, Ti, Zr, U, Th, Al, K, P, Si, Si/Al, and Mg all decrease, while Ca, Mg/Ca, Sr, Mn increase. However, Si and Si/Al reach higher values at Transect 2. This is important because the carbonate proxies increase. Owing to the debris flow in Transect 1, more siliciclastic proxies were found in Transect 1,

however, with increases in Ca, Mg/Ca, Sr, and Mn, suggest that Transect 2 was likely deposited during the early L6 HST, however, by different processes than Transect 1. As mentioned earlier, the high lateral continuity of the beds in Transect 2 suggests a sheet-like deposition of carbonates on the toe-of-slope. This is determined to represent carbonate turbidite deposits. During the L6 HST, carbonate production is, in general, high, but, as will be shown, production is inferred to have will increased in the following transects.

API in Transects							
Formation	Play	Transect	Max	Min	Difference	Average	Points per Transect
Brushy Canyon		Transect 7	53381	99.6	53281.84	26740.52	2
Cutoff	Upper Avalon	Transect 6	22772.2	49.76	22722.44	11410.98	2
Bone Spring	Middle Avalon	Transect 5	26134.48	67.08	26067.4	9389.18	4
		Transect 4	71100.64	0	71100.64	11556.07	50
		Transect 3	75180.8	3527.04	71654	27887.5	30
		Transect 2	68428.96	11468.44	56960.52	37344.38	12
	Lower Avalon	Transect 1	138920.8	21969.76	116951	82472.31	9

Table 3: Table showing Max, Min, Difference, and Average API for all transects in Bone Canyon

Transect 3 is important because the depositional environment and processes remain the same as Transect 2, providing the first real look into the progradation of the basal L6 Bone Spring carbonate turbidites. At Transect 3, average API, Si, Ti, Zr, Al, Th, K, P, Mg, Mn, Mg/Ca decrease, while Si/Al, U, Ca, and Sr increase. However, API, Mg, Si, Th, and K all reach higher values than the previous transect. The fact that some of these proxy's average values decrease is likely owing to the amount of data points collected here compared to Transect 2. Transect 3 contains 30 data points compared to 12 data points from Transect 2. It is important to mention that because more quartz/chert-rich beds were collected in Transect 3, which contain almost none or very little carbonate, the average values of certain carbonate proxies will be lower. The

decrease in terrigenous proxies, increase in main carbonate proxies, increase in the Si/Al ratio, along with the higher values reached by API, Mg, Si, Th, and K suggest that Transect 3 was deposited similarly to Transect 2, but represents a further stage (continuation) in progradation of the toe-of-slope-basal L6 carbonate strata. Similar to Transect 2, Transect 3 beds display high lateral continuity in both carbonate and chert beds, further suggesting carbonate turbidite deposition.

Transect 4 represents a continuation of the prograding basal carbonate turbidites. Here, average API, K, Si, Ti, and Zr continue to decrease from Transect 1, while average Ca is the only constant increase. From Transect 3 to Transect 4, average Si/Al, U, Sr, and Mn decrease, while Th, Al, Mg, and Mg/Ca increase. However, Transect 4 reaches higher values in U and contains generally higher Si/Al and Si. Again, it is important to mention that owing to the collection of more beds, either carbonate or chert, some interpretations may be skewed. However, owing to the general, continued decrease in terrigenous proxies and the continued increase in carbonate proxies, U and Th, and the Si/Al and Mg/Ca ratios, Transect 4 represents the continued progradation of the L6 HFS. Another important fact is that at the end (top) of Transect 4, Mg/Ca, Si/Al, Mg, U, and Si start to decrease, while K and Al start to increase.

At Transect 4 (Detailed Section 1) the average API values, as well as fluctuations in API, are much lower at 11,556.07 API. The average value decreases from Detailed Section 2 (T3) to Detailed Section 1 (T4) by 16,331.43 API. Although not as significant of a decrease as seen from previous transects, a trend can now be seen. The trend appears to start with a high interval at Transect 1, a transitional period during Transects 2 and 3 (DS2), and then a low interval at Transect 4 (DS1). Such a trend can be explained by a change from a TST to an HST in which the slope has stabilized allowing ‘normal carbonate progradation’ deposition to occur. By Detailed

Section 1 the HST is in full swing depositing carbonate mudstones in the basin, which is reflected in the pseudo-gamma ray response.

During the HST, carbonate production is high and sediment is being transported into the basin via carbonate turbidity currents. Another important aspect of deposition during this time is the settling of sediment and biota such as radiolarian and sponge spicules out of suspension in the water column and onto the basin floor. The biota is especially important in Transect 2 and Transect 3 because it is the source of silica that created the interbedded chert that is seen on the pseudo-gamma ray and lithology profiles.

In carbonate turbidites, sediment is being rapidly buried and the freshly buried sediment is then experiencing pressure from the load above. When the sediment is squeezed, pore fluids rich in silica (from biota) escape and go towards less pressure and more permeability, which is ideally back into the water column. However, because turbidites are deposited so quickly the sediment is buried deeper and usually only makes it into a more permeable layer above. Another factor with carbonate turbidites, and/or turbidite systems in general, is how the facies arrange themselves within the system both vertically and horizontally. This arrangement is otherwise known as the Bouma Sequence, which is influenced by energy and/or sediment size. In the Bone Spring Formation, most of the bouma sequences within the beds in the basin are bouma A and bouma B meaning a general proximal fan location within the. Bouma A sequences are usually considered less permeable and as you move into bouma B and C permeability increases. Since bouma A is buried first, siliceous fluid tends to migrate up into the more permeable overlying bouma B, or C, sequence. The fluid then tries to continue to migrate vertically, however, because bouma A (less permeable) is now deposited on top of bouma B the fluid can’t migrate vertically anymore so it migrates and spreads laterally forming beds and nodules. This process is believed

to happen during early diagenesis. This explanation can be seen by the fluctuations in the pseudo-gamma ray curve that resemble alternating beds of limestone and chert.

Although Transects 5-7 do not have the amount of XRF detail (data) as previous transects, important observations can be made from the XRF data when compounded with field data (notes and pictures). From Detailed Section 1 (Transect 4) to Transect 5 the average API value continues to decrease from 11,556.07 to 9,389.18 API, a difference of 2,166.89 API, following the same trend as before. Overall, API, U, Th, K, Ti, Zr, Al, Si, Si/Al, Mg, and Mg/Ca decrease, while Ca continues to increase. Continuous trends from Transect 1 to Transect 5 are seen in API, Si, Ti, Zr, and Ca. These proxy trends suggest that depositional processes to Transect 5 have remained the same. Again, this suggests that the L6 HFS represents prograding carbonate strata. However, after Transect 5 an important change is observed in both field and lab data, suggesting progradation is coming to an end, either from a decrease in carbonate production and sediment supply, or a change in depositional processes and/or environment. As previously mentioned in the field results, Transect 5 differs from Transect 4 (DS1) in that the chert in Transect 5 is more nodular, and, specifically, becoming mottled (splotchy, noncontinuous).

At Transect 6, average API, U, Th, K, Si, Ti, Zr, Sr, Mg, Mn, Si/Al, and Mg/Ca all increase, while average Al and Ca decrease. The greatest change was observed in a decrease in Mg/Ca. Transect 6 proxy values do show increases, or decreases, from Transect 5, although in general, all concentrations seem to have returned to the concentrations observed in Transect 4. Owing to the fact that the concentrations alter from the continuing previous trends, there was likely different controls and processes that influenced Transect 6. However, it is important to mention there is less data at Transect 5 than the previous transects, possibly skewing the

observations. With this in mind, it was crucial to observe the previous trends along with the field results collected directly above this transect.

By Transect 6 the chert is almost entirely mottled and noncontinuous suggesting that less silica was present in the system, during diagenesis, or the unit was not buried fast enough. When the silica-rich interstitial fluid tried to migrate, it did, but couldn't provide enough silica to the more permeable layer above, which caused silica to precipitate out in a splotchy, mottled texture. **Table 3** shows from Transect 5 to Transect 6 there's an increase in average API from 9,389.18 to 11,410.98 API. Unlike the previous transects that gradually decrease, Transect 6 has a gradual increase in API. Any change seen visually, and/or through geochemical data, reflects changes in depositional controls whether it may be sea level, sediment input, source, pathway to the basin, and so on. The fact that a change is seen at Transect 6, and again immediately above, means that the depositional regime is changing. As will be discussed next, this change in deposition was caused by the Cutoff Formation, which is reflected by more shale/mud-rich deposits that resulted from an RST and/or LST, as well as the subsequent TST and/or HST in sea level during the L7-G2 high frequency sequences.

From Transect 6 to Transect 7 the beds are primarily covered and not easily accessible. When the beds do crop out after Transect 6, they are at first muddy, fissile, and highly weathered. The beds closer to Transect 7, however, change from a shaley, fissile carbonate to a very clean and highly layered carbonate mudstone. Do to the fact there weren't outcrops in accessible locations and, when there were, fresh clean surfaces could not be found and/or made to collect data in the field, the only data collected between Transect 6 and Transect 7 were field observations and pictures.

The interval between Transect 6 and Transect 7 has been the subject of discussion in many recent works (Hurd and Kerans, 2014; Kerans and Kempter, 2002). These authors believe that this interval is known as the Cutoff Formation. The Cutoff Formation is important for many reasons. The Cutoff Formation is not defined as a chronostratigraphic boundary, but instead cuts across two chronostratigraphic boundaries, the Leonardian and the Guadalupian, creating an intraformational contact. This intraformational contact has been traced throughout the Western Escarpment and is commonly identified as a megabreccia, or a more siliciclastic (sandstone-siltstone) rich, unit dividing the Leonardian 7 HFS from the Leonardian 8 HFS. The Cutoff Formation in outcrop provides a more detailed analysis of its characteristics, such as lithology, age, and depositional processes. For this reason, the Cutoff Formation has been easily over-looked in the subsurface, which has resulted in it being grouped within the Bone Spring Formation as part of the First Bone Spring Carbonate. Within the recent past, more studies have been including the Cutoff Formation above the Bone Spring Formation in the subsurface (Plemons, 2019).

Another issue arises when discussing the Avalon Shale, both in outcrop and in the subsurface. The Avalon Shale is defined as a petroleum 'play' rather than an actual stratigraphic unit and, because of this, depending on the basinal position of the well and/or the company involved, the Avalon Shale can refer to different sets of strata. The work done by Stolz (2014) explains this in detail and defines the Avalon Shale based on research regarding the characteristics of the Avalon Shale from various companies. This thesis uses Stolz's (2014) definition of the Avalon Shale and the biostratigraphic (conodont) work done by Kerans (2016), Hurd and Kerans (2014), and Kerans and Kempter (2002) that correlates the Avalon Shale in the

subsurface to the outcrops of the Bone Spring and Cutoff Formations along the Western Escarpment, Guadalupe Mountains, West Texas.

The interval between Transect 6 and Transect 7 correlates to the Cutoff Formation (Lower, Middle, Upper), which corresponds to the L7-G4 HFS. Kerans (2016) and Hurd and Kerans (2014) correlate the Lower-Middle Cutoff Formation, known as the El Centro Member (L8-G1 HFS), to the Upper Avalon Shale based on conodont data from the subsurface and outcrop. Kerans (2016) goes further and implies that, because of this, the Middle Avalon correlates to the First Bone Spring Carbonate and, specifically, the L6 HFS. With this in mind, the strata in Bone Canyon just above Transect 6 is the mud-, or shale-, rich Upper Avalon and Transect 6 to Transect 1 correlates to the carbonate-rich Middle Avalon. To conclude the Avalon Shale, the Lower Avalon Shale is very similar to the Upper Avalon Shale in that it is more siliciclastic-rich. Looking back at the contact between L5 and L6 at Transect 1 (mouth of canyon), it is now possible to say that this is likely the contact between the Middle and Lower Avalon Shale.

Another important aspect of depositional processes, as they related to the Avalon Shale, is that both Upper and Lower Avalon units were deposited as gravity debris flows, while the Middle Avalon was deposited primarily by carbonate-rich turbidite deposits. The Lower Avalon (L5 HFS), previously discussed, was deposited sometime during the transition from the TST of the L5 HFS to the HST of the L6 HFS. The depositional processes for the Upper Avalon (L7-G1 HFS) are similar but may have been deposited in a slightly different environment.

The L7 HFS resembles the LST. During this quick fall, and subsequent quick rise (TST) during the L8 HFS, the slope became unstable once again. Transect 6 resembles the change in depositional processes from the previous transects. During this time, the sea level began to fall,

transitioning the system from an HST to the L7 LST. The unstable slope as sea level fell caused debris flows to reach lower areas of the slope and into the basin. This process is seen just above Transect 6 in the slumping structure of the lower shale unit. Directly above this slumping structure, there is a layered interval comprised of large cobbles inside of a mud matrix. These cobbles made their way into the basin after the debris flow carved the necessary path for them to travel into the basin during the L7 HFS. This cobble and mud-rich interval is directly overlain by a shale-rich interval, which was deposited during the following TST of the L8 HFS.

This process is similar to that seen in Transect 1, however, the system in Transect 1 did not reach, and does not represent, a lowstand in sea level. Furthermore, after the L6 HFS prograded, Bone Canyon was closer to the carbonate platform margin. This resulted in less sand deposition and more carbonate and shale deposition. The Upper Avalon was deposited during the RST (L6-L7 HFS), the LST of the L7 HFS, and the following TST of the L8 HFS. The Lower Avalon was deposited during the TST of the L5 HFS. This is confirmed by looking at the work done by Fitchens (1997), in which he proves that the L5 HFS represents a TST and the following L6 HFS represents an HST. The main difference is that the Upper Avalon went through a greater extent of sea level fluctuation (RST-LST-TST) compared to the Lower Avalon that resulted from a much lesser extent of sea level fluctuation (TST-HST).

After the deposition of the Lower-Early Middle Cutoff Formation (Upper Avalon) during the L8 TST, the following HST of the G1 HFS resulted in the deposition of more carbonate-rich sediment of the upper El Centro Member of the Cutoff Formation. Above the shale-rich and siliciclastic-rich interval that is above Transect 6 and below Transect 7, the “No-Name”, or “PB” Member, of the Cutoff Formation was deposited during the G2 and G3 HFS. This interval is seen as a clean carbonate mudstone that was deposited, once again, as carbonate turbidites. The

carbonate turbidites alternate between thicker, more resistant (less weathered) beds followed by thinner, less resistant (more weathered) beds. Overall, the beds are becoming more resistant (less weathered) up-section. This suggests that more resistant material is being added into the system. The process of adding more resistant material is the result of a gradual RST.

At Transect 7, average API, U, Th, K, Ti, Zr, P, Ca, Mg, and Mn increase, while average Si, Al, Si/Al, Sr, and Mg/Ca decrease. It is important to mention that the two data points collected at Transect 7 were collected on two different units, the Cutoff Conglomerate and the Brushy Canyon Sandstone, which influences the interpretation of Transect 7 overall. The lower, conglomeritic unit has a concentration value of zero in API, K, and Ti, very low concentrations of Zr and Mg/Ca, moderate concentrations of Si, Al, and Si/Al, and fairly high concentrations of U, Th, Ca, and Mg. The upper, clastic-rich unit displays low concentrations of Ca, moderate concentrations of Al, Mg, and Mg/Ca, and fairly high concentrations of API, K, Th, U, Ti, Zr, Si, and Si/Al.

Transect 7 is important because it represents the contact between the G3-G4 HFS of the Cutoff Formation and the G5 HFS of the Brushy Canyon Formation. This contact represents a change in depositional environment and processes. The lower carbonate unit is the last interval that corresponds to the HST (or RST), while the upper clastic unit is the first interval that corresponds to the LST, which lasts through the end of the Guadalupian and, therefore, the end of Permian deposition.

Another important aspect at Transect 7 is that the upper Brushy Canyon unit is seen to cut, or erode, the underlying carbonate unit of the Cutoff Formation. Furthermore, the Brushy Canyon is massively deformed. The style of deformation seen in this unit resembles soft-sediment deformation. This type of deformation occurs in subsea environments and, here in

Bone Canyon, relates to the early stages of the LST. During the RST, the underlying unit was cut. Then during the following LST, the sediment followed this newly formed route. In the following higher-order fluctuations, this sediment was overlain, which resulted in pressure to the underlying unit. Owing to the differences in lateral erosion of the underlying carbonate unit and the load overlying the first Brushy Canyon sandstone, the first Brushy Canyon sandstone was subjected to differential compaction, which then caused the soft sediment deformation in the sandstone unit. Through time this sediment was solidified and represents what is now seen. These purposed sequences are further confirmed by the correlation of Bone Canyon to Crosby's (2015) investigation into the subsurface. The interpretations of the pseudo-gamma ray response in outcrop and the subsurface closely correspond, providing further support to Bone depositional processes and paleoenvironments of the Bone Spring and Cutoff Formation.

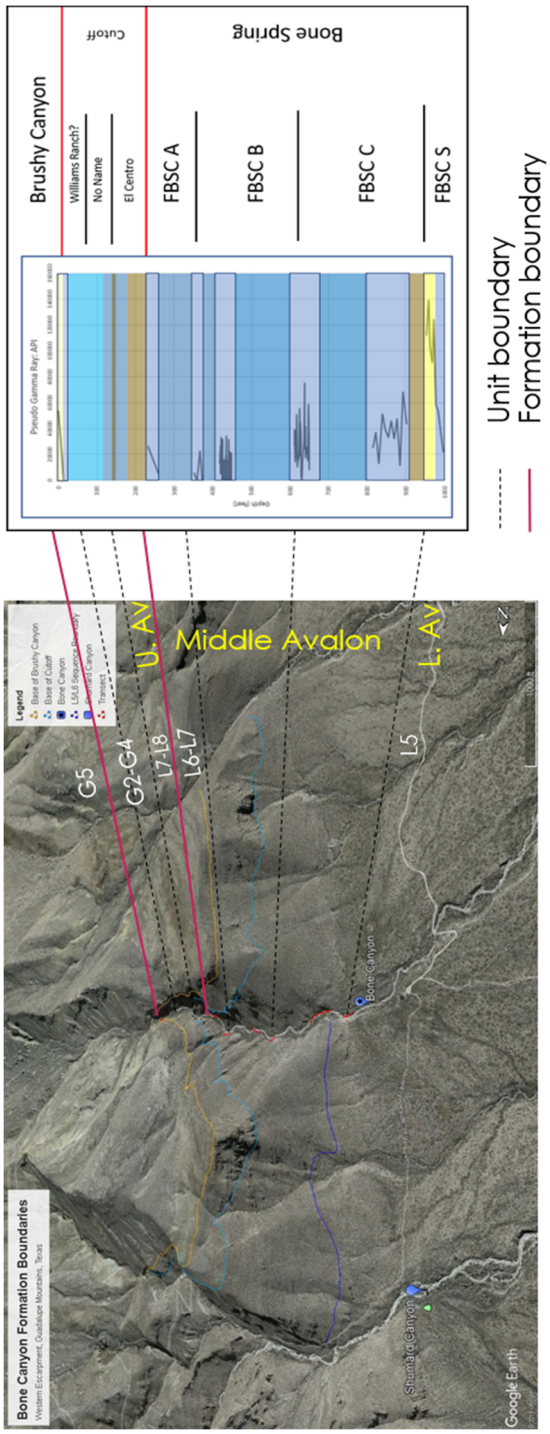

Figure 96: Google Earth Image of Bone Canyon displaying the correlation between the Units, API, and HFS.

Conclusion

The Delaware Basin occupies a negative structural depression located in western Texas and southeastern New Mexico that reaches 200 miles long and 100 miles wide, covering around 86,000 square miles comprised of 52 counties in Texas and New Mexico (Adams, 1965; ShaleExperts, 2019). The DB is bounded by the Northwestern Shelf to the North, the Central Basin Platform to the East, the Marathon-Ouachita Belt to the South, and the Diablo Platform to the West. Few channels including the San Simon Channel to the northeast, the Hovey Channel to the southwest, and the Sheffield Channel to the southeast, played important roles connecting the Delaware Basin, Midland Basin, and Panthalassic Ocean together (Crosby, 2015).

Numerous tectonic and depositional, and/or erosional, phases from multiple orogenies (i.e. Grenville and Variscan) led to the creation of the Delaware Basin. Tectonism during the Permian was owing to waning events of the Variscan Orogeny that resulted in extensive sedimentation into the previously (Pennsylvanian) created accommodation space. The Permian is divided into four depositional phases known as the Wolfcampian, Leonardian, Guadalupian, and Ochoan. The early phases of the Permian are associated with rapid subsidence and extensive sedimentation. These processes resulted in loading, uplift, and the formation of ridges around the basin. This resulted in a more constricted circulation in the basin in the Middle-Late Permian. A few important channels, however, allowed surface water to circulate and promote organic production. Tectonics and subsidence slowed at the end of the Permian and the tilting and deepening of the Delaware Basin was the primary tectonic influence, however, it eventually stopped and the basin was structurally stable during the Ochoan. Tectonic activity increased in the Cretaceous-Cenozoic during the Laramide Orogeny the Basin and Range formation. These events created the Guadalupe Mountains, as well as other structural features seen today.

One of the most important aspects defining the Delaware Basin is the accumulation of Phanerozoic, organic-rich sediments in the deep, poorly circulated basin and the conversion of these sediments into kerogen (Hills, 1984). Although some hydrocarbons became trapped in the basin, without significant tectonics to create structural traps, large amounts of hydrocarbons migrated into carbonate reservoirs. The low amount of tectonic activity, coupled with sedimentary overburden, allowed numerous generations of oil and gas to form (Hills, 1984). During the end of the Permian, thick evaporite beds were deposited that created seals to the traps and allowed the preservation of the hydrocarbons (Hills, 1984).

The Bone Spring Formation is comprised of alternating units of carbonate and siliciclastic sediment, which is generally thought to correspond to 3rd order cycles of relative sea level. Carbonate deposition corresponds to highstands, whereas clastic/siliciclastic deposition corresponds to lowstands in sea level. This pattern of sedimentation, known as *reciprocal sedimentation*, refers to these alternating depositional environments and their associated facies. The four Permian series correlate to these 3rd order cycles and relate to the depositional environments, processes, stratigraphy, and, therefore, the generation of petroleum.

The Upper Leonardian Bone Spring Formation, Cutoff Formation, and Early Guadalupian Brushy Canyon Formation are analyzed in the outcrops of Bone Canyon located along the Western Escarpment of the Guadalupe Mountains in West Texas. This investigation focuses on the high-order (3rd-4th) sequences within these formations primarily through XRF and thin-section petrographic analysis in order to further the understanding of the depositional environments and processes that created and made them into the prolific petroleum plays that they are today. From this study it is suggested that the Bone Spring Formation presented in Bone Canyon consisted of eight to nine 3rd order sequences, from the Leonardian to Guadalupian,

which record the effects of global and relative fluctuations in sea level changes in sediment supply and rate, episodes of subaqueous erosion and basin physiography. These controls upon deposition are seen in Bone Canyon through variations in gravity debris flows, carbonate turbidites, mud drapes, and siliciclastic-clastic fans. The sequences are bounded by intraformational contacts, the Leonardian Unconformity, and the Cutoff Unconformity and reflect 3rd and 2nd order sequence boundaries.

For the observed parasequence sets, Bone Canyon reveals four 2nd order and seven 3rd order sea level fluctuations that represent (2nd order) HST, TST, HST, and RST or LST and (3rd order) TST, HST, LST, TST, HST, RST, and LST, respectively. The first unit in the canyon is identified to be the Lower Avalon Shale and represents the L5 HFS that was deposited as a gravity debris flow that resulted from slope failure during the late stage of the first 3rd order TST (transgressive systems tract or rising sea level). The ensuing 3rd order HST (highstand systems tract or high sea level) of the L6 HFS is identified to be the Upper Bone Spring Carbonate, also known as the Middle Avalon Shale, which is comprised of carbonate turbidite deposits. These turbidite deposits show bouma sequence deposition and alternate between thicker, less permeable carbonate beds followed by thinner, more permeable chert beds.

The Upper Avalon Shale, where at this location it is known as the Shumard and El Centro Members of the Cutoff Formation, represents the late RST of the L6 HFS, the 3rd order LST of the L7 HFS, and the earliest stage of the 3rd order L8 TST. This unit is identified in Bone Canyon by a mud- and shale-rich unit that shows soft-sediment deformation and slumping of the L6 RST, an interval of megabreccia inside of a mud matrix representing erosion of the L7 LST, and a layered, fissile shale of the L8 TST. The Upper Avalon, similar to the Lower Avalon, was

deposited as a gravity debris flow during slope failure, which was caused by these fluctuations in the sea level.

The following 3rd order HST of the G1-G2 HFS resulted in more carbonate turbidite deposition and is seen in Bone Canyon between the Leonardian and Cutoff Unconformities. These turbidite deposits have a thicker, less weathered bed followed by a thinner, more weathered bed and have an overall less weathered trend up-section. These deposits differ from the previous turbidite deposits owing to the type and concentration of silica.

Above these turbidite deposits is a unit known here as the Cutoff Conglomerate, also referred to in this work as the No Name Member, and represents an RST. Directly above this unit is a sandstone unit known as the Brushy Canyon Formation, which eroded the underlying No Name Member and was deposited during the LST. This final LST was the last interval analyzed in this thesis. The LST lasted until the end of the Guadalupian and, therefore, the end of Permian deposition.

The Permian Basin is a very prolific oil and gas province. Oil and gas exploration and production in the Permian Basin, and the Delaware Basin within, has occurred for close to a century. As of 2018, the Permian has produced more than 33.4 billion barrels of oil and around 118 trillion cubic feet of natural gas with proven reserves exceeding 5 billion barrels of oil and 19.1 cubic feet of natural gas, resulting in one of the largest hydrocarbon producing basins in the world. (EIA, 2018). However, there is still a great mystery about its tectonic development, including deformation and subsidence, degrees of sedimentary fill, thermal maturities, and remaining exploration and production potential (Lew et al., 2013).

Advancements in technology and the continued success rate of the Permian Basin, and the Delaware Basin within, have created more interest of the area and sparked questions as to

how the basin has become so prolific. Formations in outcrop are now able to be studied, not just in the field, but also in great detail. The fine-scale heterogeneities of these three formations in Bone Canyon are delineated through the pseudo-gamma ray and geochemical proxies that were generated from analysis by the hand held x-ray fluorescence (XRF), and reveal the internal complexities of the petroleum system(s) created from reciprocal sedimentation. The analysis correlates terrigenous concentrations to lowstands and carbonate concentrations to highstands in sea level, which provide fine-scale observations into the depositional environments and processes. Compositional and paleoenvironment proxies reveal ideal source and reservoir rocks. The analysis shows transgressive system tracts produce more permeable gravity debris flow deposits in a more anoxic environment that result in high hydrocarbon generation.

Future Work

The Guadalupe Mountains, Western Escarpment, and Bone Canyon are ideal places for high-resolution studies of Permian stratigraphy. The outcrops in these areas allow for many more detailed and multidiscipline studies. The fact that most of the previous works in this area, both in outcrop and the subsurface, focus on 3rd-4th order sequences makes these areas perfect for investigations into higher order sequences. Although owing to the thin thicknesses of some of these strata, energy companies cannot focus their drilling efforts into individual beds, it is possible that finding trends in individual bed sets could prove useful to their objectives. As seen in this study, fine-scale trends in physical and chemical properties can be seen at scales around 5-10 feet. It is possible that oil generation, maturation, or migration could be related to certain trends at this scale. It is certainly possible to determine diagenetic trends at these fine-scales and, therefore, diagenetic studies in these areas may be beneficial to various disciplines.

Being able to fill in the gaps within Bone Canyon would help provide a more detailed analysis of the depositional processes that created Bone Canyon. Also, a more complete set of data is necessary in determining the number of high-resolution sequences. Determining the number of sequences would provide a better understanding of the controls that influenced the deposition of Permian formations. Similarly, determining the ages of the units within individual Permian formations would provide a more detailed understanding of the fine-scale, high-order controls.

Although energy companies typically have focused on lower order sequences, it is my understanding that this focus is owing to the fact that the technology necessary to analyze higher order sequences has been limited. As a result, fine-scale processes, and the factors that

influenced them, is not well understood. Seismic data resolution is not good enough to see the high-order sequences. Although cores can be analyzed at this scale and detail, they do not allow for investigations into the lateral variability, at any scale. This lack of information highlights the need to, not only investigate fine-scale sequences through depth, but to also investigate the lateral variability of high-order sequences. Studies of outcrops are the best means for this type of investigation.

Lateral variation provides insight into depositional processes for lower order sequences, however, at a fine scale, lateral variation may provide insight into fluid migration. The migration of silica is an important factor in Permian formations and their petroleum production. It is possible that determining fluid migration pathways from fine-scale investigations may allow 'sweet spots' to be found that otherwise would not be uncovered. Although fluid migrates upwards, it is possible that fluids also migrate based on other factors at a finer scale. These sweet spots may be found trapped at lower elevations owing to differences in diagenetic processes, both vertically and laterally.

It is also possible to use biota to aid in determining finer-scale processes and influences as mentioned above. By looking at biota at finer scales, and how they vary vertically and laterally, it is possible that trends could be found that aid in further determination of hydrocarbon exploration sweet spots. Knowledge of higher order sequences may make it possible in the near future for companies to be better able to determine where oil and gas may be discovered and produced or where sweet spots can be found within lower order sequences. These factors make understanding fine scale, high order stratigraphy important.

References

Adams, J.E., M.G. Cheney, R.K. DeFord, R.I. Dickey, C.O. Dunbar, J.M. Hills, R.E. King, E.R. Lloy, A. K. Miller, and C. E. Needham, 1939, Standard Permian Section of North America: AAPG Bulletin, v. 23, p. 1673-1681.

Adams, J.E., 1965, Stratigraphic-Tectonic Development of Delaware Basin: Bulletin of the American Association of Petroleum Geologists, v. 49.11, p. 2140-2148.

Algeo, T.J., and H. Rowe, 2012, Paleoceanographic Applications of Trace-metal Concentration Data: Chemical Geology, v. 324-325, p. 6-18.

Algeo, T.J. and N. Tribovillard, 2009, Environmental Analysis of Paleoceanographic Systems Based on Molybdenum–uranium Co-variation: Chemical Geology, v. 268.3-4, p. 211-225.

Algeo, T.J., and J.B. Maynard, 2008, Trace-metal Co-variation as a Guide to Water- mass Conditions in Ancient Anoxic Marine Environments: Geosphere, v. 4.5, p. 872-887.

Barker, C.E. and R.B. Halley, 1986, Fluid Inclusion, Stable Isotope, and Vitrinite Reflectance; Evidence for the Thermal History of the Bone Spring Limestone, Southern Guadalupe Mountains, Texas: SEPM Special Publications, v. 38, p. 189-203.

Bassett, D. A., 2012, Evaluation of Chemostratigraphy in Interpreting Stratigraphic Architecture of the Bone Spring Formation in the Delaware Basin, Eddy County, New Mexico: Master‘s thesis. Oklahoma State University, 2012, Stillwater, Oklahoma, p. 260

Blakey, R., 2013, Global Paleogeography, Northern Arizona University. <http://www2.nau.edu/rcb7/nam.html>.

Boyd, D. G., 1958, Permian sedimentary facies, central Guadalupe Mountains, New Mexico: New Mexico Bureau of Mines and Mineral Resources Bulletin 49, p. 100Brumsack, H.J., 2006, The trace metal content of recent organic carbon-rich sediments: Implications for Cretaceous black shale formation: Paleogeography, Paleoclimatology, Paleoecology, v. 232, p. 344-361

Catuneanu, O., W.E. Galloway, C.G.St.C Kendall, A.D. Miall, H.W. Posamentier, A. Strasser, and M.E. Tucker, 2011, Sequence Stratigraphy: Methodology and Nomenclature: Newletters on Stratigraphy, v. 44/3, p. 173-245.

Catuneanu, O., V. Abreu, J.P. Bhattacharya, M.D. Blum, R.W. Dalrymple, P.G. Eriksson, C.R. Fielding, W.L. Fisher, W.E. Galloway, M.R. Gibling, K.A. Giles,J.M. Holbrook, R. Jordan, C.G.St.C. Kendall, B. Macurda, O.J. Martinsen, A.D. Miall, J.E. Neal, D. Nummedal, L. Pomar, H.W. Posamentier, B.R. Pratt, J.F. Sarg, K.W. Shanley, R.J. Steel, A. Strasser, M.E. Tucker, and C. Winker, 2009, Towards the Standardization of Sequence Stratigraphy: Earth-Science Reviews, v. 92.1-2, p. 1-33.

Crosby, C. B., 2015, Depositional history and high-resolution sequence stratigraphy of the Leonardian Bone Spring Formation, Northern Delaware Basin, Eddy and Lea Counties, New Mexico: Norman, OK, University of Oklahoma.

Dunham, R. J., 1962, Classification of carbonate rocks according to depositional texture, in Ham, W. E., ed., Classifications of carbonate rocks-a symposium: American Association of Petroleum Geologists Memoir NO. I, p. 108-1 21.

EIA, 2018, U.S. Crude Oil and Natural Gas Proved Reserves, 2017 *<http://www.eia.gov/naturalgas/crudeoilreserves/pdf/usreserves.pdf>*

EIA, 2014, U.S. Crude Oil and Natural Gas Proved Reserves, 2013 *<http://www.eia.gov/naturalgas/crudeoilreserves/?src=home-b1>*

Enverus. 2017. Midland Basin Blog. <https://www.enverus.com/tag/midland-basin/>

Fitchen, W. M., 1992, Sequence stratigraphy of the upper San Andres Formation and Cherry Canyon Tongue (Permian, Guadalupian), southern Brokeoff Mountains, New Mexico: The University of Texas at Austin, Master's thesis, 155 p. 1993, Sequence stratigraphic framework of the Upper San Andres Formation and equivalent basinal strata in the Brokeoff Mountains, Otero County, New Mexico, in Love, D. W., and others, eds., New Mexico Geological Society Guidebook, 44th Field Conference, Carlsbad Region, New Mexico and West Texas, p. 185-1 93. 1994, Leonardian carbonate platform sequences, Sierra Diablo, West Texas: composite relative sea-level control on sequence attributes (abs.): American Association of Petroleum; Lower Permian Sequence Stratigraphy of the Western Delaware Basin Margin, Sierra Diablo, West Texas, PhD Dissertation, 1997 University of Texas at Austin.

Galley, John E. "Oil and geology in the Permian basin of Texas and New Mexico: North America." (1958): 395-446.

Goldhammer, R. K., Lehmann, P. J., and Dunn, P. A., 1993, The origin of high-frequency platform carbonate cycles and third-order sequences (Lower Ordovician El Paso Group, West Texas): constraints from outcrop data and stratigraphic modeling: Journal of Sedimentary Petrology, V. 63, p. 31 8-359.

Harris, P. M., Kerans, Charles, and Bebout, D. G., 1993, Ancient and modern examples of platform carbonate cycles-implications for subsurface correlation and understanding reservoir heterogeneity, in Loucks, R. G., and Sarg, J. F., eds., Carbonate sequence stratigraphy: recent development and applications: American Association of Petroleum Geologists Memoir 57, p. 475-492.Haq, B. U., and S. R. Schutter, 2008, A Chronology of Paleozoic Sea-Level Changes: Science, v. 322, p. 64-68.

Hart, B.S., 1997, New Targets in the Bone Spring Formation, Permian Basin: Oil & Gas Journal, p. 85-88.

Hart, B.S., 1997, New Targets in the Bone Spring Formation, Permian Basin: Oil & Gas Journal, p. 85-88.

Hill, C.A., 1996, Geology of the Delaware Basin, Guadalupe, Apache, and Glass Mountains, New Mexico and West Texas: Society for Sedimentary Geology, Albuquerque, New Mexico, v. 96-39.

Hills, J.M., 1984, Sedimentation, Tectonism, and Hydrocarbon Generation in Delaware Basin, West Texas and Southeastern New Mexico: AAPG Bulletin, v. 68.3, p. 250-267.

Horak, R. L., 1985, Tectonic and Hydrocarbon Maturation History in the Permian Basin: Oil and Gas Journal, v. 83, no.21.

Hornbuckle, John S "Process Sedimentology of the Guadalupian Rader Limestone, Delaware Basin" *The University of Oklahoma*, 2017

Hurd, Gregory, Kerans, Charlie, 2014, Advances in the Stratigraphic Model of the Cutoff Formation with Implications for Upper Bone Spring and Avalon Reservoirs, Western Escarpment, Guadalupe Mountains: WTGS 2014 Fall Symposium Field Trip, Publication #14-128.

Keller, G.R., J.M. Hills, and R. Djeddi, 1980, A Regional Geological and Geophysical Study of the Delaware Basin, New Mexico and West Texas: New Mexico Geological Society Guidebook, p. 105-111.

Kerans, Charles, Fitchen, W. M., Gardner, M. H., and Wardlaw, B. R., 1993, A contribution of the evolving stratigraphic framework of Middle Permian strata of the Delaware Basin, Texas and New Mexico, in Love, D. W., and others, eds., New Mexico Geological Society Guidebook, 44th Field Conference, Carlsbad Region, New Mexico and West Texas, p. 175-184.

Kerans, Charles, Fitchen, W. M., Gardner, M. H., Sonnenfeld, M. D., Tinker, S. W., and Wardlaw, B. R., 1992, Styles of sequence development within uppermost Leonardian through Guadalupian strata of the Guadalupe Mountains, Texas and New Mexico, in Mruk, D. H., and Curran, B. C., eds., Permian Basin exploration and production strategies: applications of sequence stratigraphic and reservoir characterization concepts: West Texas Geological Society Symposium, Publication No. 92-91, p. 1-7.

Kerans, Charles, and Ruppel, S. C., 1994, San Andres sequence framework, Guadalupe Mountains: implications for San Andres type section and subsurface reservoirs, in Garber, R. A., and Keller, D. R., eds., Field guide to the Paleozoic Section of the San Andres Mountains: Permian Basin Section, Society of Economic Paleontologists and Mineralogists Publication 94-35, p. 105-116.King, P. B., 1948, Geology of the southern Guadalupe Mountains: U.S. Geological Survey Professional Paper 215, p. 183.

Lew C. L., Baharuddin, S. B., and Pigott, J.D., 2013. Deepwater Basin Model for the Permian Basin:Delaware Basin example, The international Petroleum Technology Conference in Bejing, China.

Mack, G.H., and P.A. Dinterman, 2002, Depositional Environments and Paleogeography of the Lower Permian (Leonardian) Yeso and Correlative Formations in New Mexico: The Mountain Geologist, v. 39.4, p. 75-88.

Madhavaraju, J. and Y.I. Lee, 2009, Geochemistry of the Dalmiapuram Formation of the Uttatur Group (Early Cretaceous), Cauvery basin, southeastern India:Implications on provenance and paleo-redox conditions: Revista Mexicana de Ciencias Geologicas, v. 26.2, p. 380-394.

Mccullough, B.J., 2014, Sequence-Stratigraphic Framework and Characterization of the Woodford Shale on the Southern Cherokee Platform of Central Oklahoma: Master‘s thesis, University of Oklahoma, Norman, Oklahoma, 210 p.

McManus, J., W.M. Berelson, G.P. Klinkhammer, D.E. Hammond, and C. Holm, 2004, Authigenic uranium: relationship to oxygen penetration depth and organic carbon rain: Geochimica et Cosmochimica Acta, v. 69.1, p. 95-108.

Meissner, F. F., 1972, Cyclic sedimentation in Middle Permian strata of the Permian Basin, west Texas and New Mexico: West Texas Geological Society Publication 72-60, p. 11 8-142.

Montgomery, S.L., 1998, The Permian Bone Spring Formation, Delaware Basin: Petroleum Frontiers, v. 14.3, p. 1-89.

Mullins, H.T., and H.E. Cook, 1986, Carbonate Apron Models: Alternatives to the Submarine Fan Model for Paleoenvironmental Analysis and Hydrocarbon Exploration: Sedimentary Geology, v. 48.1-2, p. 37-79.

Nance, H.S. and H.D. Rowe, 2014, Nested Cyclicity in Mudrock Successions: Bone Spring Formation, Delaware Basin, West Texas: AAPG Search and Discovery #90189.

Nance, S. and H.D. Rowe, 2013, Chemostratigraphy of Mudrocks: Bone Spring Formation, Delaware Basin, West Texas: AAPG Search and Discovery #90163.

Pigott, John D. and Bryant W. Bradley, 2014, Application of production decline curve analysis to clastic reservoir facies characterization with a sequence stratigraphic framework: Example – Frio Formation South Texas, BCABS Journal, Vol 3, p. 112-133.

Pigott, K.L., J.D. Pigott, M.H. Engel and R.P. Philip, High Resolution Chemical Sequence Stratigraphy in Carbonates: Oxfordian Smackover USA Ramp Proxy AAPG European Region Conference Athens, Greece 2007.

Plemons, T.O., An Integrated Lidar-Xrf Study and Geomechanical Lithofacies Analysis of The Leonardian Upper Bone Spring Formation, Bone Canyon, Texas, Master’s Thesis, University of Oklahoma 2019

Read, J. F., 1985, Carbonate platform facies models: American Association of Petroleum Geologists Bulletin, v. 69, p. 1-21.

Ross, C.A. and J.R.P. Ross, 1995, Permian Sequence Stratigraphy in P.A. Scholle, T.M. Peryt, and D.S. Ulmer-Scholle, eds., The Permian of Northern Pangea: Berlin: Springer-Verlag, v. 1, p. 98-113.

Ross, C.A. and J.R.P. Ross, 1994, Permian Sequence Stratigraphy and Fossil Zonation: Canadian Society of Petroleum Geologists, v. 17, p. 219-231.

Ross, C. A., and Ross, J. R. P., 1987, Late Paleozoic sea levels and depositional sequences, in Ross, C. A., and Haman, D., eds., Timing and depositional history of eustatic sequences: constraints on seismic stratigraphy: Cushman Foundation for Foraminiferal Research, Special Publication 24, p. 137-149.

Ruppel, Stephen C., and W. Bruce Ward, 2013, Outcrop-based Characterization of the Leonardian Carbonate Platform in West Texas: Implications for Sequence- stratigraphic Styles in the Lower Permian: AAPG Bulletin, v. 97.2, p. 223-250.

Sarg, J. F., J. R. Markello, and L. J. Weber, 1999, The Second-Order Cycle, Carbonate- Platform Growth, and Reservoir, Source, and Trap Prediction: SEPM Special Publication, v. 63, p. 11-34.

Sarg, J. F., and Lehmann, P. J., 1986, Lower-Middle Guadalupian facies and stratigraphy, San Andres- Grayburg Formations, Permian Basin, Guadalupe Mountains, New Mexico, in Moore, G. E., and Wilde, G. L., eds., Lower and Middle Guadalupian facies, stratigraphy, and reservoir geometries, San Andres- Grayburg Formations, Guadalupe Mountains, New Mexico and Texas: Permian Basin Section, Society of Economic Paleontologists and Mineralogists Special Publication No. 86-25, p. 1-36. Saller, A.H., J.W. Barton, and R.E. Barton, 1989, Slope Sedimentation Associated with a Vertically Building Shelf, Bone Spring Formation, Mescalero Escarpe Field, Southeastern New Mexico: SEPM Special Publication, v. 44, p. 275-288.

Shale Experts. 2019. Permian Basin Overview. <https://www.shaleexperts.com/plays/permian-basin/Overview>

Silver, B.A. and R.G. Todd, 1969, Permian Cyclic Strata, Northern Midland and Delaware Basins, West Texas and Southeastern New Mexico: AAPG Bulletin, v. 53.11, p. 2223-2251.

Slatt, R.M., 2013 GEOL 5970: Reservoir Characterization I. Fall 2013. Unpublished Lecture Notes.

Slatt, R. M., 2006, Stratigraphic Reservoir Characterization for Petroleum Geologists, Geophysicists, and Engineers, v. 10, Elsevier.

Smith, C.N., and A. Malicse, 2010, Rapid Handheld X-ray Fluorescence (HHXRF) Analysis of Gas Shales: AAPG Search and Discovery #90108.

Stolz, Dustin J., 2014. Reservoir Character of the Avalon Shale (Bone Spring Formation) of the Delaware Basin, West Texas and Southeast New Mexico: Effect of Carbonate-rich Sediment Gravity Flows, p. 23.

Tang, Carol Marie. 2007. Permian Basin Area, Texas, United States. Encyclopedia Britannica, Inc. <https://www.britannica.com/place/Permian-Basin>

Thermo Fisher Scientific. (2010). XL3 Analyzer: User‘s Guide Version 7.0.1.

Treanton, J. A., 2014, Outcrop-derived Chemostratigraphy of the Woodford Shale, Murray County, Oklahoma: Master‘s thesis, University of Oklahoma, Norman, Oklahoma, 83 p.

Tribovillard, N., T.J. Algeo, T. Lyons, A. Riboulleau, 2006, Trace metals as paleoredox and paleoproductivity proxies: An Update: Chemical Geology, v. 232, p. 12-32.

Turner, B., Roger Slatt and Jessica Treanton, The Use of Chemostratigraphy to Refine Ambiguous Sequence Stratographic Correlations in Marine Shales: An Example from the Woodford Shale, Oklahoma, Unconventional Resources Technology Conference, San Antonio, Texas, July 2015.

West Texas Geological Society. Northwest-Southwest. 1964. Delaware and Val Verde Basins Geology of Mina Plomosas-Placer De Gaudalupe Area, Paleozoic. Pub. 64-49.

Wiggins, W.D. and P.M. Harris, 1985, Burial Diagenetic Sequence in Deep-Water Allochthonous Dolomites, Permian Bone Spring Formation, Southeast New Mexico: The Society of Economic Paleontologists and Mineralogists, v. CW 6, p. 140-173.

Yang, K.M. and S.L. Dorobek, 1995, The Permian Basin of West Texas and New Mexico: Tectonic History of a ―Composite‖ Foreland Basin and Its Effects on Stratigraphic Development: SEPM Special Publication, v. 52, p. 149-174.

Yang, K.-M., and Dorobek, S. L., 1992, Mechanisms for late Paleozoic synorogenic subsidence of the Midland and Delaware Basins, Permian Basin, Texas and New Mexico, in Mruk, D. H., and Curran, B. C., eds., Permian Basin exploration and production strategies: applications of sequence stratigraphic and reservoir characterization concepts: West Texas Geological Society Publication 92-91, p. 45-60.]

Zhou, Y., 2014, High Resolution Spectral Gamma Ray Sequence Stratigraphy of Shelf Edge to Basin Floor Upper Capitan Permian Carbonates, Guadalupe Mountains, Texas and Delaware Basin, New Mexico: Master‘s thesis, University of Oklahoma, Norman, Oklahoma, p. 131.

Appendix A: Bone Canyon Geochemistry (Average & Mean)

	Uav	Um	Thav	Thm	Kav	Km
T7	10.86	10.86	4.43	4.43	1664.75	1664.75
T6	7.04	7.04	3.505	3.505	997.36	997.36
T5	6.3425	6.37	3.44	4.34	438.513	167.54
T4	5.384	5.47	3.994	4.24	644.133	484.37
T3	6.485	6.54	3.60167	3.6	1738.83	1546.13
T2	4.8525	5.695	3.73583	3.89	2330.66	2365.25
T1	7.80222	7.4	6.52556	5.8	5148.99	5676.17

Table 4: Bone Canyon Radiation Proxy Average and Mean.

	Siav	Sim	Tiav	Tim	Zrav	Zrm	Si/Alav	Si/Alm	Alav	Alm
T7	34436.1	34436.1	1116.68	1116.68	654.29	654.29	11.7243	11.7243	2946.99	2946.99
T6	44167.5	44167.5	508.46	508.46	13.05	13.05	13.6294	13.6294	2993.97	2993.97
T5	39225.7	39846.1	226.73	272.645	12.615	13.18	11.4675	11.0761	3355.6	3446.07
T4	38569.2	23843.3	619.266	588.36	24.1068	22.9	11.9798	7.07848	3342.6	3213.18
T3	39910.7	36332.5	820.548	805.08	28.145	26.77	12.8868	12.4017	3120.35	3105.08
T2	44253.2	44241.2	1035.4	989.975	44.0242	40.725	12.0688	11.1333	3705.13	3638.51
T1	45288.9	48388.6	1495.85	1756.38	97.0311	74.31	11.758	11.7264	3903.88	3743.75

Table 5: Bone Canyon Terrigenous Proxy Average and Mean.

	Pav	Pm	Caav	Cam	Srav	Srm	Mgav	Mgm	Mnav	Mnm	Mg/Caav	Mg/Cam
T7	2669.33	2669.33	168783	168783	46.99	46.99	9794	9794	264.44	264.44	0.39792	0.39792
T6	1394.54	1394.54	161326	161326	191.965	191.965	8426.65	8426.65	253.935	253.935	0.92733	0.92733
T5	1724.42	1702.93	188260	192776	158.02	158.87	5787.52	7155.06	153.913	153.915	0.3235	0.11953
T4	1555.33	1210.82	175729	265802	247.149	251.84	9989.53	8820.19	188.214	169.31	0.6679	0.06103
T3	1602.34	1144.65	149823	182666	393.026	376.5	9396.47	8380.66	235.365	207.04	0.57734	0.0694
T2	2217.42	2610.48	126627	92923.1	201.036	220.065	9522.62	9287.41	438.285	296.205	0.84414	0.47356
T1	2447.49	2393.5	86056.3	66598.3	167.242	170.85	9902.86	10211.4	293.881	270.87	0.25819	0.12658

Table 6: Bone Canyon Carbonate Proxy Average and Mean.

	Moav	Mom	Vav	Vm	Uav	Um	Niav	Nim	Cuav	Cum	Mn*av	Mn*m
T7	10.3	10.3	0	0	10.86	10.86	72.915	72.915	54.68	54.68	0.67755	0.67755
T6	2.965	2.965	0	0	6.38	6.38	78.535	78.535	36.53	36.53	1.63388	1.63388
T5	4.7575	4.71	0	0	6.3425	6.37	97.8925	104.53	49.515	52.81	1.52507	1.52901
T4	4.6394	4.82	0	0	5.384	5.47	90.8304	101.27	41.7062	44.365	1.32745	1.37857
T3	4.30167	4.11	2.65767	0	6.485	6.54	83.799	94.64	31.9057	35.92	1.41135	1.41615
T2	3.8175	4.245	1.025	0	4.8525	5.695	77.7367	89.265	37.2042	35.795	1.50015	1.43239
T1	4.26222	4.23	5.11444	0	7.80222	7.4	93.4533	78.68	46.97	41.43	1.29448	1.29532

Table 7: Bone Canyon Paleoredox Proxy Average and Mean.

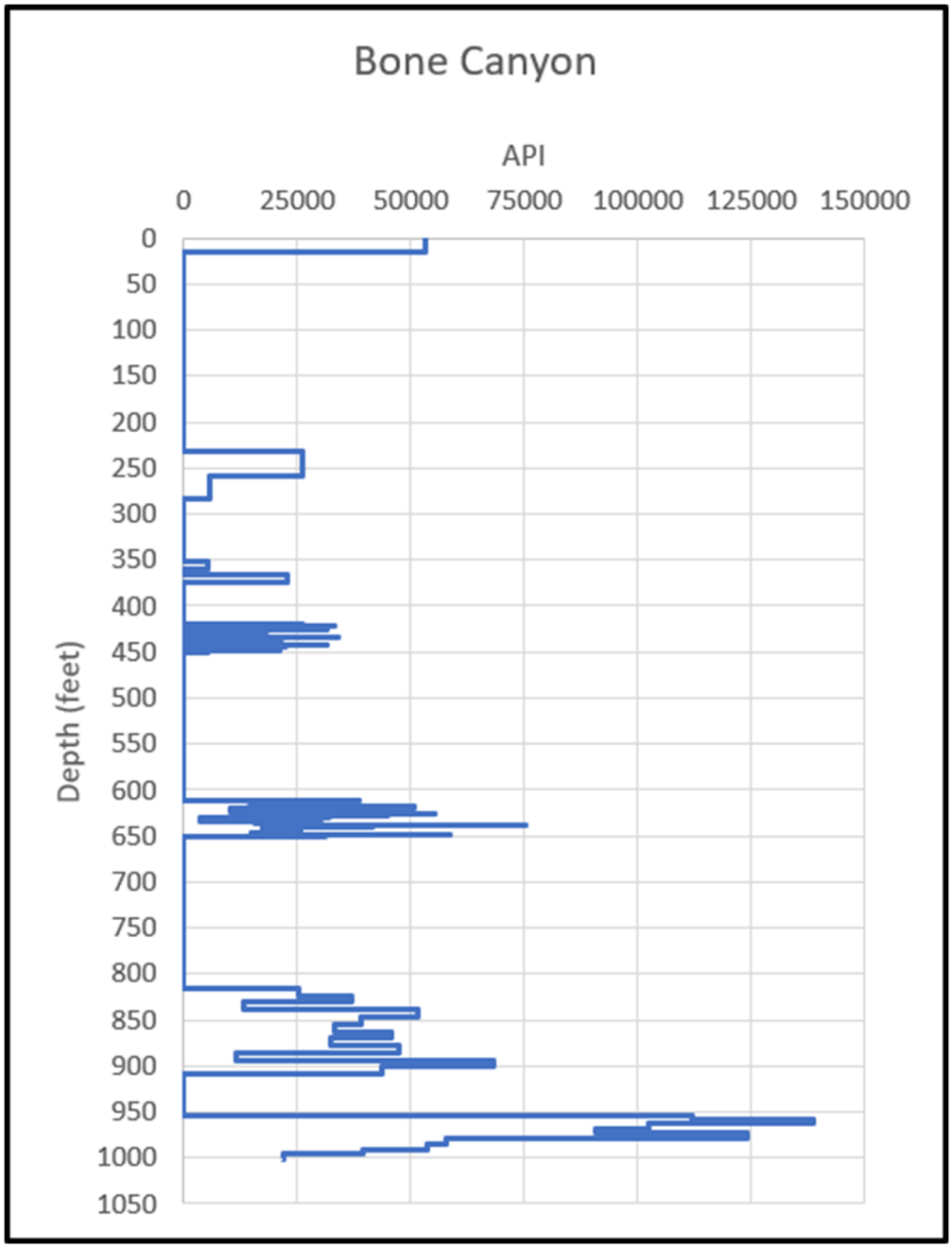

Figure 97: Bone Canyon Pseudo-Gamma Ray in API.

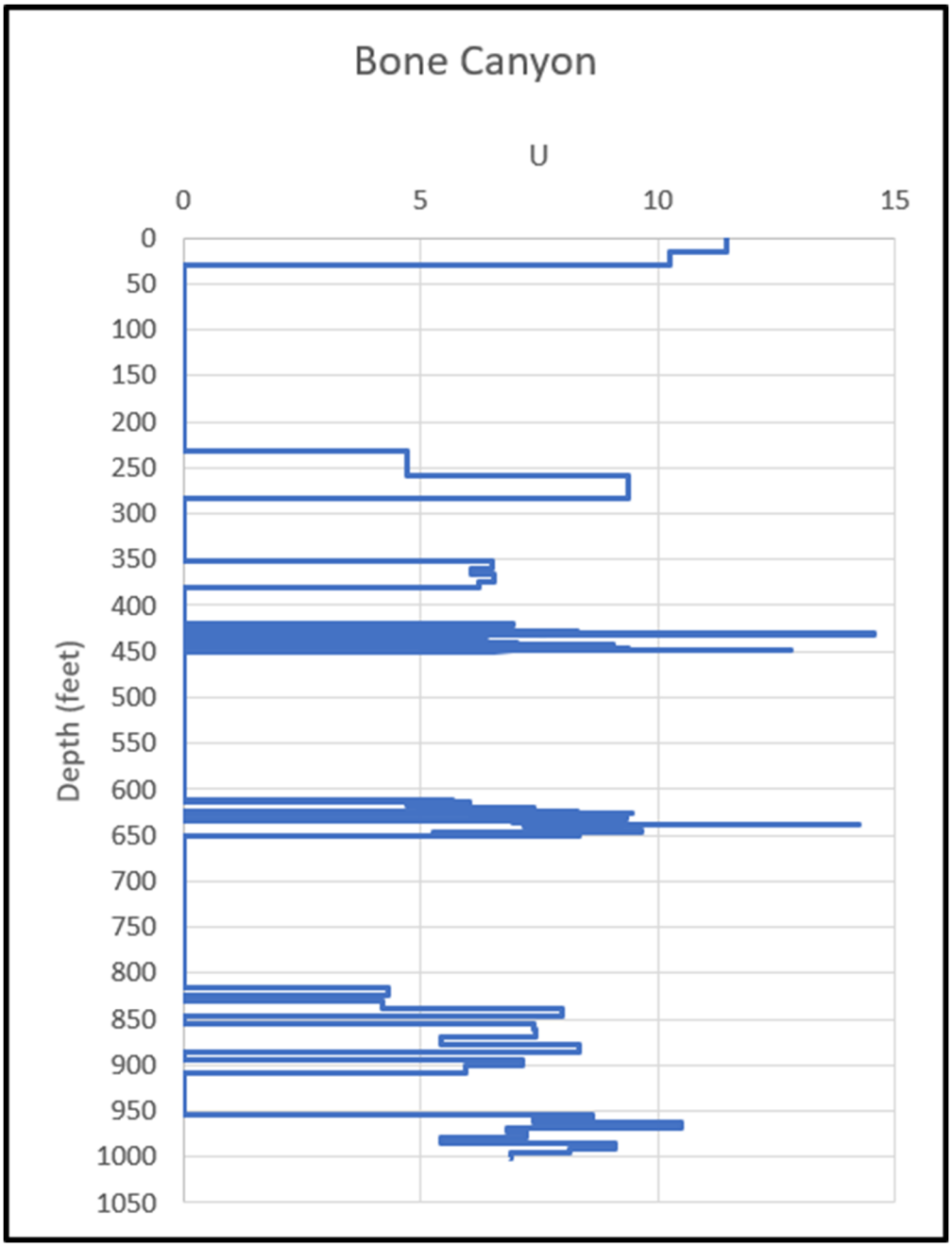

Figure 98: Bone Canyon Radiation Proxy Uranium.

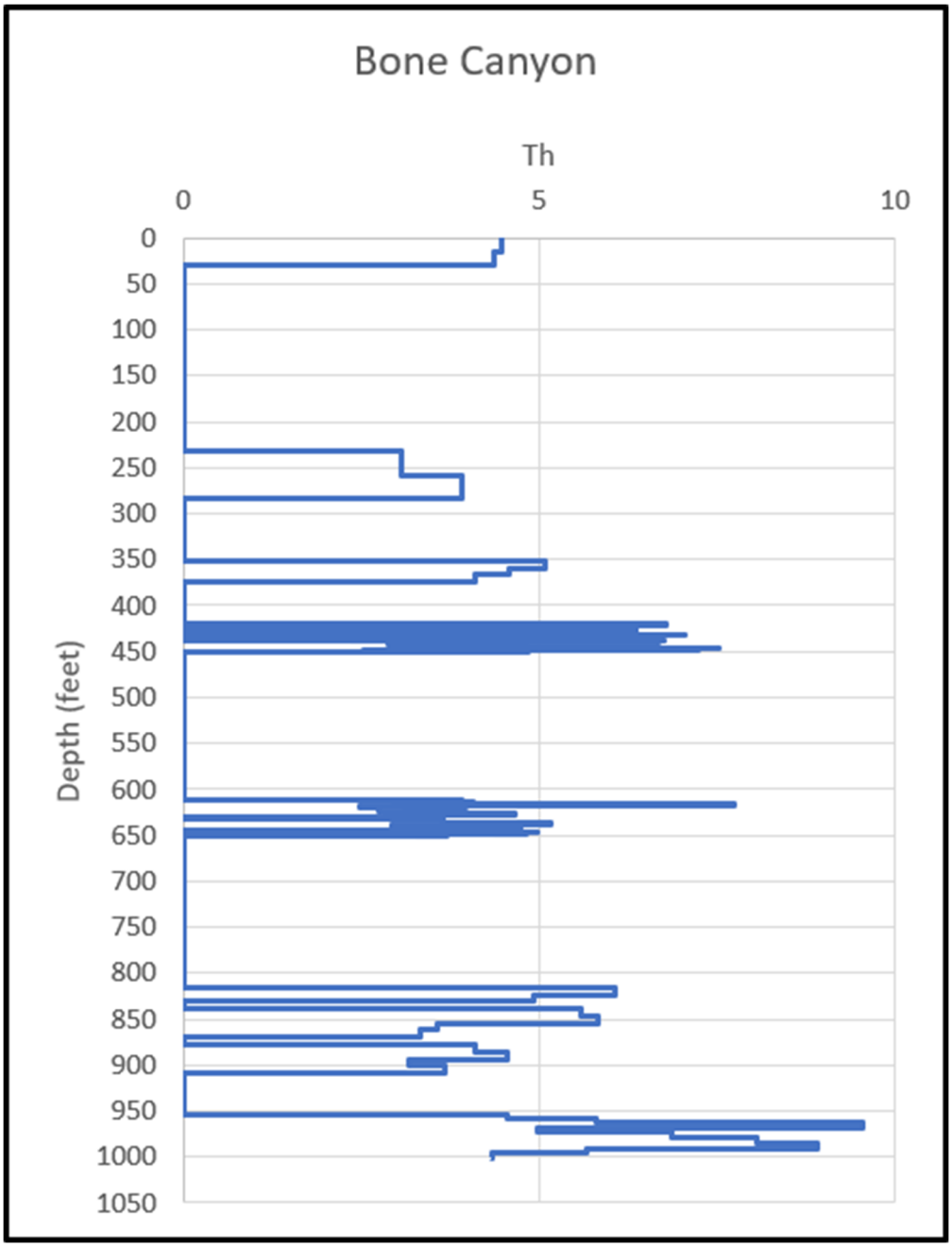

Figure 99: Bone Canyon Radiation Proxy Thorium.

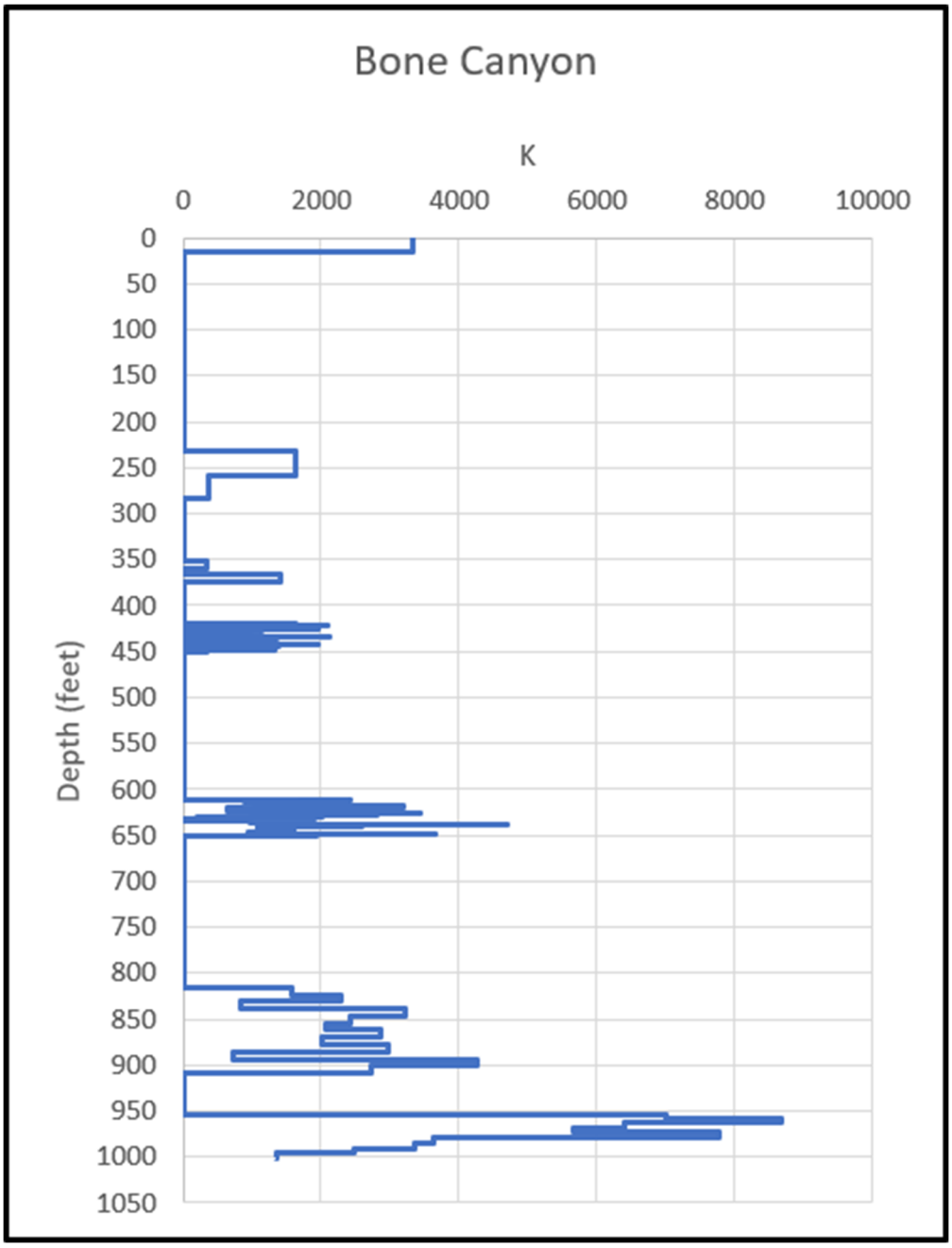

Figure 100: Bone Canyon Radiation and Terrigenous Proxy Potassium.

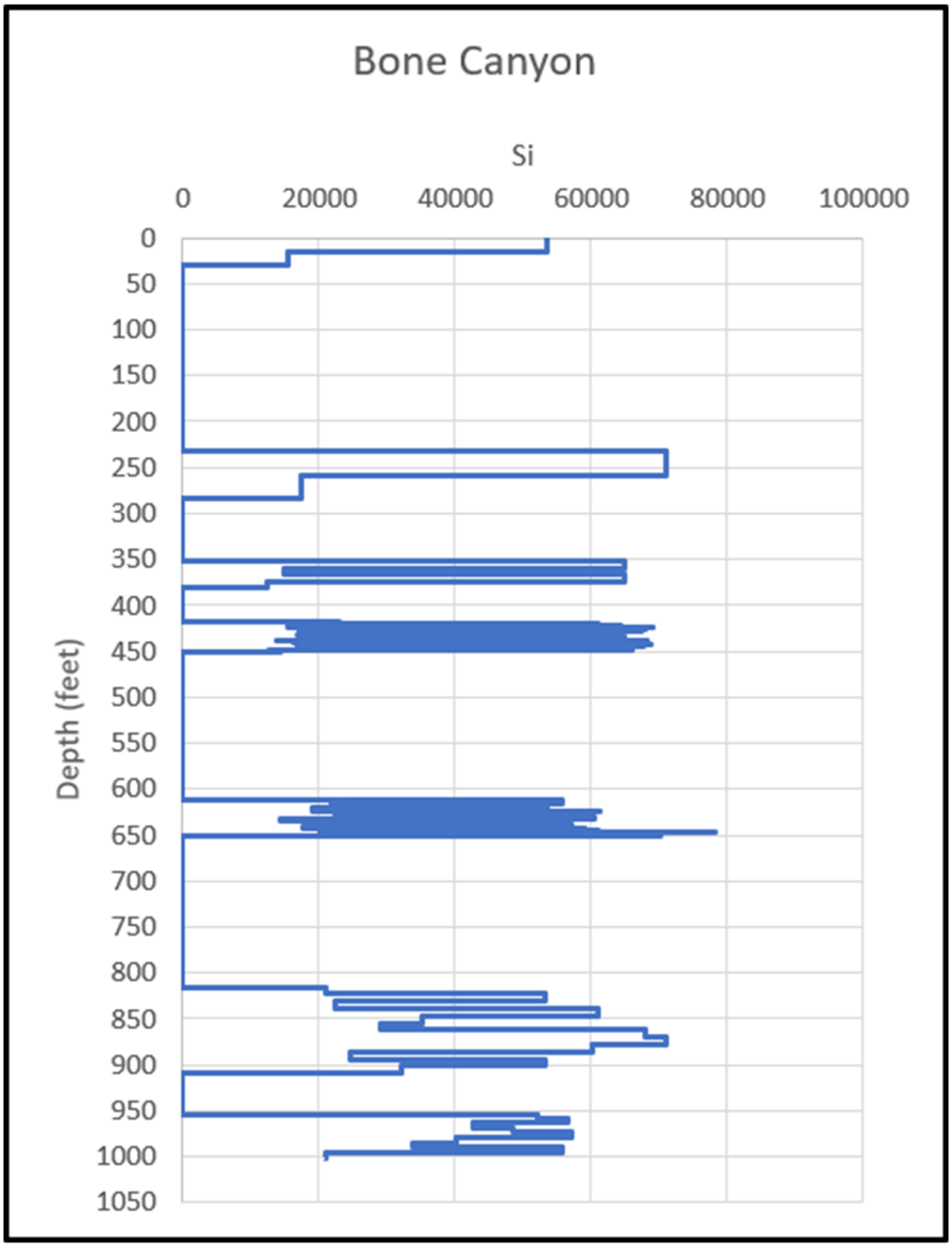

Figure 101: Bone Canyon Terrigenous Proxy Silica.

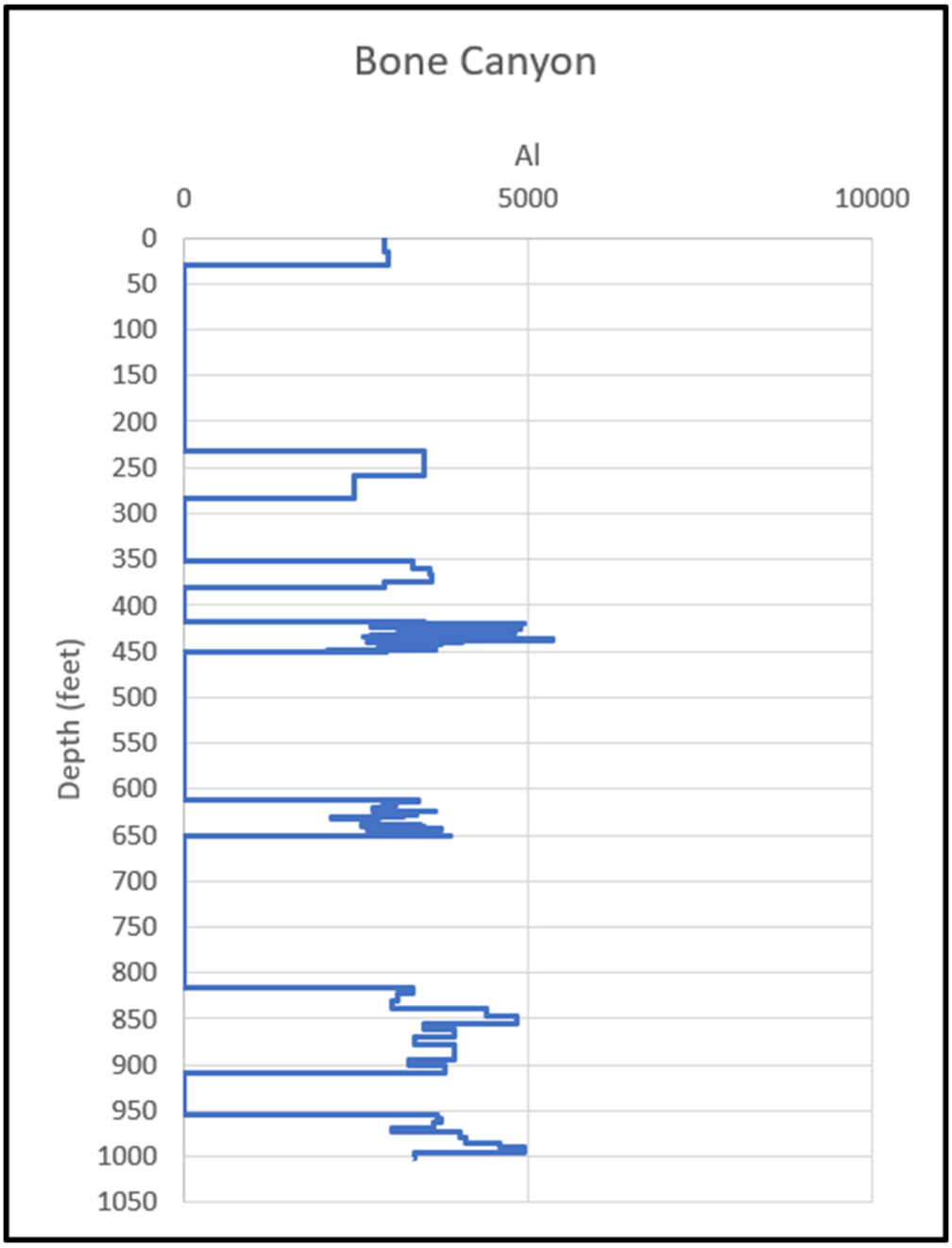

Figure 102: Bone Canyon Terrigenous Proxy Aluminum.

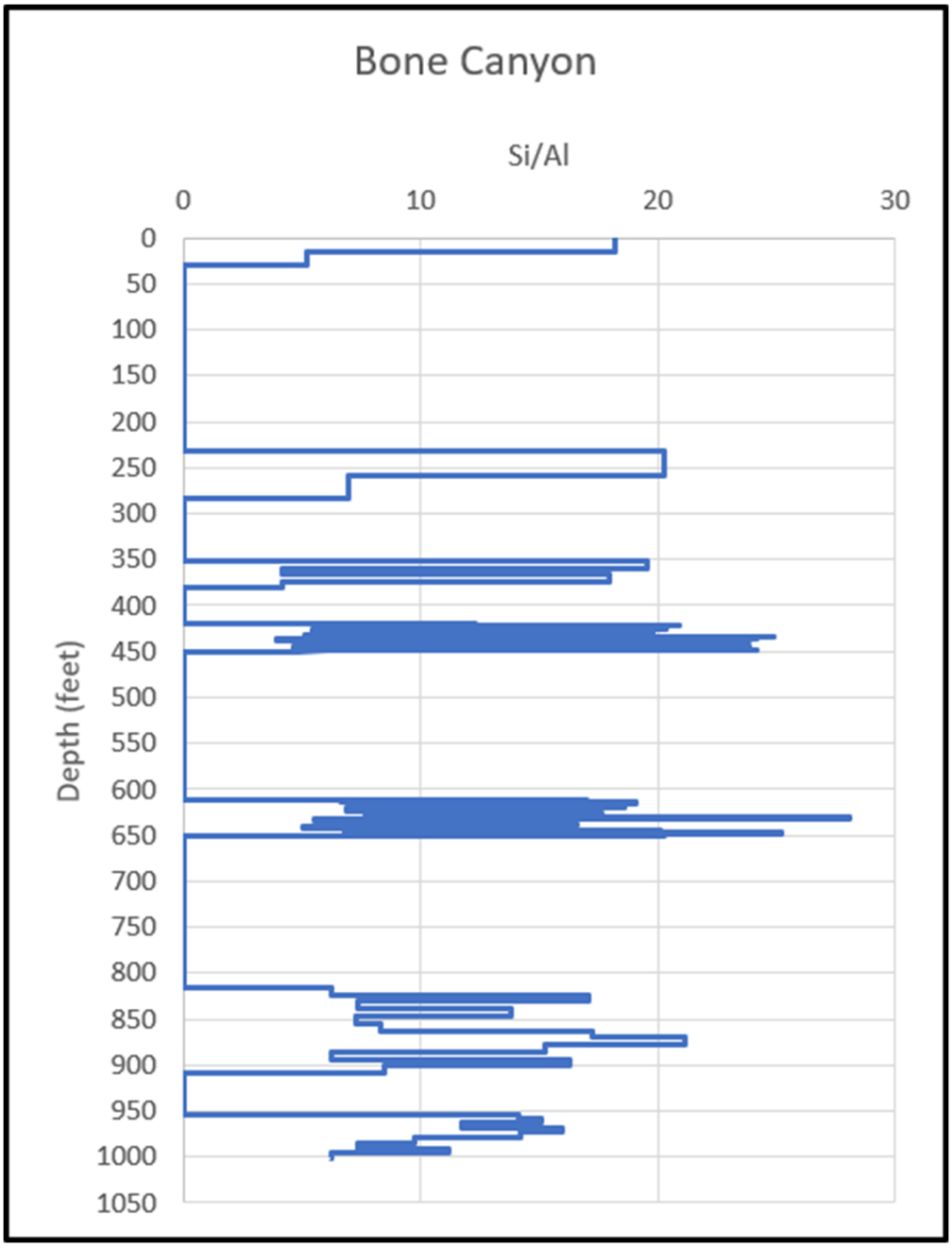

Figure 103: Bone Canyon Si/Al Ratio for Type/Origin of Silica.

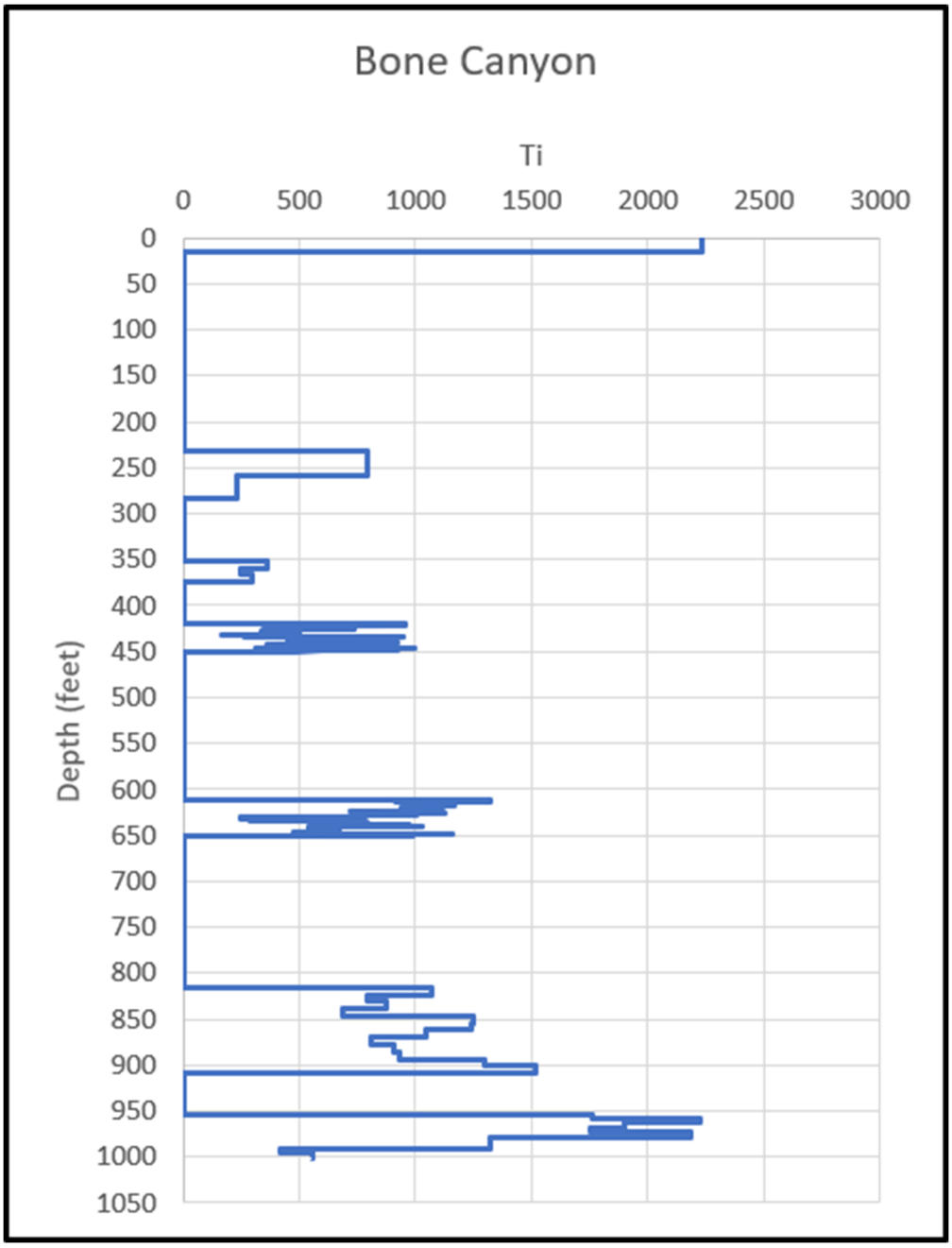

Figure 104: Bone Canyon Terrigenous Proxy Titanium.

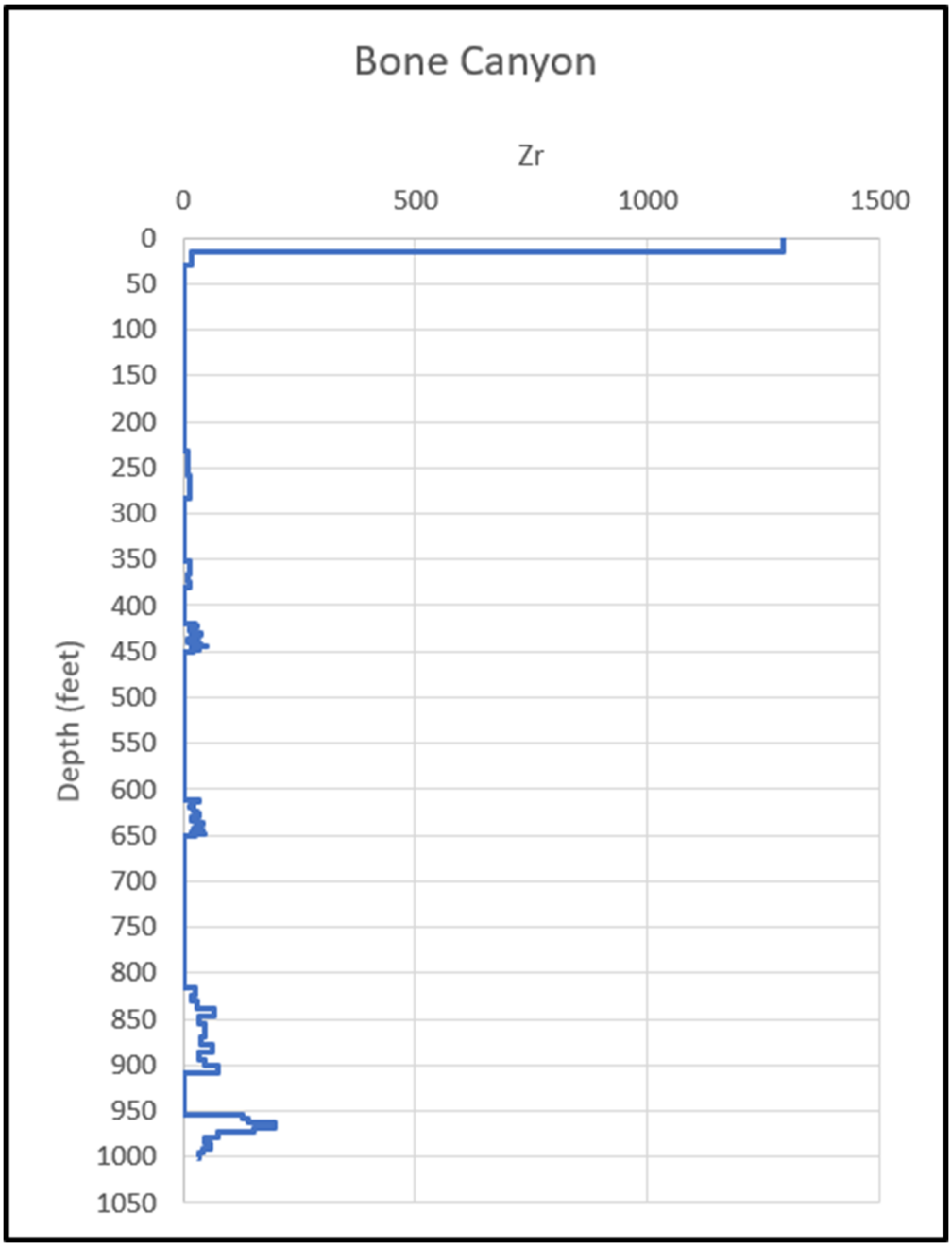

Figure 105: Bone Canyon Terrigenous Proxy Zirconium.

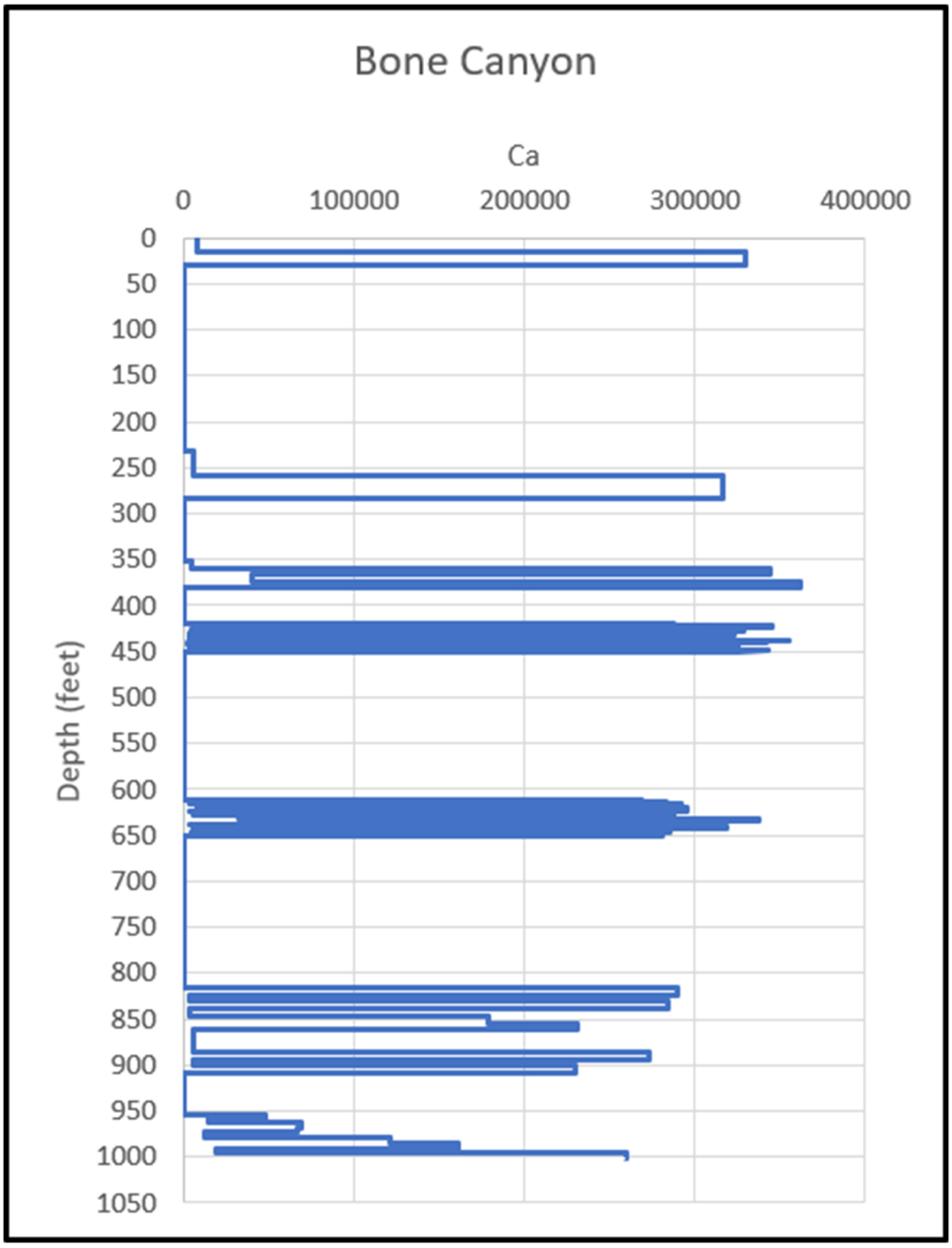

Figure 106: Bone Canyon Carbonate Proxy Calcium.

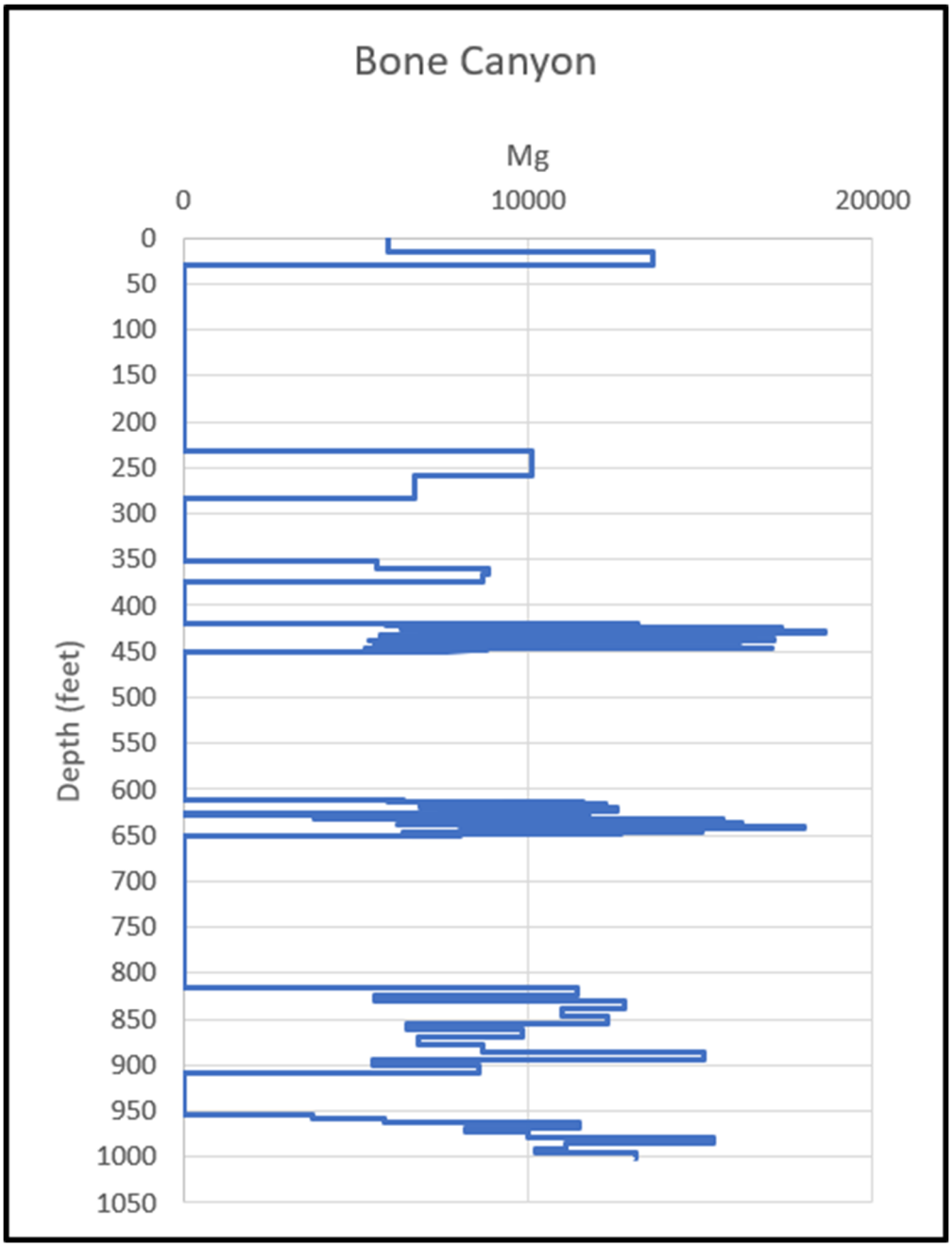

Figure 107: Bone Canyon Carbonate Proxy Magnesium.

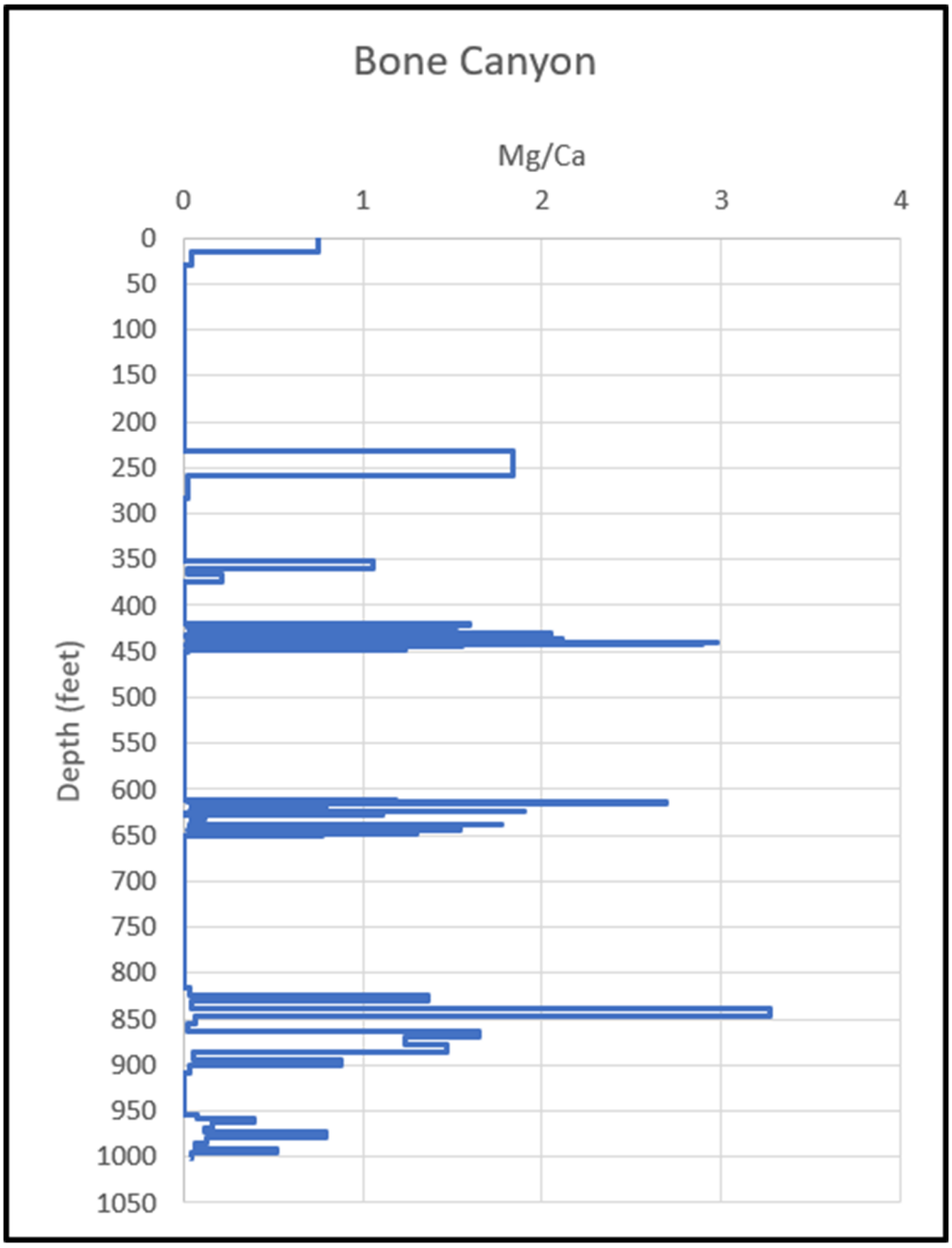

Figure 108: Bone Canyon Carbonate Proxy Mg/Ca Ratio for Dolomite.

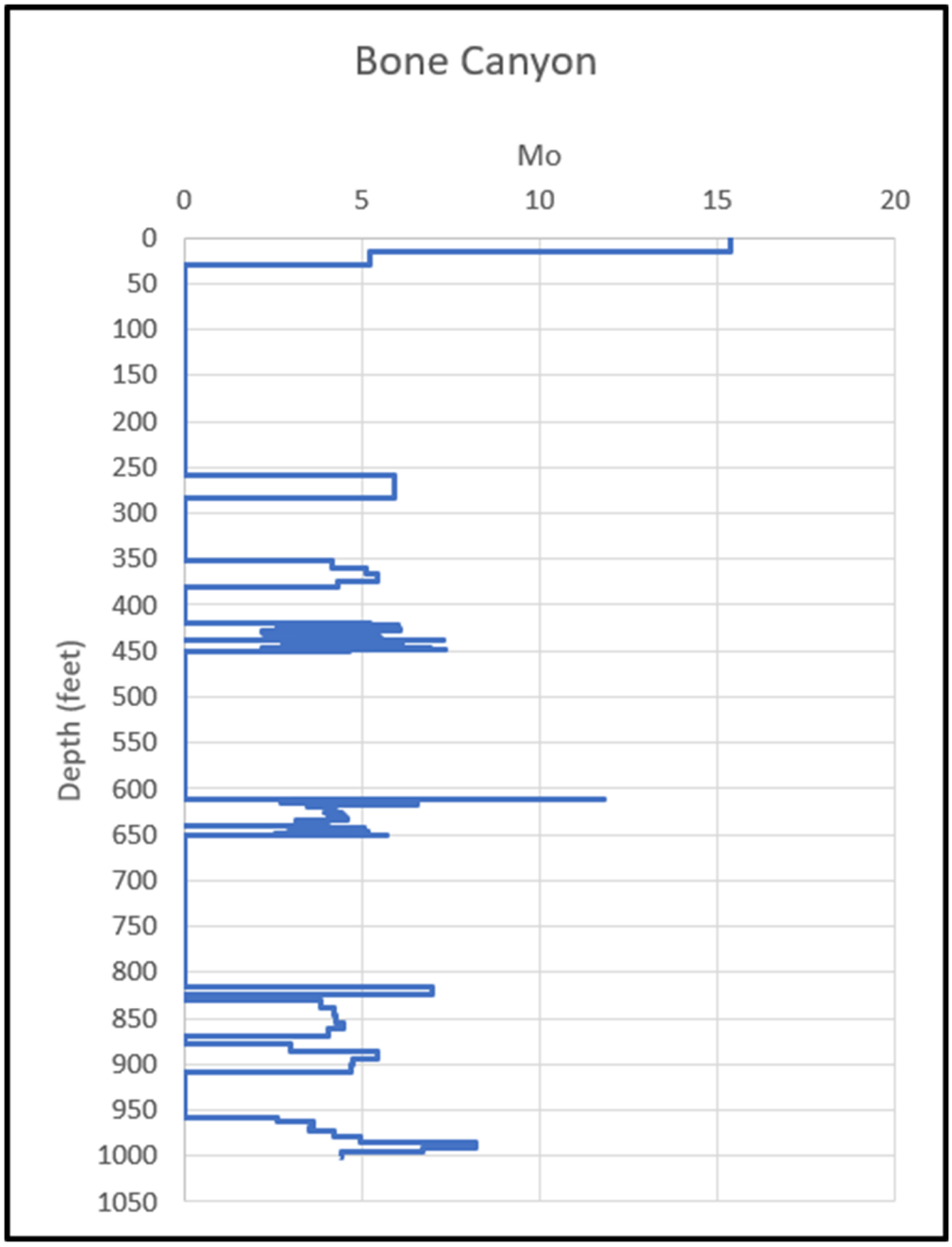

Figure 109: Bone Canyon Paleoredox Proxy Molybdenum.

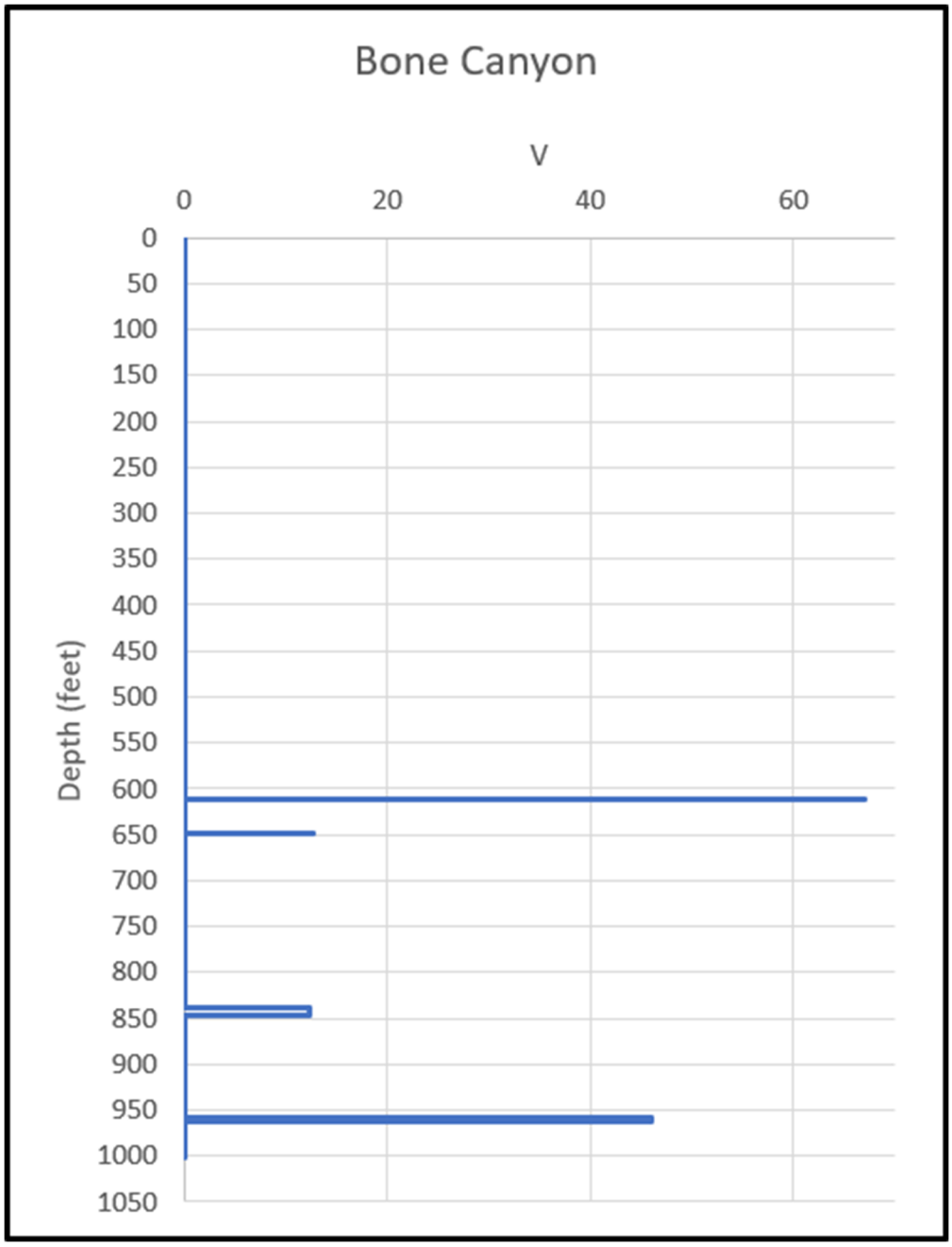

Figure 110: Bone Canyon Paleoredox Proxy Vanadium.

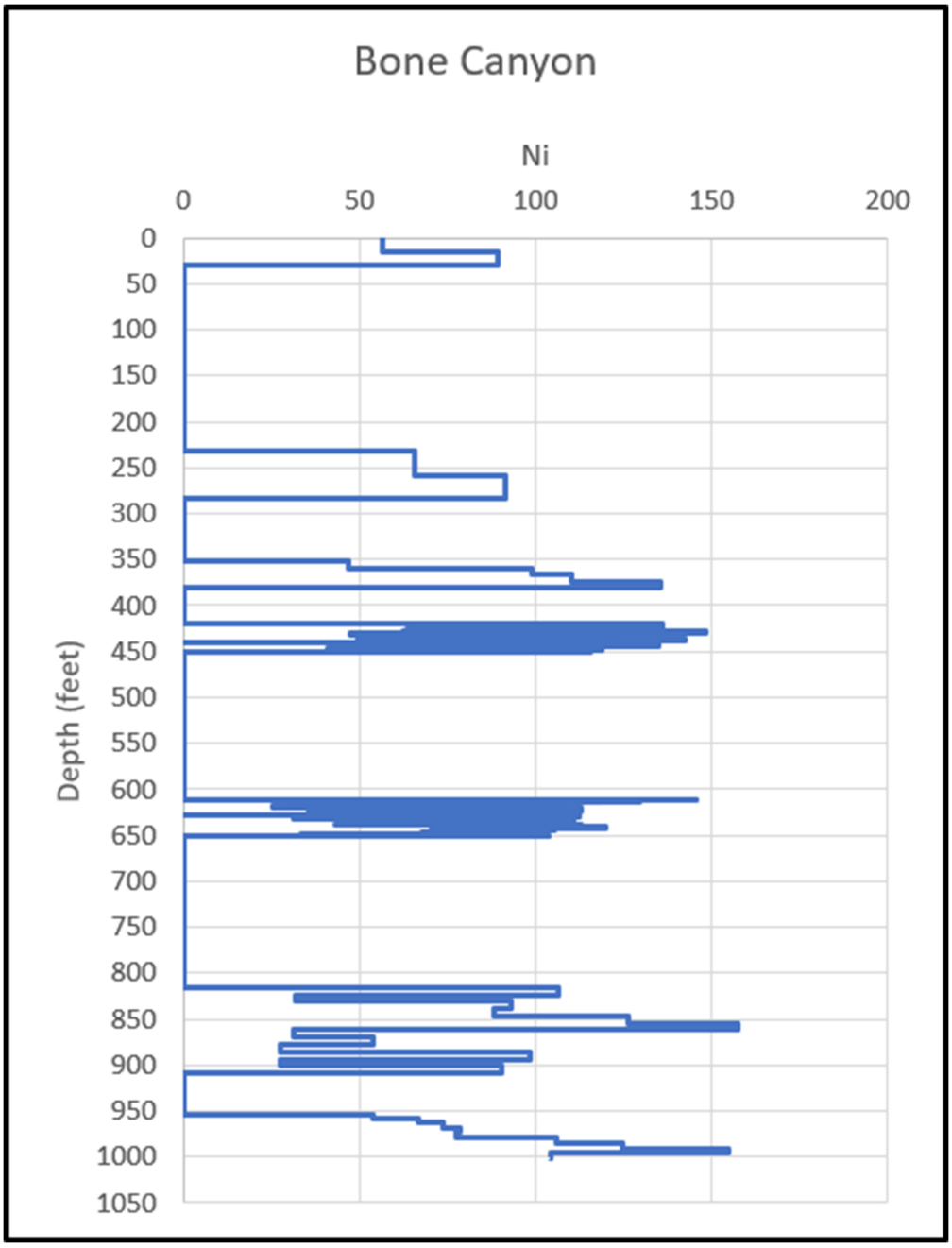

Figure 111: Bone Canyon Paleoredox Proxy Nickel.

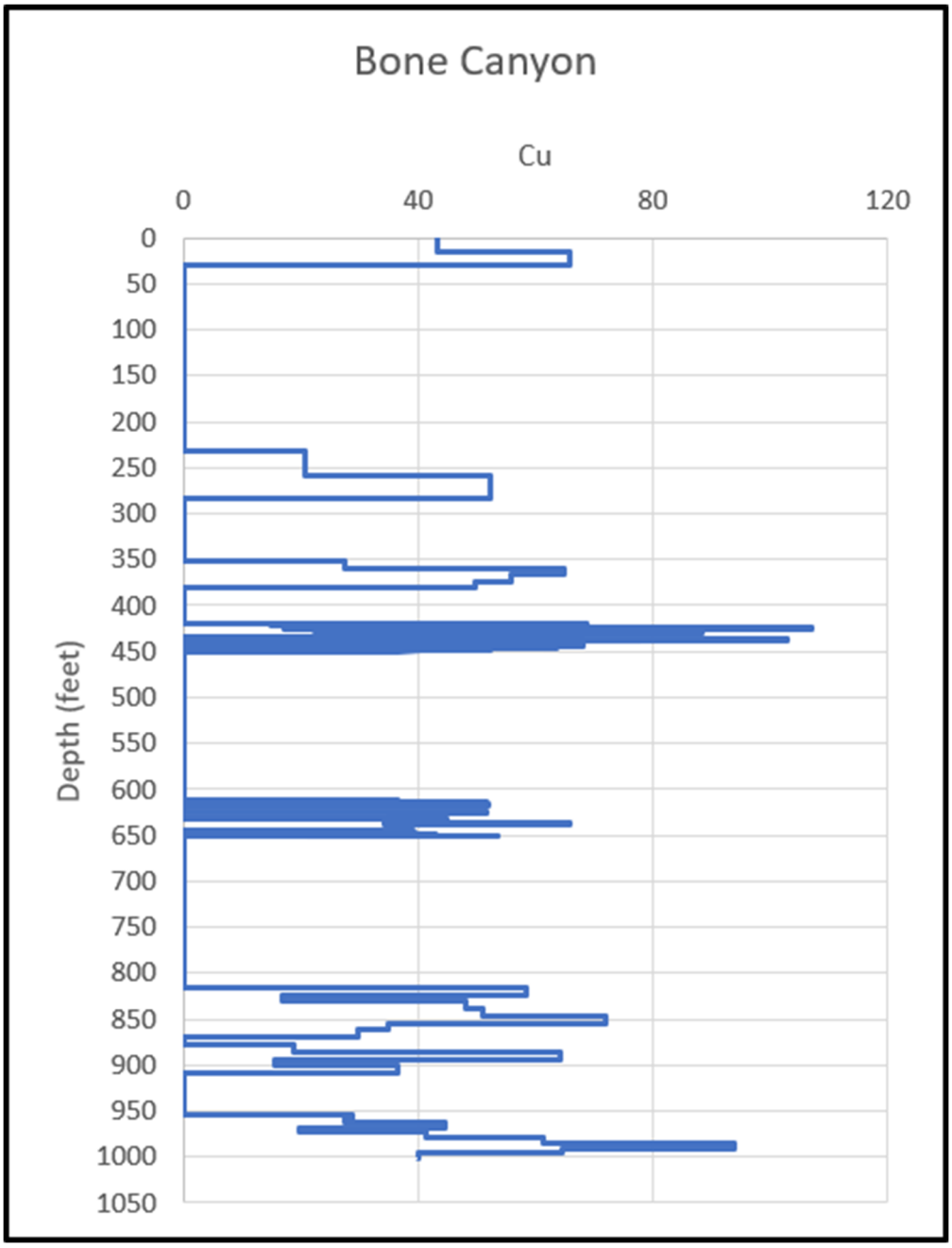

Figure 112: Bone Canyon Paleoredox Proxy Copper.

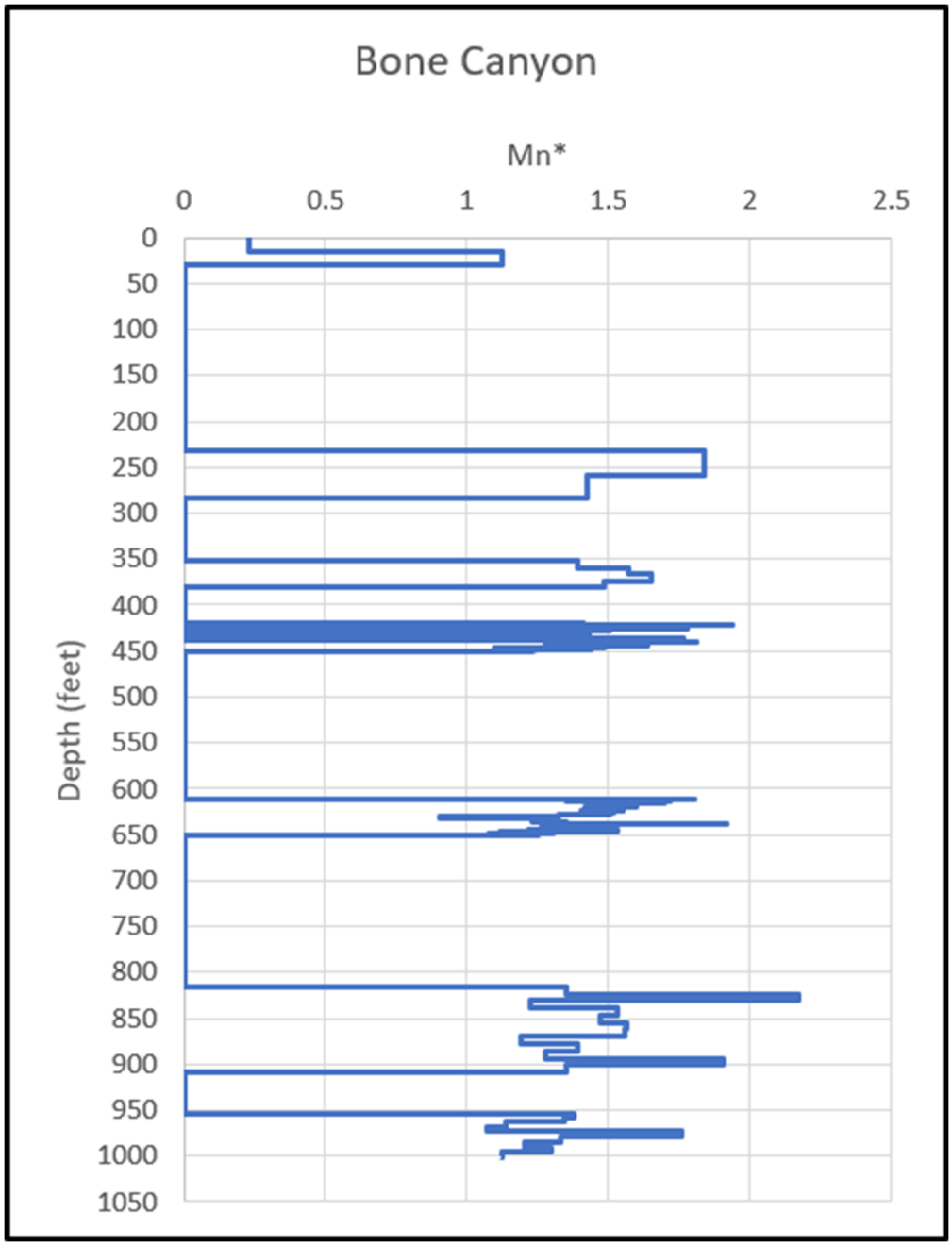

Figure 113: Bone Canyon Paleoredox Proxy Manganese (adjusted for relation to Fe (Iron)).